biomolecules

Special Issue Reprint

Versatility of Glutathione Transferase Proteins

Edited by
Bengt Mannervik

mdpi.com/journal/biomolecules

MDPI

Versatility of Glutathione Transferase Proteins

Versatility of Glutathione Transferase Proteins

Editor

Bengt Mannervik

MDPI

Basel • Beijing • Wuhan • Barcelona • Belgrade • Novi Sad • Cluj • Manchester

Editor
Bengt Mannervik
Stockholm University
Stockholm
Sweden

Editorial Office
MDPI
St. Alban-Anlage 66
4052 Basel, Switzerland

This is a reprint of articles from the Special Issue published online in the open access journal *Biomolecules* (ISSN 2218-273X) (available at: https://www.mdpi.com/journal/biomolecules/special_issues/V1FP5F489N).

For citation purposes, cite each article independently as indicated on the article page online and as indicated below:

Lastname, A.A.; Lastname, B.B. Article Title. *Journal Name* **Year**, *Volume Number*, Page Range.

ISBN 978-3-7258-0453-5 (Hbk)
ISBN 978-3-7258-0454-2 (PDF)
doi.org/10.3390/books978-3-7258-0454-2

Contents

Bengt Mannervik
Versatility of Glutathione Transferase Proteins
Reprinted from: *Biomolecules* **2023**, *13*, 1749, doi:10.3390/biom13121749 . . . . . **1**

Aaron J. Oakley
Hidden Glutathione Transferases in the Human Genome
Reprinted from: *Biomolecules* **2023**, *13*, 1240, doi:10.3390/biom13081240 . . . . . **5**

Aslam M. A. Mazari, Leilei Zhang, Zhi-Wei Ye, Jie Zhang, Kenneth D. Tew and Danyelle M. Townsend
The Multifaceted Role of Glutathione S-Transferases in Health and Disease
Reprinted from: *Biomolecules* **2023**, *13*, 688, doi:10.3390/biom13040688 . . . . . **24**

Oleksii Kupreienko, Fotini Pouliou, Konstantinos Konstandinidis, Irene Axarli, Eleni Douni, Anastassios C. Papageorgiou and Nikolaos E. Labrou
Inhibition Analysis and High-Resolution Crystal Structure of *Mus musculus* Glutathione Transferase P1-1
Reprinted from: *Biomolecules* **2023**, *13*, 613, doi:10.3390/biom13040613 . . . . . **41**

Tiffany M. Russell and Des R. Richardson
Glutathione-*S*-Transferases as Potential Targets for Modulation of Nitric Oxide-Mediated Vasodilation
Reprinted from: *Biomolecules* **2022**, *12*, 1292, doi:10.3390/biom12091292 . . . . . **56**

Michele Scian, Lorela Paço, Taylor A. Murphree, Laura M. Shireman and William M. Atkins
Reversibility and Low Commitment to Forward Catalysis in the Conjugation of Lipid Alkenals by Glutathione Transferase A4-4
Reprinted from: *Biomolecules* **2023**, *13*, 329, doi:10.3390/biom13020329 . . . . . **67**

Mathieu Schwartz, Valentin Boichot, Stéphane Fraichard, Mariam Muradova, Patrick Senet, Adrien Nicolai, et al.
Role of Insect and Mammal Glutathione Transferases in Chemoperception
Reprinted from: *Biomolecules* **2023**, *13*, 322, doi:10.3390/biom13020322 . . . . . **82**

Eva Mocchetti, Laura Morette, Guillermo Mulliert, Sandrine Mathiot, Benoît Guillot, François Dehez, et al.
Biochemical and Structural Characterization of Chi-Class Glutathione Transferases: A Snapshot on the Glutathione Transferase Encoded by *sll0067* Gene in the Cyanobacterium *Synechocystis* sp. Strain PCC 6803
Reprinted from: *Biomolecules* **2022**, *12*, 1466, doi:10.3390/biom12101466 . . . . . **100**

Shawna M. Hubert, Paul B. Samollow, Helena Lindström, Bengt Mannervik and Nancy H. Ing
Conservation of Glutathione Transferase mRNA and Protein Sequences Similar to Human and Horse Alpha Class GST A3-3 across Dog, Goat, and Opossum Species
Reprinted from: *Biomolecules* **2023**, *13*, 1420, doi:10.3390/biom13091420 . . . . . **119**

Yaman Musdal, Aram Ismail, Birgitta Sjödin and Bengt Mannervik
Potent GST Ketosteroid Isomerase Activity Relevant to Ecdysteroidogenesis in the Malaria Vector *Anopheles gambiae*
Reprinted from: *Biomolecules* **2023**, *13*, 976, doi:10.3390/biom13060976 . . . . . **134**

Kana Ebihara and Ryusuke Niwa
Compounds Inhibiting Noppera-bo, a Glutathione *S*-transferase Involved in Insect Ecdysteroid Biosynthesis: Novel Insect Growth Regulators
Reprinted from: *Biomolecules* **2023**, *13*, 461, doi:10.3390/biom13030461 . . . . . **144**

biomolecules

MDPI

Editorial

Versatility of Glutathione Transferase Proteins

Bengt Mannervik [1,2]

[1] Department of Biochemistry and Biophysics, Arrhenius Laboratories, Stockholm University, SE-10691 Stockholm, Sweden; bengt.mannervik@dbb.su.se
[2] Department of Chemistry, Scripps Research, La Jolla, CA 92037, USA

For more than 60 years, glutathione transferases (GSTs) have attracted attention, but the research field of the GSTome [1] has not yet matured. Originally discovered in the research on cellular protection against carcinogens and mutagens [2], GSTs were, by contrast, in cancer cells found to protect tumors against anti-cancer drugs. The biotransformation of other drugs was also established, in many cases following metabolic activation by cytochrome P450 enzymes. It was further concluded that a crucial GST function was the inactivation of genotoxic electrophiles such as unsaturated aldehydes formed in endogenous processes [3]. The engineering of GSTs for biotechnical applications followed suit [4]. Since then, new aspects have emerged every few years, and a full understanding of the scope of the GST proteins is not yet in sight.

The human genome encodes 17 GST proteins in seven classes, which are expressed as the "canonical" or cytosolic GST enzymes. In addition, homologous sequences forming chloride channels [5] or having other functions are known. Oakley has extended the gene family to 39 members [6] by mining databases for sequences and protein structures by use of artificial intelligence algorithms; in particular, AlphaFold [7] and AlphaFold-Multimer [8]. With the exception of prostaglandin E synthase 2 and the previously characterized GSTs, the new homologous proteins were not recognized as enzymes but were associated with other molecular activities. Oakley's analysis also predicted that the dimeric canonical GST enzymes could form heterodimers, including subunits from different classes. However, the natural occurrence of inter-class hybrids is so far lacking experimental evidence, even though the existence of intra-class heterodimers is well-documented [9].

The review by Mazari et al. [10] addresses the role of GSTs related to diseases, with particular emphasis on cancer. In addition to protection against toxicants and a role in drug resistance [11], the interactions with other proteins and their functions in cellular signaling is indicated. The glutathionylation of SH groups in proteins is considered a posttranslational modification of biochemical significance. Townsend and Tew have forwarded GST P1-1 as a catalyst of this thiol–disulfide interchange. Recent findings reporting increased severity of SARS-CoV-2 (COVID-19) infections in GST-null individuals, lacking the *GSTM1* or *GSTT1* genes, are also reviewed.

A search for GST P1-1 inhibitors for possible use in overcoming anti-cancer drug resistance was published by Kupreienko et al. [12]. The crystal structure of *Mus musculus* GST P1-1 was solved, and a library of registered pesticides was screened for possible repurposing as inhibitors of the enzyme. The most potent compound found was the fungicide iprodione, which was observed intercalated between the active-site residues Phe8 and Tyr108 (with the authors' numbering omitting the initiator Met1). Iprodione shows minimal toxicity to mammals and may therefore serve as a lead in the search for more potent inhibitors.

Russell and Richardson review the role of GSTs in nitric oxide (NO) metabolism [13]. The enzymes contribute to the release of the pharmacologically active NO from various drugs including the classical angina medicine nitroglycerin [14]. These drugs have applications as anti-cancer agents and as vasodilators for clinical use [15]. The GST proteins

Citation: Mannervik, B. Versatility of Glutathione Transferase Proteins. *Biomolecules* **2023**, *13*, 1749. https://doi.org/10.3390/biom13121749

Received: 25 November 2023
Revised: 3 December 2023
Accepted: 4 December 2023
Published: 6 December 2023

can also serve in the cellular storage of NO in the form of a stable dinitrosyl–iron complex with glutathione [16].

Scian et al. [17] propose that GST A4-4 plays a role as an enzyme regulating the cellular steady-state levels of lipid alkenals such as 4-hydroxynonenal. These products of lipid peroxidation have an important function as intracellular "second messengers" that contribute to homeostasis by managing the Nrf2-mediated phase-2 response involving the expression of anti-oxidant enzymes. High concentrations of the alkenals are cytotoxic and are counteracted by glutathione conjugation, followed by the exporting of the conjugate from the cell [18]. The conjugation reaction is reversible, and the backward direction safeguards an adequate fraction of unconjugated alkenal for regulatory functions. GST A4-4 efficiently catalyzes both forward and backward reactions and thereby makes sure that the alkenals are not completely eliminated by unidirectional detoxication.

Aldehydes and other low-molecular-mass molecules are among the odorous compounds that bind to GSTs and react with glutathione if they carry suitable functional groups. Schwartz et al. [19] are summarizing the evidence indicating that GSTs present in the olfactory tissues provide protection against toxic compounds. In addition, the enzymes appear to play a pivotal role in chemoperception by rapidly degrading bound odorants, thereby terminating the signal and preparing the receptors for new inputs [20]. GSTs occur abundantly in mammals as well as in insects, and in the various species investigated, the enzymes appear to play similar roles in their olfactory systems. In mammals, alpha-, mu-, and pi-class GSTs are implicated, whereas in insects, delta- and epsilon-class members are engaged. Notably, the former mammalian GST classes do not occur in insects [21], and the latter insect GST classes are absent in mammals. Thus, the development of GST functions in chemosensory perception seems to be an example of convergent evolution, which is enabled by the versatility of the GST protein fold.

A novel class of canonical GSTs was discovered in cyanobacteria by Wiktelius and Stenberg and was named chi [22]. The photosynthesis carried out by cyanobacteria caused the Earth's atmosphere to change from an anaerobic reducing state to an oxygen-containing environment >2 billion years ago. The novel oxidizing conditions necessitated the emergence of protective agents such as glutathione, and it is a reasonable assumption that the evolution of GST was first established in cyanobacteria [22]. Mocchetti et al. [23] have solved the crystal structure of the chi-class GST from the cyanobacterium *Synechocystis*, and furthermore, they have compared it with primary structures from other species. The chi-class proteins featured a well-conserved Ser-Arg-Ala-Ser amino acid motif in the active site of the N-terminal region, but a Ser residue appeared to be non-essential for catalytic activity, as indicated by mutagenesis of the *Synechocystis* GST. By contrast, Ser in a similar position of GSTs from other classes plays a role in stabilizing the thiolate form of glutathione in the catalyzed reaction. In the chi-class, the Ser sidechain interacts instead with the protein backbone. Overall, the *Synechocystis* structure was similar to the known canonical GSTs of different classes, although the length of its α4 and α5 helices in the core of the protein was diminished as a consequence of a shorter primary structure. A phylogenetic analysis identified several hundred homologs to the *Synechocystis* GST, of which 147 featured the characteristic Ser-Arg-Ala-Ser sequence.

A physiological role of GST A3-3 in steroid hormone biosynthesis in humans and a few other mammals has been identified, which involves the double-bond isomerization of 5-androsten-3,17-dione and 5-pregnen-3,20-dione, precursors of testosterone, estradiol, and progesterone [24]. Although man and horse feature the enzyme GST A3-3 with prominent ketosteroid isomerase activity, cow, rat, and mouse do not have a GST with a corresponding high isomerase activity. Hubert et al. have cloned mammalian GSTs homologous to GST A3-3 from a broader phylogenetic range [25] in order to further explore the occurrence of the high-steroid isomerase activity in the GSTome.

In insects, a high-ketosteroid isomerase activity contributed by an epsilon-class GST was furthermore discovered in the malaria-transmitting mosquito *Anopheles gambiae* [26]. The catalytic efficiency ($k_{cat}/K_m = 6.9 \times 10^6\ M^{-1}s^{-1}$) of the mosquito GSTE8 matches

that of the most active mammalian GST A3-3. A corresponding GSTE14 in *Drosophila melanogaster* had previously been identified as one of several enzymes essential to the biosynthesis of the insect steroid hormone ecdysone [27,28]. The fruit fly mutant deficient in the enzyme was named *noppera-bo* and the GST was consequently called Noppera-bo (or Nobo). The mutant insect is not viable, since ecdysone is required for metamorphosis, including hatching, molting, pupation, and eclosion. The cognate substrate of GSTE8/Nobo is unknown, but the prominent activity discovered with 5-androsten-3,17-dione, a steroid not found in insects, suggests that a similar ketosteroid related to ecdysone may be the natural counterpart.

Nobo has been identified in the orders *Diptera* and *Lepidoptera* but is absent in other insects. Thus, the enzyme has been recognized as an ideal target in combatting insects carrying infectious diseases. Selective inhibitors of Nobo would serve as insect growth regulators that would not jeopardize bees and other insects of agricultural importance, which do not express Nobo. Ebihara and Niwa [29] have directed particular attention to inhibitors of Nobo from the yellow-fever vector *Aedes aegypti* and identified flavonoids with high potency. The strongest inhibitor (IC_{50} = 0.287 μM) was desmethylglycitein, and the insecticidal activity was verified experimentally with larvae from *A. aegypti* [30].

The Special Issue on the "Versatility of Glutathione Transferase Proteins" exemplifies various aspects of GST research ranging from human genes and disease to metabolism and insects. The cyanobacterial GSTs point to a vast field of unchartered enzymology in the realm of prokaryotes. Not represented here is the research on plant GSTs and membrane-associated GSTs.

Funding: The author's research has, over the last decades, been funded by the Swedish Research Council, the Swedish Cancer Society, and the Swedish Childhood Cancer Fund.

Conflicts of Interest: The author declares no conflict of interest.

References

1. Mannervik, B. Five Decades with Glutathione and the GSTome. *J. Biol. Chem.* **2012**, *287*, 6072–6083. [CrossRef] [PubMed]
2. Boyland, E.; Chasseaud, L.F. The Role of Glutathione and Glutathione S-Transferases in Mercapturic Acid Biosynthesis. *Adv. Enzymol. Relat. Areas Mol. Biol.* **1969**, *32*, 173–219. [CrossRef] [PubMed]
3. Berhane, K.; Mannervik, B. Inactivation of the Genotoxic Aldehyde Acrolein by Human Glutathione Transferases of Classes Alpha, Mu, and Pi. *Mol. Pharmacol.* **1990**, *37*, 251–254.
4. Perperopoulou, F.; Pouliou, F.; Labrou, N.E. Recent Advances in Protein Engineering and Biotechnological Applications of Glutathione Transferases. *Crit. Rev. Biotechnol.* **2018**, *38*, 511–528. [CrossRef] [PubMed]
5. Cromer, B.A.; Morton, C.J.; Board, P.G.; Parker, M.W. From Glutathione Transferase to Pore in a CLIC. *Eur. Biophys. J.* **2002**, *31*, 356–364. [CrossRef] [PubMed]
6. Oakley, A. Hidden Glutathione Transferases in the Human Genome. *Biomolecules* **2023**, *13*, 1240. [CrossRef]
7. Jumper, J.; Evans, R.; Pritzel, A.; Green, T.; Figurnov, M.; Ronneberger, O.; Tunyasuvunakool, K.; Bates, R.; Žídek, A.; Potapenko, A.; et al. Highly Accurate Protein Structure Prediction with AlphaFold. *Nature* **2021**, *596*, 583–589. [CrossRef]
8. Evans, R.; O'Neill, M.; Pritzel, A.; Antropova, N.; Senior, A.; Green, T.; Žídek, A.; Bates, R.; Blackwell, S.; Yim, J.; et al. Protein Complex Prediction with AlphaFold-Multimer. *bioRxiv* **2022**. [CrossRef]
9. Mannervik, B.; Morgenstern, R. *Comprehensive Toxicology*, 4th ed.; Elsevier: New York, NY, USA, 2024; Chapter 10.16.
10. Mazari, A.; Zhang, L.; Ye, Z.; Zhang, J.; Tew, K.; Townsend, D. The Multifaceted Role of Glutathione S-Transferases in Health and Disease. *Biomolecules* **2023**, *13*, 688. [CrossRef]
11. Tew, K.D. Glutathione-Associated Enzymes in Anticancer Drug Resistance. *Cancer Res.* **1994**, *54*, 4313–4320. [CrossRef]
12. Kupreienko, O.; Pouliou, F.; Konstandinidis, K.; Axarli, I.; Douni, E.; Papageorgiou, A.; Labrou, N. Inhibition Analysis and High-Resolution Crystal Structure of Mus musculus Glutathione Transferase P1-1. *Biomolecules* **2023**, *13*, 613. [CrossRef] [PubMed]
13. Russell, T.; Richardson, D. Glutathione-S-Transferases as Potential Targets for Modulation of Nitric Oxide-Mediated Vasodilation. *Biomolecules* **2022**, *12*, 1292. [CrossRef] [PubMed]
14. Tsuchida, S.; Maki, T.; Sato, K. Purification and Characterization of Glutathione Transferases with an Activity toward Nitroglycerin from Human Aorta and Heart. Multiplicity of the Human Class Mu Forms. *J. Biol. Chem.* **1990**, *265*, 7150–7157. [CrossRef] [PubMed]
15. Andrabi, S.M.; Sharma, N.S.; Karan, A.; Shahriar, S.M.S.; Cordon, B.; Ma, B.; Xie, J. Nitric Oxide: Physiological Functions, Delivery, and Biomedical Applications. *Adv. Sci.* **2023**, *10*, e2303259. [CrossRef] [PubMed]

16. De Maria, F.; Pedersen, J.Z.; Caccuri, A.M.; Antonini, G.; Turella, P.; Stella, L.; Bello, M.L.; Federici, G.; Ricci, G. The Specific Interaction of Dinitrosyl-Diglutathionyl-Iron Complex, a Natural NO Carrier, with the Glutathione Transferase Superfamily: Suggestion for an Evolutionary Pressure in the Direction of the Storage of Nitric Oxide. *J. Biol. Chem.* **2003**, *278*, 42283–42293. [CrossRef] [PubMed]
17. Scian, M.; Paço, L.; Murphree, T.; Shireman, L.; Atkins, W. Reversibility and Low Commitment to Forward Catalysis in the Conjugation of Lipid Alkenals by Glutathione Transferase A4-4. *Biomolecules* **2023**, *13*, 329. [CrossRef] [PubMed]
18. Awasthi, Y.C.; Ramana, K.V.; Chaudhary, P.; Srivastava, S.K.; Awasthi, S. Regulatory Roles of Glutathione-S-Transferases and 4-Hydroxynonenal in Stress-Mediated Signaling and Toxicity. *Free Radic. Biol. Med.* **2017**, *111*, 235–243. [CrossRef] [PubMed]
19. Schwartz, M.; Boichot, V.; Fraichard, S.; Muradova, M.; Senet, P.; Nicolai, A.; Lirussi, F.; Bas, M.; Canon, F.; Heydel, J.; et al. Role of Insect and Mammal Glutathione Transferases in Chemoperception. *Biomolecules* **2023**, *13*, 322. [CrossRef]
20. Ben-Arie, N.; Khen, M.; Lancet, D. Glutathione S-Transferases in Rat Olfactory Epithelium: Purification, Molecular Properties and Odorant Biotransformation. *Biochem. J.* **1993**, *292*, 379–384. [CrossRef]
21. Koirala, B.K.S.; Moural, T.; Zhu, F. Functional and Structural Diversity of Insect Glutathione S-Transferases in Xenobiotic Adaptation. *Int. J. Biol. Sci.* **2022**, *18*, 5713–5723. [CrossRef]
22. Wiktelius, E.; Stenberg, G. Novel Class of Glutathione Transferases from Cyanobacteria Exhibit High Catalytic Activities Towards Naturally Occurring Isothiocyanates. *Biochem. J.* **2007**, *406*, 115–123. [CrossRef]
23. Mocchetti, E.; Morette, L.; Mulliert, G.; Mathiot, S.; Guillot, B.; Dehez, F.; Chauvat, F.; Cassier-Chauvat, C.; Brochier-Armanet, C.; Didierjean, C.; et al. Biochemical and Structural Characterization of Chi-Class Glutathione Transferases: A Snapshot on the Glutathione Transferase Encoded by sll0067 Gene in the Cyanobacterium Synechocystis sp. Strain PCC 6803. *Biomolecules* **2022**, *12*, 1466. [CrossRef] [PubMed]
24. Mannervik, B.; Ismail, A.; Lindström, H.; Sjödin, B.; Ing, N.H. Glutathione Transferases as Efficient Ketosteroid Isomerases. *Front. Mol. Biosci.* **2021**, *8*, 765970. [CrossRef]
25. Hubert, S.; Samollow, P.; Lindström, H.; Mannervik, B.; Ing, N. Conservation of Glutathione Transferase mRNA and Protein Sequences Similar to Human and Horse Alpha Class GST A3-3 across Dog, Goat, and Opossum Species. *Biomolecules* **2023**, *13*, 1420. [CrossRef]
26. Musdal, Y.; Ismail, A.; Sjödin, B.; Mannervik, B. Potent GST Ketosteroid Isomerase Activity Relevant to Ecdysteroidogenesis in the Malaria Vector Anopheles gambiae. *Biomolecules* **2023**, *13*, 976. [CrossRef] [PubMed]
27. Chanut-Delalande, H.; Hashimoto, Y.; Pelissier-Monier, A.; Spokony, R.; Dib, A.; Kondo, T.; Bohère, J.; Niimi, K.; Latapie, Y.; Inagaki, S.; et al. Pri Peptides Are Mediators of Ecdysone for the Temporal Control of Development. *Nat. Cell Biol.* **2014**, *16*, 1035–1044. [CrossRef] [PubMed]
28. Enya, S.; Ameku, T.; Igarashi, F.; Iga, M.; Kataoka, H.; Shinoda, T.; Niwa, R. A Halloween Gene Noppera-Bo Encodes a Glutathione S-Transferase Essential for Ecdysteroid Biosynthesis via Regulating the Behaviour of Cholesterol in Drosophila. *Sci. Rep.* **2014**, *4*, 6586. [CrossRef]
29. Ebihara, K.; Niwa, R. Compounds Inhibiting Noppera-bo, a Glutathione S-transferase Involved in Insect Ecdysteroid Biosynthesis: Novel Insect Growth Regulators. *Biomolecules* **2023**, *13*, 461. [CrossRef]
30. Inaba, K.; Ebihara, K.; Senda, M.; Yoshino, R.; Sakuma, C.; Koiwai, K.; Takaya, D.; Watanabe, C.; Watanabe, A.; Kawashima, Y.; et al. Molecular Action of Larvicidal Flavonoids on Ecdysteroidogenic Glutathione S-Transferase Noppera-Bo in Aedes aegypti. *BMC Biol.* **2022**, *20*, 43. [CrossRef]

biomolecules

MDPI

Article

Hidden Glutathione Transferases in the Human Genome

Aaron J. Oakley

School of Chemistry and Molecular Bioscience, Faculty of Science, Medicine and Health, University of Wollongong, Wollongong, NSW 2522, Australia; aarono@uow.edu.au; Tel.: +61-2-4221-4347

Abstract: With the development of accurate protein structure prediction algorithms, artificial intelligence (AI) has emerged as a powerful tool in the field of structural biology. AI-based algorithms have been used to analyze large amounts of protein sequence data including the human proteome, complementing experimental structure data found in resources such as the Protein Data Bank. The EBI AlphaFold Protein Structure Database (for example) contains over 230 million structures. In this study, these data have been analyzed to find all human proteins containing (or predicted to contain) the cytosolic glutathione transferase (cGST) fold. A total of 39 proteins were found, including the alpha-, mu-, pi-, sigma-, zeta- and omega-class GSTs, intracellular chloride channels, metaxins, multisynthetase complex components, elongation factor 1 complex components and others. Three broad themes emerge: cGST domains as enzymes, as chloride ion channels and as protein–protein interaction mediators. As the majority of cGSTs are dimers, the AI-based structure prediction algorithm AlphaFold-multimer was used to predict structures of all pairwise combinations of these cGST domains. Potential homo- and heterodimers are described. Experimental biochemical and structure data is used to highlight the strengths and limitations of AI-predicted structures.

Keywords: glutathione transferase; intracellular chloride channel; metaxin; failed axon connections homolog; ganglioside-induced differentiation-associated protein; glutathione S-transferase C-terminal domain-containing protein; multi-tRNA synthetase complex; eukaryotic elongation factor 1; structure prediction

Citation: Oakley, A.J. Hidden Glutathione Transferases in the Human Genome. *Biomolecules* **2023**, *13*, 1240. https://doi.org/10.3390/biom13081240

Academic Editor: Bengt Mannervik

Received: 20 June 2023
Revised: 8 August 2023
Accepted: 8 August 2023
Published: 12 August 2023

1. Introduction

Since glutathione transferase (GST) activity was discovered in rat liver and was postulated to play a role in drug detoxification [1], decades of research has led to the identification and isolation of multiple classes of GST from bacteria to man with a considerable array of catalytic and binding activities. In 1991, the first glutathione transferase structure was determined [2,3], the pi-class isozyme from pig in complex with glutathione-sulfonic acid (PDB ID 2GSR). Several features of that structure are now known to be typical of the cytosolic GSTs (cGSTs): it is a dimer, and each monomer contains an N-terminal domain (NDT) (having the thioredoxin-like βαβαββα topology) and a unique C-terminal domain (CTD) composed of α-helixes. Many crystal structures of cGSTs have revealed the binding location of glutathione (GSH) in the N-terminal domain (the "G-site") and the adjacent binding site for (often hydrophobic) co-substrates (the "H-site"). While hundreds of GST structures have been reported in organisms ranging from bacteria to man, the set of human proteins known to adopt the cGST fold can be regarded as incomplete. However, recent advances in protein structure prediction provide the tools to discover and analyze these "hidden" GSTs. Not considered here are the microsomal GSTs, which are trimeric, integral membrane proteins, and the mitochondrial kappa-class GST that form a distinct family of thioredoxin-fold-containing proteins [4].

With the availability of deep learning algorithms such as AlphaFold [5] and RoseTTAfold [6], we now have tools to make reliable predictions of protein structures. Briefly, these artificial intelligence (AI) systems use a neural network to extract the relationship between a protein's sequence and its 3D structure based on existing experimental data. Employed for the bulk of this

study is AlphaFold, which uses a three-stage process to predict protein structures. In the first stage, a multiple sequence alignment (MSA) is generated for the target protein(s). In the second stage, the "evoformer block", consisting of a series of interconnected layers, processes the input amino acid sequence using an "attention mechanism" that captures evolutionary information from related protein sequences. This mechanism allows the network to selectively focus on different parts of the sequence based on their importance for predicting the protein's structure. Information from the evoformer feeds into the third stage, the "structure module", which creates an explicit 3D structure. In a typical prediction run, the information from the structure prediction module is recycled three times through the evoformer and structure modules. Along with 3D models, AlphaFold provides a per-residue confidence metric called predicted local distance difference test (pLDDT) on the interval [0, 1]. A higher pLDDT implies higher confidence. In predicted structures, well-structured regions typically have high pLDDT scores. Loops and regions near termini (often missing in crystal structures) tend to have low pLDDT scores.

As of this writing, the EBI AlphaFold database contains over 230 million predictions of 3D protein structures from hundreds of organisms including humans. In this study, a structure-based search of this database was used to reveal all human proteins predicted to contain the cGST fold. A limitation of this database is that it contains only monomeric structures. Since many classes of GST-domain-containing proteins form dimers, I used AlphaFold-multimer [7] to predict complexes of all pairwise combinations of human GST-domain-containing proteins to reproduce known and predict new homo- and heterodimer structures. The quality of the predictions were assessed using metrics that AlphaFold generates for its models and using published structural and biochemical data. Insights gained include possible functions of poorly understood proteins and proposals for new protein–protein interactions involving cGST-containing domains.

2. Materials and Methods

Crystal structures of human proteins containing the cytosolic GST fold were obtained from the Protein Data Bank (PDB) and were used in DALI [8] searches through the set of human protein structures in the European Bioinformatics Institute AlphaFold database (EBI, Cambridge, UK). Redundant structures were removed.

Using amino acid sequences corresponding to the cGST domains in the proteins identified above, AlphaFold-multimer (ColabFold distribution, version 1.5.0; [9]) was used to predict the structures of all pairwise domain combinations. Within ColabFold, the "alphafold2_multimer_v3" model was used, which uses weights derived from training on PDB structures deposited up to September 30, 2021. For each prediction, five models were generated, and the top-ranked prediction was selected for further analysis. Assessment of model quality was based on AlphaFold's intrinsic model accuracy estimate: predicted template modeling-score (pTM). AlphaFold-multimer gives a modified score for interactions between residues of different chains: interface pTM (ipTM). To assess the quality of predictions, model confidence (MC) was calculated "$= 0.8 \times \text{ipTM} + 0.2 \times \text{pTM}$" [7].

ChimeraX [10] was used for structure alignment and figure production. Clustal Omega [11] was used to generate a phylogram based on the GST-domain sequences.

3. Results

Searches of the EBI AlphaFold database revealed a total of 39 human proteins predicted to contain the cGST fold (Table 1) that will be briefly described here. The domain organization of all hits are shown in Figure 1. The structures of the domains colored by pLDDT value are shown in Figure S1 and a phylogram based on the sequences is shown in Figure S2.

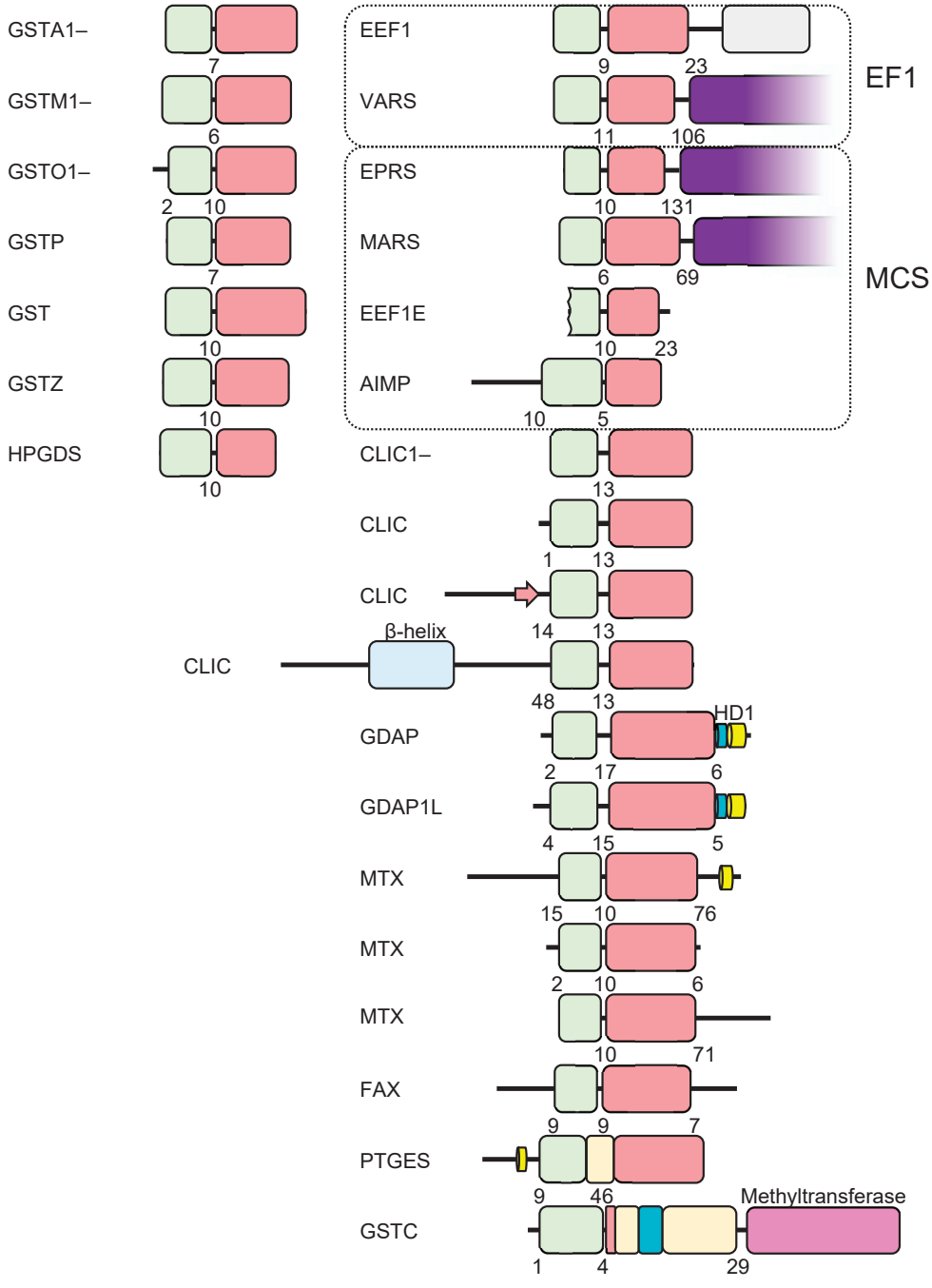

Figure 1. Domain organization of cGSTs in the human genome. The thioredoxin and C-terminal domains are indicated in pale green and pink, respectively. Numbers indicate the length of sequence before, between and after the NTDs and CTDs. Putative trans-membrane helices are indicated in yellow. tRNA synthetase domains are indicated in purple. Additional structure elements are described in the text.

Slightly less than half of the proteins identified fall into previously identified classes of GST, including the alpha, mu, pi, theta, zeta and omega classes (18 proteins). The alpha-, mu- and pi-class GSTs are common in mammalian genomes and are well known for their role in phase II detoxification. They form a distinct clade in the phylogram (Figure S2). Most characterized reactions involve GSH-conjugating activity with electrophiles. Some GSTs have additional roles. For example, the human pi-class GST modulates the activities of the mitogen-activated protein kinase (MAPK) signaling pathway via direct interactions with apoptosis signal-regulating kinase (ASK1) [12] and c-Jun N-terminal kinase 1 (JNK1) [13].

The hematopoietic prostaglandin D synthase (HPGDS), also known as sigma-class GST (GSTS1), was identified. HPGDS catalyzes the GSH-dependent conversion of prostaglandin H_2 (PGH_2) to prostaglandin D_2 (PGD_2) [14].

Prostaglandin E Synthase 2 (PTGES2), also known as microsomal prostaglandin E synthase type 2, was found. It catalyzes conversion of PGH_2 to prostaglandin E_2 (PGE_2) [15]. In addition to cGST-like motifs, this protein contains an insertion between the N- and C-terminal domains that results in an unusual dimerization interaction.

Three proteins classified as metaxins (MTX1, MTX2 and MTX3), which are associated with mitochondrial import and trafficking [16], were found.

Six intracellular chloride channels (CLIC1 to CLIC6) were identified. The CLICs pose an interesting challenge for structure prediction algorithms. While most experimental CLIC protein structures are characterized by the cGST fold, CLICs have both soluble and integral membrane forms [17]. Furthermore, CLIC1 has been shown to adopt two distinct soluble conformations [18].

Several hits correspond to protein domains involved in the organization of tRNA synthetase. These include eukaryotic translation elongation factor 1 epsilon 1 (EEF1E1), Aminoacyl tRNA synthetase complex interacting multifunctional protein 2 (AIMP2), Glutamyl-prolyl-tRNA synthetase 1 (EPRS1) and Methionyl-tRNA synthetase 1 (MARS1), which are components of the multi-tRNA synthetase complex (MSC) [19]. Eukaryotic translation elongation factor 1 gamma (EEF1G) and Valyl-tRNA synthetase 1 (VARS1) are components of the eukaryotic elongation factor 1 (eEF1) complex [20].

The remaining hits are relatively poorly characterized proteins: ganglioside-induced differentiation-associated protein 1 (GADP1), ganglioside-induced differentiation-associated protein-1-like 1 (GADP1L1), failed axon connections homolog (FAXC) and glutathione S-transferase C-terminal domain-containing protein (GSTCD).

Table 1. Glutathione-transferase-fold-containing proteins in the human genome.

Gene [1]	Location	Name	Comment [2]
GSTA1	6p12.2	Glutathione S-transferase alpha 1	Substrates: Δ^5AD, BCDE, BPDE, Busulfan, Chlorambucil, DBADE, DBPDE, BPhDE, *N*-a-PhIP
GSTA2	6p12.2	Glutathione S-transferase alpha 2	CuOOH, DBPDE, 7-chloro-4-nitrobenz-2-oxa-1,3-diazole
GSTA3	6p12.2	Glutathione S-transferase alpha 3	Substrates: Δ^5AD, Δ^5-pregnene-3,20-dione, DBPDE
GSTA4	6p12.2	Glutathione S-transferase alpha 4	Substrates: COMC-6, EA, 4-hydroxynonenal, 4-hydroxydecenal
GSTA5	6p12.2	Glutathione S-transferase alpha 5	Uncharacterized
GSTM1	1p13.3	Glutathione S-transferase mu 1	Substrates: *trans*-4-phenyl-3-buten-2-one, BPDE, CDE, DBADE, *trans*-stilbene oxide, styrene-7,8-oxide
GSTM2	1p13.3	Glutathione S-transferase mu 2	Substrates: COMC-6, 1,2-dichloro-4-nitrobenzene, aminochrome, dopa *O*-quinone, $PGH_2 \rightarrow PGE_2$
GSTM3	1p13.3	Glutathione S-transferase mu 3	Substrates: BCNU, $PGH_2 \rightarrow PGE_2$
GSTM4	1p13.3	Glutathione S-transferase mu 4	CDNB
GSTM5	1p13.3	Glutathione S-transferase mu 5	Uncharacterized

Table 1. *Cont.*

Gene [1]	Location	Name	Comment [2]
GSTO1	10q25.1	Glutathione S-transferase omega 1	Substrates: MMA, dehydroascorbate, S-(4-nitrophenacyl)glutathione
GSTO2	10q25.1	Glutathione S-transferase omega 2	Glutaredoxin-like activities
GSTP1	11q13.2	Glutathione S-transferase pi 1	Substrates: CDNB, acrolein, base propenals, BPDE, CDE, Chlorambucil, COMC-6, EA, Thiotepa
GSTT1	22q11.23	Glutathione S-transferase theta 1	A pseudogene in the reference genome. Protein coding in some individuals. Substrates: BCNU, butadiene epoxide, CH_2Cl_2, EPNP, ethylene oxide
GSTT2	22q11.23	Glutathione S-transferase theta 2	CuOOH, 1-menaphthyl sulfate
GSTT2B	22q11.23	Glutathione S-transferase theta 2B	A pseudogene in some individuals. Substrates: CuOOH, 1-menaphthyl sulfate
GSTT4	22q11.23	Glutathione S-transferase theta 4	Uncharacterized
GSTZ1	14q24.3	Maleylacetoacetate isomerase	Substrates: dichloroacetate, fluoroacetate, 2-chloropropionate, malelyacetoacetate
HPGDS	4q22.3	Hematopoietic prostaglandin D synthase	$PGH_2 \rightarrow PGD_2$
PTGES2	9q34.11	Prostaglandin E synthase 2	$PGH_2 \rightarrow PGE_2$
GDAP1	8q21.11	Ganglioside-induced differentiation-associated protein 1	Mitochondrial transport
GDAP1L1	20q13.12	Ganglioside-induced differentiation-associated protein-1-like 1	Mitochondrial transport
CLIC1	6p21.33	Chloride intracellular channel 1	Intracellular chloride ion channel
CLIC2	Xq28	Chloride intracellular channel 2	Intracellular chloride ion channel
CLIC3	9q34.3	Chloride intracellular channel 3	Intracellular chloride ion channel
CLIC4	1p36.11	Chloride intracellular channel 4	Intracellular chloride ion channel
CLIC5	6p21.1	Chloride intracellular channel 5	Intracellular chloride ion channel
CLIC6	21q22.12	Chloride intracellular channel 6	Intracellular chloride ion channel
MTX1	1q22	Metaxin 1	Mitochondrial outer membrane component
MTX2	2q31.1	Metaxin 2	Mitochondrial outer membrane component
MTX3	5q14.1	Metaxin 3	Mitochondrial outer membrane component
FAXC	6q16.2	Failed axon connections homolog	
GSTCD	4q24	Glutathione *S*-transferase C-terminal domain-containing protein	Probable methyltransferase
EEF1E1	6p24.3	Eukaryotic translation elongation factor 1 epsilon 1	MSC component
AIMP2	7p22.1	Aminoacyl tRNA synthetase complex interacting multifunctional protein 2	MSC component
EPRS1	1q41	Glutamyl-prolyl-tRNA synthetase 1	MSC component
MARS1	12q13.3	Methionyl-tRNA synthetase 1	MSC component
EEF1G	11q12.3	Eukaryotic translation elongation factor 1 gamma	eEF1 component
VARS1	6p21.33	Valyl-tRNA synthetase 1	eEF1 component

[1] HUGO Gene Nomenclature Committee recommended names used. [2] Abbreviations: Δ^5AD, Δ^5-androstene-3,17-dione; BCDE, benzo[*g*]chrysene diol epoxide; BCNU, 1,3-bis(2-chloroethyl)-1-nitrosourea; BPDE, benzo[*a*]pyrene diol epoxide; BPhDE, benzo[*c*]phenanthrene diol epoxide; CDE, chrysene1,2-diol 3,4-epoxide; CDNB, 1-chloro-2,4-dinitrobenzene; COMC-6, crotonyloxymethyl-2-cyclohexenone; DBADE, dibenz[*a*,*h*]anthracene diol epoxide; DBPDE, dibenzo[*a*,*l*]pyrene diol epoxide; EA, ethacrynic acid; EPNP, 1,2-epoxy-3-(*p*-nitrophenoxy)propane; *N*-a-PhIP, *N*-acetoxy-2-amino-1-methyl-6-phenylimidazo[4,5-*b*]pyridine; MMA, mono-methylarsonic acid; MSC, Multi-tRNA synthetase complex. Substrate data from [21] and elsewhere.

RMSD-based comparisons show that the predicted GST structures are very similar to high-resolution crystal structures of human wild-type proteins (where they are available) (Table 2). In general, the greatest deviations occur in surface loops or near the termini. In general, these regions are poorly ordered in crystal structures and show lower pLDDT scores in predictions (Figure S1). Specific cases will be detailed below.

Table 2. Comparison of predicted structures of human cGST-domain-containing proteins with crystal structures.

Protein	PDB ID	Resolution (Å)	RMSD (Å) [1]	RMSD (Å) [1]
GSTA1	1K3Y	1.3	0.353 (220)	0.490 (221)
GSTA2	2VCT	2.1	0.431 (220)	0.459 (221)
GSTA3	2VCV	1.8	0.414 (219)	0.414 (219)
GSTA4	3IK7	1.97	0.425 (218)	0.550 (220)
GSTM1	7BEU	1.59	0.484 (215)	0.551 (218)
GSTM2 [2]	2C4J	1.35	0.356 (214)	0.438 (217)
GSTM3	3GTU	2.8	0.533 (210)	1.682 (224)
GSTM4	4GTU	3.3	0.586 (216)	0.611 (217)
GSTO1	5YVN	1.33	0.540 (229)	1.082 (238)
GSTO2 [3]	3Q18	1.70	0.374 (235)	0.412 (236)
GSTP1	5J41	1.19	0.251 (208)	0.251 (208)
GSTT1	2C3N	1.5	0.393 (239)	0.393 (239)
GSTT2	4MPF	2.10	0.302 (243)	0.385 (244)
GSTT2B	4MPC	1.95	0.189 (243)	0.189 (243)
GSTZ1	1FW1	1.90	0.301 (207)	0.334 (208)
HPGDS	7JR8	1.13	0.536 (196)	0.609 (199)
PTGES2 [4]	1Z9H	2.60	0.490 (266)	0.794 (274)
GDAP1	7AIA	2.2	0.721 (206)	7.511 (259)
CLIC1	1K0M	1.4	0.559 (220)	2.180 (236)
	1RK4 [5]	1.79	0.569 (165)	7.472 (213)
CLIC2	2R4V	1.85	0.573 (211)	1.962 (226)
CLIC3	3KJY	1.95	0.488 (211)	0.948 (217)
CLIC4	2D2Z	2.20	0.521 (221)	0.828 (229)
CLIC5	6Y2H	2.15	0.518 (210)	1.291 (223)
EEF1E1	2UZ8	2.00	0.677 (154)	1.747 (164)
EEF1G	5JPO	2.00	0.322 (214)	0.322 (214)
AIMP2	5A5H	2.32	0.473 (187)	1.914 (209)
EPRS1 [6]	5A1N	2.1	0.612 (166)	0.737 (167)
MARS1	4BVX	1.60	0.652 (197)	0.829 (203)

[1] RMSD values calculated in ChimeraX. The number of Cα atoms used for comparison is provided in parentheses. The first column gives the pruned set of residues that provide the best fit. The second provides RMSD over all matching residues. [2] T210S mutant. [3] C80S, C121S, C136S, C140S, C170S, C214S mutant. [4] From *Macaca fascicularis*. [5] Oxidized form. [6] S156D mutant.

3.1. Prediction of GST Homo- and HeteroDimers

AlphFold predicted homodimers of all human alpha-, mu-, pi-, theta- and omega-class GSTs and HPGDS are consistent with crystallographic results obtained to date. For example, the homodimers GSTA1-1, GSTM1-1 and GSTP1-1 superimpose with RMSD values of 0.64 Å (over 422 Cα atoms), 0.58 Å (over 434 Cα atoms) and 0.35 Å (416 Cα atoms), respectively (Figure 2a–c). Of note is PTGES2, which has an unusual mode of dimerization thanks to a 46-residue insertion between the N- and C-terminal domains (Figure 1). Nevertheless, AlphaFold predicted the structure of this insertion and the dimerization interaction correctly (RMSD 1.92 Å over 548 Cα atoms) (Figure 2d). These RMSD values are similar to those obtained when comparing crystal structures of the same proteins.

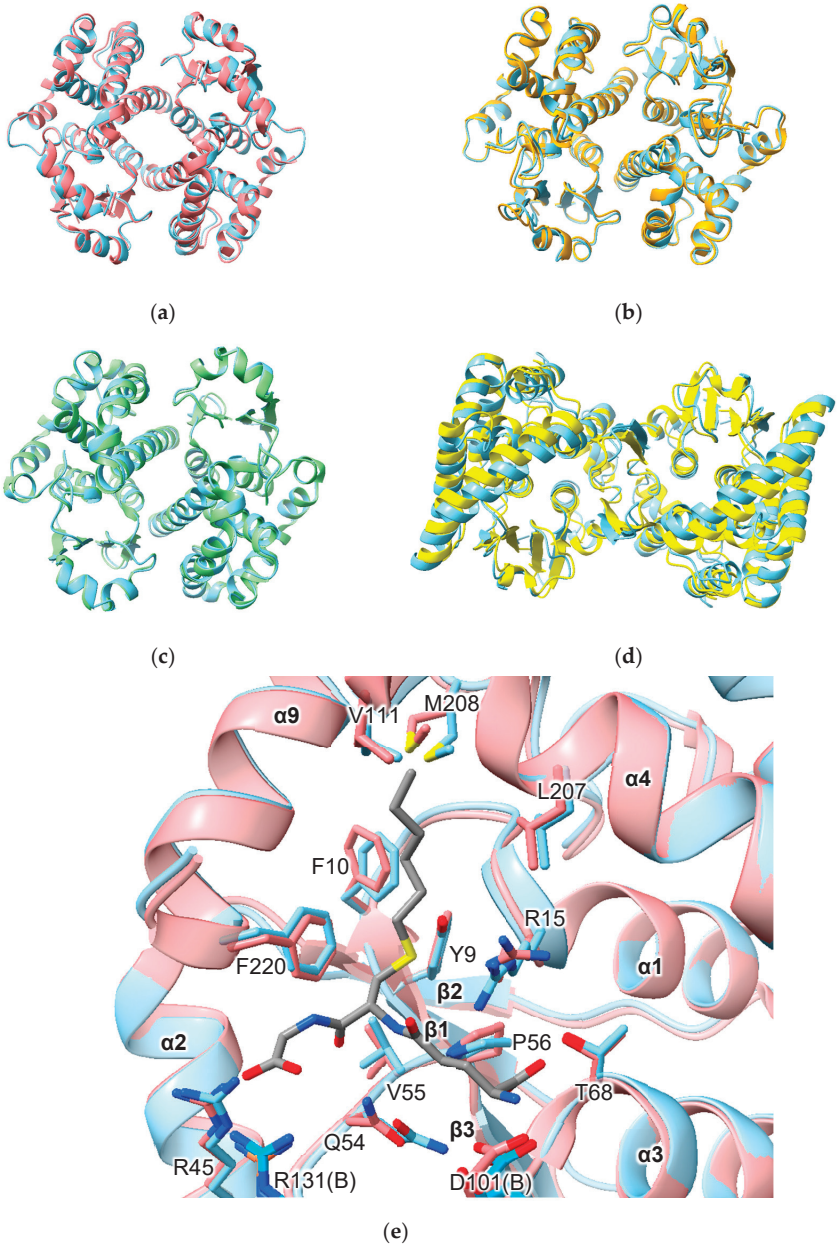

Figure 2. Comparison of predicted human versus experimentally determined structures of GST dimers. (**a**) human GSTA1-1 (PDB ID 1K3Y); (**b**) human GSTM1-1 (PDB ID7 BEU); (**c**). human GSTP1-1 (PDB ID 5J41); (**d**) *Macaca fascicularis* PTGES2 (PDB ID 1Z9H); (**e**) active site of GSTA1-1 with S-hexyl glutathione bound. In all cases, the predicted structure is indicated in sky blue.

There are relatively few biochemical studies of GST heterodimers. Within the alpha, mu- and theta-class GSTs, all isoforms are predicted, based on model confidence scores, to form heterodimers (Table S1). Data concerning the human alpha-class GSTs provide valuable context for the interpretation of predicted heterodimer models. Within the human

alpha-class GSTs, the A4 isozyme, a phylogenetic outlier (Figure S2), has residues in its interface that distinguish it from the other alpha-class isozymes. Co-expression of human GSTA4 and GSTA1 in *E. coli* shows that, while each subunit prefers to form homodimers, it is possible to form the GSTA1-4 heterodimer. While both subunits were active with substrates CDNB, HNE or Δ^5AD in the heterodimer, the specific activities and k_{cat} values were lower than the average values of the parent isozymes [22]. By contrast, the catalytic efficiencies (k_{cat}/K_M) of various heterodimers of rat alpha-class GSTs toward CDNB were predictable from the activities of their corresponding homodimers [23]. The model confidence for the predicted GSTA1-4 heterodimer structure is the same as for the GSTA1-1 homodimer (0.94). In fact, the model confidence for the GSTA1-4 heterodimer is higher than that for the GSTA4-4 homodimer (0.92). These data show that that model confidence scores should not be used as a proxy for multimerization preference or activity. While heterodimer formation is possible, and structures of heterodimers predicted with high confidence, they may not be preferred in vitro or in vivo.

An important aspect of structure prediction is the fidelity with which the algorithm reproduces the conformation of binding-site residues. Comparison of the active site of predicted and crystal structures of GSTA1-1 indicates that some side-chains show small differences in conformation. Of 14 residues in the active site, different rotamers were assigned to three residues in the model versus the crystal structure (Figure 2e). Residue R13 is assigned the **mtt**-180° rotamer in the model but adopts the **mtt**-85° rotamer in the crystal structure. Residue Q54 is assigned the **pt**-20° rotamer in the model but adopts the **mt**-30° conformation in the crystal structures. Finally, residue M208 is assigned the **mtm** rotamer in the model but adopts the **ttp** rotamer in the crystal structure. The consequence of these differences is that the placement of side-chains is similar but not identical. It is important to note that, while AlphaFold does not build ligands into predicted structures, the effects of ligand binding nonetheless may be imprinted on the structures on which the AI was trained. Thus, while the C-terminal helix (α9) is disordered in the unliganded structures (e.g., PDB 1GSD), it is nonetheless present in the predicted structures in a conformation observed in ligand-bound GSTA1-1 structures.

Few crystal structures of cGST domain-based heterodimers have been deposited in the PDB. However, published examples offer the opportunity to assess the quality of AlphaFold predictions of such assemblies. Comparison of the human GSTM2-M3 crystal structure solved at 2.8 Å resolution (PDB 3GTU) with the predicted structure yielded a RMSD of 0.69 Å over 434 Cα atoms. Comparison of the 2.6 Å crystal structure of the heterodimer of GST-like domains from EPRS1 and AIMP2 (PDB 5A34) with the AlphaFold prediction yielded an RMSD of 0.71 Å over 349 Cα atoms. The crystal structure of the GST-like domains of MARS1 and EEF1E1 (PDB 4BL7) with the predicted structure gave an RMSD of 0.80 Å over 366 Cα atoms.

A remarkable result is the prediction, with high confidence, of heterodimers of alpha-, mu-, pi- and theta-class—as well as other classes of—GST. (Selected heterodimers are shown in Figure 3.) While heterodimers within classes of GST are well known, there are few reports of heterodimers between classes of GST. Heterodimers of mu- and pi-class GSTs have been observed by incubation of rat GSTM2 and pig GSTP1 enzymes in phosphate buffer at 4 °C for 24 h [24]. The same researchers were unable to detect heterodimers of rat GSTs A1, A2 or A3 with the pi-class GST. However, the dissociation kinetics under experimental conditions may have been too slow to allow detection.

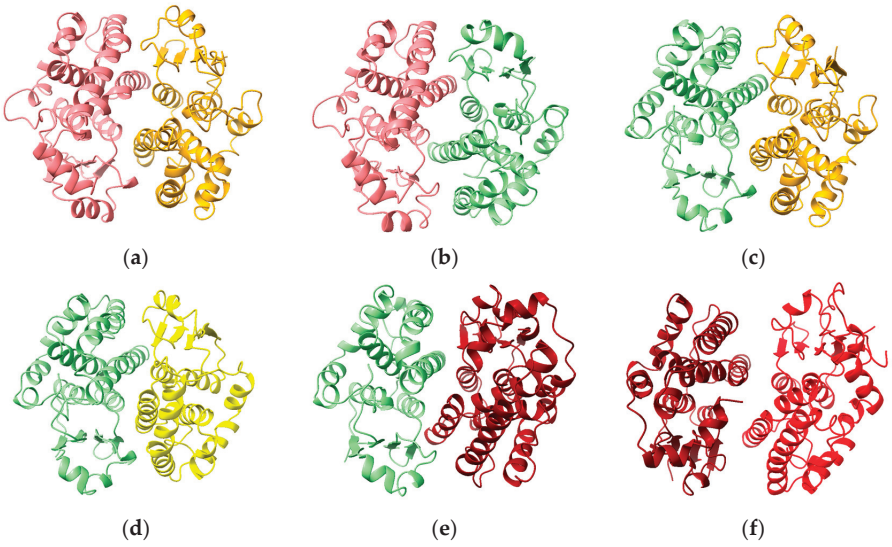

Figure 3. Predicted structures of heterodimers containing cGST domains: (**a**) GSTA1-M1; (**b**) GSTA1-P1; (**c**) GSTP1-M1; (**d**) GSTP1-HPGDS; (**e**) GSTP1-T1; (**f**) GSTT1-Z1.

3.2. Metaxins and FAXC

Metaxin (from the Greek μεταξύ; "between") was first identified in mice as essential for embryonic development [25] and later shown to be a mitochondrial outer membrane component [26]. In humans, three metaxins have been described (MTX1, MTX2 and MTX3). These proteins have been identified as components of the mitochondrial intermembrane space bridging (MIB) complex that includes SAM50 (also a component of the Sorting and Assembly Machinery or SAM complex), DNAJC11 and several other components [27]. Mandibuloacral dysplasia associated with MTX2 (MADaM) is a sever condition with symptoms including growth retardation and arises from homozygous null mutations in the human *MTX2* gene [28].

The GST-like domains of the metaxins are predicted to incorporate helices inserted between the canonical α4 and α5 helices cover the "G-site", which in these models is blocked and would be unable to bind GSH (Figure 4). In line with earlier predictions that MTX1 has a transmembrane domain near its C-terminus (Figure 1; residues 421 to 443) that is predicted to play a role in apoptosis [29], a hydrophobic helix is predicted for this region. The pattern of pairwise dimer predictions involving MTX2 and its close relatives suggests that MTX2 acts as a key interaction domain. The structures with the highest MC scores are MTX2 with MTX1, MTX3 and FAXC. Predicted heterodimers of MTX1-MTX2 and FAXC-MTX2 are shown in Figure 4b,c, respectively. Curiously, the MTX2 homodimer appears to be disfavored (MC = 0.28) and is predicted to form heterodimers with MTX1, MTX3 and FAXC, but not to form homodimers (Table S1).

There is little experimental or clinical data concerning FAXC ("Failed Axon Connections Homolog"). Transcriptomics reveal high levels of expression in the brain [30]. One report describes patients with developmental delay due to a 6q16.1 deletion that included the FAXC gene [31]. The human protein with the highest sequence similarity to FAXC is MTX2, with which FAXC is predicted to form a homodimer (MC = 0.90). Like MTX1 and MTX3, AlphaFold predictions of FAXC with other GST domains produced low ipTM scores with the exception of MTX2 (MC = 0.90). These data and phylogenetic analysis (Figure S2) suggest that FAXC is an outlying member of the metaxin family and, like MTX1 and MTX3, may form a heterodimer with MTX2.

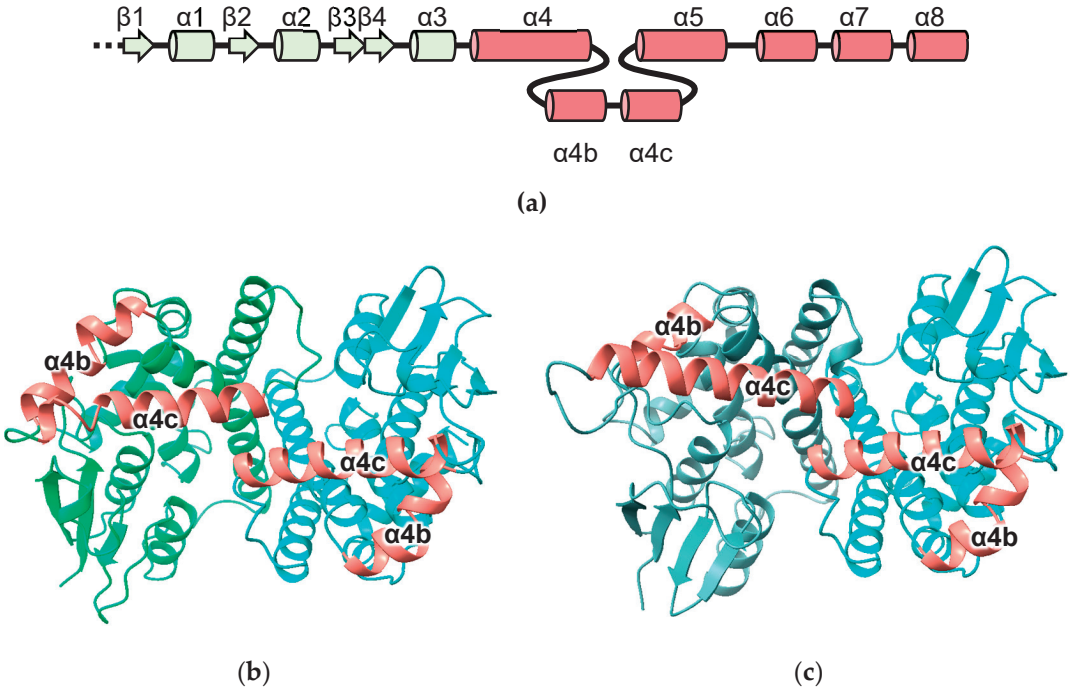

Figure 4. Predicted metaxin and FAXC structures: (**a**) topology diagram of metaxins and FAXC indicating helices inserted into the cGST domain (α4b and α4c); (**b**) MTX1-MTX2 (**c**) FAXC-MTX2.

3.3. GDAP1 and GDAP1L1

Ganglioside-Induced Differentiation-Associated Protein 1 (GDAP1) is a mitochondrial outer membrane protein involved in mitochondrial fission. GDAP1 mutations are associated with the autosomal recessive neurological disorder Charcot–Marie–Tooth disease type 4A. Mutations in GDAP1 that are associated with disease (mostly missense mutations) impede mitochondrial dynamics. Crystal structures of the mouse [32] and human [33] GDAP1 homologs confirmed the presence of the cGST fold. Efforts to detect the GSH-conjugating activity of GDAP have yielded mixed results, with some groups detecting no activity [32,34], and others detecting GSH-conjugating activity with EA, *p*-nitrobenzylchloride and EPNP [35]. GDAP1L1 is a paralogue of GDAP1 (59% sequence identity) and appears to function in mitochondrial fission. Expression of GDAP1L1 in macrophages is implicated in T-cell- and dendritic-cell-driven skin inflammation disease [36]. GDAP1 and GDAP1L1 appear to be distant relatives of the CLICs (Figure S2).

In addition to the cGST domain, GDAP has a sequence inserted between regions corresponding to helix α4 and α5, and an auto-inhibitory hydrophobic domain (HD1) followed by a trans-membrane domain (TMD) near its C-terminus (Figures 1 and 5a). Mitochondrial fission and GST activity are dependent on HD1. Huber and co-workers proposed that HD1 switches between an autoinhibited mode, where HD1 blocks the catalytic site, and an active mode, where HD1 dissociates from the catalytic site and associates with the membrane [35]. HD1 is in a position to influence the position of the loop between strand β1 and helix α1. The GDAP1L1 sequence also features the HD1 and TMD motifs.

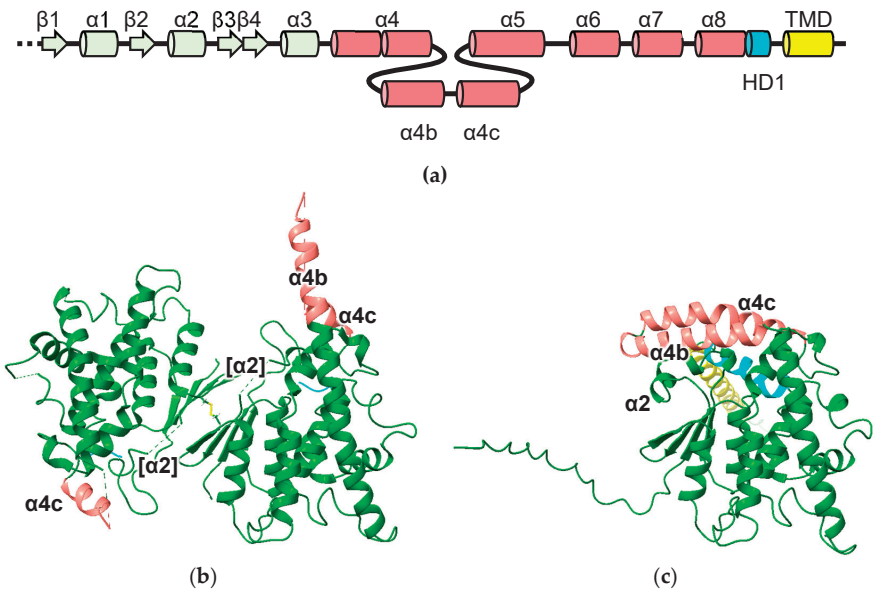

Figure 5. Experimental and predicted GDAP1 structures: (**a**) topology diagram of GDAP1 and GDAP1L1 indicating helices inserted into the cGST domain (α4b and α4c), HD1 and TMD domains; (**b**) Crystal structure of human GDAP1 residues 23 to 302 (PDB ID 7ALM) with the C88 disulfide in stick representation; (**c**) AlphaFold model of human GDAP1. Regions corresponding to inserted sequence (designated helices α4b and α4c in (**a**) are highlighted in pink. The HD1 domain (truncated in the crystal structure) is highlighted in cyan and the TMD domain in yellow. The region corresponding to helix α2 disordered in the crystal structure is indicated as [α2].

Crystal structures of mouse and human GDAP1 omit extensions at the N- and C-termini and are dimers with an atypical arrangement: the beta-sheets form a sandwich stabilized by an inter-chain disulfide bond between C88 of each monomer (Figure 5b). None of the GDAP1 crystal structures reported to date appear be competent at binding GSH due to helix α2 and flanking regions being disordered (Figure 5b) and residue P78 adopting a *trans* conformation. The equivalent proline in catalytically active cGSTs is in the *cis* conformation, is essential for GSH binding and is the only completely conserved G-site residue in the cGSTs. Intriguingly, the AlphaFold model of GDAP1 adopts a classic cGST-like structure including *cis*-proline in this region compatible with GSH binding (Figure 5c). Another key difference between model and crystal structures is the insertion between helices α4 and α5 (residues 154 to 200 in GDAP). In the AlphaFold model, this region consists of two helices forming a lid over the active site that contacts helix α2 like that seen in the predicted metaxin structures. This region is mostly disordered in crystal structures (Figure 5b). However, the residues that are present do not align with the AlphaFold model, leading to a higher RMSD (7.511 Å over 259 residues) compared to other models for which experimental structures are available (Table 2).

3.4. CLICs

Paradoxically, CLICs were first identified as chloride ion channels, yet they have a soluble form that adopts the cGST fold [37]. Several CLICs have been reported to spontaneously integrate into lipid bilayers. In addition to overall topology, CLICs contain features conserved in GSTs including the G-site *cis*-proline. They contain a conserved motif located between strand β1 and helix α1 that is also observed in glutaredoxins: CP(F/Y)C.

A similar motif is also seen on the Omega-class GSTs (CPFA and CPYS in human GSTO1 and O2, respectively).

The predicted structures of the human CLICs all have the cGST fold and are in excellent agreement with experimentally determined structures (where available) (Table 2). A noteworthy exception is the oxidized form of CLIC1, represented by PDB structure 1RK4. This contains an intramolecular disulfide between residues C24 and C59 and the N-terminal domain is rearranged [18]. The predicted model of CLIC1 matches the reduced, cGST-like form of CLIC1 (RMSD = 2.18 Å over 236 Cα atoms) and not the exceptional oxidized structure (RMSD = 7.47 Å over 213 Cα atoms) (Figure 6d).

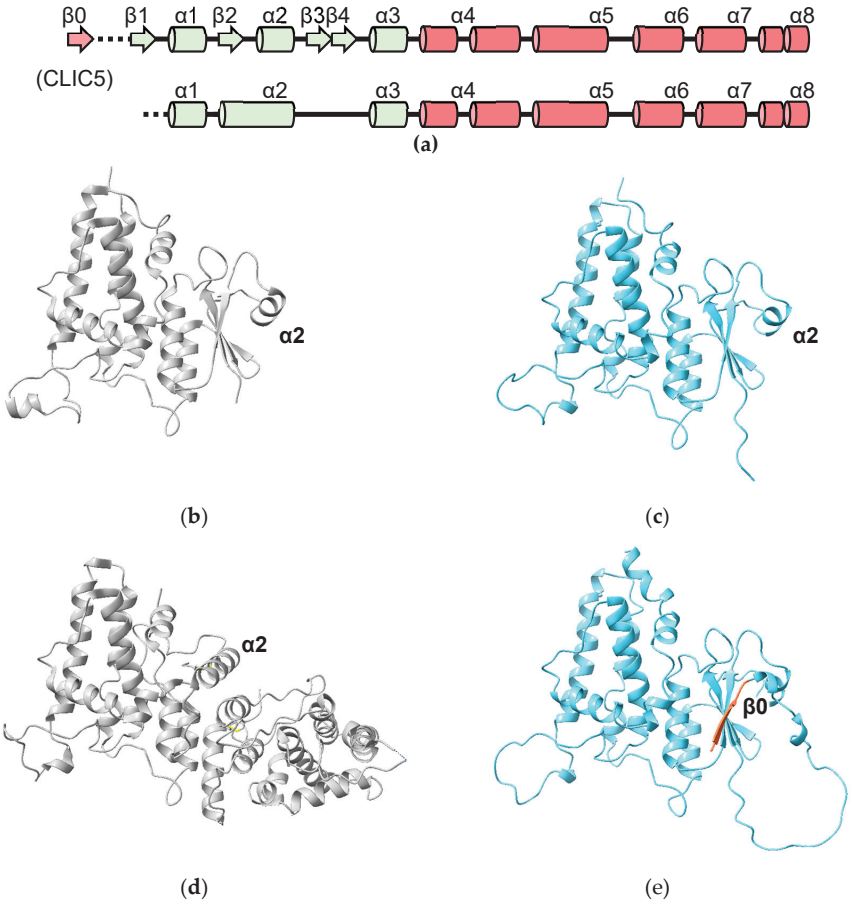

Figure 6. Experimental and predicted CLIC structures: (**a**) topology diagram of CLICs. The additional β-strand ("β0") is found in CLIC5. Below, the topology of oxidized CLIC1 is shown; (**b**) crystal structure of human CLIC1 (PDB ID 1K0M); (**c**) AlphaFold model of human CLIC1; (**d**) crystal structure of oxidized CLIC1 (PDB ID 1RK4); (**e**) predicted structure of CLIC5 (residue 141–410) with additional strand β0 highlighted in pink.

CLIC 4, 5 and 6 have N-terminal extensions predicted to be largely disordered. The N-terminal extension on CLIC5 is predicted to contain an additional β-strand "β0" that runs parallel to strand β2 (Figure 6a,e). The N-terminal extension is deleted in the crystal structure of human CLIC5 (PDB ID 6Y2H) which, thus, does not contain this additional β-strand. The longest N-terminal extension (487 residues) in CLIC6 includes 14 copies of a decapeptide motif (consensus sequence AEGPAGDSVD; residues 150 to 295) [38]. This

repeat region is predicted to form a right-handed, 15-stranded β-helix. The relationship between the secondary structure of the beta helix and the repeat is illustrated in Figure 7. The function of this domain is unknown. A DALI search of the PDB using this domain as a search model reveals an ice-binding protein from perennial ryegrass, *Lolium perenne* (PDB 3ULT), adhesin UspA1 from the Gram-negative bacterium *Moraxella catarrhalis* (PDB 3PR7) and tailspike protein TSP3 from bacteriophage CBA120 (PDB 6NW9).

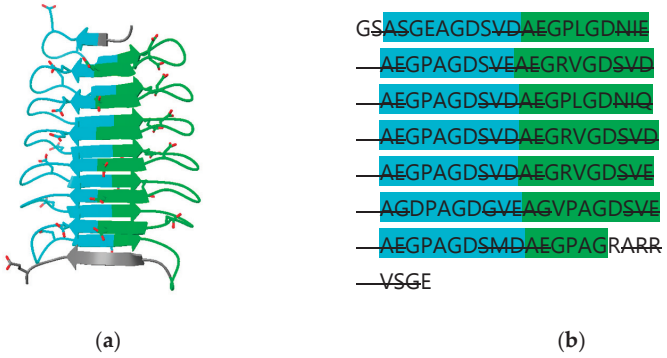

(**a**) (**b**)

Figure 7. Predicted β-helix domain (residues 150-295) of human CLIC6: (**a**) cartoon diagram with acidic residues in stick form; (**b**) amino acid sequence with odd- and even-numbered repeats highlighted in cyan and green, respectively. β-strand regions are indicated with strikethrough.

In keeping with their known monomeric structures, no human CLIC is predicted to form dimers (Table S1). Predictions of heterodimers of CLIC GST domains with other GST-domain proteins produced negative results except with AIMP2. In a study investigating the role of CLIC4 in pancreatic β-cell apoptosis, mass spectrometry experiments demonstrated an interaction between CLIC4 and AIMP2 [39].

3.5. GSTCD

GSTCD has been implicated in the development of Chronic Obstructive Pulmonary Disease. GSTCD$^{-/-}$ mice showed an increased lung TNF production in response to lipopolysaccharide. It was predicted to contain a methyltransferase domain [40].

Of the human proteins predicted to contain the cGST fold, the AlphaFold-predicted structure of the Glutathione S-transferase C-terminal domain-containing protein (GSTCD) is the greatest outlier (Figures 1 and 8). The thioredoxin domain has a region containing a two-stranded β-sheet (β1b + β1c) inserted between strand β1 and helix α2. Following strand β2, a loop and another beta strand (β2b) that forms part of the classic NTD beta sheet is inserted. While the NTD contains the *cis*-proline conserved in cGSTs, the G-site appears to be degenerate; superposition of the GSTCD model with cGST/GSH complexes show clashes with GSH (data not shown). Consistent with this is a lack of detectable GST activity [40]. With the exception of a short helix corresponding to helix α4, the rest of the CTD is rotated approximately 90° with respect to its usual position relative to the NTD. Between helices α5 and α6, a 93-residue helical bundle including a likely disordered 31 residue loop is inserted. Following helix α8 is another extended loop and, finally, the methyltransferase domain. A DALI search of the PDB using human GSTCD as a template yields the methyltransferase domain of *Anabaena variabilis* Hen1-C (PDB ID 3JWH) [41]. Hen1-C is responsible for methylation (using *S*-adenosyl methionine; SAM) of 2′-OH groups at the 3′ ends of small RNAs. Based on crystal structures, it is trivial to model S-adenosyl methionine in GSTCD (Figure 8b,c). A cluster of cysteine residues near the proposed SAM hint at a Zn^{2+} binding site that may be involved in catalysis. The role that the cGST-like components of GSTCD play in function remains unclear, as these parts of the protein do not approach the putative SAM and substrate RNA-binding sites of the methyltransferase domain.

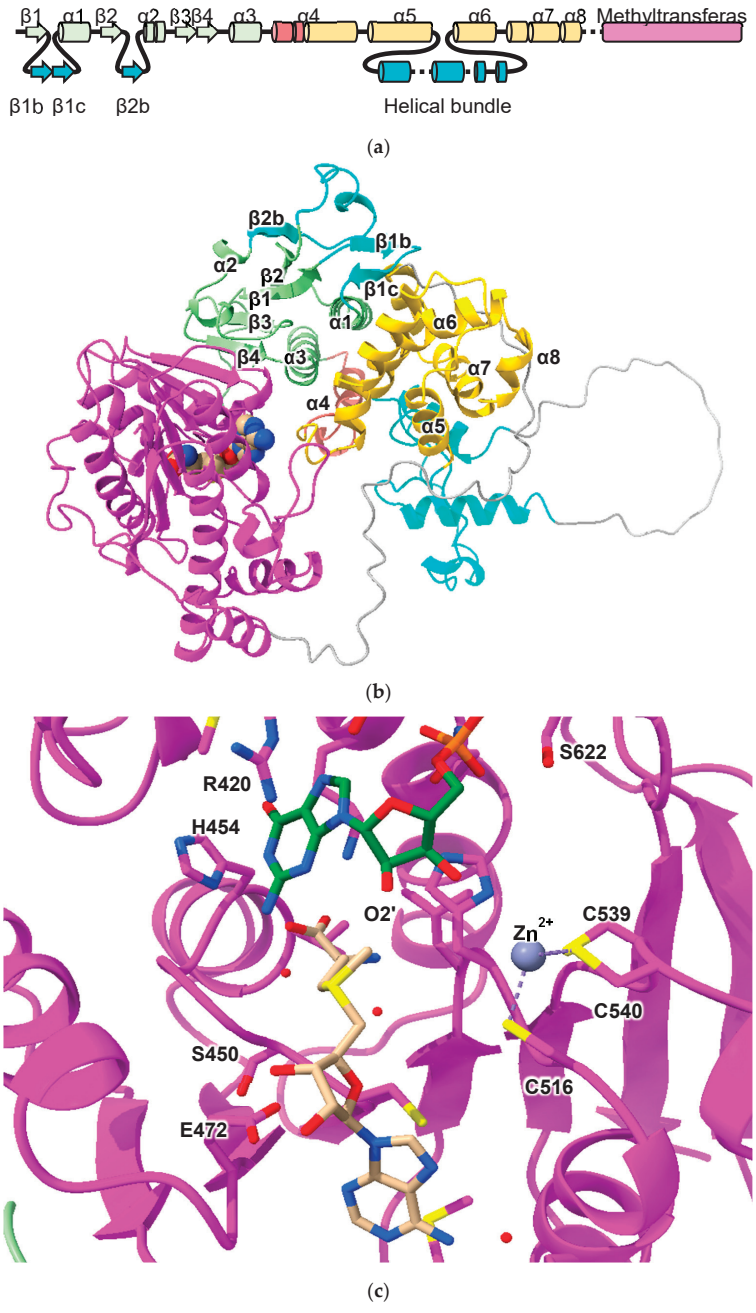

Figure 8. Predicted structure of GSTCD: (**a**) topology diagram of GSTCD indicating strands and helices inserted into the cGST domain (β1b, β1c and β2b). The component of the cGST CTD that is offset from its usual position is colored yellow. The methyltransferase domain is colored purple. (**b**) Predicted structure of GSTCD with the same color scheme in cartoon representation. SAM atoms are shown as spheres. (**c**) Cartoon diagram of GSTCD model with SAM (tan carbon atoms), Zn^{2+} and substrate RNA (green carbon atoms). Residues involved in binding these entities are shown in stick form.

3.6. MCS Components

Aminoacyl-tRNA synthetases (ARSs) are enzymes that ligate amino acids to their corresponding tRNAs (reviewed by [42]). In eukaryotes, synthetases have been observed to form a complex termed the multisynthetase complex (MSC), an assembly held together by a variety of domains appended to the synthetases as well as structural adapter proteins. The human MSC includes nine ARSs (glutamyl-, prolyl-, isoleucyl-, leucyl-, methionyl-, glutaminyl-, lysyl-, arginyl- and aspartyl-tRNA synthetase). cGST domains appear in four MSC proteins: EPRS1 (glutamyl-prolyl-tRNA synthetase 1), MARS1 (MRS, methionyl-tRNA synthetase 1), AIMP2 (ARS-interacting multifunctional protein 2) and EEF1E1 (eukaryotic translation elongation factor 1 epsilon 1, also known as AIMP3). The cGST domains are essential to the MCS assembly through canonical and non-canonical cGST-dimerization interactions. EEF1E1 has a severely truncated N-terminal domain, missing strand β1 and helix α2. Conversely, AIMP2 has additional secondary structure elements in its N-terminal domain, including an N-terminal α-helix ("α0") and a strand introduced between β1 and β2 ("β2b") (Figures 1 and 9a). These novel features were correctly predicted by AlphaFold.

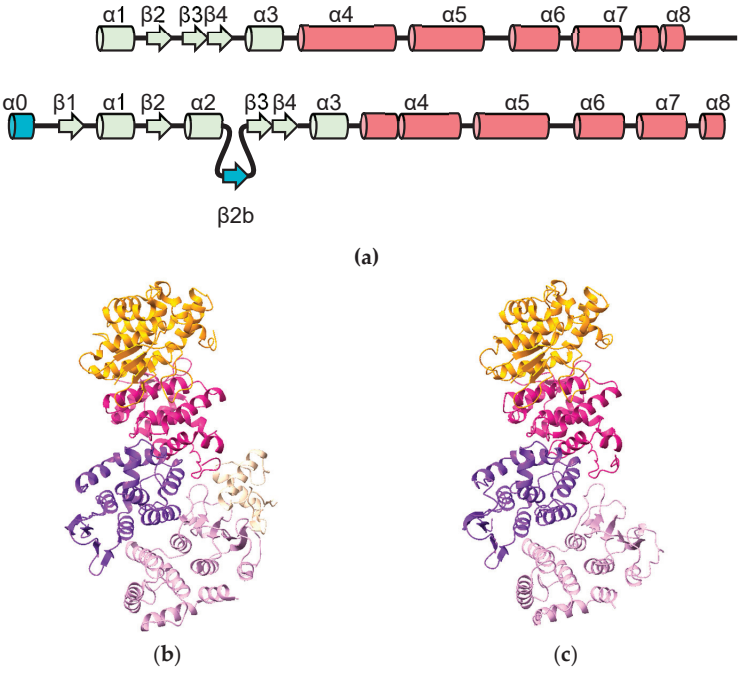

Figure 9. Structures of MCS components: (**a**) topology diagram of EEF1E1 and AIMP2 indicating strands and helices inserted into the cGST domain (α0 and β2b). (**b**) Crystal structure of MARS1 (gold), EEF1E1 (violet-red), EPRS1 (blue-violet) and AIMP2 (plum) complex with DARS1 fragment (peach) (PDB ID 5Y6L). (**c**) AlphaFold prediction of MARS1-EEF1E1-EPRS1-AIMP2 complex with the same color scheme.

The crystal structures of EPRS1, AIMP2, EEF1E1 and MARS1 with a fragment of aspartyl-tRNA synthetase 1 (DARS1) (PDB ID 5Y6L) reveal canonical heterodimer interactions between AIMP2 and EPRS and between EEF1E1 and MARS1 and a non-canonical interaction between EPRS1 and EEF1E1 (Figure 9b) [19]. AlphaFold models of AIMP2-EPRS1 (MC score 0.93) and EEF1E1 and MARS1 (MC score 0.93) agree with the crystal structures. Despite the interaction between EPRS1 and EEF1E1 being a non-canonical dimerization interaction, AlphaFold correctly predicted the interaction (MC score 0.93). It should be noted that non-canonical complexes of the domains were also predicted, albeit

with lower MC scores: EEF1E1-EPRS and EEF1E1-AIMP2 with MC scores 0.89 and 0.86, respectively. Intriguingly, some promiscuity in heterodimer formation is predicted with the four MCS cGST domains. MC scores over 0.9 were observed with GSTP1 with the theta-class GSTs, GSTP1 and CLIC1 (Table S1). The aforementioned CLIC4-AIMP2 complex has an MC of 0.84. Finally, prediction of the complex of the four subunits together was successful (Figure 9c).

Interestingly, EEF1E1, in addition to forming a heterodimer with MARS1, has also been observed to form a homodimer in an X-ray structure (PDB ID 2UZ8) [43]. The MC scores of the predicted complexes are 0.93 and 0.89, respectively.

3.7. X EEF1 Components

Eukaryotic elongation factor 1A (eEF1A) binds aminoacyl-tRNAs and delivers them to the ribosome A-site in a GTP-dependent manner. If the correct codon–anticodon interaction occurs, GTP hydrolysis is triggered at eEF1A. GDP-bound eEF1A is then released from the A-site. Translation-elongation factor complex eEF1B facilitates GDP/GTP exchange on eEF1A [44]. Like the MCS, eEF1B is formed from multiple subunits: eEF1Bα (also called elongation factor 1-beta; EF1B), eEF1Bβ (also called elongation factor 1-delta; EF1D) and eEF1Bγ (also known as EEF1G). Additionally, VARS1 interacts with eEF1 to form a "heavy" complex (eEF1H) [45]. Weak GST activity has been found in the rice EEF1G homolog [46].

Two components of EEF1 contain (or are predicted to contain) cGST domains: EEF1G and VARS1 (Figure 1). EEF1G is a two-domain protein. Unpublished crystal structures of the human EEF1G N-terminal domain with eEF1Bα (EF1B) (PDB ID 5DQS) and EEF1Bα (EF1D) (PDB ID 5JPO) reveal classic cGST homodimers (Figure 10a). The C-terminal domain of EEF1G was determined by NMR and consists of a five stranded anti-parallel β-sheet surrounded by α-helices [47]. There are no experimental structural data for VARS1. However, the structure predicted by AlphaFold has a cGST-domain at its N-terminus (residues 1 to 213) (Figure 10b). The VARS1 cGST domain is not predicted to contain a residue equivalent to the catalytic residues of catalytically active GSTs and therefore appears unlikely to have enzymatic activity.

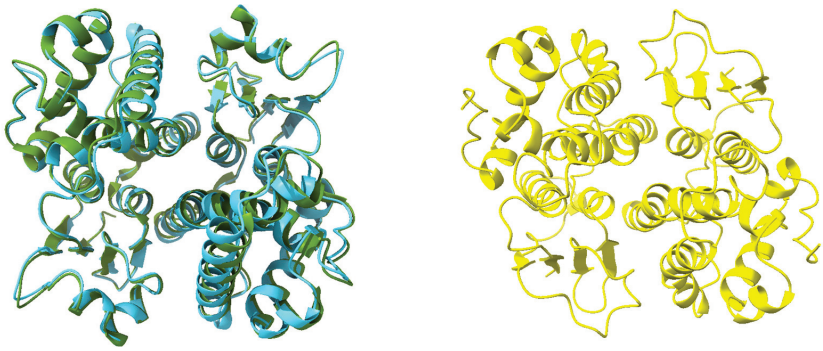

(**a**) (**b**)

Figure 10. Structures of cGST domains of EEF1 components: (**a**) dimer of the N-terminal domain of EEF1G (crystal structure PDB 5JPO, olive green; predicted structure sky blue); (**b**) predicted structure of VARS1 dimer cGST domain (residues 1–213).

Reconstitution of the rabbit eEF1H complex in vitro showed that the cGST domain of VARS1 interacts with eEF1Bβ [48]. The existence of the cGST domains of EEF1G and VARS1 prompts consideration of the possibilities for homo- and heterodimer formation in EEF1H complex formation. Human EEF1G is observed to form classic cGST homodimers in available crystal structures (Figure 10a). However, no experimental structures exist for the VARS1 cGST domain. Pairwise predictions support both homo- and heterodimer formation of EEF1G and VARS1 cGST domains (Table S1). Interestingly, the EEF1G/VARS1

heterodimer gives a higher MC score (0.91) than the VARS1 homodimer (0.84; Figure 10b). Nevertheless, a VARS1 cGST-domain homodimer could be the basis for the reported presence of two copies of VARS1 in the eEF1H complex [49].

4. Discussion

The recent advancements in protein structure prediction are leading a revolution in structural biology. While such advances pose obvious opportunities to accelerate research, it is important to determine the strengths and limitations of such tools. The algorithms described and used in this study do not predict the binding of co-factors, metal ions or post-translational modifications. There are also biases associated with the structures used to train the AI, which naturally represent a small fraction of all protein structures. In this study, a bias appears to manifest in the predicted structure of GDAP1, which resembles an archetypal cGST domain more than the available GDAP1 crystal structures. Nevertheless, high-quality predictions can inform experimental strategies. For enzymes such as GSTs, predicted structures could be used (for example) to identify active-site residues for mutagenesis and kinetics studies investigating catalytic mechanism or enzyme–substrate interactions. Where proteins act as adapters for protein–protein interactions, models can be used to identify likely binding interfaces that can again inform mutagenesis studies. For structure determination, the models predict disordered regions likely to inhibit crystallization. Constructs for expression could therefore be designed that truncate or omit such regions.

Based on available experimental data, predicted structures of human cGST-domain-containing dimers appear to be largely correct. Again, one exception is GDAP1: the mode of dimerization is unlike any other known cGST-domain-containing dimer and was not correctly predicted. Nevertheless, the successes found here compare favorably with recent benchmarking studies. Yin and co-workers [50] tested AlphaFold against a set of 152 diverse heterodimer complexes and reported near-native structure predictions for 43% of models. Again, success rates will be influenced by the training data and, therefore, some classes of dimer will be more accurately predicted than others.

Comparisons of predictions of heterodimers with biochemical data yields important lessons. Biochemical detection of heterodimers of mu- and pi-class GSTs [24] support the possibilities presented by predictions of heterodimers between classes of cGSTs (Table S1). As noted above, the propensity for heterodimer formation in alpha-class GSTs is not reflected in MC or ipTM scores. This suggests that these confidence scores should be interpreted as indicating that an interaction is feasible but not necessarily thermodynamically favorable. Multimer formation in vivo will depend on expression levels as well as thermodynamic stability.

Supplementary Materials: The following supporting information can be downloaded at: https://www.mdpi.com/article/10.3390/biom13081240/s1, Table S1: Model confidence, ipTM and pTM scores for pairwise predictions of cGST-domain-containing proteins. Where experimental structure data are available, pairs are highlighted in red. Figure S1: AlphaFold predictions of GST-domain-containing proteins in the human genome shown in Cartoon form. Structures are colored by pLDDT (key at bottom right). Only the GST domains are shown, except for GSTCD where the whole protein is shown. Figure S2: Phylogram of 39 GST-domain sequences.

Funding: This research received no external funding.

Institutional Review Board Statement: Not applicable.

Informed Consent Statement: Not applicable.

Data Availability Statement: Available in Table S1.

Conflicts of Interest: The author declares no conflict of interest.

References

1. Booth, J.; Boyland, E.; Sims, P. An enzyme from rat liver catalysing conjugations with glutathione. *Biochem. J.* **1961**, *79*, 516–524. [CrossRef] [PubMed]
2. Reinemer, P.; Dirr, H.W.; Ladenstein, R.; Schaffer, J.; Gallay, O.; Huber, R. The 3-dimensional structure of class-pi glutathione-S-transferase in complex with glutathione sulfonate at 2.3 Å resolution. *EMBO J.* **1991**, *10*, 1997–2005. [CrossRef] [PubMed]
3. Dirr, H.; Reinemer, P.; Huber, R. Refined crystal structure of porcine class Pi glutathione S-transferase (pGST P1-1) at 2·1 Å resolution. *J. Mol. Biol.* **1994**, *243*, 72–92. [CrossRef]
4. Wang, B.; Peng, Y.; Zhang, T.; Ding, J. Crystal structures and kinetic studies of human Kappa class glutathione transferase provide insights into the catalytic mechanism. *Biochem. J.* **2011**, *439*, 215–225. [CrossRef] [PubMed]
5. Jumper, J.; Evans, R.; Pritzel, A.; Green, T.; Figurnov, M.; Ronneberger, O.; Tunyasuvunakool, K.; Bates, R.; Žídek, A.; Potapenko, A.; et al. Highly accurate protein structure prediction with AlphaFold. *Nature* **2021**, *596*, 583–589. [CrossRef]
6. Baek, M.; DiMaio, F.; Anishchenko, I.; Dauparas, J.; Ovchinnikov, S.; Lee, G.R.; Wang, J.; Cong, Q.; Kinch, L.N.; Schaeffer, R.D.; et al. Accurate prediction of protein structures and interactions using a three-track neural network. *Science* **2021**, *373*, 871–876. [CrossRef] [PubMed]
7. Richard, E.; Michael, O.N.; Alexander, P.; Natasha, A.; Andrew, S.; Tim, G.; Augustin, Ž.; Russ, B.; Sam, B.; Jason, Y.; et al. Protein complex prediction with AlphaFold-Multimer. *BioRxiv* **2021**. [CrossRef]
8. Holm, L. Using Dali for Protein Structure Comparison. *Methods Mol. Biol.* **2020**, *2112*, 29–42. [CrossRef]
9. Mirdita, M.; Schütze, K.; Moriwaki, Y.; Heo, L.; Ovchinnikov, S.; Steinegger, M. ColabFold: Making protein folding accessible to all. *Nat. Methods* **2022**, *19*, 679–682. [CrossRef]
10. Pettersen, E.F.; Goddard, T.D.; Huang, C.C.; Meng, E.C.; Couch, G.S.; Croll, T.I.; Morris, J.A.-O.; Ferrin, T.A.-O. UCSF ChimeraX: Structure visualization for researchers, educators, and developers. *Protein Sci.* **2021**, *30*, 70–82. [CrossRef]
11. Sievers, F.; Wilm, A.; Dineen, D.; Gibson, T.J.; Karplus, K.; Li, W.; Lopez, R.; McWilliam, H.; Remmert, M.; Söding, J.; et al. Fast, scalable generation of high-quality protein multiple sequence alignments using Clustal Omega. *Mol. Syst. Biol.* **2011**, *7*, 539. [CrossRef] [PubMed]
12. Wu, Y.; Fan, Y.; Xue, B.; Luo, L.; Shen, J.; Zhang, S.; Jiang, Y.; Yin, Z. Human glutathione S-transferase P1-1 interacts with TRAF2 and regulates TRAF2-ASK1 signals. *Oncogene* **2006**, *25*, 5787–5800. [CrossRef] [PubMed]
13. Adler, V.; Yin, Z.; Fuchs, S.Y.; Benezra, M.; Rosario, L.; Tew, K.D.; Pincus, M.R.; Sardana, M.; Henderson, C.J.; Wolf, C.R.; et al. Regulation of JNK signaling by GSTp. *EMBO J.* **1999**, *18*, 1321–1334. [CrossRef] [PubMed]
14. Jowsey, I.R.; Thomson, A.M.; Flanagan, J.U.; Murdock, P.R.; Moore, G.B.; Meyer, D.J.; Murphy, G.J.; Smith, S.A.; Hayes, J.D. Mammalian class Sigma glutathione S-transferases: Catalytic properties and tissue-specific expression of human and rat GSH-dependent prostaglandin D2 synthases. *Biochem. J.* **2001**, *359*, 507–516. [CrossRef]
15. Yamada, T.; Komoto, J.; Watanabe, K.; Ohmiya, Y.; Takusagawa, F. Crystal structure and possible catalytic mechanism of microsomal prostaglandin E synthase type 2 (mPGES-2). *J. Mol. Biol.* **2005**, *348*, 1163–1176. [CrossRef]
16. Zhao, Y.; Song, E.; Wang, W.; Hsieh, C.H.; Wang, X.; Feng, W.; Wang, X.; Shen, K. Metaxins are core components of mitochondrial transport adaptor complexes. *Nat. Commun.* **2021**, *12*, 83. [CrossRef]
17. Cromer, B.A.; Gorman, M.A.; Hansen, G.; Adams, J.J.; Coggan, M.; Littler, D.R.; Brown, L.J.; Mazzanti, M.; Breit, S.N.; Curmi, P.M.; et al. Structure of the Janus protein human CLIC2. *J. Mol. Biol.* **2007**, *374*, 719–731. [CrossRef]
18. Littler, D.R.; Harrop, S.J.; Fairlie, W.D.; Brown, L.J.; Pankhurst, G.J.; Pankhurst, S.; DeMaere, M.Z.; Campbell, T.J.; Bauskin, A.R.; Tonini, R.; et al. The intracellular chloride ion channel protein CLIC1 undergoes a redox-controlled structural transition. *J. Biol. Chem.* **2004**, *279*, 9298–9305. [CrossRef]
19. Cho, H.Y.; Lee, H.J.; Choi, Y.S.; Kim, D.K.; Jin, K.S.; Kim, S.; Kang, B.S. Symmetric Assembly of a Decameric Subcomplex in Human Multi-tRNA Synthetase Complex Via Interactions between Glutathione Transferase-Homology Domains and Aspartyl-tRNA Synthetase. *J. Mol. Biol.* **2019**, *431*, 4475–4496. [CrossRef]
20. Bondarchuk, T.V.; Shalak, V.F.; Lozhko, D.M.; Fatalska, A.; Szczepanowski, R.H.; Liudkovska, V.; Tsuvariev, O.Y.; Dadlez, M.; El'skaya, A.V.; Negrutskii, B.S. Quaternary organization of the human eEF1B complex reveals unique multi-GEF domain assembly. *Nucleic Acids Res.* **2022**, *50*, 9490–9504. [CrossRef]
21. Hayes, J.D.; Flanagan, J.U.; Jowsey, I.R. Glutathione transferases. *Annu. Rev. Pharmacol. Toxicol.* **2005**, *45*, 51–88. [CrossRef]
22. Gustafsson, A.; Nilsson, L.O.; Mannervik, B. Hybridization of alpha class subunits generating a functional glutathione transferase A1-4 heterodimer. *J. Mol. Biol.* **2002**, *316*, 395–406. [CrossRef]
23. Danielson, U.H.; Mannervik, B. Kinetic independence of the subunits of cytosolic glutathione transferase from the rat. *Biochem. J.* **1985**, *231*, 263–267. [CrossRef]
24. Pettigrew, N.E.; Colman, R.F. Heterodimers of glutathione S-transferase can form between isoenzyme classes pi and mu. *Arch. Biochem. Biophys.* **2001**, *396*, 225–230. [CrossRef] [PubMed]
25. Bornstein, P.; McKinney, C.E.; LaMarca, M.E.; Winfield, S.; Shingu, T.; Devarayalu, S.; Vos, H.L.; Ginns, E.I. Metaxin, a gene contiguous to both thrombospondin 3 and glucocerebrosidase, is required for embryonic development in the mouse: Implications for Gaucher disease. *Proc. Natl. Acad. Sci. USA* **1995**, *92*, 4547–4551. [CrossRef] [PubMed]
26. Armstrong, L.C.; Komiya, T.; Bergman, B.E.; Mihara, K.; Bornstein, P. Metaxin is a component of a preprotein import complex in the outer membrane of the mammalian mitochondrion. *J. Biol. Chem.* **1997**, *272*, 6510–6518. [CrossRef] [PubMed]

27. Huynen, M.A.; Mühlmeister, M.; Gotthardt, K.; Guerrero-Castillo, S.; Brandt, U. Evolution and structural organization of the mitochondrial contact site (MICOS) complex and the mitochondrial intermembrane space bridging (MIB) complex. *Biochim. Biophys. Acta* **2016**, *1863*, 91–101. [CrossRef] [PubMed]
28. Elouej, S.; Harhouri, K.; Le Mao, M.; Baujat, G.; Nampoothiri, S.; Kayserili, H.; Menabawy, N.A.; Selim, L.; Paneque, A.L.; Kubisch, C.; et al. Loss of MTX2 causes mandibuloacral dysplasia and links mitochondrial dysfunction to altered nuclear morphology. *Nat. Commun.* **2020**, *11*, 4589. [CrossRef]
29. Long, G.L.; Winfield, S.; Adolph, K.W.; Ginns, E.I.; Bornstein, P. Structure and organization of the human metaxin gene (MTX) and pseudogene. *Genomics* **1996**, *33*, 177–184. [CrossRef]
30. Fagerberg, L.; Hallström, B.M.; Oksvold, P.; Kampf, C.; Djureinovic, D.; Odeberg, J.; Habuka, M.; Tahmasebpoor, S.; Danielsson, A.; Edlund, K.; et al. Analysis of the human tissue-specific expression by genome-wide integration of transcriptomics and antibody-based proteomics. *Mol. Cell. Proteom.* **2014**, *13*, 397–406. [CrossRef]
31. Okazaki, T.; Kawaguchi, T.; Saiki, Y.; Aoki, C.; Kasagi, N.; Adachi, K.; Saida, K.; Matsumoto, N.; Nanba, E.; Maegaki, Y. Clinical course of a Japanese patient with developmental delay linked to a small 6q16.1 deletion. *Hum. Genome Var.* **2022**, *9*, 14. [CrossRef]
32. Googins, M.R.; Woghiren-Afegbua, A.O.; Calderon, M.; St Croix, C.M.; Kiselyov, K.I.; VanDemark, A.P. Structural and functional divergence of GDAP1 from the glutathione S-transferase superfamily. *FASEB J.* **2020**, *34*, 7192–7207. [CrossRef] [PubMed]
33. Nguyen, G.T.T.; Sutinen, A.; Raasakka, A.; Muruganandam, G.; Loris, R.; Kursula, P. Structure of the Complete Dimeric Human GDAP1 Core Domain Provides Insights into Ligand Binding and Clustering of Disease Mutations. *Front. Mol. Biosci.* **2020**, *7*, 631232. [CrossRef]
34. Shield, A.J.; Murray, T.P.; Board, P.G. Functional characterisation of ganglioside-induced differentiation-associated protein 1 as a glutathione transferase. *Biochem. Biophys. Res. Commun.* **2006**, *347*, 859–866. [CrossRef]
35. Huber, N.; Bieniossek, C.; Wagner, K.M.; Elsässer, H.P.; Suter, U.; Berger, I.; Niemann, A. Glutathione-conjugating and membrane-remodeling activity of GDAP1 relies on amphipathic C-terminal domain. *Sci. Rep.* **2016**, *6*, 36930. [CrossRef] [PubMed]
36. Alalaiwe, A.; Chen, C.Y.; Chang, Z.Y.; Sung, J.T.; Chuang, S.Y.; Fang, J.Y. Psoriasiform Inflammation Is Associated with Mitochondrial Fission/GDAP1L1 Signaling in Macrophages. *Int. J. Mol. Sci.* **2021**, *22*, 10410. [CrossRef]
37. Harrop, S.J.; DeMaere, M.Z.; Fairlie, W.D.; Reztsova, T.; Valenzuela, S.M.; Mazzanti, M.; Tonini, R.; Qiu, M.R.; Jankova, L.; Warton, K.; et al. Crystal structure of a soluble form of the intracellular chloride ion channel CLIC1 (NCC27) at 1.4-A resolution. *J. Biol. Chem.* **2001**, *276*, 44993–45000. [CrossRef]
38. Friedli, M.; Guipponi, M.; Bertrand, S.; Bertrand, D.; Neerman-Arbez, M.; Scott, H.S.; Antonarakis, S.E.; Reymond, A. Identification of a novel member of the CLIC family, CLIC6, mapping to 21q22.12. *Gene* **2003**, *320*, 31–40. [CrossRef]
39. Patel, D.; Ythier, D.; Brozzi, F.; Eizirik, D.L.; Thorens, B. Clic4, a novel protein that sensitizes β-cells to apoptosis. *Mol. Metab.* **2015**, *4*, 253–264. [CrossRef] [PubMed]
40. Henry, A.P.; Probert, K.; Stewart, C.E.; Thakker, D.; Bhaker, S.; Azimi, S.; Hall, I.P.; Sayers, I. Defining a role for lung function associated gene GSTCD in cell homeostasis. *Respir. Res.* **2019**, *20*, 172. [CrossRef]
41. Mui Chan, C.; Zhou, C.; Brunzelle, J.S.; Huang, R.H. Structural and biochemical insights into 2′-O-methylation at the 3′-terminal nucleotide of RNA by Hen1. *Proc. Natl. Acad. Sci. USA* **2009**, *106*, 17699–17704. [CrossRef] [PubMed]
42. Rubio Gomez, M.A.; Ibba, M. Aminoacyl-tRNA synthetases. *RNA* **2020**, *26*, 910–936. [CrossRef] [PubMed]
43. Kim, K.J.; Park, M.C.; Choi, S.J.; Oh, Y.S.; Choi, E.C.; Cho, H.J.; Kim, M.H.; Kim, S.H.; Kim, D.W.; Kim, S.; et al. Determination of three-dimensional structure and residues of the novel tumor suppressor AIMP3/p18 required for the interaction with ATM. *J. Biol. Chem.* **2008**, *283*, 14032–14040. [CrossRef]
44. Blanchet, S.; Ranjan, N. Translation Phases in Eukaryotes. *Methods Mol. Biol.* **2022**, *2533*, 217–228. [CrossRef]
45. Negrutskii, B.S.; Shalak, V.F.; Kerjan, P.; El'skaya, A.V.; Mirande, M. Functional interaction of mammalian valyl-tRNA synthetase with elongation factor EF-1alpha in the complex with EF-1H. *J. Biol. Chem.* **1999**, *274*, 4545–4550. [CrossRef]
46. Kobayashi, S.; Kidou, S.; Ejiri, S. Detection and characterization of glutathione S-transferase activity in rice EF-1betabeta'gamma and EF-1gamma expressed in Escherichia coli. *Biochem. Biophys. Res. Commun.* **2001**, *288*, 509–514. [CrossRef] [PubMed]
47. Vanwetswinkel, S.; Kriek, J.; Andersen, G.R.; Güntert, P.; Dijk, J.; Canters, G.W.; Siegal, G. Solution structure of the 162 residue C-terminal domain of human elongation factor 1Bgamma. *J. Biol. Chem.* **2003**, *278*, 43443–43451. [CrossRef]
48. Bec, G.; Kerjan, P.; Waller, J.P. Reconstitution in vitro of the valyl-tRNA synthetase-elongation factor (EF) 1 beta gamma delta complex. Essential roles of the NH2-terminal extension of valyl-tRNA synthetase and of the EF-1 delta subunit in complex formation. *J. Biol. Chem.* **1994**, *269*, 2086–2092. [CrossRef]
49. Jiang, S.; Wolfe, C.L.; Warrington, J.A.; Norcum, M.T. Three-dimensional reconstruction of the valyl-tRNA synthetase/elongation factor-1H complex and localization of the delta subunit. *FEBS Lett.* **2005**, *579*, 6049–6054. [CrossRef]
50. Yin, R.; Feng, B.Y.; Varshney, A.; Pierce, B.G. Benchmarking AlphaFold for protein complex modeling reveals accuracy determinants. *Protein Sci.* **2022**, *31*, e4379. [CrossRef]

biomolecules

MDPI

Review

The Multifaceted Role of Glutathione S-Transferases in Health and Disease

Aslam M. A. Mazari [1,*], Leilei Zhang [1], Zhi-Wei Ye [1], Jie Zhang [1], Kenneth D. Tew [1] and Danyelle M. Townsend [2]

[1] Department of Cell and Molecular Pharmacology and Experimental Therapeutics, Medical University of South Carolina, 70 President Street, DDB410, Charleston, SC 29425, USA
[2] Department of Pharmaceutical and Biomedical Sciences, Medical University of South Carolina, 274 Calhoun Street, MSC141, Charleston, SC 29425, USA
* Correspondence: mua205@musc.edu

Abstract: In humans, the cytosolic glutathione S-transferase (GST) family of proteins is encoded by 16 genes presented in seven different classes. GSTs exhibit remarkable structural similarity with some overlapping functionalities. As a primary function, GSTs play a putative role in Phase II metabolism by protecting living cells against a wide variety of toxic molecules by conjugating them with the tripeptide glutathione. This conjugation reaction is extended to forming redox sensitive post-translational modifications on proteins: S-glutathionylation. Apart from these catalytic functions, specific GSTs are involved in the regulation of stress-induced signaling pathways that govern cell proliferation and apoptosis. Recently, studies on the effects of GST genetic polymorphisms on COVID-19 disease development revealed that the individuals with higher numbers of risk-associated genotypes showed higher risk of COVID-19 prevalence and severity. Furthermore, overexpression of GSTs in many tumors is frequently associated with drug resistance phenotypes. These functional properties make these proteins promising targets for therapeutics, and a number of GST inhibitors have progressed in clinical trials for the treatment of cancer and other diseases.

Keywords: Glutathione S-transferases (GSTs); antioxidants; cancer-cell signaling; cell survival; chemoresistance; xenobiotic compounds; metabolism; GST inhibitors; glutathionylation; oxidative stress; JNK; apoptosis; GST Polymorphism; SARS-CoV-2; COVID-19

Citation: Mazari, A.M.A.; Zhang, L.; Ye, Z.-W.; Zhang, J.; Tew, K.D.; Townsend, D.M. The Multifaceted Role of Glutathione S-Transferases in Health and Disease. *Biomolecules* **2023**, *13*, 688. https://doi.org/10.3390/biom13040688

Academic Editor: Bengt Mannervik

Received: 28 February 2023
Revised: 12 April 2023
Accepted: 13 April 2023
Published: 18 April 2023

1. Introduction

Glutathione transferases (GSTs), also referred to as glutathione *S*-transferases, belong to the supergene family of phase II detoxification enzymes that are ubiquitously present in almost all cellular life forms. On the basis of their sub-cellular distribution, GSTs are classified into three major protein families as either Cytosolic, Mitochondrial or Kappa and Microsomal (also known as Membrane-Associated Proteins in Eicosanoid and Glutathione (MAPEG)) [1]. The cytosolic GSTs constitute the largest family and are sub-divided into seven distinct classes based on their amino acid sequence and other structural similarities, represented by Greek letter names with alphanumeric letter designations, namely alpha (A), mu (M), omega (O), pi (P), sigma (S), theta (T), and zeta (Z) [2–4]. Cytosolic GSTs are structurally distinct from mitochondrial and microsomal classes of enzymes and are composed of two subunits (~25 kDa each), either homodimers of a single gene product or heterodimers encoded by a different gene. Each subunit of the dimeric isozyme consists of two functional domains, the more conserved N-terminal domain containing catalytically active cysteine, serine, or tyrosine residues, and the C-terminal domain. There are two substrate binding sites in each subunit: the GSH binding site or G-site and an adjacent H-site for binding structurally diverse hydrophobic xenobiotics or the products of oxidative stress [1,5]. As principal phase II detoxification enzymes, GSTs protect living cells by catalyzing the conjugation of glutathione (GSH) to a wide variety of electrophilic molecules of both endogenous and exogenous origin. GSH is a tripeptide (γ-l-glutamyl-l-cysteinyl

glycine) synthesized in the cytoplasm of every cell in a two-step ATP-requiring enzymatic process catalyzed by glutamate-cysteine ligase and glutathione synthetase enzymes. GST tissue distribution and expression levels vary according to the class. A recent review summarizes the tissue distribution of soluble GSTs [6]. The variations in GST tissue distribution suggest possible differences in the ways by which individual human tissues can detoxify or otherwise handle xenobiotics and or drugs. Furthermore, certain chemicals, including those occurring naturally in fruits and cruciferous vegetables can act as inducers of GST genes through a range of responsive elements and such inductions are part of GSTs adaptive response mechanisms to chemical insult caused by electrophiles [7].

Apart from their essential role as detoxification enzymes, GSTs are involved in several other important functions such as cell signaling, post-translational modifications, and chemotherapeutic drug resistance [8]. For example, the pi and mu classes of GSTs modulate the mitogen-activated protein kinase (MAPK) signaling pathway responsible for stress response, cell proliferation, and apoptosis via direct interactions with c-Jun N-terminal kinase 1 (JNK1) and apoptosis signal-regulating kinase (ASK1) [8,9]. Furthermore, GSTs are known to facilitate protein S-glutathionylation reactions, and a number of proteins have been shown to be common substrates for GST-mediated protein S-glutathionylation including protein disulfide isomerase (PDI), p53, and peroxiredoxin-VI (Prdx-VI) [10]. Overexpression of GSTs, particularly GSTP1-1 is often considered as a possible mechanism of tumor cell drug resistance [11–13]. Hence, GSTs remain a viable therapeutic target, and inhibitors of GST catalytic activity have emerged as potential therapeutic tools in cancer cell drug resistance [14,15]. This review focuses on the diverse role these versatile enzymes play in human health and disease.

2. Role in Detoxification

GSTs function in cellular protection by catalyzing the conjugation of GSH with numerous hydrophobic and electrophilic intermediates, including many carcinogens, therapeutic agents, and products of oxidative stress, rendering them less toxic and facilitating their export from the cell. An overview of xenobiotic detoxification is shown below in (Figure 1).

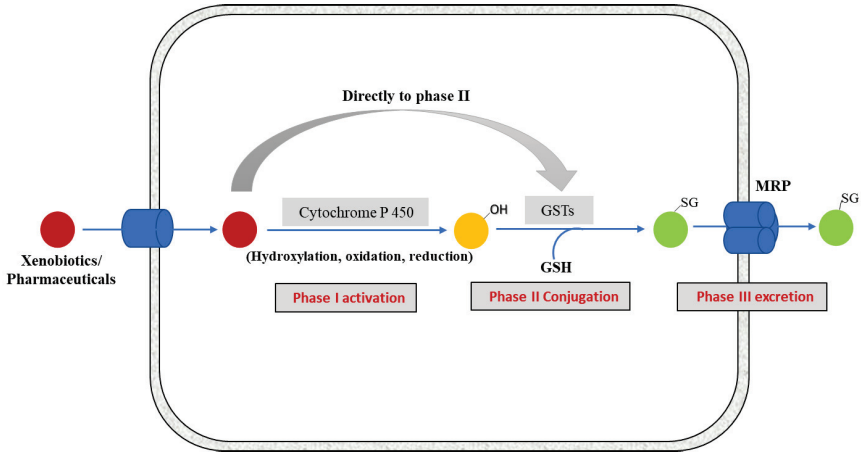

Figure 1. Overview of xenobiotic biotransformation pathway. Once inside the cell, the toxic molecules are targeted by different enzymes of detoxification system. Lipophilic molecules are metabolized by Phase I enzymes, i.e., Cytochrome P450s. The activated xenobiotics are subsequently conjugated with GSH by phase II detoxification enzyme GSTs and are finally exported out of the cell in phase III by trans-membrane multidrug resistance-associated proteins (MRPs) from the C family of ABC transporters [1]. Some compounds (polar or hydrophilic in nature) may enter in Phase II metabolism directly.

The human genome encodes 16 cytosolic GST enzymes with overlapping, but non-identical, substrate specificities, and there is no clear reason for such diversity. A possible explanation could be based on the physiological role of these isoenzymes. Functionally, they comprise a "chemical immune system" that must be capable of dealing with a broad spectrum of substrates, including those it has not previously encountered, and without interfering with non-toxic endogenous metabolites. A single, multifaceted enzyme would be incapable of the latter, whereas too many specific enzymes could be too costly to maintain from an energy efficiency standpoint. Perhaps the evolved optimal number of GST isoenzymes in each class is co-determined by the occurrence of xenobiotics in the distinctive environment of each species [16]. Early in mammalian development, rapid gene duplication and subsequent adoptive evolution of the replicated genes is essentially a divergent process, but may eventually have resulted in multiple isoenzymes acquiring specificities for a given substrate by convergent evolution rather than by a common ancestry.

Traditionally, the catalytic activities of GSTs are measured with 1-chloro-2, 4-dinitrobenzene (CDNB) and cumene hydroperoxide (CuOOH) as substrates. Because they also possess selenium-independent GPx activity, GSTs are able to reduce hydroperoxides of phospholipids and free fatty acids as well as cholesterol hydroperoxides [17–19]. In this regard, GST's can impact the regulation of certain electrophilic intermediates indirectly controlling critical regulatory pathways. For example, 4-hydroxy-2-trans-nonenal (4-HNE), is a potentially toxic stable end product of lipid peroxidation, a common denominator in stress-mediated signaling and a pro-apoptotic second messenger that alters cell cycle signaling pathways in a concentration-dependent manner [20,21]. Steady-state intracellular levels of 4-HNE are maintained by the balance between its production, due to lipid peroxidation, and its removal via different pathways. GSTs are a major determinant of the intracellular concentration of 4-HNE as they catalyze the conjugation of GSH with 4-HNE [22]. In particular, the GSTA4-4 isoform possesses a higher affinity for 4-HNE [23] than other xenobiotics, implying a critical role in regulating 4-HNE homeostasis. The GS-HNE adduct formed is then transported out of the cell in an ATP-dependent manner, similar to the system that exports other GSH conjugates [24,25] (Figure 1).

It is generally accepted that the conjugation of GSH with xenobiotics almost always results in the formation of less reactive metabolites that are more readily excreted. However, in some cases, GSH conjugates can be more reactive than their parental compounds. Examples include short-chain alkyl halides bearing two functional groups. The conjugation of GSH with dichloromethane results in the formation of highly unstable s-chloromethylglutathione adducts, containing an electrophilic center capable of modifying DNA [26,27], with subsequent toxic effects. Cisplatin, a commonly used anticancer agent, leads to nephrotoxicity [28]. This occurs when GSH conjugates of platinum are metabolized in the proximal tubule cells of kidneys [29,30]. It was subsequently shown that this occurs in a GSTpi-dependent manner using both genetic and pharmacological inhibition in vivo [31,32]. Cisplatin-induced nephrotoxicity could be diminished using GSH mimetics [33] (Figure 2).

The capacity of cells to maintain cellular redox homeostasis during oxidative stress resides in their ability to induce a battery of protective enzymes critical to mounting a cellular defense against ROS/RNS or toxic electrophiles. In this context, the Nrf2/Keap1 transcription complex in animals is the primary finely tuned system that regulates the expression of many oxidative stress-related genes, including antioxidant and phase II detoxification enzymes. This is achieved via interactions with antioxidant response elements (ARE) in their promoter regions [34,35]. Under unstressed conditions, Nrf2 binds to Keap1 in the cytosol where it is instantly ubiquitinated and destined for proteasomal degradation. However, under conditions of elevated oxidative stress, Keap1 becomes oxidized, and this inhibits its binding to Nrf2. The activation and translocation of Nrf2 into the nucleus is facilitated by various cellular protein kinases [36,37]. Once inside the nucleus, Nrf2, along with other small Maf proteins, binds to the ARE of target genes and induces their expression. In this way, the induction of antioxidant and phase II detoxification enzymes contributes to cytoprotection against chemical insults that cause direct or indirect oxidative stress.

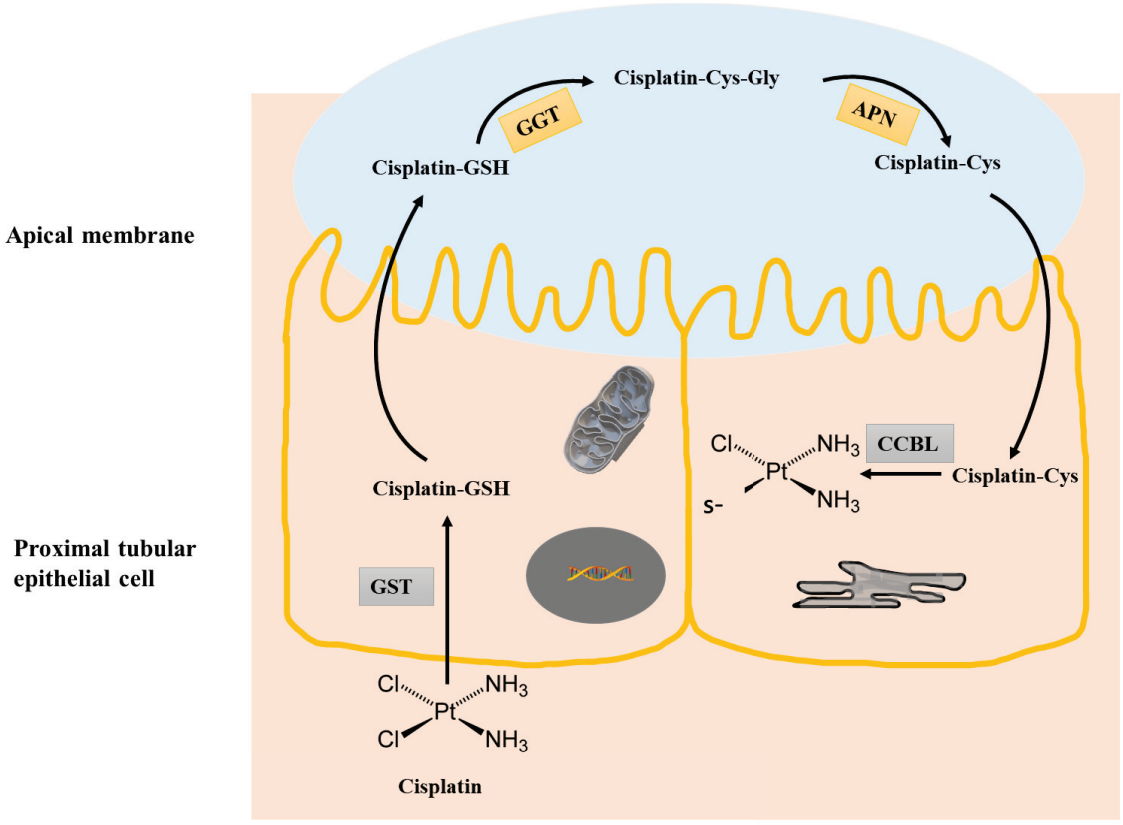

Figure 2. Bioactivation of cisplatin to a nephrotoxin. In the first step, Cisplatin can be conjugated with GSH by GST. The Cisplatin–GSH conjugate then passes through to the tubule lumen by MRP2 effluxes, where it is cleaved to a cysteinyl–glycine conjugate by g-glutamyl transpeptidase (GGT) followed by further cleavage to Cisplatin–Cysteine by aminopeptidase (APN). The Cisplatin–Cys conjugate is then re absorbed by the proximal tubule, where Cisplatin–CYS is further metabolized by a pyridoxal 5′-phosphate-dependent enzyme, cysteine S-conjugate beta-lyase (CCBL) to form a reactive thiol that can bind proteins and contribute to toxicity.

3. Role in Protein S-Glutathionylation

Protein post-translational modifications (PTMs) complement functional proteomics by regulating enzymatic activities, stability, localization, and their interactions with other cellular proteins [38]. Because of the valence flexibility of sulfur, the redox reactions of cysteine thiols can be exceptionally dynamic. Oxidative stress can preferentially react and oxidize protein thiolates (RS^-). Protein S-glutathionylation is a redox-sensitive, reversible PTM that adds GSH to a cysteine residue in a acceptor protein [39,40]. Cysteines on the surfaces of globular proteins are generally readily accessible to GSH and GSSG and can undergo spontaneous S-glutathionylation [41], which can be altered by antioxidant enzyme systems such as thioredoxin (Trx) [42], glutaredoxin (Grx) [43], or sulfiredoxin (Srx) [44]. Grx isoenzymes have been shown to metabolize both glutathionylation and deglutathionylation reactions and are controlled by the overall redox state of the GSH pool, where a more oxidized (GSSG) environment favors glutathionylation while restoration of reduced (GSH) levels steers deglutathionylation [45].

Of relevance, a prerequisite for a cysteine residue modification is its accessibility by the solvent and reactivity influenced by adjacent amino acids. The estimated pKa of the

cysteine thiol under physiological pH ranges from 8.0 to 8.7, contributing to low reactive potential. GSTs can effectively lower this pKa of the cysteine thiol, creating a more reactive nucleophilic thiolate anion [46]. Several GST isoenzymes have been reported to facilitate S-glutathionylation reactions. In particular, GSTP1-1 has been shown to catalyze glutathionylation of numerous cellular proteins, particularly under oxidative stress conditions both in vitro [9,47,48] and in vivo [10,49].

Peroxiredoxins (Prdxs) are important thiol-dependent peroxidase enzymes that are ubiquitously expressed and are known targets for GSTP1-1 mediated reversible S-glutathionylation. They perform their antioxidant functions by using intracellular thiols to catalyze the reduction of H_2O_2, and other alkyl hydroperoxides. There are two major sub-classes of peroxiredoxins, 1-cys Prdx (commonly known as Prdx VI) and 2-cys Prdx. It has been shown that the catalytically active cysteine residue of Prdx VI undergoes oxidation and results in the loss of peroxidase activity. The heterodimerization of Prdx VI with GSTP1-1 facilitates the S-glutathionylation of the previously oxidized catalytic cysteine residue and restores the enzyme's peroxidase activity [50]. Interestingly, studies suggest that polymorphic variants of GSTP1-1 may differentially mediate the activation of Prdx VI and hence influence an individual's response to oxidant stress. For example, GSTP1-1A, is the most abundant variant of GSTP1-1 and shows a higher affinity for Prdx VI than those of GSTP1-1B or 1D variants. Furthermore, the transient transfection of GSTP1-1A in MCF-7 breast cancer cells exhibited higher peroxidase activity than that of the GSTP1-1B variant. The variations in catalytic activity between different polymorphic isoforms could be attributed to the relative distance between oxidized cysteine of Prdx VI and the activated GSH bound to the GSTP1-1 molecule [51]. Such information might imply that polymorphisms in the human population can regulate response to oxidative stress and influence factors in responding to such stress.

S-glutathionylation reactions have also been shown to influence the functions of many endoplasmic reticulum (ER) resident proteins involved in regulating the unfolded protein response (UPR). Protein disulfide isomerase (PDI) is a multifaceted ER resident protein that plays a pivotal role in cellular protein folding through its chaperone and isomerase activities. GSTP1-1 has been shown to S-glutathionylate PDI in cells exposed to oxidative or nitrosative stress, including cigarette smoke [52,53]. GSTP1-1-mediated S-glutathionylation of PDI results in impaired isomerase activity and is potentially an upstream signaling event in UPR that could influence the functionality of other client proteins with enormous impact on cellular proteostasis [52]. Although, GSTP1-1 is primarily considered a cytosolic protein, its sub-cellular distribution in the nucleus [54], mitochondria [55], and ER [49] has been reported.

Non-enzymatic S-glutathionylation reactions depend upon the GSH/GSSG ratio within the cell and occur through thiol-disulfide exchange reactions between GSSG and the protein cysteinyl residues, or by the reaction of GSH with an oxidized thiol derivative such as S-nitrosyl (-SNO), thiyl radical (-S•), or sulfenic acid (-SOH) (Figure 3) [56].

The importance of S-glutathionylation as a post-translational modification in modulating cellular processes is underscored by the ubiquity of these reactions in mammalian cells. Indeed, reversible S-glutathionylation reactions have been shown to control an array of cellular processes that include calcium homeostasis, cell signaling, chemotaxis, immune cell function, energy metabolism, and glycolysis [57]. Moreover, deregulated glutathionylation reactions have been shown to be involved in pathogenesis of many human diseases, including cardiovascular, neurological, and metabolic disorders, cataracts, and impaired embryonic development [50]. Collectively, these reactions are critical to the oversight of cellular protection against environmental insults of many different types.

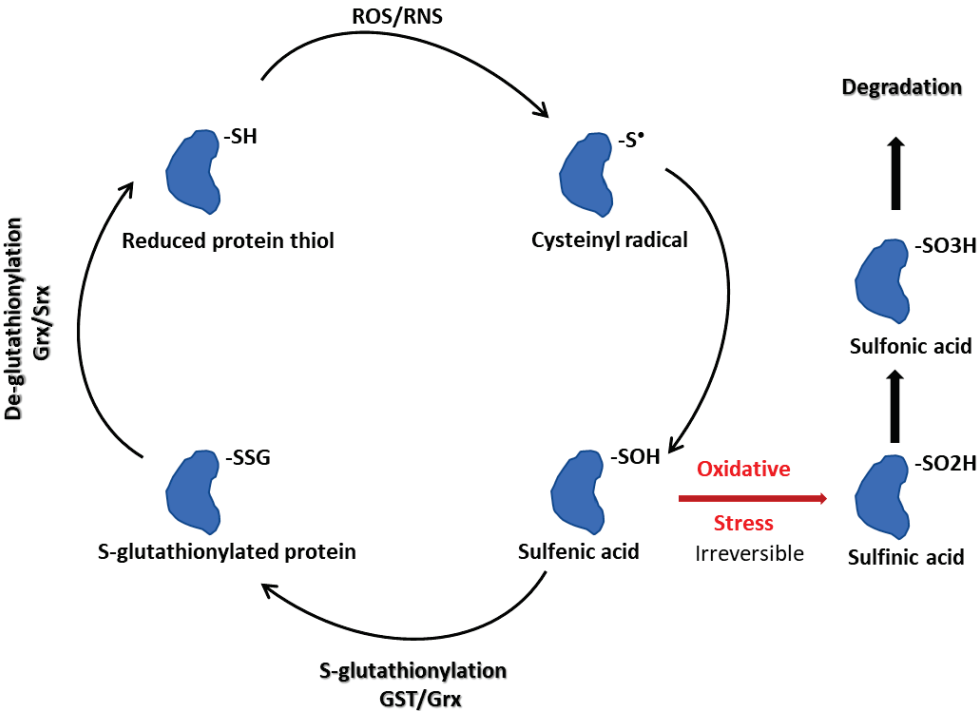

Figure 3. S-glutathionylation schematic.

4. Role in Signaling

Cells are constantly exposed to internal or external stressors that trigger signaling cascades and result in the activation of numerous biological processes such as cell stress response, differentiation, proliferation, and apoptosis. Control of these pathways is complex and is regulated by upstream activation of members of the mitogen-activated protein kinase (MAPK) family. Jun-terminal kinases (JNKs) are a sub-class of MAPK kinases, initially identified as stress-activated protein kinases in mouse liver treated with cycloheximide to induce inflammation and apoptosis [58]. JNKs are transiently activated by several stress stimuli including ROS/RNS, UV irradiation, heat or osmotic shock, or inflammatory cytokines [59]. JNK activation can result in subsequent phosphorylation of multiple nuclear substrates that can include transcription factor c-Jun, activating transcription factor 2 (ATF2), p53, and others, and further stimulate downstream targets and contribute to stress response through alterations in the cell cycle, DNA damage repair, and/or programmed cell death [59].

GSTs exhibit significant ligand-binding properties, and several GST isoenzymes have been shown to interact with stress kinases during regulation of cell signaling pathways responsible for stress response, cell proliferation, and apoptosis. Acting in a non-enzymatic chaperone role, GSTP1-1 negatively regulates signaling by sequestering the JNK kinase in a complex, preventing its capacity to act upon its downstream effectors. In unstressed cells, the basal activity of JNK is necessarily maintained at low levels by sequestration within the protein complex that includes at least GSTP1-1 and JNK [9]. However, under oxidative or chemical stress conditions, GSTP1-1 dissociates from the complex and accumulates in oligomeric structures, resulting in the release and activation of JNK for subsequent phosphorylation of downstream targets regulating cell proliferation and apoptosis [60]. Furthermore, GSTP1-1 has been documented to interact with, and inhibit, tumor necrosis factor (TNF) receptor-associated factor 2 (TRAF2), an upstream regulator of JNK, hence

modulating the MAPK signaling cascade at multiple levels. The inhibitory effects of GSTP1-1 on TRAF2 were shown in human cervical cancer cells, where overexpression of GSTP1-1 suppressed TRAF2-induced activation of both JNK and p38. Additionally, GSTP1-1 has been shown to weaken the effects of TRAF2 on apoptosis signal-regulating kinase-1 (ASK1) and inhibit TRAF2-ASK1-induced apoptosis by suppressing the interaction between these two proteins. In comparison, reducing GSTP1-1 levels triggers TRAF2-ASK1 association and results in the activation of both ASK1 and JNK [61]. Biochemical analysis of the complex revealed that GSTP1-1 interacts with TRAF2 through both G and H sites. Even though the engagement of GSTP1-1 with TRAF2 is dimeric in form, only one monomer is involved in binding with TRAF2 and therefore the other monomer may still perform catalytic functions [62].

Furthermore, GSTP1-1 has been implicated in modulating the transcription factor nuclear factor kappa B (NF-κB) [63], which promotes the activation of pro-inflammatory signaling cascades [64,65]. An in vitro study using unstimulated mouse lung alveolar epithelial cells showed a constitutive association between GSTP1-1 and IκBα, and resulted in the inhibition of NF-κB, potentially by preventing the phosphorylation and ubiquitination of IκBα. However, LPS stimulation led to a rapid decrease in GSTP1-1/IκBα association and increased interaction between GSTP1-1 and IKKβ, along with increased IKKβ-SSG levels. These results were supported by decreased S-glutathionylation of IKKβ after siRNA-mediated knockdown of GSTP1-1 in LPS exposed cells. GSTP1-1 ablation also promoted NF-κB nuclear translocation, transcriptional activity, and pro-inflammatory cytokine production, suggesting a potential inhibitory activity of GSTP1-1 on IKKβ [63]. Similar results to that of GSTP1-1 knockdown were observed by using isotype-selective GSTP1-1 inhibitor TLK 117, which also enhanced NF-κB transcriptional activity and pro-inflammatory cytokine production in LPS-treated cells, indicating that GSTP1-1 catalytic activity is essential in repressing NF-κB activation. Such results suggest that S-glutathionylation of IKK proteins may represent a model through which GSTP1-1 can attenuate NF-κB [63]. The possible mechanistic model anticipates that, in the absence of a stimulus, GSTP1-1 averts IκBα degradation and GSTP1-1-mediated S-glutathionylation shuts down IKK activity, providing a versatile mechanism by which GSTP1-1 represses NF-κB activation.

Notably, the direct interaction of GSTs with MAP Kinases is not limited to GSTP1-1. Other GST isoenzymes have also been shown to be involved in regulating MAPK signaling pathways. For example, GSTM1-1 can bind to, and inhibit, the activity of ASK1. Under stress conditions, the GSTM1-1–ASK1 complex dissociates, causing the oligomerization of GSTM1-1 and the activation of ASK1, which subsequently activates JNK and P38 pathways, leading to apoptosis [66]. Elevated expression of GSTM1-1 has been associated with an impaired clinical response to therapies in a number of different types of cancers.

GSTA1-1 can also bind to and suppress activation of JNK signaling by pro-inflammatory cytokines or oxidative stress, implying a protective role in JNK-mediated apoptosis [67]. More recently, it has been documented that GSTA1-1 negatively regulates the mTOR signaling pathway and the over-expression of the isoenzyme in hepatocellular carcinoma cells showed enhanced AMPK activity and subsequent inhibition of the mTOR pathway. Moreover, cancer patients with high expression of GSTA1-1 in their tumors had better prognoses, and the isoenzyme may serve a protective role against hepatocellular carcinoma by suppressing the AMPK/mTOR-signaling pathway [68]. Additionally, GSTO1-1 has been shown to modulate Akt and MEK1/2 kinase pathways in human neuroblastoma SH-SY5Y cells, where the catalytic activities of the isoenzyme was shown to suppress the activation of these two kinases (either directly or in a complex) to maintain basal levels [69].

5. GST Polymorphism and SARS-CoV-2 (COVID-19) Disease Susceptibility

COVID-19 is a highly infectious disease caused by severe acute respiratory syndrome coronavirus 2 (SARS-CoV-2). The disease emerged in late 2019 and was declared a global pandemic in March 2020 by World Health Organization. Severe illness and death rates were more prevalent in elderly people and in those having underlying health conditions.

However, the majority of the individuals infected with COVID-19 showed mild symptoms and did not require hospitalization. The severity of the infection was driven by the host's response to the disease, triggering a cascade of inflammatory responses and respiratory dysfunction [70]. Individuals with COVID-19 infections have been reported to have markedly higher levels of inflammatory cytokines that trigger a pro-inflammatory response and cause tissue damage, thus contributing to the severity of the disease [71,72]. There is mounting evidence to support the concept that inflammatory disease progression is associated with increased ROS production and resultant oxidative stress. Imbalanced redox homeostasis linked to COVID-19 [73] may contribute to inter-individual differences in patient clinical manifestations, influenced by genetic variation in antioxidant enzyme systems. GST polymorphisms are common in humans and range from frequencies as high as 20% to 60 % in some populations, including the null genotypes of GST Mu and Theta class ($GSTM1^{-/-}$ and $GSTT1^{-/-}$, respectively), whereby individuals lack a catalytically active enzyme [74]. In a study comprising 269 RT-PCR-confirmed COVID-19 patients (with both mild and severe conditions), Abbas et al. [75] reported the relationship between GSTM1 and/or GSTT1 genotypes with COVID-19 vulnerability and its outcome in Northern Indian populations. The results indicated that the frequencies of $GSTM1^{-/-}$, $GSTT1^{-/-}$ and $GSTM1^{-/-}/GSTT1^{-/-}$ were more pronounced in patients with severe COVID-19 symptoms than those with mild. Overall, patients with $GSTT1^{-/-}$ genotypes had higher mortality rates than those with $GSTT1^{+/+}$. In another study, Saadat [76] suggested that individuals with the $GSTT1^{-/-}$ genotype showed a positive association with COVID-19 mortality, but no correlation with COVID-19 prevalence. However, individuals with a low frequency of the GSTT1-null genotype exhibited higher numbers of COVID-19 deaths in East Asian countries.

Tatjana et al. [77] recently reported in Serbian populations that individuals carrying GSTO1*AA and GSTO2*GG polymorphic variants had a significantly increased risk of COVID-19 development as compared to the wild-type genotype. Vesna et al. [78] studied the distribution of GST genotypes among COVID-19 patients of both genders with common COVID-19 co-morbidities such as hypertension, diabetes, and obesity. The results indicated a significant association between GSTP1 and GSTM3 polymorphisms and COVID-19 susceptibility and clinical manifestation. Individuals carrying the GSTP1* (Ile105Val rs1695) or GSTP1* (Ala114Val rs1138272) variants were less prone to develop COVID-19 as compared to the GSTP1 wild type genotypes. Similarly, individuals with GSTM3*AC (rs1332018) variants showed lower odds of developing COVID-19 compared to the wild type GSTM3. The combined GSTP1* and GSTM3* polymorphisms showed a cumulative risk regarding COVID-19 prevalence and severity. These results have shed some light on the involvement of genetic susceptibility in COVID-19 development and further pointed out the multifaceted role of GSTP1-1 as being the dominant GST class in lungs.

Extensive research efforts have documented the relevance of GST polymorphisms in governing cancer susceptibility [65,79,80], and with disease progression or response in various communicable or non-communicable lung diseases [65,81]. In particular, the homozygous GSTP1* Val allele was found to be associated with a reduced risk of asthma and improved lung function [82]. Ding et al. [83] reported the association of GSTT1 and/or GSTM1-null genotypes with an increased risk of developing pulmonary fibrosis in patients with chronic obstructive pulmonary disease (COPD), one of the more important COVID-19 complications characterizing long-term respiratory problems.

Taken together, the polymorphic studies reviewed in the current article revealed that GSTT1 and GSTM1-null genotypes show differential behavior against COVID-19 mortality. Individuals with a lower frequency of GSTT1-null genotype showed higher COVID-19 mortality rates, while GSTM1-null genotype increased the odds of severe disease outcome. The carriers of GSTM3* (rs1332018) and GSTP1* (rs1695) heterozygotes and GSTP1* (rs1138272) Val allele showed a reduced risk of developing COVID-19 as compared to the wild-type carriers. The cumulative effect of GST gene polymorphisms on COVID-19

disease development shows that the individuals with a higher number of risk-associated genotypes had a higher risk of developing COVID-19.

6. GST Inhibitors and Their Therapeutic Importance

GSTs emerged as viable therapeutic targets because specific GST isoenzymes have been shown to be over-expressed in numerous tumors. Involvement in the pathogenesis of other diseases including allergic asthma, multiple sclerosis, and neurodegenerative diseases has also been considered [84–87]. Over the years, attempts have been made to develop specific and potent inhibitors of GSTs with the goal of diminishing tumor growth and enhancement of the cytotoxic effects of existing chemotherapeutic agents [88–91]. The first clinical study was carried out on ethacrynic acid, an approved diuretic drug that nonspecifically inhibits GSTα, GSTμ, and GSTπ isoforms [92]. Although ethacrynic acid showed encouraging inhibitory properties in several cancers, its strong diuretic properties and lack of isozyme specificity made it less favorable for its clinical use as a modulator of anticancer drugs. A further disadvantage was its propensity for enzymatic cleavage as the γ-glu-cys peptide bond in the GSH conjugates is sensitive to γ-glutamyl transpeptidase enzymes. Thus, attempts have been made to develop GSH analogues/prodrugs with improved stability and clinical properties. Newer ethacrynic acid derivatives have been developed and tested for their antiproliferative properties in vitro [93]. Ethacraplatin is a platinum (IV)-based prodrug designed to overcome GST mediated cisplatin resistance. The cisplatin molecule is incorporated between two ethacrynate ligand moieties that inhibit the enzymatic activity of GSTP1-1 and liberates the cisplatin molecule as a consequence of binding, which in turn results in the increased localized diffusion of Pt ions and reversion of platinum drug resistance [94].

NBDHEX (6-(7-nitro-2,1,3-benzoxadiazol-4-ylthio) hexanol) is another inhibitor of GSTP1-1 and other GSTs that has shown anti-proliferative activities in various cancer cells [95,96]. NBDHEX acts as a mechanism-based inhibitor of GSTP1-1, where it is first recognized as a substrate and makes a spontaneous intermediate σ- complex with GSH, which binds very tightly to the enzyme and results in the loss of both the GSH-conjugating activity as well as the ability to form complexes with partner proteins JNK1 and TRAF2 [62,95,97]. NBDHEX was tested on several human osteosarcoma cell lines resistant to cisplatin, doxorubicin or methotrexate and proved to be active against the majority of drug-resistant cell lines [98].

GSH is the most abundant low molecular weight thiol in the cell and a number of GST inhibitors have been designed on the structural basis of the GSH moiety. Ezatiostat hydrochloride (Telintra, TLK199) is a peptidomimetic analogue of GSH and a well characterized inhibitor of GSTP1-1 [15]. Studies conducted on mouse fibroblasts, showed that after intracellular de-esterification to TLK117, it binds to and inhibits GSTP1-1 and can disrupt the binding of GSTP1-1 to JNK. This results in the activation and restoration of JNK and MAPK pathways, which subsequently promotes MAPK-mediated cellular proliferation and differentiation pathways [99]. In addition to GSTP1-1 inhibition, TLK199 has been shown to effectively inhibit multidrug resistance-associated protein 1 MRP1 (encoded by ABCC1 gene), which plays an essential role in multidrug resistance by its ability to effectively export an array of chemotherapeutic and other drugs out of the cell [100]. Studies conducted on MRP1-transfected NIH3T3 mouse fibroblasts with minute GSTP1-1 levels, TLK199 showed significant inhibition of ATP-dependent efflux and resulted in the enhanced retention and subsequent reversal of numerous resistant phenotypes including doxorubicin, daunorubicin, etoposide, mitoxantrone and vincristine [101]. Additionally, in phase I/II clinical studies, TLK199 was tested in patients with myelodysplastic syndrome (MDS), a diverse group of bone marrow stem cell disorders largely affecting individuals with median ages of 65–70 years at diagnosis. The results of ezatiostat treatment in patients with lower to mild risk MDS were encouraging in patients with trilineage cytopenias. Hematologic Improvement-Erythroid (HI-E) was observed in 11 out of 38 patients (29% cases), HI-Neutrophil (HI-N) was reported in 11 out of 26 patients (42% cases), while

HI-Platelet (HI-P) was observed in 12 out of 24 patients (50% cases). HI-E was also reported in a few patients with red blood cells (RBC) transfusion dependency with no prior record of receiving any therapy with hypomethylating agents [15,102]. Overall, the available clinical data showed encouraging results for ezatiostat in MDS patients with favorable tolerability and hematopoietic-promoting activities, indicating the worthiness of the drug for further evaluation in randomized phase II/III clinical trials.

Idiopathic pulmonary fibrosis (IPF) is a chronic and progressive lung fibrotic disease that results in the thickening of alveolar walls and diminished lung function [103]. The pathogenic mechanism of the disease is not yet completely understood. Hence, therapies of IPF still remain a clinical challenge. Changes in the expression levels of GSTs have been reported in pulmonary fibrosis cells, murine models, and in IPF patients [15,81,104]. This suggests an important role for GSTs in pulmonary fibrosis. Oropharyngeal administration of TLK117 has been shown to reduce the severity of pulmonary fibrosis. Furthermore, the synergetic effects of TLK117 with pirfenidone showed better therapeutic outcomes in pulmonary fibrosis mice models than by using pirfenidone alone [104].

To date, clinical experiences with GST inhibitors have been limited. Ethacrynic acid in both animals and humans caused the expected diuretic effects and the Phase II clinical trial was stopped because of severe fluid and electrolyte imbalance [105]. This had less to do with the GST-inhibitory effect but was more related to the thiol-mediated diuresis' impact on the kidney [106,107]. In Phase I/II clinical trials, Telintra was dose-limited by the unusual toxicity of patients displaying unpleasant sulfurous odors, primarily because of metabolism of the peptidomimetic [15]. While there are now reports of the involvement of GST isozymes in myeloproliferation, none of the GST inhibitors so far developed appear to be restricted in their pharmacological effects by myelotoxicities. In summary, the rodent model and early clinical experiences with direct GST-inhibitory drugs would suggest that neither acute nor chronic treatments are accompanied by serious dose-limiting toxicities.

Canfosfamide (TLK 286, TELCYTA) is a glutathione analogue prodrug that is preferentially activated by GSTP1-1 into a vinyl sulfone derivative of the GSH backbone and an alkylating metabolite phosphorodiamidate that spontaneously forms aziridinium ring structures [108–110]. The rationale behind designing this prodrug was to address the issue of anticancer drug resistance due to overexpression of GSTP1-1 in many tumors and to limit the off-target adverse effects. In vitro studies showed that TLK286 had higher antiproliferative activity in cells overexpressing GSTP1-1. In vivo studies using xenograft models in nude mice showed that tumor growth inhibition or regression was positively corelated with GSTP1-1 expression levels in response to TLK286 treatment, and a mild bone marrow toxicity was observed as a side effect [111]. These promising results led to several clinical studies where the prodrug was demonstrated to be active and safe, as a single agent or in combination regimens with other established drugs, including anthracyclines, platinums, and taxanes. The clinical efficacy of the prodrug in phase II and III clinical trials was observed in both relapsed patients with ovarian and non-small cell lung cancers, and in the first-line treatment setting in non-small cell lung cancer patients [112,113].

Advances in structural studies have been instrumental in designing isotype-specific inhibitors since different GST isoforms have unique glutathione binding sites [114]. The efforts to use glutathione as a prototype to develop G-site specific inhibitors provides an efficient platform. However, higher levels of intracellular GSH present a challenge for developing G-site-specific inhibitors [115,116]. Shishido et al. have developed GSH derivatives by introducing a sulfonyl fluoride (SF) onto the sulfhydryl group of GSH, GS-ESF, that irreversibly inhibited GSTP1-1 by a covalent bond with Tyr 108 of the isozyme [117]. However, due to the polarity of the GSH moiety, the cell permeability presented a challenge that was addressed by introducing cell-membrane-permeable benzene sulfonyl fluoride (BSF)-type covalent inhibitors [118]. The in vitro studies of these covalent inhibitors showed a prolonged inactivation of the GSTP1-1 in human non-small-cell lung adenocarcinoma cells, which served as lead compounds for the further development of potent inhibitors of GSTP1-1 in cancer.

A library of 20 dichlorotriazine probes was synthesized by Crawford et al. via tosylating 4-pent-yn-1-ol and evaluated for covalent protein labeling in Hela cell lysates [119]. Of all the compounds investigated, only one showed the potency and specificity for covalent modification of GSTP1-1 in cellular context. Mass spectrometry and mutagenesis analysis identified Y108 as the site of covalent modification of GSTP1-1 by LAS17, thus providing a unique mode of irreversible inhibition by targeting a functional tyrosine residue (Y108). Cell cultures treated with LAS17 showed impaired GST activity and reduced cell survival [120]. Daily administration of LAS17 significantly reduced breast tumor xenograft growth.

More recently Jeffery et al. [121] introduced sulfur-triazole exchange (SuTEx) chemistry as an adaptive platform for developing covalent probes with broad applications for chemical proteomics and protein ligand discovery purposes. They have previously demonstrated that modifications to the triazole leaving group can equip sulfonyl probes with enhanced chemoselectivity for tyrosines (over other nucleophilic residues). By using these probes, they identified that the tyrosine residues with enhanced nucleophilicity are more enriched in enzymatic, protein–protein interactions and nucleotide recognition domains [89]. GSTP1-1 has a reactive tyrosine Y8 in its active site and a known site for phosphorylation [122]. By using SuTEx fragments, they discovered JWB152 and JWB198 as efficient ligands of GSTP1-1 Y8. In vitro studies revealed equivalent inhibitory activities for both ligands, however, only JWB198 could ligand the Y8 site of GSTP1-1 in live cells. Proteome-wide reactivity evaluations of JWB198 were encouraging as it maintained ~70% blockade of GSTP1-1 Y8 in live DM93 cells while being substantially less reactive to the other tyrosine residues within the protein [121].

7. Conclusions

The various functional properties of GSTs have drawn a lot of attention from researchers all over the world for decades. Initially, the enzymes were best known for their catalytic functions in the detoxification process of endogenously produced and or xenobiotic electrophiles. However, advances in the field have brought research to focus on additional biologically important roles ascribed to this versatile enzyme family including cell signaling and post-translational modifications, as well as conferring resistance to chemotherapy, since many GST isoforms have been shown to be overexpressed in numerous cancers. In this context, it is not surprising that a large number of GST inhibitors and prodrugs have been designed and tested for their therapeutic applications. Some of these inhibitors have entered into phase II/III clinical trials, and in the future we may welcome the approval of GST inhibitors/prodrugs as therapies for patients. Moreover, the data on the effects of GST genetic polymorphisms on COVID-19 disease severity and clinical manifestations is inconclusive, but it may add to our understanding of the risk factors that contribute to the severity of the disease and may potentially be useful for better selecting targeted pharmacological strategies for individual COVID-19 patient needs.

8. Perspectives

There has been much progress since the discovery and early descriptions of GST isozymes in the 1960s. Their role in detoxification have been described in detail and the isozyme family provides a broad-ranging capacity to conjugate small electrophilic chemicals with GSH. While the early years focused attention on the catalytic properties of isozymes and their organ distribution, subsequent publications have served to exemplify their ligand binding properties, influence on cell signaling, thioltransferase activities and their general involvement in human pathologies. Pharmacology, particularly in cancer, has produced a variety of small molecular drugs that either inhibit GST pathways or serve as prodrugs that might be activated by GST. Since cancer is characterized by aberrant energy production and signaling pathways, as well as maintaining a redox homeostasis distinct from normal cells, there has been much interest in how GST expression patterns may differ in malignant disease and how they might be targeted. Many types of cancer and drug-resistant tumor cells express extremely high levels of GST, particularly GSTP, and

oncology studies continue to extend the role of this isozyme in regulating signaling pathway cascades. Some of these studies consider the involvement of GST in regulating energy production and may yield information pertinent to how cancer cells use glycolysis versus the pentose phosphate pathway, the so-called Warburg effect. Moreover, post-translational modification of the proteome extends structure/function properties of many proteins, and the involvement of, for example, GSTP1-1 and GST omega in S-glutathionylation and deglutathionylation reactions. There is a continually expanding literature documenting the substantial corpus of proteins that are subject to this cysteine modification. In brief, despite the nearly 60 years of published studies documenting GST, there still remains a significant amount to be learned about this ubiquitous and adaptable family of enzymes.

Funding: This work was supported by grants from National Institutes of Health 5P20GM103542—South Carolina COBRE in Oxidants, Redox Balance and Stress Signaling, the South Carolina Centers of Economic Excellence program, and American Cancer Society Institutional Research Grant (ACS-IRG) IRG-19-137-20.

Institutional Review Board Statement: Not applicable.

Informed Consent Statement: Not applicable.

Data Availability Statement: Not applicable.

Conflicts of Interest: The authors declare no conflict of interest.

References

1. Hayes, J.D.; Flanagan, J.U.; Jowsey, I.R. Glutathione transferases. *Annu. Rev. Pharmacol. Toxicol.* **2005**, *45*, 51–88. [CrossRef] [PubMed]
2. Mannervik, B.; Board, P.G.; Hayes, J.D.; Listowsky, I.; Pearson, W.R. Nomenclature for Mammalian Soluble Glutathione Transferases. *Methods Enzymol.* **2005**, *401*, 1–8. [PubMed]
3. Townsend, D.M.; Tew, K.D. Cancer Drugs, Genetic Variation and the Glutathione-S-Transferase Gene Family. *Am. J. PharmacoGenomics* **2003**, *3*, 157–172. [CrossRef] [PubMed]
4. Josephy, P.D.; Mannervik, B. *Molecular Toxicology*; Oxford University Press on Demand: New York, NY, USA, 2006.
5. Mannervik, B.; Danielson, U.H. Glutathione transferases—Structure and catalytic activity. *Crit. Rev. Biochem.* **1988**, *23*, 283–337. [CrossRef]
6. Buratti, F.M.; Darney, K.; Vichi, S.; Turco, L.; Di Consiglio, E.; Lautz, L.S.; Béchaux, C.; Dorne, J.-L.C.M.; Testai, E. Human variability in glutathione-S-transferase activities, tissue distribution and major polymorphic variants: Meta-analysis and implication for chemical risk assessment. *Toxicol. Lett.* **2020**, *337*, 78–90. [CrossRef]
7. Hayes, J.D.; Pulford, D.J. The glutathione S-transferase supergene family: Regulation of GST and the contribution of the isoenzymes to cancer chemoprotection and drug resistance. *Crit. Rev. Biochem. Mol. Biol.* **1995**, *30*, 445–600. [CrossRef]
8. Tew, K.D.; Townsend, D.M. Regulatory functions of glutathione S-transferase P1-1 unrelated to detoxification. *Drug Metab. Rev.* **2011**, *43*, 179–193. [CrossRef]
9. Zhang, J.; Ye, Z.-W.; Singh, S.; Townsend, D.M.; Tew, K.D. An evolving understanding of the S-glutathionylation cycle in pathways of redox regulation. *Free. Radic. Biol. Med.* **2018**, *120*, 204–216. [CrossRef]
10. Adler, V.; Yin, Z.; Fuchs, S.Y.; Benezra, M.; Rosario, L.; Tew, K.D.; Pincus, M.R.; Sardana, M.; Henderson, C.J.; Wolf, C.R.; et al. Regulation of JNK signaling by GSTp. *EMBO J.* **1999**, *18*, 1321–1334. [CrossRef]
11. Townsend, D.M.; Manevich, Y.; He, L.; Hutchens, S.; Pazoles, C.J.; Tew, K.D. Novel role for glutathione S-transferase pi. Regulator of protein S-Glutathionylation following oxidative and nitrosative stress. *J. Biol. Chem.* **2009**, *284*, 436–445. [CrossRef]
12. Schisselbauer, J.C.; Silber, R.; Papadopoulos, E.; Abrams, K.; LaCreta, F.P.; Tew, K.D. Characterization of glutathione S-transferase expression in lymphocytes from chronic lymphocytic leukemia patients. *Cancer Res* **1990**, *50*, 3562–3568. [PubMed]
13. Townsend, D.M.; Shen, H.; Staros, A.L.; Gaté, L.; Tew, K.D. Efficacy of a glutathione S-transferase pi-activated prodrug in platinum-resistant ovarian cancer cells. *Mol. Cancer Ther.* **2002**, *1*, 1089–1095. [PubMed]
14. Zhang, J.; Ye, Z.-W.; Chen, W.; Culpepper, J.; Jiang, H.; Ball, L.E.; Mehrotra, S.; Blumental-Perry, A.; Tew, K.D.; Townsend, D.M. Altered redox regulation and S-glutathionylation of BiP contribute to bortezomib resistance in multiple myeloma. *Free. Radic. Biol. Med.* **2020**, *160*, 755–767. [CrossRef] [PubMed]
15. Townsend, D.M.; Findlay, V.L.; Tew, K.D. Glutathione S-Transferases as Regulators of Kinase Pathways and Anticancer Drug Targets. *Methods Enzymol.* **2005**, *401*, 287–307.
16. Zhang, J.; Ye, Z.-W.; Janssen-Heininger, Y.; Townsend, D.M.; Tew, K.D. Development of Telintra as an Inhibitor of Glutathione S-Transferase P. *Handb. Exp. Pharmacol.* **2021**, *264*, 71–91. [PubMed]
17. Zimniak, P. Detoxification reactions: Relevance to aging. *Ageing Res. Rev.* **2008**, *7*, 281–300. [CrossRef] [PubMed]

18. Hurst, R.; Bao, Y.; Jemth, P.; Mannervik, B.; Williamson, G. Phospholipid hydroperoxide glutathione peroxidase activity of human glutathione transferases. *Biochem. J.* **1998**, *332*, 97–100. [CrossRef]
19. Yang, Y.; Sharma, R.; Zimniak, P.; Awasthi, Y.C. Role of alpha class glutathione S-transferases as antioxidant enzymes in rodent tissues. *Toxicol. Appl. Pharmacol.* **2002**, *182*, 105–115. [CrossRef]
20. Hiratsuka, A.; Yamane, H.; Yamazaki, S.; Ozawa, N.; Watabe, T. Subunit Ya-specific Glutathione Peroxidase Activity toward Cholesterol 7-Hydroperoxides of Glutathione S-Transferases in Cytosols from Rat Liver and Skin. *J. Biol. Chem.* **1997**, *272*, 4763–4769. [CrossRef]
21. Singhal, S.S.; Singh, S.P.; Singhal, P.; Horne, D.; Singhal, J.; Awasthi, S. Antioxidant role of glutathione S-transferases: 4-Hydroxynonenal, a key molecule in stress-mediated signaling. *Toxicol. Appl. Pharmacol.* **2015**, *289*, 361–370. [CrossRef]
22. Dwivedi, S.; Sharma, A.; Patrick, B.; Sharma, R.; Awasthi, Y.C. Role of 4-hydroxynonenal and its metabolites in signaling. *Redox Rep.* **2007**, *12*, 4–10. [CrossRef] [PubMed]
23. Ålin, P.; Danielson, U.H.; Mannervik, B. 4-Hydroxyalk-2-enals are substrates for glutathione transferase. *FEBS Lett.* **1985**, *179*, 267–270. [CrossRef] [PubMed]
24. Hubatsch, I.; Ridderström, M.; Mannervik, B. Human glutathione transferase A4-4: An alpha class enzyme with high catalytic efficiency in the conjugation of 4-hydroxynonenal and other genotoxic products of lipid peroxidation. *Biochem. J.* **1998**, *330*, 175–179. [CrossRef] [PubMed]
25. Awasthi, S.; Cheng, J.; Singhal, S.S.; Saini, M.K.; Pandya, U.; Pikula, S.; Bandorowicz-Pikula, J.; Singh, S.V.; Zimniak, P.; Awasthi, Y.C. Novel function of human RLIP76: ATP-dependent transport of glutathione conjugates and doxorubicin. *Biochemistry* **2000**, *39*, 9327–9334. [CrossRef]
26. Cheng, J.-Z.; Sharma, R.; Yang, Y.; Singhal, S.S.; Sharma, A.; Saini, M.K.; Singh, S.V.; Zimniak, P.; Awasthi, S.; Awasthi, Y.C. Accelerated Metabolism and Exclusion of 4-Hydroxynonenal through Induction of RLIP76 and hGST5.8 Is an Early Adaptive Response of Cells to Heat and Oxidative Stress. *J. Biol. Chem.* **2001**, *276*, 41213–41223. [CrossRef]
27. Wheeler, J.B.; Stourman, N.V.; Thier, R.; Dommermuth, A.; Vuilleumier, S.; Rose, J.A.; Armstrong, R.N.; Guengerich, F.P. Conjugation of Haloalkanes by Bacterial and Mammalian Glutathione Transferases: Mono- and Dihalomethanes. *Chem. Res. Toxicol.* **2001**, *14*, 1118–1127. [CrossRef]
28. Guengerich, F.P.; McCormick, W.A.; Wheeler, J.B. Analysis of the kinetic mechanism of haloalkane conjugation by mammalian theta-class glutathione transferases. *Chem. Res. Toxicol.* **2003**, *16*, 1493–1499. [CrossRef]
29. Zhang, J.; Ye, Z.-W.; Tew, K.D.; Townsend, D.M. Cisplatin chemotherapy and renal function. *Adv. Cancer Res.* **2021**, *152*, 305–327.
30. Townsend, D.M.; Hanigan, M.H. Inhibition of gamma-glutamyl transpeptidase or cysteine S-conjugate beta-lyase activity blocks the nephrotoxicity of cisplatin in mice. *J. Pharmacol. Exp. Ther.* **2002**, *300*, 142–148. [CrossRef]
31. Townsend, D.M.; Deng, M.; Zhang, L.; Lapus, M.G.; Hanigan, M.H. Metabolism of Cisplatin to a Nephrotoxin in Proximal Tubule Cells. *J. Am. Soc. Nephrol.* **2003**, *14*, 1–10. [CrossRef]
32. Townsend, D.M.; Marto, J.A.; Deng, M.; Macdonald, T.J.; Hanigan, M.H. High Pressure Liquid Chromatography and Mass Spectrometry Characterization of the Nephrotoxic Biotransformation Products of Cisplatin. *Drug Metab. Dispos.* **2003**, *31*, 705–713. [CrossRef] [PubMed]
33. Townsend, D.M.; Tew, K.D.; He, L.; King, J.B.; Hanigan, M.H. Role of glutathione S-transferase Pi in cisplatin-induced nephrotoxicity. *Biomed. Pharmacother.* **2009**, *63*, 79–85. [CrossRef] [PubMed]
34. Jenderny, S.; Lin, H.; Garrett, T.; Tew, K.D.; Townsend, D.M. Protective effects of a glutathione disulfide mimetic (NOV-002) against cisplatin induced kidney toxicity. *Biomed. Pharmacother.* **2010**, *64*, 73–76. [CrossRef]
35. Surh, Y.-J.; Kundu, J.K.; Na, H.-K. Nrf2 as a Master Redox Switch in Turning on the Cellular Signaling Involved in the Induction of Cytoprotective Genes by Some Chemopreventive Phytochemicals. *Planta Medica* **2008**, *74*, 1526–1539. [CrossRef] [PubMed]
36. Nguyen, T.; Nioi, P.; Pickett, C.B. The Nrf2-antioxidant response element signaling pathway and its activation by oxidative stress. *J. Biol. Chem.* **2009**, *284*, 13291–13295. [CrossRef] [PubMed]
37. Kim, S.G.; Lee, S.J. PI3K, RSK, and mTOR Signal Networks for the GST Gene Regulation. *Toxicol. Sci.* **2006**, *96*, 206–213. [CrossRef] [PubMed]
38. Hayes, J.D.; Dinkova-Kostova, A.T.; Tew, K.D. Oxidative Stress in Cancer. *Cancer Cell* **2020**, *38*, 167–197. [CrossRef]
39. Gallogly, M.M.; Starke, D.W.; Mieyal, J.J. Mechanistic and kinetic details of catalysis of thiol-disulfide exchange by glutaredoxins and potential mechanisms of regulation. *Antioxid. Redox Signal.* **2009**, *11*, 1059–1081. [CrossRef]
40. Graminski, G.F.; Kubo, Y.; Armstrong, R.N. Spectroscopic and kinetic evidence for the thiolate anion of glutathione at the active site of glutathione S-transferase. *Biochemistry* **1989**, *28*, 3562–3568. [CrossRef]
41. Ghezzi, P. Regulation of protein function by glutathionylation. *Free Radic. Res.* **2005**, *39*, 573–580. [CrossRef]
42. Arnér, E.S.J.; Holmgren, A. Physiological functions of thioredoxin and thioredoxin reductase. *Eur. J. BioChem.* **2000**, *267*, 6102–6109. [CrossRef] [PubMed]
43. Fernandes, A.P.; Holmgren, A. Glutaredoxins: Glutathione-Dependent Redox Enzymes with Functions Far Beyond a Simple Thioredoxin Backup System. *Antioxidants Redox Signal.* **2004**, *6*, 63–74. [CrossRef] [PubMed]
44. Findlay, V.J.; Townsend, D.M.; Morris, T.E.; Fraser, J.P.; He, L.; Tew, K.D. A Novel Role for Human Sulfiredoxin in the Reversal of Glutathionylation. *Cancer Res.* **2006**, *66*, 6800–6806. [CrossRef] [PubMed]
45. Gallogly, M.M.; Mieyal, J.J. Mechanisms of reversible protein glutathionylation in redox signaling and oxidative stress. *Curr. Opin. Pharmacol.* **2007**, *7*, 381–391. [CrossRef]

46. Atkins, W.M.; Wang, R.W.; Bird, A.W.; Newton, D.J.; Lu, A.Y. The catalytic mechanism of glutathione S-transferase (GST). Spectroscopic determination of the pKa of Tyr-9 in rat alpha 1-1 GST. *J. Biol. Chem.* **1993**, *268*, 19188–19191. [CrossRef]
47. Manevich, Y.; Feinstein, S.I.; Fisher, A.B. Activation of the antioxidant enzyme 1-CYS peroxiredoxin requires glutathionylation mediated by heterodimerization with pi GST. *Proc. Natl. Acad. Sci. USA* **2004**, *101*, 3780–3785. [CrossRef]
48. Klaus, A.; Zorman, S.; Berthier, A.; Polge, C.; Ramirez, S.; Michelland, S.; Seve, M.; Vertommen, D.; Rider, M.; Lentze, N.; et al. Glutathione S-Transferases Interact with AMP-Activated Protein Kinase: Evidence for S-Glutathionylation and Activation In Vitro. *PLoS ONE* **2013**, *8*, e62497. [CrossRef]
49. Ye, Z.-W.; Zhang, J.; Ancrum, T.; Manevich, Y.; Townsend, D.M.; Tew, K.D. Glutathione*S*-Transferase P-Mediated Protein S-Glutathionylation of Resident Endoplasmic Reticulum Proteins Influences Sensitivity to Drug-Induced Unfolded Protein Response. *Antioxidants Redox Signal.* **2017**, *26*, 247–261. [CrossRef]
50. Manevich, Y.; Fisher, A.B. Peroxiredoxin 6, a 1-Cys peroxiredoxin, functions in antioxidant defense and lung phospholipid metabolism. *Free. Radic. Biol. Med.* **2005**, *38*, 1422–1432. [CrossRef]
51. Manevich, Y.; Hutchens, S.; Tew, K.; Townsend, D. Allelic variants of glutathione S-transferase P1-1 differentially mediate the peroxidase function of peroxiredoxin VI and alter membrane lipid peroxidation. *Free. Radic. Biol. Med.* **2012**, *54*, 62–70. [CrossRef]
52. Townsend, D.M. S-Glutathionylation: Indicator of Cell Stress and Regulator of the Unfolded Protein Response. *Mol. Interv.* **2007**, *7*, 313–324. [CrossRef] [PubMed]
53. Kenche, H.; Ye, Z.W.; Vedagiri, K.; Richards, D.M.; Gao, X.H.; Tew, K.D.; Townsend, D.M.; Blumental-Perry, A. Adverse Outcomes Associated with Cigarette Smoke Radicals Related to Damage to Protein-disulfide Isomerase. *J. Biol. Chem.* **2016**, *291*, 4763–4778. [CrossRef] [PubMed]
54. Kamada, K.; Goto, S.; Okunaga, T.; Ihara, Y.; Tsuji, K.; Kawai, Y.; Uchida, K.; Osawa, T.; Matsuo, T.; Nagata, I.; et al. Nuclear glutathione S-transferase π prevents apoptosis by reducing the oxidative stress-induced formation of exocyclic dna products. *Free. Radic. Biol. Med.* **2004**, *37*, 1875–1884. [CrossRef] [PubMed]
55. Goto, S.; Kawakatsu, M.; Izumi, S.-I.; Urata, Y.; Kageyama, K.; Ihara, Y.; Koji, T.; Kondo, T. Glutathione S-transferase π localizes in mitochondria and protects against oxidative stress. *Free. Radic. Biol. Med.* **2009**, *46*, 1392–1403. [CrossRef] [PubMed]
56. Janssen-Heininger, Y.M.W.; Nolin, J.; Hoffman, S.M.; van der Velden, J.; Tully, J.E.; Lahue, K.G.; Abdalla, S.T.; Chapman, D.; Reynaert, N.L.; van der Vliet, A.; et al. Emerging mechanisms of glutathione-dependent chemistry in biology and disease. *J. Cell. Biochem.* **2013**, *114*, 1962–1968. [CrossRef]
57. Mailloux, R.J.; Gill, R.; Young, A. Chapter 13—Protein S-glutathionylation and the regulation of cellular functions. In *Oxidative Stress*; Sies, H., Ed.; Academic Press: New York, NY, USA, 2020; pp. 217–247.
58. Xia, Z.; Dickens, M.; Raingeaud, J.; Davis, R.J.; Greenberg, M.E. Opposing Effects of ERK and JNK-p38 MAP Kinases on Apoptosis. *Science* **1995**, *270*, 1326–1331. [CrossRef]
59. Davis, R.J. Signal transduction by the JNK group of MAP kinases. *Cell* **2000**, *103*, 239–252. [CrossRef]
60. Tew, K.D.; Townsend, D.M.; Palumbo, C.; De Luca, A.; Rosato, N.; Forgione, M.; Rotili, D.; Caccuri, A.M.; Weich, N.; Ferri, C.; et al. Glutathione-S-Transferases As Determinants of Cell Survival and Death. *Antioxidants Redox Signal.* **2012**, *17*, 1728–1737. [CrossRef]
61. Wu, Y.; Fan, Y.; Xue, B.; Luo, L.; Shen, J.; Zhang, S.; Jiang, Y.; Yin, Z. Human glutathione S-transferase P1-1 interacts with TRAF2 and regulates TRAF2–ASK1 signals. *Oncogene* **2006**, *25*, 5787–5800. [CrossRef]
62. De Luca, A.; Mei, G.; Rosato, N.; Nicolai, E.; Federici, L.; Palumbo, C.; Pastore, A.; Serra, M.; Caccuri, A.M. The fine-tuning of TRAF2–GSTP1-1 interaction: Effect of ligand binding and in situ detection of the complex. *Cell Death Dis.* **2014**, *5*, e1015. [CrossRef]
63. Jones, J.T.; Qian, X.; van der Velden, J.L.; Chia, S.B.; McMillan, D.H.; Flemer, S.; Hoffman, S.M.; Lahue, K.G.; Schneider, R.W.; Nolin, J.D.; et al. Glutathione S-transferase pi modulates NF-κB activation and pro-inflammatory responses in lung epithelial cells. *Redox Biol.* **2016**, *8*, 375–382. [CrossRef] [PubMed]
64. Karin, M.; Lin, A. NF-kappaB at the crossroads of life and death. *Nat. Immunol.* **2002**, *3*, 221–227. [CrossRef] [PubMed]
65. van de Wetering, C.; Elko, E.; Berg, M.; Schiffers, C.H.; Stylianidis, V.; van den Berge, M.; Nawijn, M.C.; Wouters, E.F.; Janssen-Heininger, Y.M.; Reynaert, N.L. Glutathione S-transferases and their implications in the lung diseases asthma and chronic obstructive pulmonary disease: Early life susceptibility? *Redox Biol.* **2021**, *43*, 101995. [CrossRef]
66. Dorion, S.; Lambert, H.; Landry, J. Activation of the p38 signaling pathway by heat shock involves the dissociation of glutathione S-transferase Mu from Ask1. *J. Biol. Chem.* **2002**, *277*, 30792–30797. [CrossRef]
67. Romero, L.; Andrews, K.; Ng, L.; O'Rourke, K.; Maslen, A.; Kirby, G. Human GSTA1-1 reduces c-Jun N-terminal kinase signalling and apoptosis in Caco-2 cells. *Biochem. J.* **2006**, *400*, 135–141. [CrossRef] [PubMed]
68. Liu, X.; Sui, X.; Zhang, C.; Wei, K.; Bao, Y.; Xiong, J.; Zhou, Z.; Chen, Z.; Wang, C.; Zhu, H.; et al. Glutathione S-transferase A1 suppresses tumor progression and indicates better prognosis of human primary hepatocellular carcinoma. *J. Cancer* **2020**, *11*, 83–91. [CrossRef]
69. Saisawang, C.; Wongsantichon, J.; Robinson, R.C.; Ketterman, A.J. Glutathione transferase Omega 1-1 (GSTO1-1) modulates Akt and MEK1/2 signaling in human neuroblastoma cell SH-SY5Y. *Proteins* **2019**, *87*, 588–595. [CrossRef]
70. Yuki, K.; Fujiogi, M.; Koutsogiannaki, S. COVID-19 pathophysiology: A review. *Clin. Immunol.* **2020**, *215*, 108427. [CrossRef]
71. Merad, M.; Martin, J.C. Pathological inflammation in patients with COVID-19: A key role for monocytes and macrophages. *Nat. Rev. Immunol.* **2020**, *20*, 355–362. [CrossRef]

72. Gadotti, A.C.; Lipinski, A.L.; Vasconcellos, F.T.; Marqueze, L.F.; Cunha, E.B.; Campos, A.C.; Oliveira, C.F.; Amaral, A.N.; Baena, C.P.; Telles, J.P.; et al. Susceptibility of the patients infected with Sars-Cov2 to oxidative stress and possible interplay with severity of the disease. *Free Radic. Biol. Med.* **2021**, *165*, 184–190. [CrossRef]
73. Polonikov, A. Endogenous Deficiency of Glutathione as the Most Likely Cause of Serious Manifestations and Death in COVID-19 Patients. *ACS Infect. Dis.* **2020**, *6*, 1558–1562. [CrossRef] [PubMed]
74. Nissar, S.; Sameer, A.S.; Rasool, R.; Chowdri, N.A.; Rashid, F.J.J.C.M. Glutathione S Transferases: Biochemistry, Polymorphism and Role in Colorectal Carcinogenesis. *J. Carcinog. Mutagen* **2017**, *8*, 287. [CrossRef]
75. Abbas, M.; Verma, S.; Verma, S.; Siddiqui, S.; Khan, F.H.; Raza, S.T.; Siddiqi, Z.; Eba, A.; Mahdi, F. Association of GSTM1 and GSTT1 gene polymorphisms with COVID-19 susceptibility and its outcome. *J. Med. Virol.* **2021**, *93*, 5446–5451. [CrossRef]
76. Saadat, M. An evidence for correlation between the glutathione S-transferase T1 (GSTT1) polymorphism and outcome of COVID-19. *Clin. Chim. Acta.* **2020**, *508*, 213–216. [CrossRef] [PubMed]
77. Djukic, T.; Stevanovic, G.; Coric, V.; Bukumiric, Z.; Pljesa-Ercegovac, M.; Matic, M.; Jerotic, D.; Todorovic, N.; Asanin, M.; Ercegovac, M.; et al. GSTO1, GSTO2 and ACE2 Polymorphisms Modify Susceptibility to Developing COVID-19. *J. Pers. Med.* **2022**, *12*, 458. [CrossRef]
78. Coric, V.; Milosevic, I.; Djukic, T.; Bukumiric, Z.; Savic-Radojevic, A.; Matic, M.; Jerotic, D.; Todorovic, N.; Asanin, M.; Ercegovac, M.; et al. GSTP1 and GSTM3 Variant Alleles Affect Susceptibility and Severity of COVID-19. *Front. Mol. Biosci.* **2021**, *8*, 747493. [CrossRef]
79. Nørskov, M.S.; Dahl, M.; Tybjærg-Hansen, A. Genetic Variation in GSTP1, Lung Function, Risk of Lung Cancer, and Mortality. *J. Thorac. Oncol.* **2017**, *12*, 1664–1672. [CrossRef]
80. Pljesa-Ercegovac, M.; Savic-Radojevic, A.; Matic, M.; Coric, V.; Djukic, T.; Radic, T.; Simic, T. Glutathione Transferases: Potential Targets to Overcome Chemoresistance in Solid Tumors. *Int. J. Mol. Sci.* **2018**, *19*, 3785. [CrossRef]
81. McMillan, D.H.; van der Velden, J.L.; Lahue, K.G.; Qian, X.; Schneider, R.W.; Iberg, M.S.; Nolin, J.D.; Abdalla, S.; Casey, D.T.; Tew, K.D.; et al. Attenuation of lung fibrosis in mice with a clinically relevant inhibitor of glutathione-S-transferase π. *JCI Insight* **2016**, *1*, e85717. [CrossRef]
82. Fryer, A.A.; Bianco, A.; Hepple, M.; Jones, P.W.; Strange, R.C.; Spiteri, M.A. Polymorphism at the Glutathione *S*-transferase GSTP1 Locus. *Am. J. Respir. Crit. Care Med.* **2000**, *161*, 1437–1442. [CrossRef]
83. Ding, Z.; Wang, K.; Li, J.; Tan, Q.; Tan, W.; Guo, G. Association between glutathione S-transferase gene M1 and T1 polymorphisms and chronic obstructive pulmonary disease risk: A meta-analysis. *Clin. Genet.* **2018**, *95*, 53–62. [CrossRef] [PubMed]
84. Tew, K.D. Glutathione-associated enzymes in anticancer drug resistance. *Cancer Res.* **1994**, *54*, 4313–4320. [CrossRef] [PubMed]
85. Baez, S.; Segura-Aguilar, J.; Widersten, M.; Johansson, A.-S.; Mannervik, B. Glutathione transferases catalyse the detoxication of oxidized metabolites (o-quinones) of catecholamines and may serve as an antioxidant system preventing degenerative cellular processes. *Biochem. J.* **1997**, *324*, 25–28. [CrossRef] [PubMed]
86. Mapp, C.E.; Fryer, A.A.; De Marzo, N.; Pozzato, V.; Padoan, M.; Boschetto, P.; Strange, R.C.; Hemmingsen, A.; Spiteri, M.A. Glutathione S-transferase GSTP1 is a susceptibility gene for occupational asthma induced by isocyanates. *J. Allergy Clin. Immunol.* **2002**, *109*, 867–872. [CrossRef] [PubMed]
87. Kumar, A.; Dhull, D.K.; Gupta, V.; Channana, P.; Singh, A.; Bhardwaj, M.; Ruhal, P.; Mittal, R. Role of Glutathione-S-transferases in neurological problems. *Expert Opin. Ther. Patents* **2016**, *27*, 299–309. [CrossRef]
88. Robin, S.K.; Ansari, M.; Uppugunduri, C.R.S. Spectrophotometric Screening for Potential Inhibitors of Cytosolic Glutathione S-Transferases. *J. Vis. Exp.* **2020**, *164*, e61347.
89. Wu, J.H.; Batist, G. Glutathione and glutathione analogues; Therapeutic potentials. *Biochim. Biophys. Acta (BBA)-Gen. Subj.* **2013**, *1830*, 3350–3353. [CrossRef]
90. Musdal, Y.; Hegazy, U.M.; Aksoy, Y.; Mannervik, B. FDA-approved drugs and other compounds tested as inhibitors of human glutathione transferase P1-1. *Chem. Interact.* **2013**, *205*, 53–62. [CrossRef]
91. Lee, K.G.Z.; Babak, M.V.; Weiss, A.; Dyson, P.J.; Nowak-Sliwinska, P.; Montagner, D.; Ang, W.H. Development of an Efficient Dual-Action GST-Inhibiting Anticancer Platinum(IV) Prodrug. *Chemmedchem* **2018**, *13*, 1210–1217. [CrossRef]
92. Mulder, G.J.; Ouwerkerk-Mahadevan, S. Modulation of glutathione conjugation in vivo: How to decrease glutathione conjugation in vivo or in intact cellular systems in vitro. *Chem. Interactions* **1997**, *105*, 17–34. [CrossRef]
93. Mignani, S.; El Brahmi, N.; El Kazzouli, S.; Eloy, L.; Courilleau, D.; Caron, J.; Bousmina, M.M.; Caminade, A.M.; Cresteil, T.; Majoral, J.P. A novel class of ethacrynic acid derivatives as promising drug-like potent generation of anticancer agents with established mechanism of action. *Eur. J. Med. Chem.* **2016**, *122*, 656–673. [CrossRef] [PubMed]
94. Parker, L.J.; Italiano, L.C.; Morton, C.J.; Hancock, N.C.; Ascher, D.B.; Aitken, J.B.; Harris, H.H.; Campomanes, P.; Rothlisberger, U.; De Luca, A.; et al. Studies of glutathione transferase P1-1 bound to a platinum(IV)-based anticancer compound reveal the molecular basis of its activation. *Chemistry* **2011**, *17*, 7806–7816. [CrossRef] [PubMed]
95. Turella, P.; Cerella, C.; Filomeni, G.; Bullo, A.; De Maria, F.; Ghibelli, L.; Ciriolo, M.R.; Cianfriglia, M.; Mattei, M.; Federici, G.; et al. Proapoptotic Activity of New Glutathione *S*-Transferase Inhibitors. *Cancer Res* **2005**, *65*, 3751–3761. [CrossRef]
96. Turella, P.; Filomeni, G.; Dupuis, M.L.; Ciriolo, M.R.; Molinari, A.; De Maria, F.; Tombesi, M.; Cianfriglia, M.; Federici, G.; Ricci, G.; et al. A strong glutathione S-transferase inhibitor overcomes the P-glycoprotein-mediated resistance in tumor cells 6-(7-Nitro-2,1,3-benzoxadiazol-4-ylthio)hexanol (NBDHEX) triggers a caspase-dependent apoptosis in MDR1-expressing leukemia cells. *J. Biol. Chem.* **2006**, *281*, 23725–23732. [CrossRef]

97. Sau, A.; Filomeni, G.; Pezzola, S.; D'Aguanno, S.; Tregno, F.P.; Urbani, A.; Serra, M.; Pasello, M.; Picci, P.; Federici, G.; et al. Targeting GSTP1-1 induces JNK activation and leads to apoptosis in cisplatin-sensitive and -resistant human osteosarcoma cell lines. *Mol. Biosyst.* **2011**, *8*, 994–1006. [CrossRef] [PubMed]
98. Pasello, M.; Michelacci, F.; Scionti, I.; Hattinger, C.M.; Zuntini, M.; Caccuri, A.M.; Scotlandi, K.; Picci, P.; Serra, M. Overcoming Glutathione *S*-Transferase P1–Related Cisplatin Resistance in Osteosarcoma. *Cancer Res.* **2008**, *68*, 6661–6668. [CrossRef]
99. Lyons, R.M.; Wilks, S.T.; Young, S.; Brown, G.L. Oral ezatiostat HCl (Telintra®, TLK199) and Idiopathic Chronic Neutropenia (ICN): A case report of complete response of a patient with G-CSF resistant ICN following treatment with ezatiostat, a glutathione S-transferase P1-1 (GSTP1-1) inhibitor. *J. Hematol. Oncol.* **2011**, *4*, 43. [CrossRef]
100. Cole, S.; Bhardwaj, G.; Gerlach, J.H.; Mackie, J.E.; Grant, C.E.; Almquist, K.C.; Stewart, A.J.; Kurz, E.U.; Duncan, A.M.; Deeley, R.G. Overexpression of a transporter gene in a multidrug-resistant human lung cancer cell line. *Science* **1992**, *258*, 1650–1654. [CrossRef]
101. O'Brien, M.L.; Vulevic, B.; Freer, S.; Boyd, J.; Shen, H.; Tew, K.D. Glutathione peptidomimetic drug modulator of multidrug resistance-associated protein. *J. Pharmacol. Exp. Ther.* **1999**, *291*, 1348–1355.
102. Raza, A.; Galili, N.; Callander, N.; Ochoa, L.; Piro, L.; Emanuel, P.; Williams, S.; Burris, H.; Faderl, S.; Estrov, Z.; et al. Phase 1-2a multicenter dose-escalation study of ezatiostat hydrochloride liposomes for injection (Telintra, TLK199), a novel glutathione analog prodrug in patients with myelodysplastic syndrome. *J. Hematol. Oncol.* **2009**, *2*, 20. [CrossRef]
103. Lomas, N.J.; Watts, K.L.; Akram, K.M.; Forsyth, N.R.; Spiteri, M.A. Idiopathic pulmonary fibrosis: Immunohistochemical analysis provides fresh insights into lung tissue remodelling with implications for novel prognostic markers. *Int. J. Clin. Exp. Pathol.* **2012**, *5*, 58–71. [PubMed]
104. He, N.; Bai, S.; Huang, Y.; Xing, Y.; Chen, L.; Yu, F.; Lv, C. Evaluation of Glutathione S-Transferase Inhibition Effects on Idiopathic Pulmonary Fibrosis Therapy with a Near-Infrared Fluorescent Probe in Cell and Mice Models. *Anal. Chem.* **2019**, *91*, 5424–5432. [CrossRef] [PubMed]
105. Tew, K.D.; Gaté, L. Glutathione S-transferases as emerging therapeutic targets. *Expert Opin. Ther. Targets* **2001**, *5*, 477–489. [CrossRef] [PubMed]
106. Molnar, J.; Somberg, J.C. The Clinical Pharmacology of Ethacrynic Acid. *Am. J. Ther.* **2009**, *16*, 86–92. [CrossRef] [PubMed]
107. LaCreta, F.P.; Brennan, J.M.; Nash, S.L.; Comis, R.L.; Tew, K.D.; O'Dwyer, P.J. Pharmakokinetics and bioavailability study of ethacrynic acid as a modulator of drug resistance in patients with cancer. *Experiment* **1994**, *270*, 1186–1191.
108. Lyttle, M.H.; Satyam, A.; Hocker, M.D.; Bauer, K.E.; Caldwell, C.G.; Hui, H.C.; Morgan, A.S.; Mergia, A.; Kauvar, L.M. Glutathione-S-transferase Activates Novel Alkylating Agents. *J. Med. Chem.* **1994**, *37*, 1501–1507. [CrossRef]
109. Dourado, D.F.A.R.; Fernandes, P.; Ramos, M.J.; Mannervik, B. Mechanism of Glutathione Transferase P1-1-Catalyzed Activation of the Prodrug Canfosfamide (TLK286, TELCYTA). *Biochemistry* **2013**, *52*, 8069–8078. [CrossRef]
110. Tew, K.D. TLK-286: A novel glutathione*S*-transferase-activated prodrug. *Expert Opin. Investig. Drugs* **2005**, *14*, 1047–1054. [CrossRef]
111. Morgan, A.S.; Sanderson, P.E.; Borch, R.F.; Tew, K.D.; Niitsu, Y.; Takayama, T.; Von Hoff, D.D.; Izbicka, E.; Mangold, G.; Paul, C.; et al. Tumor efficacy and bone marrow-sparing properties of TER286, a cytotoxin activated by glutathione S-transferase. *Cancer Res.* **1998**, *58*, 2568–2575.
112. Sequist, L.V.; Fidias, P.M.; Temel, J.S.; Kolevska, T.; Rabin, M.S.; Boccia, R.V.; Burris, H.A.; Belt, R.J.; Huberman, M.S.; Melnyk, O.; et al. Phase 1-2a multicenter dose-ranging study of canfosfamide in combination with carboplatin and paclitaxel as first-line therapy for patients with advanced non-small cell lung cancer. *J. Thorac. Oncol.* **2009**, *4*, 1389–1396. [CrossRef]
113. Vergote, I.; Finkler, N.J.; Hall, J.B.; Melnyk, O.; Edwards, R.P.; Jones, M.; Keck, J.G.; Meng, L.; Brown, G.L.; Rankin, E.M.; et al. Randomized Phase III Study of Canfosfamide in Combination With Pegylated Liposomal Doxorubicin Compared With Pegylated Liposomal Doxorubicin Alone in Platinum-Resistant Ovarian Cancer. *Int. J. Gynecol. Cancer* **2010**, *20*, 772–780. [CrossRef] [PubMed]
114. Wu, B.; Dong, D. Human cytosolic glutathione transferases: Structure, function, and drug discovery. *Trends Pharmacol. Sci.* **2012**, *33*, 656–668. [CrossRef] [PubMed]
115. Lushchak, V.I. Glutathione Homeostasis and Functions: Potential Targets for Medical Interventions. *J. Amino Acids* **2012**, *2012*, 736837. [CrossRef]
116. Singh, R.R.; Reindl, K.M. Glutathione S-Transferases in Cancer. *Antioxidants* **2021**, *10*, 701. [CrossRef] [PubMed]
117. Shishido, Y.; Tomoike, F.; Kimura, Y.; Kuwata, K.; Yano, T.; Fukui, K.; Fujikawa, H.; Sekido, Y.; Murakami-Tonami, Y.; Kameda, T.; et al. A covalent G-site inhibitor for glutathione S-transferase Pi ($GSTP_{1-1}$). *Chem. Commun.* **2017**, *53*, 11138–11141. [CrossRef]
118. Shishido, Y.; Tomoike, F.; Kuwata, K.; Fujikawa, H.; Sekido, Y.; Murakami-Tonami, Y.; Kameda, T.; Abe, N.; Kimura, Y.; Shuto, S.; et al. A Covalent Inhibitor for Glutathione S-Transferase Pi (GSTP(1-1)) in Human Cells. *Chembiochem* **2019**, *20*, 900–905. [CrossRef]
119. Crawford, L.A.; Weerapana, E. A tyrosine-reactive irreversible inhibitor for glutathione S-transferase Pi (GSTP1). *Mol. Biosyst.* **2016**, *12*, 1768–1771. [CrossRef]
120. Louie, S.M.; Grossman, E.A.; Crawford, L.A.; Ding, L.; Camarda, R.; Huffman, T.R.; Miyamoto, D.K.; Goga, A.; Weerapana, E.; Nomura, D.K. GSTP1 Is a Driver of Triple-Negative Breast Cancer Cell Metabolism and Pathogenicity. *Cell Chem. Biol.* **2016**, *23*, 567–578. [CrossRef]

121. Hahm, H.S.; Toroitich, E.K.; Borne, A.L.; Brulet, J.W.; Libby, A.H.; Yuan, K.; Ware, T.B.; McCloud, R.L.; Ciancone, A.M.; Hsu, K.-L. Global targeting of functional tyrosines using sulfur-triazole exchange chemistry. *Nat. Chem. Biol.* **2019**, *16*, 150–159. [CrossRef]
122. Okamura, T.; Singh, S.; Buolamwini, J.; Haystead, T.; Friedman, H.; Bigner, D.; Ali-Osman, F. Tyrosine Phosphorylation of the Human Glutathione S-Transferase P1 by Epidermal Growth Factor Receptor. *J. Biol. Chem.* **2009**, *284*, 16979–16989. [CrossRef]

biomolecules

MDPI

Article

Inhibition Analysis and High-Resolution Crystal Structure of *Mus musculus* Glutathione Transferase P1-1

Oleksii Kupreienko [1], Fotini Pouliou [1], Konstantinos Konstandinidis [1], Irene Axarli [1], Eleni Douni [2,3], Anastassios C. Papageorgiou [4] and Nikolaos E. Labrou [1,*]

[1] Laboratory of Enzyme Technology, Department of Biotechnology, School of Applied Biology and Biotechnology, Agricultural University of Athens, 75 Iera Odos Street, 11855 Athens, Greece
[2] Laboratory of Genetics, Department of Biotechnology, School of Applied Biology and Biotechnology, Agricultural University of Athens, 75 Iera Odos Street, 11855 Athens, Greece
[3] Alexander Fleming, Institute for Bioinnovation, Biomedical Sciences Research Center, 16672 Vari, Greece
[4] Turku Bioscience Centre, University of Turku and Åbo Akademi University, 20521 Turku, Finland
* Correspondence: lambrou@aua.gr; Tel./Fax: +30-(210)-5294308

Abstract: Multidrug resistance is a significant barrier that makes anticancer therapies less effective. Glutathione transferases (GSTs) are involved in multidrug resistance mechanisms and play a significant part in the metabolism of alkylating anticancer drugs. The purpose of this study was to screen and select a lead compound with high inhibitory potency against the isoenzyme GSTP1-1 from *Mus musculus* (*Mm*GSTP1-1). The lead compound was selected following the screening of a library of currently approved and registered pesticides that belong to different chemical classes. The results showed that the fungicide iprodione [3-(3,5-dichlorophenyl)-2,4-dioxo-N-propan-2-ylimidazolidine-1-carboxamide] exhibited the highest inhibition potency (IC_{50} = 11.3 ± 0.5 μM) towards *Mm*GSTP1-1. Kinetics analysis revealed that iprodione functions as a mixed-type inhibitor towards glutathione (GSH) and non-competitive inhibitor towards 1-chloro-2,4-dinitrobenzene (CDNB). X-ray crystallography was used to determine the crystal structure of *Mm*GSTP1-1 at 1.28 Å resolution as a complex with S-(p-nitrobenzyl)glutathione (Nb-GSH). The crystal structure was used to map the ligand-binding site of *Mm*GSTP1-1 and to provide structural data of the interaction of the enzyme with iprodione using molecular docking. The results of this study shed light on the inhibition mechanism of *Mm*GSTP1-1 and provide a new compound as a potential lead structure for future drug/inhibitor development.

Keywords: anticancer drugs; cancer; human glutathione transferase P1-1 (hGSTP1-1); glutathione transferase; enzyme inhibition; multidrug resistance; pesticide

Citation: Kupreienko, O.; Pouliou, F.; Konstandinidis, K.; Axarli, I.; Douni, E.; Papageorgiou, A.C.; Labrou, N.E. Inhibition Analysis and High-Resolution Crystal Structure of *Mus musculus* Glutathione Transferase P1-1. *Biomolecules* **2023**, *13*, 613. https://doi.org/10.3390/biom13040613

Academic Editor: Bengt Mannervik

Received: 28 February 2023
Revised: 20 March 2023
Accepted: 22 March 2023
Published: 29 March 2023

1. Introduction

A large superfamily of enzymes known as glutathione transferases (GSTs; EC 2.5.1.18) catalyze the nucleophilic attack of the reduced tripeptide glutathione (GSH, L-Glu-L-Cys-Gly) on nonpolar molecules that contain an electrophilic carbon, oxygen, or sulfur atom [1–3]. GSTs play a crucial role in Phase II of the cell detoxification process and are considered essential components of this process [4–6]. Beyond their primary detoxification function, some GSTs are also involved in the biosynthesis of hormones in mammals, catabolism of amino acids, signalling pathways, synthesis of prostaglandins and leukotrienes, breakdown of reactive oxygen species (ROS), and other significant intracellular processes [3].

GSTs are primarily classified based on their structure and sequence [1]. They are classified into three separate families, cytosolic, mitochondrial, and microsomal GSTs, with members found in various kingdoms and phyla. The cytosolic family is comprised of the following classes: α (alpha), β (beta), δ (delta), ε (epsilon), ζ (zeta), θ (theta), μ (mu), ν (nu), π (pi), σ (sigma), τ (tau), φ (phi), and ω (omega) [1,3,5].

GSTs function as dimers consisting of two similar or different subunits, each with an average sequence length of 200–250 amino acids. Each subunit of GSTs has at least two binding sites, the G-site and the H-site [1,5,7], which are able to bind GSH and the electrophilic substrate, respectively. The G-site is located at the N-terminal region and its structure is strictly conserved among GSTs that belong to different classes. It consists of β-strands (β1, β2, β3, and β4), three of which are antiparallel to each other (β1, β2, and β3). This structural region of the β-strands is sandwiched between α-helices, resulting in a βαβαββα structural motif. The C-terminal region is entirely helical and is formed by five or six α-helices. Some GST classes, such as alpha, omega, tau, and theta may have an additional α-helix. The H-site is located at the C-terminal region. Its structure is less conserved than that of the G-site and contributes to the broad specificity of GSTs towards electrophilic substrates [1,8–10].

The catalytic role of GSTs in multidrug resistance (MDR) of cancer cells is mainly due to their overexpression, leading to rapid detoxification of anticancer drugs [9,11,12]. The GST classes that are associated with the development of MDR cancer cells in humans are alpha, mu, and pi [13–15]. Human GSTP1-1 (hGSTP1-1) is the most well-studied member of the GST family. It is involved in apoptosis resistance and metabolism of various chemotherapeutic agents, such as platinum-based drugs [16,17]. In addition, hGSTP1-1 regulates calcium channels by reducing the apoptotic mobilization of calcium ions [18] and modulating the function of apoptotic signalling of JNK1 [19,20] and Bax [21]. Additionally, hGSTP1-1 regulates calcium channels by reducing the apoptotic mobilization of calcium ions [18], modulating the function of apoptotic signalling of JNK1 [19,20] and Bax [21]. The regulation of tumor necrosis factor (TNF), TNF-receptor factor 2 (TRAF2), and apoptosis signal-regulating kinase 1 (ASK1) is another crucial function of hGSTP1-1 [22]. Through a redox mechanism, nuclear factor (NF)-κB and activator protein 1 both mediate the control of hGSTP1-1 [23]. Therefore, identifying GSTP1-1 inhibitors may be valuable for developing new therapeutic strategies for cancer [5,17,20].

A range of synthetic and natural substances has been tested for their ability to inhibit GSTs in an attempt to lessen or even abolish multidrug resistance in cancer cells. 2,2′-dihydroxybenzophenones [24], benzoxazole [25], selenium compounds [26], diselenides and benzisoselenazolones [27], benzoxadiazoles [28,29], auranofin [30], piperlongumine [31], and curcumin analogs [32,33] have been recently reported.

The use of approved compounds (e.g., FDA-approved drugs, pesticides) as a source of molecular scaffolds is an effective way to reduce the cost and time required for new lead development. Reuse of existing chemical scaffolds, with chemical and toxicological profiles that are already established, can provide a significant advantage in terms of safety and reduce the risk associated with new drug development. For example, Musdal et al. [34], in a library of FDA-approved drugs, have identified merbromine, hexachlorophene, and ethacrynic acid as the most effective hGSTP1-1 inhibitors with IC_{50} values in the low micromolar range. Recently, Bodourian et al. [33], using the human GSTM1-1 (hGSTM1-1) as a model enzyme, exploited a diverse pesticide library to identify the carbamate insecticide pirimicarb as a strong inhibitor of hGSTM1-1. The present study aimed to identify a new lead compound from a pesticide library as an inhibitor of *Mus musculus* GSTP1-1 (*Mm*GSTP1-1) and provide the basis for further research and development.

2. Materials and Methods

2.1. Materials

Glutathione (reduced form, GSH), 1-chloro-2,4-dinitrobenzene (CDNB), acetochlor, butachlor, metazachlor, and bovine serum albumin (BSA, fraction V) were purchased from Sigma-Aldrich (St. Louis, MI, USA). Alachlor and malathion were purchased from Fluka (Darmstadt, Germany). Other pesticides were obtained from Riedel de Haen (Hanover, Germany).

2.2. Methods

2.2.1. Cloning, Expression, and Purification of MmGSTP1-1

First-strand cDNA synthesis was performed using Poly(A)-mRNA, oligo-p(dT)15 primer and Superscript II reverse transcriptase according to the manufacturer's recommendations (Thermo Fisher Scientific, Waltham, MA, USA). The PCR-primers: 5′ GAA GGA GAT ATA CAT ATG ATG GCC GGG AAG CCC GTG CTT CAC-3′ (forward primer) and 5′-GTG ATG GTG GTG ATG ATG TTA TCA CTG AAT CTT GAA AGC CTT CCT TGC TTC-3′ (reverse primer) were designed according to the *Mm*GSTP1-1 gene sequence (GenBank accession number: BC061109.1, accessed on 5 October 2016). The PCR reaction was carried out in a total volume of 50 μL containing 10 pmol of each primer, 1μg template cDNA, 0.2 mM of each dNTP, 5 μL 10× buffer, and 1 unit of Accura High-Fidelity DNA polymerase (Lucigen, Middlesex, UK). The PCR procedure comprised of 25 cycles of 45 s at 94 °C, 15 s at 65 °C, and 1 min at 72 °C. A final extension time at 72 °C for 10 min was performed after the 25 cycles. The PCR products were run on a 1% (*w*/*v*) agarose gel, and the single PCR product (630 bp) was excised, purified by adsorption to silica beads and cloned to the expression plasmid pETite C-His. The resulting expression construct was used to transform competent *E. coli* HI-Control BL21 (DE3) cells for expression. Nucleotide sequencing was performed along both strands for sequence validation.

Competent *E. coli* HI-Control BL21 (DE3) cells were grown in Luria–Bertani (LB) medium containing kanamycin (25 μg/mL). GST synthesis was induced by the addition of 1 mM isopropyl-β-D-thiogalactopyranoside (IPTG) when the absorbance at 600 nm had reached 0.6. Following incubation, the cells were harvested by centrifugation at 8000× *g* for 20 min, resuspended in phosphate buffer (20 mM, pH 7), sonicated, and centrifuged at 13,000× *g* for 5 min. The supernatant was loaded onto an epoxy-activated Sepharose CL-6B column coupled to GSH (1,4-butanediol diglycidyl ether-GSH-Sepharose-CL6B, 1 mL), which was previously equilibrated with potassium phosphate buffer (20 mM, pH 7). The bound enzyme was eluted by the equilibration buffer containing GSH (1 mM). The purity of the protein was judged by SDS-PAGE (Supplementary Figure S1).

2.2.2. Assay of Protein and Enzyme Activity

Determination of enzyme activity was performed by monitoring the formation of a conjugate between GSH (2.5 mM) and CDNB (1 mM) at 340 nm (ε = 9.6 $mM^{-1}cm^{-1}$) at 37 °C, pH = 6.5, using a published method [35]. Observed reaction velocities were corrected for spontaneous reaction rates when necessary. Turnover numbers were calculated based on the presence of one active site per subunit. All the initial velocities were determined at least three times in buffers equilibrated at a constant temperature. As defined, one enzyme unit is the amount of enzyme that produces 1 μmole of product per minute at pH = 6.5 and 37 °C.

2.2.3. Pesticides Screening

In total, 49 pesticides were included in the analysis. Inhibition potency evaluation was carried out in the same assay system as described above in the presence of 25 μM of pesticide dissolved in acetone. The percentage of enzyme inhibition was calculated as follows:

$$\%(\text{Inhibition}) = [(R_u - R_i)/R_u] \times 100, \quad (1)$$

where R_u is the rate of absorbance increase for the reaction in the absence of the inhibitor and R_i is the rate of absorbance increase for the reaction in the presence of the inhibitor.

Both R_u and R_i were measured at the same substrate concentration (GSH and CDNB). No reaction between GSH and pesticide was observed during the enzyme assay (60 s).

2.2.4. IC_{50} Value Determination for Iprodione

The IC_{50} value of iprodione was determined using the assay system described above [35], and the *Mm*GSTP1-1 activity was measured at different concentrations of iprodione (0–75 μM).

The IC_{50} value was calculated by fitting the following equation to the concentration-response data:

$$\%(\text{Inhibition}) = 100/[1 + (IC_{50}/[I])], \quad (2)$$

where [I] is the concentration of the inhibitor (e.g., iprodione). The IC_{50} value was determined by fitting the above equation to the experimental data using a non-linear curve fitting method via GraphPad Prism v7.00 (GraphPad Software Inc., Boston, MA, USA).

2.2.5. Kinetic Inhibition Study of MmGSTP1 in Presence of Iprodione

A kinetic study of *Mm*GSTP1-1 using GSH as a variable substrate was performed using the assay system mentioned above with different GSH concentrations (18.75–3375 μM) in the presence of different (0–10 μM) concentrations of iprodione. Using CDNB as a variable substrate, the same assay system was used with different CDNB concentrations (30–1500 μM) in the presence of variable (0–10 μM) concentrations of iprodione. The kinetic parameters (K_m, k_{cat}) were determined via GraphPad Prism v7.00 (GraphPad Software Inc.)

2.2.6. X-ray Crystallography

*Mm*GSTP1-1 was co-crystallized in the presence of 2.5 mM Nb-GSH using the hanging drop vapor diffusion method. The well solution consisted of 0.1 M Tris-HCl, PEG 6000 20% (*w*/*v*) and 0.2 M calcium chloride dihydrate, pH 8.0. X-ray diffraction data from a single crystal were collected on the P13 beamline (EMBL-Hamburg) to 1.28 Å resolution at 100 K using glycerol 10% (*v*/*v*) as cryoprotectant. The initial phases were determined using molecular replacement with the previously determined structure of mouse liver GSTP1-1 at 1.8 Å resolution (PDB ID: 1GLQ; sequence identity 100%) as a search model in Phaser [36]. The crystals of the 1GLQ structure also belong to the orthorhombic $P2_12_12_1$ space group with similar unit cell dimensions as the ones reported here but the axes have been assigned differently. The structure was refined with Phenix v. 1.20.1-4487 [37].

2.2.7. Molecular Docking of Iprodione

Molecular docking of iprodione was performed using AutoDock4.2 (version 4.2.6) and AutoDockTools4 [38]. Ligand-free *Mm*GSTP1-1 and iprodione were used as the receptor and ligand, respectively. The grid was centred at −31, 0, 23 coordinates (with grid sides having 100, 125, and 100 points, spaced at 0.375 Å). AutoDock4.2 was then used for the docking analysis, carrying 100 independent genetic algorithm cycles with a population of 300 individuals. The docked ligand clusters were then further analyzed using PyMOL [39]. The refined crystal structure of *Mm*GSTP1-1 resolved in the present study at 1.28 Å resolution was used.

3. Results and Discussion

3.1. Purification and Kinetic Analysis

Recombinant *Mm*GSTP1-1 was purified in a single step by affinity chromatography using Sepharose-immobilized GSH as an affinity ligand. Kinetics analysis was carried out using the model GST compounds CDNB and GSH as substrates. The enzyme was found to obey Michaelis–Menten kinetics (Figure 1) with $K_m{}^{CDNB}$ 0.80 ± 0.04 mM and $K_m{}^{GSH}$ 0.22 ± 0.01 mM. Both parameters are close to those reported for the hGSTP1-1 isoenzyme [40–42].

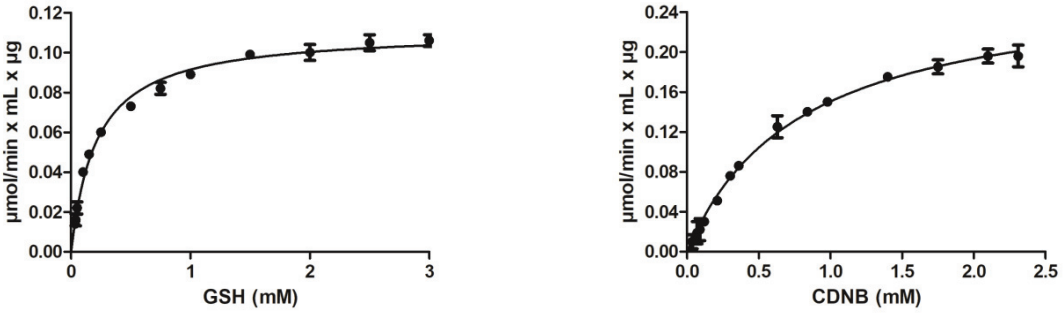

Figure 1. (**a**) Kinetics analysis of *Mm*GSTP1-1 using CDNB at saturated concentration and GSH varied. (**b**) Kinetics analysis of *Mm*GSTP1-1 using GSH at saturated concentration and CDNB varied.

The substrate specificity of the purified enzyme was assessed using a panel of model GST substrates. The results are presented in Table 1. *Mm*GSTP1-1 exhibits a range of diverse activities including transferase activity towards alkyl-halides or unsaturated compounds and hydroperoxidase activity using cumene hydroperoxide as substrate. GSTs are known to participate in oxidative stress defense mechanisms, catalyzing the GSH-dependent inactivation of organic hydroperoxides, such as cumene hydroperoxide and converting them into non-toxic alcohols [43]. tert-Butyl-hydroperoxide did not appear to be an acceptable substrate for the enzyme. Significant activity is exhibited towards ethacrynic acid, a well-known inhibitor of GSTs [34]. Significant activity was also observed with phenethyl isothiocyanate as a substrate, suggesting that *Mm*GSTP1-1 catalyzes with high efficiency the addition of the thiol of GSH to the electrophilic central carbon of the isothiocyanate group. Similar substrate specificity towards the reported electrophilic substrates has also been observed for hGSTP1-1 [40–42,44].

Table 1. Substrate specificity of *Mm*GSTP1-1. The results represent the mean of triplicate determinations, with a variation of less than 5% in all cases. The specific activity of the enzyme against the model substrate CDNB is defined as 100%.

Electrophile Substrates	U/mg (%)
1-Chloro-2,4-dinitrobenzene	100
1-Bromo-2,4-dinitrobenzene	188.8
1-Iodo-2,4-dinitrobenzene	14.4
4-Chloro-7-nitrobenzofurazan	-
p-Nitrobenzyl chloride	1.7
Bromosulfalein	8.7
Cumene hydroperoxide	2.7
tert-Butyl hydroperoxide	-
Dehydroascorbate	-
Sulphanilamide	0.2
2,3-Dichloro-4-[2-methylene-butyryl]phenoxy)acetic acid (Ethacrynic acid)	19.1
trans-4-Phenyl-3-buten-2-one	-
Allyl isothiocyanate	-
Phenethyl isothiocyanate	41.1

3.2. Pesticides Library Screening

A library of 49 different pesticides belonging to diverse chemical classes, including insecticides, herbicides, and fungicides, was selected to assess their inhibitory potency against the *Mm*GSTP1-1 isoenzyme. The selected pesticides represent a mixed collection of compounds with diverse structural and physicochemical properties. The results of the screening are illustrated in Figure 2 in the form of a heatmap.

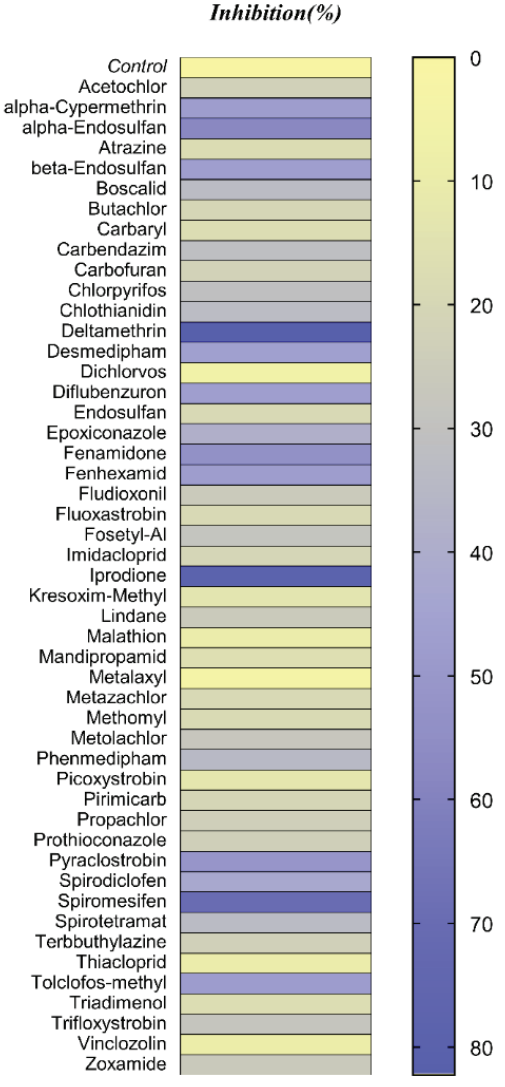

Figure 2. Screening of the inhibitory potency of pesticides (25 μM) against *Mm*GSTP1-1. The enzyme was assayed in all measurements using the CDNB-GSH assay system. The colour scale represents the mean values of three inhibition assays (%) for each pesticide against the tested enzyme with a variation of less than 5% in all cases.

The results showed that the insecticide deltamethrin and the fungicide iprodione display the highest inhibition potencies, 82% and 78%, respectively. Considering that among deltamethrin and iprodione, the latter displays much less toxicity [e.g., acute oral

toxicity LD_{50} (rat) > 5 g/kg and acute dermal toxicity LD_{50} (rabbit) > 2 g/kg], iprodione was selected for further studies.

Other pesticides with significant but much lower inhibition potency compared to iprodione, include spiromesifen (70% inhibition), α-endosulfan (58% inhibition), and fenamidone (53% inhibition).

The concentration–inhibition curve for iprodione allowed the determination of the half maximal inhibitory concentration (IC_{50}) which was 11.3 ± 0.5 μM (R^2 = 0.989) (Figure 3). This value lies within the range expected for a strong GST inhibitor [24,25,27,32,33].

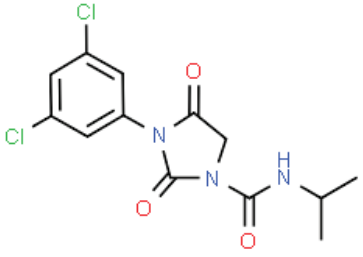

(**a**)

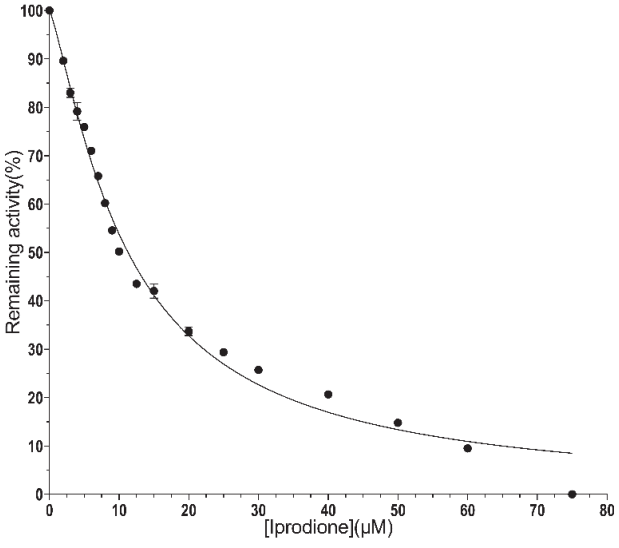

(**b**)

Figure 3. (**a**) The 2D structure of iprodione ($C_{13}H_{13}Cl_2N_3O_3$). (**b**) Concentration–response curve for iprodione. The IC_{50} for *Mm*GSTP1−1 was determined by fitting Equation (2) to the data using nonlinear curve-fitting methods.

3.3. Kinetic Inhibition Study

A kinetic inhibition study was performed with the aim of determining the inhibition pattern of iprodione with the enzyme, and the results are illustrated in Figures 4 and 5. The data suggest that iprodione behaves as a mixed-type inhibitor towards GSH (Figure 4) and a non-competitive inhibitor towards CDNB (Figure 5).

The mixed-type inhibitor indicates that iprodione can bind to both the free enzyme and the enzyme–substrate complex (E-GSH) with different affinities for each enzyme ($K_{iE} \neq K_{iES}$). The analysis reveals that the inhibition constants K_{iE} and K_{iEGSH} for iprodione, using GSH as a variable substrate, are 5.2 ± 0.1 μM (R^2 = 0.99) and 14.8 ± 4 μM (R^2 = 0.99), respectively.

The measured K_i values (K_{iE} and K_{iEGSH}) suggest that iprodione shows preferential binding and greater affinity for the free form of *Mm*GSTP1-1. This suggests that the recognition elements of binding for the inhibitor are not completely overlapping with those of the substrate, and therefore, the substrate and inhibitor binding sites may be thought to be distinct. Thus, the binding of iprodione to *Mm*GSTP1-1 may not preclude GSH binding. The non-competitive inhibition constant using CDNB as a variable substrate is K_i = 6.6 ± 2.6 μM (R^2 = 0.98).

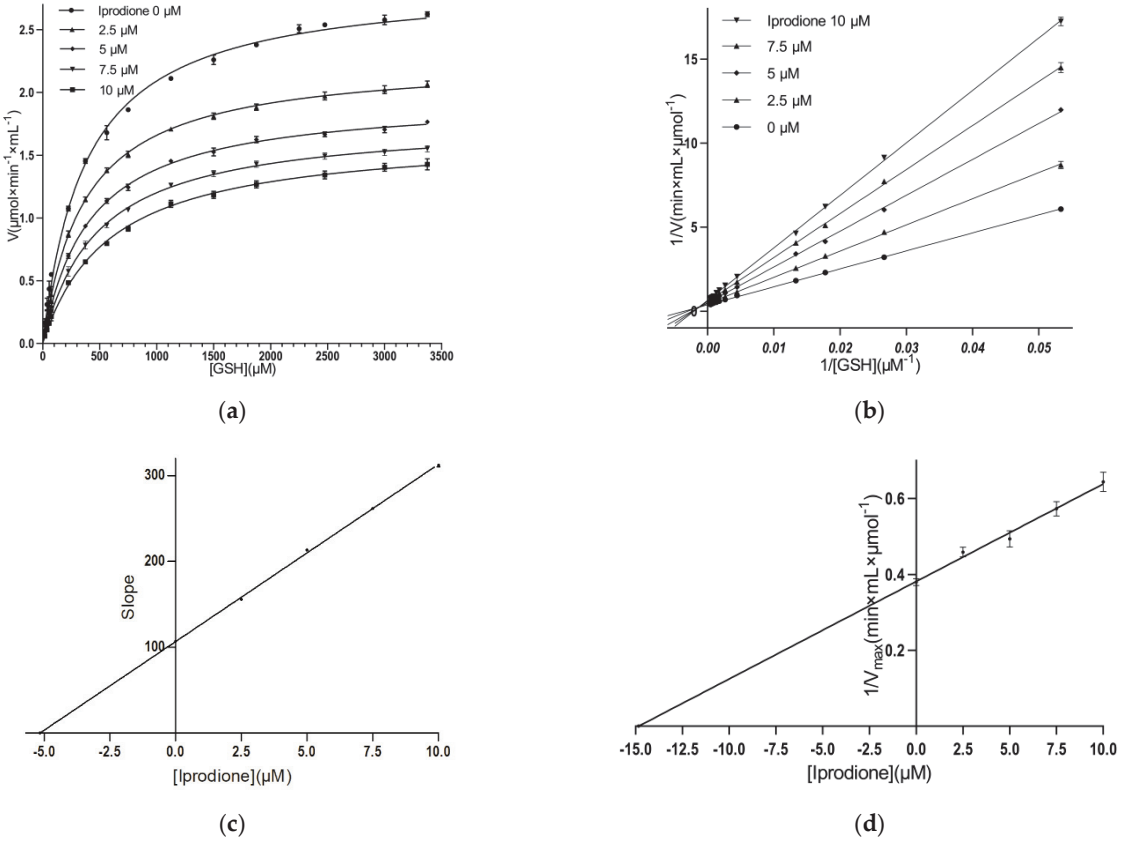

Figure 4. Kinetic inhibition of *Mm*GSTP1−1 by iprodione. The concentration of CDNB was constant, while the concentration of GSH was varied. (**a**) Michaelis–Menten plot and (**b**) Lineweaver–Burk plot for the inhibition of *Mm*GSTP1-1 with iprodione at different GSH concentrations. Iprodione concentrations: 0–10 μM. (**c**) Secondary plot for the determination of K_{iE} for the GSH. The slope values were obtained from a Lineweaver–Burk plot. (**d**) Secondary plot for the determination of K_{iES} for the GSH. The $1/V_{max}$ values are the intersection points of lines on the ordinate axis of the Lineweaver–Burk plot.

It is well established that the inhibition pattern that is obeyed by different GST isoenzymes when studied with different inhibitory compounds is inhibitor- and substrate-dependent and cannot be predicted based on structural information of the particular inhibitor or the enzyme. However, the vast majority of kinetic inhibition studies have revealed that the most potent inhibitors function as non-competitive/mixed-type inhibitors [24,25,27,32,33].

3.4. Crystallization of MmGSTP1-1 and Structural Analysis

The crystal structure of *Mm*GSTP1-1 was refined to 1.28 Å resolution with final R_{work} and R_{free} values of 0.175 and 0.199, respectively (Table 2). *Mm*GSTP1-1 was crystallized with two molecules in the asymmetric unit. The final refined structure contains 4083 non-hydrogen atoms. Of them, 3338 belong to the protein and 602 are water molecules. Compared to the previously determined *Mm*GSTP1-1 structure (PDB ID: 1GLQ, 1.8 Å resolution) [45] which has 148 water molecules, the high-resolution structure reported here shows a significant improvement in the number of water molecules.

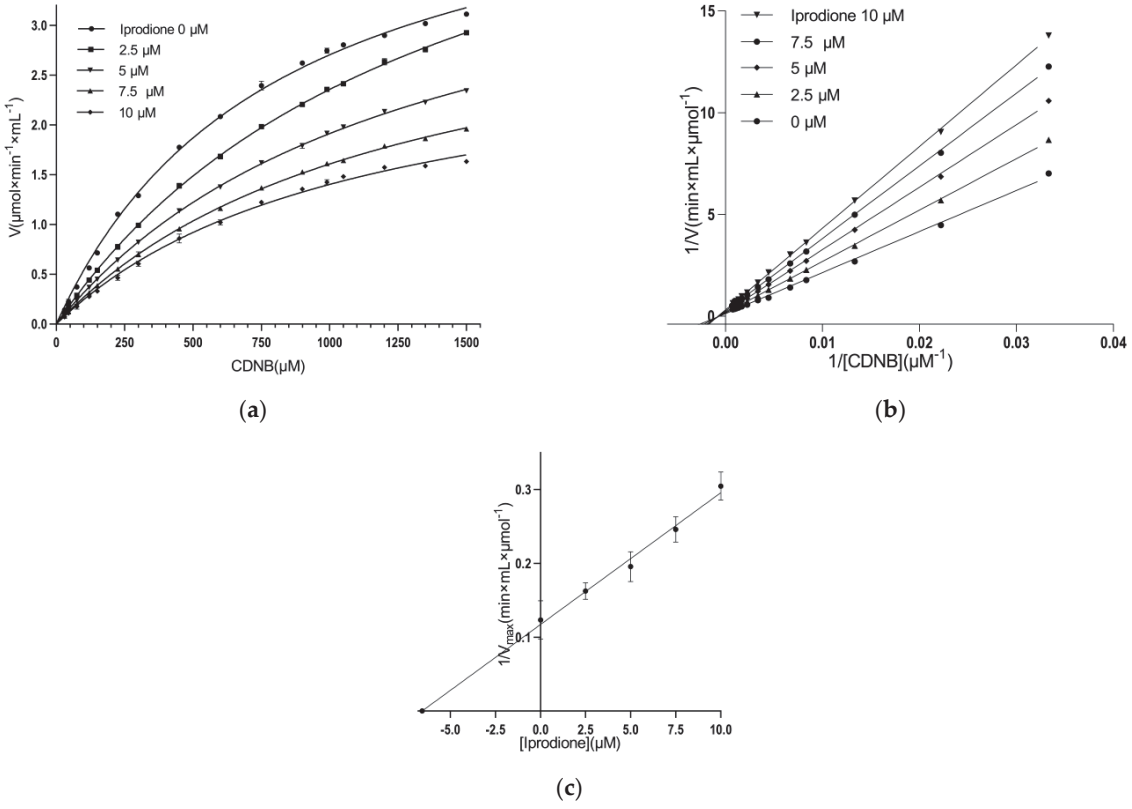

Figure 5. Kinetic inhibition study of *Mm*GSTP1−1 with iprodione. The concentration of GSH was constant, while the concentration of CDNB was varied. (**a**) Michaelis–Menten plot. (**b**) Lineweaver–Burk plot for inhibition. Iprodione concentrations: 0–10 μM. (**c**) Secondary plot for K_i determination.

A molecule of Nb-GSH was found bound in the active site of each molecule of the dimer (Figure 6a,b; Supplementary Figure S2). A structural comparison with the previously determined *Mm*GSTP1-1 structure at a lower resolution (1.8 Å) [45] showed a root mean square deviation (RMSD) between the two structures of 0.315 Å for 209 atom pairs, suggesting subtle differences between them.

The amino acid residues that contribute to the binding of Nb-GSH are strictly conserved in all mammalian GSTP1-1 enzymes as well as in *Mm*GSTP1-1 (Figure 6a). Notably, Tyr108 makes a π-π aromatic–aromatic interaction with the nitrobenzyl group of the bound Nb-GSH.

An interesting finding that has not been described previously is the presence of four calcium ions in the present structure. The source of the calcium ions is the salt used during crystallization. Among them, one calcium ion was found in each of the active sites (Figure 6c). Their B-factors were 21.4 and 28.2 $Å^2$, indicating stable binding. Each of them is located in the vicinity of the H-site and forms 24 van der Waals interactions in total with protein atoms. Important van der Waals interactions are formed with the hydroxyl groups of the key residues Tyr7 and Tyr108 and with the side chains of Val104 and Arg13. In addition, the calcium ion interacts with the sulfur group of Nb-GSH.

All these interactions seem to contribute towards stabilizing and fixing the orientation of the aromatic groups of Tyr7 and Tyr108, allowing the formation of aromatic–aromatic interactions with the nitrobenzyl group of the bound Nb-GSH.

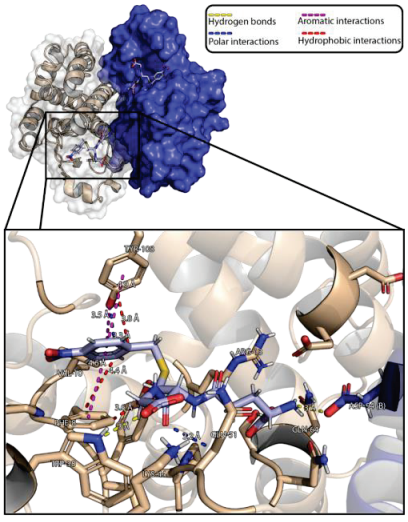

(**a**)

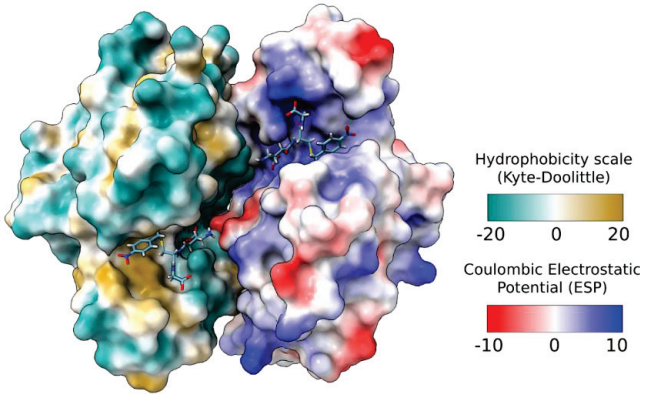

(**b**)

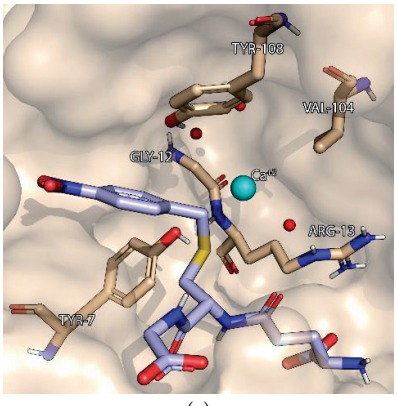

(**c**)

Figure 6. (**a**) The structure of *Mm*GSTP1−1 at 1.28 Å resolution. Each subunit is shown in a different color. The bound Nb-GSH is shown in a stick representation and colored according to the atom type. The figure was produced using the PyMOL program [39]. Close up: The amino acids that contribute to Nb-GSH binding. The close-up figure was created using PyMOL [39]. Interactions were calculated using the web server Arpeggio [46]. (**b**) The electrostatic and hydrophobicity potential of *Mm*GSTP1-1. One subunit is colored according to the electrostatic potential. Negative, positive, and neutral charges are shown as shades of red, blue, and white, respectively. The other subunit is colored according to the hydropathic character of the protein [47]. Hydrophilic to hydrophobic residues are colored from pale green to yellow brown. The bound NB-GSH is shown in a stick representation. The figure was created using the UCSF ChimeraX program [48,49]. (**c**) The interactions of the Ca^{2+} in the vicinity of H-site with important amino acid residues. Ca^{2+} is shown as a green sphere and water molecules as red spheres. Nb-GSH is shown in a stick representation and colored according to the atom type.

3.5. Characterization of the Iprodione Binding Site Using Molecular Docking

The crystal structure of *Mm*GSTP1-1 that was determined in the present study was used to map the iprodione-binding site using molecular docking. As co-crystallization of the *Mm*GSTP1-1/iprodione complex was not achieved despite extensive crystallization screens, an in silico molecular docking approach was adopted using AutoDock 4.2 [38].

Based on the most credible conformation cluster, iprodione appears to bind to the region that partially overlaps with the H-site (Figure 7a). Its aromatic ring is sandwiched between the aromatic groups of Tyr108 and Phe8. It also forms two hydrogen bonds with residues Arg100 and Asn204 and two polar interactions with residues Tyr7 and Arg13 (Figure 7a). Superposition of the binding site of iprodione and Nb-GSH showed that iprodione overlaps only with the nitrobenzyl group of the bound Nb-GSH (Figure 7b,c).

This binding mode is consistent with the observed mixed-type inhibition towards GSH and non-competitive inhibition towards CDNB, as found in the present study (Figure 5).

Based on the estimation made by AutoDock 4.2, the free energy of binding is equal to −7.17 kcal/mol and the inhibition constant K_i is equal to 5.68 μM. This theoretical value is very close to that which was measured experimentally for iprodione using GSH as a variable substrate (K_{iE} = 5.2 ± 0.1 μM) and using CDNB as a variable substrate (K_i = 6.6 ± 2.6 μM), supporting the accuracy of the in silico docking studies.

Table 2. X-ray data collection and refinement statistics.

Data Collection	***Mm*GSTP1-1**
Beamline	P13 (EMBL, Hamburg)
Wavelength (Å)	1.033
Resolution (Å)	56.62–1.28 (1.30–1.28)
Space group	$P2_12_12_1$
Unit cell (Å)	
a, b, c	56.62, 77.37, 101.44
No. of unique reflections	114,851 (5532)
Completeness (%)	99.7 (98.3)
Multiplicity	6.4 (6.3)
Mosaicity (°)	0.11
R_{meas}	0.059 (2.485)
$CC_{1/2}$	0.99 (0.35)
Mean (I/σ(I))	12.7 (0.9)
Wilson B-factor (Å^2)	18.3
Refinement	
No. of reflections used	114,744
R_{work}/R_{free}	0.175/0.199
No. of non-H atoms (protein/ligand/solvent)	3338/143/602
Protein residues	418
RMSD in bonds (Å)	0.006
RMSD in angles (°)	0.93
Average B-factor (all/protein/ligands/solvent) (Å^2)	28.2/26.6/28.8/36.8
Ramachandran favored/outliers (%)	97.8/0.0
Rotamer outliers (%)	0.0
Clashscore	3.5
PDB ID	8C5D

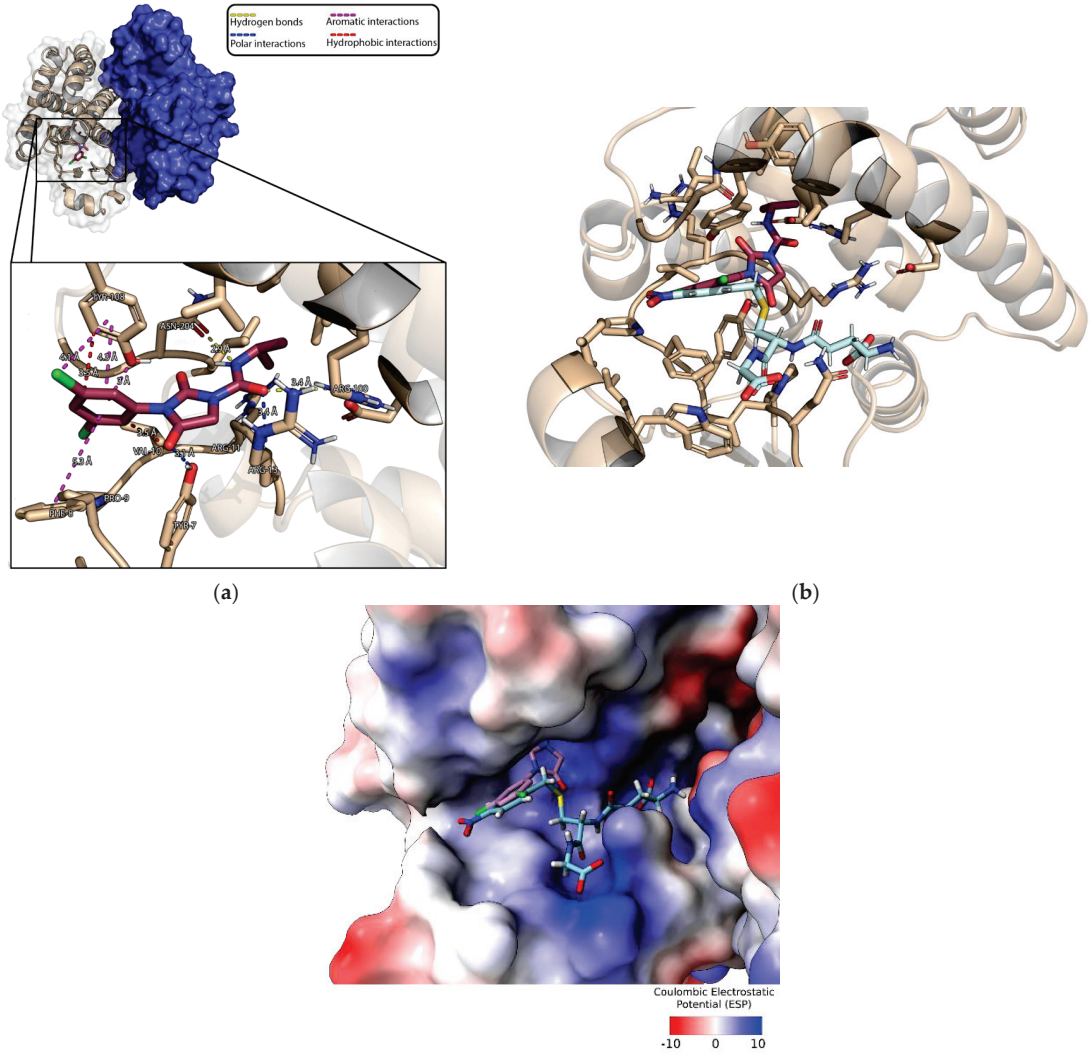

(**a**) (**b**)

(**c**)

Figure 7. (**a**) Predicted favorable binding mode of iprodione in *Mm*GSTP1−1. Iprodione is shown in a stick representation. Close up: Side chains of the interacting amino acids are shown and labelled. Interactions were calculated using the Arpeggio web server [46]. The dashed lines represent interactions. (**b**) Superposition of bound iprodione and Nb-GSH in *Mm*GSTP1-1. Both ligands are shown in stick representation. Side chains of the interacting amino acids are shown. (**c**) Superposition of bound iprodione and Nb-GSH. Both ligands are shown in stick representation. The enzyme subunit is shown as the surface and colored according to the Coulombic electrostatic potential. Negative, positive, and neutral charges are shown as shades of red, blue, and white, respectively.

4. Conclusions

The discovery of GST inhibitors remains a challenging task [50]. This is probably a consequence of the high plasticity and conformational flexibility of GSTs. The results of the present study allowed the identification of the fungicide iprodione as an inhibitor of *Mm*GSTP1-1.

Iprodione acts as a mixed-type inhibitor towards GSH and as a non-competitive inhibitor towards CDNB. X-ray crystallography was used to determine the crystal structure of *Mm*GSTP1-1 in complex with Nb-GSH and molecular docking was used to investigate the interaction between *Mm*GSTP1-1 and iprodione.

Iprodione exhibits minimal toxicity to mammals and, therefore, can be considered as a new lead compound that can be further investigated. Repurposing already approved drugs seems to be a very attractive approach given the investment (cost, time, and effort) required for implementing a new drug discovery project. In this way, the drug development timeline can be shortened since several existing compounds already have known technology, safety, and toxicity profiles.

Supplementary Materials: The following supporting information can be downloaded at: https://www.mdpi.com/article/10.3390/biom13040613/s1, Figure S1. SDS-PAGE analysis of the eluted fraction of recombinant MmGSTP1-1; Figure S2. SigmaA-weighted 2Fo-Fc electron density map of Nb-GSH with surrounding residues at 1 sigma level. The figure was created using Coot [51].

Author Contributions: Conceptualization, N.E.L.; formal analysis, O.K., F.P., K.K., I.A., A.C.P. and N.E.L.; investigation, O.K., F.P., K.K., I.A., A.C.P. and N.E.L.; resources, E.D.; writing—original draft preparation, O.K., F.P., K.K., I.A., E.D., A.C.P. and N.E.L.; supervision, N.E.L. All authors have read and agreed to the published version of the manuscript.

Funding: This research received no external funding.

Institutional Review Board Statement: Not applicable.

Informed Consent Statement: Not applicable.

Data Availability Statement: Data is contained within the article or Supplementary Materials.

Acknowledgments: ACP thanks Biocenter Finland and Academy of Finland for infrastructure support. We thank Sandrine Le Hello for help during crystallizations. Access to EMBL-Hamburg was provided by iNEXT, project number 653706, funded by the Horizon 2020 program.

Conflicts of Interest: The authors declare no conflict of interest.

Abbreviation

CDNB, 1-chloro-2, 4-dinitrobenzene; GSH, glutathione; GST, glutathione transferase; G-site, GSH-binding site; H-site, hydrophobic-binding site; iprodione, ([3-(3,5-dichlorophenyl)-N-(1-methylethyl)-2,4-dioxo-1-imidazolidinecarboxamide]); Nb-GSH, S-(p-nitrobenzyl)glutathione.

References

1. Mannervik, B. Evolution of Glutathione Transferases and Related Enzymes for the Protection of Cells against Electrophiles. *Biochem. Soc. Trans.* **1996**, *24*, 878–880. [CrossRef] [PubMed]
2. Mannervik, B. The Isoenzymes of Glutathione Transferase. In *Advances in Enzymology and Related Areas of Molecular Biology*; Meister, A., Ed.; John Wiley & Sons, Inc.: Hoboken, NJ, USA, 2006; pp. 357–417, ISBN 978-0-470-12303-4.
3. Hayes, J.D.; Flanagan, J.U.; Jowsey, I.R. GLUTATHIONE TRANSFERASES. *Annu. Rev. Pharmacol. Toxicol.* **2005**, *45*, 51–88. [CrossRef]
4. Jakoby, W.B.; Ziegler, D.M. The Enzymes of Detoxication. *J. Biol. Chem.* **1990**, *265*, 20715–20718. [CrossRef]
5. Perperopoulou, F.; Pouliou, F.; Labrou, N.E. Recent Advances in Protein Engineering and Biotechnological Applications of Glutathione Transferases. *Crit. Rev. Biotechnol.* **2018**, *38*, 511–528. [CrossRef] [PubMed]
6. Vašková, J.; Kočan, L.; Vaško, L.; Perjési, P. Glutathione-Related Enzymes and Proteins: A Review. *Molecules* **2023**, *28*, 1447. [CrossRef] [PubMed]
7. Board, P.G.; Menon, D. Glutathione Transferases, Regulators of Cellular Metabolism and Physiology. *Biochim. Biophys. Acta Gen. Subj.* **2013**, *1830*, 3267–3288. [CrossRef]
8. Oakley, A. Glutathione Transferases: A Structural Perspective. *Drug Metab. Rev.* **2011**, *43*, 138–151. [CrossRef] [PubMed]
9. Mannervik, B.; Berhane, K.; Castro, V.M.; Olin, B.; Ridderström, M.; Vignani, R.; Kozarich, J.W.; Ringborg, U. Glutathione-Linked Enzymes in Normal and Tumor Cells and Their Role in Resistance against Genotoxic Agents. *Princess Takamatsu Symp.* **1990**, *21*, 253–262.

10. Mannervik, B.; Cameron, A.D.; Fernandez, E.; Gustafsson, A.; Hansson, L.O.; Jemth, P.; Jiang, F.; Alwyn Jones, T.; Larsson, A.-K.; Nilsson, L.O.; et al. An Evolutionary Approach to the Design of Glutathione-Linked Enzymes. *Chem. Biol. Interact.* **1998**, *111–112*, 15–21. [CrossRef]
11. Kaur, G.; Gupta, S.K.; Singh, P.; Ali, V.; Kumar, V.; Verma, M. Drug-Metabolizing Enzymes: Role in Drug Resistance in Cancer. *Clin. Transl. Oncol.* **2020**, *22*, 1667–1680. [CrossRef]
12. Pljesa-Ercegovac, M.; Savic-Radojevic, A.; Matic, M.; Coric, V.; Djukic, T.; Radic, T.; Simic, T. Glutathione Transferases: Potential Targets to Overcome Chemoresistance in Solid Tumors. *Int. J. Mol. Sci.* **2018**, *19*, 3785. [CrossRef] [PubMed]
13. Bocedi, A.; Noce, A.; Marrone, G.; Noce, G.; Cattani, G.; Gambardella, G.; Di Lauro, M.; Di Daniele, N.; Ricci, G. Glutathione Transferase P1-1 an Enzyme Useful in Biomedicine and as Biomarker in Clinical Practice and in Environmental Pollution. *Nutrients* **2019**, *11*, 1741. [CrossRef] [PubMed]
14. Laborde, E. Glutathione Transferases as Mediators of Signaling Pathways Involved in Cell Proliferation and Cell Death. *Cell Death Differ.* **2010**, *17*, 1373–1380. [CrossRef] [PubMed]
15. Cui, J.; Li, G.; Yin, J.; Li, L.; Tan, Y.; Wei, H.; Liu, B.; Deng, L.; Tang, J.; Chen, Y.; et al. GSTP1 and Cancer: Expression, Methylation, Polymorphisms and Signaling (Review). *Int. J. Oncol.* **2020**, *56*, 867–878. [CrossRef]
16. Sawers, L.; Ferguson, M.J.; Ihrig, B.R.; Young, H.C.; Chakravarty, P.; Wolf, C.R.; Smith, G. Glutathione S-Transferase P1 (GSTP1) Directly Influences Platinum Drug Chemosensitivity in Ovarian Tumour Cell Lines. *Br. J. Cancer* **2014**, *111*, 1150–1158. [CrossRef] [PubMed]
17. Potęga, A. Glutathione-Mediated Conjugation of Anticancer Drugs: An Overview of Reaction Mechanisms and Biological Significance for Drug Detoxification and Bioactivation. *Molecules* **2022**, *27*, 5252. [CrossRef] [PubMed]
18. Dulhunty, A.; Gage, P.; Curtis, S.; Chelvanayagam, G.; Board, P. The Glutathione Transferase Structural Family Includes a Nuclear Chloride Channel and a Ryanodine Receptor Calcium Release Channel Modulator. *J. Biol. Chem.* **2001**, *276*, 3319–3323. [CrossRef]
19. Wang, T.; Arifoglu, P.; Ronai, Z.; Tew, K.D. Glutathione S-Transferase P1–1 (GSTP1–1) Inhibits c-Jun N-Terminal Kinase (JNK1) Signaling through Interaction with the C Terminus. *J. Biol. Chem.* **2001**, *276*, 20999–21003. [CrossRef] [PubMed]
20. Russell, T.M.; Richardson, D.R. The Good Samaritan Glutathione-S-Transferase P1: An Evolving Relationship in Nitric Oxide Metabolism Mediated by the Direct Interactions between Multiple Effector Molecules. *Redox Biol.* **2023**, *59*, 102568. [CrossRef]
21. Kampranis, S.C.; Damianova, R.; Atallah, M.; Toby, G.; Kondi, G.; Tsichlis, P.N.; Makris, A.M. A Novel Plant Glutathione S-Transferase/Peroxidase Suppresses Bax Lethality in Yeast. *J. Biol. Chem.* **2000**, *275*, 29207–29216. [CrossRef]
22. Wu, Y.; Fan, Y.; Xue, B.; Luo, L.; Shen, J.; Zhang, S.; Jiang, Y.; Yin, Z. Human Glutathione S-Transferase P1-1 Interacts with TRAF2 and Regulates TRAF2–ASK1 Signals. *Oncogene* **2006**, *25*, 5787–5800. [CrossRef]
23. Duvoix, A.; Schnekenburger, M.; Delhalle, S.; Blasius, R.; Borde-Chiché, P.; Morceau, F.; Dicato, M.; Diederich, M. Expression of Glutathione S-Transferase P1-1 in Leukemic Cells Is Regulated by Inducible AP-1 Binding. *Cancer Lett.* **2004**, *216*, 207–219. [CrossRef]
24. Georgakis, N.D.; Karagiannopoulos, D.A.; Thireou, T.N.; Eliopoulos, E.E.; Labrou, N.E.; Tsoungas, P.G.; Koutsilieris, M.N.; Clonis, Y.D. Concluding the Trilogy: The Interaction of 2,2′-Dihydroxy-Benzophenones and Their Carbonyl N-Analogues with Human Glutathione Transferase M1-1 Face to Face with the P1-1 and A1-1 Isoenzymes Involved in MDR. *Chem. Biol. Drug Des.* **2017**, *90*, 900–908. [CrossRef]
25. Ertan-Bolelli, T.; Bolelli, K.; Musdal, Y.; Yildiz, I.; Aki-Yalcin, E.; Mannervik, B.; Yalcin, I. Design and Synthesis of 2-Substituted-5-(4-Trifluoromethylphenyl-Sulphonamido)Benzoxazole Derivatives as Human GST P1-1 Inhibitors. *Artif. Cells Nanomed. Biotechnol.* **2018**, *46*, 510–517. [CrossRef] [PubMed]
26. Bartolini, D.; Torquato, P.; Piroddi, M.; Galli, F. Targeting Glutathione S-Transferase P and Its Interactome with Selenium Compounds in Cancer Therapy. *Biochim. Biophys. Acta Gen. Subj.* **2019**, *1863*, 130–143. [CrossRef] [PubMed]
27. Krasowska, D.; Iraci, N.; Santi, C.; Drabowicz, J.; Cieslak, M.; Kaźmierczak-Barańska, J.; Palomba, M.; Królewska-Golińska, K.; Magiera, J.; Sancineto, L. Diselenides and Benzisoselenazolones as Antiproliferative Agents and Glutathione-S-Transferase Inhibitors. *Molecules* **2019**, *24*, 2914. [CrossRef]
28. Sha, H.; Wang, Z.; Dong, S.; Hu, T.; Liu, S.; Zhang, J.; Wu, Y.; Ma, R.; Wu, J.; Chen, D.; et al. 6-(7-Nitro-2,1,3-Benzoxadiazol-4-Ylthio) Hexanol: A Promising New Anticancer Compound. *Biosci. Rep.* **2018**, *38*, BSR20171440. [CrossRef] [PubMed]
29. Fulci, C.; Rotili, D.; De Luca, A.; Stella, L.; della Rocca, B.M.; Forgione, M.; Di Paolo, V.; Mai, A.; Falconi, M.; Quintieri, L.; et al. A New Nitrobenzoxadiazole-Based GSTP1-1 Inhibitor with a Previously Unheard of Mechanism of Action and High Stability. *J. Enzyme Inhib. Med. Chem.* **2017**, *32*, 240–247. [CrossRef]
30. De Luca, A.; Hartinger, C.G.; Dyson, P.J.; Lo Bello, M.; Casini, A. A New Target for Gold(I) Compounds: Glutathione-S-Transferase Inhibition by Auranofin. *J. Inorg. Biochem.* **2013**, *119*, 38–42. [CrossRef]
31. Harshbarger, W.; Gondi, S.; Ficarro, S.B.; Hunter, J.; Udayakumar, D.; Gurbani, D.; Singer, W.D.; Liu, Y.; Li, L.; Marto, J.A.; et al. Structural and Biochemical Analyses Reveal the Mechanism of Glutathione S-Transferase Pi 1 Inhibition by the Anti-Cancer Compound Piperlongumine. *J. Biol. Chem.* **2017**, *292*, 112–120. [CrossRef]
32. Larasati, Y.A.; Yoneda-Kato, N.; Nakamae, I.; Yokoyama, T.; Meiyanto, E.; Kato, J. Curcumin Targets Multiple Enzymes Involved in the ROS Metabolic Pathway to Suppress Tumor Cell Growth. *Sci. Rep.* **2018**, *8*, 2039. [CrossRef] [PubMed]
33. Pantiora, P.; Furlan, V.; Matiadis, D.; Mavroidi, B.; Perperopoulou, F.; Papageorgiou, A.C.; Sagnou, M.; Bren, U.; Pelecanou, M.; Labrou, N.E. Monocarbonyl Curcumin Analogues as Potent Inhibitors against Human Glutathione Transferase P1-1. *Antioxidants* **2022**, *12*, 63. [CrossRef] [PubMed]

34. Musdal, Y.; Hegazy, U.M.; Aksoy, Y.; Mannervik, B. FDA-Approved Drugs and Other Compounds Tested as Inhibitors of Human Glutathione Transferase P1-1. *Chem. Biol. Interact.* **2013**, *205*, 53–62. [CrossRef] [PubMed]
35. Labrou, N.E.; Mello, L.V.; Clonis, Y.D. Functional and Structural Roles of the Glutathione-Binding Residues in Maize (Zea Mays) Glutathione S-Transferase I. *Biochem. J.* **2001**, *358*, 101–110. [CrossRef]
36. McCoy, A.J.; Grosse-Kunstleve, R.W.; Adams, P.D.; Winn, M.D.; Storoni, L.C.; Read, R.J. *Phaser* Crystallographic Software. *J. Appl. Crystallogr.* **2007**, *40*, 658–674. [CrossRef]
37. Liebschner, D.; Afonine, P.V.; Baker, M.L.; Bunkóczi, G.; Chen, V.B.; Croll, T.I.; Hintze, B.; Hung, L.-W.; Jain, S.; McCoy, A.J.; et al. Macromolecular Structure Determination Using X-Rays, Neutrons and Electrons: Recent Developments in *Phenix*. *Acta Crystallogr. Sect. Struct. Biol.* **2019**, *75*, 861–877. [CrossRef]
38. Morris, G.M.; Huey, R.; Lindstrom, W.; Sanner, M.F.; Belew, R.K.; Goodsell, D.S.; Olson, A.J. AutoDock4 and AutoDockTools4: Automated Docking with Selective Receptor Flexibility. *J. Comput. Chem.* **2009**, *30*, 2785–2791. [CrossRef]
39. *The PyMOL Molecular Graphics System*, Version 1.8; Schrödinger, LLC: New York, NY, USA, 2015.
40. Zimniak, P.; Nanduri, B.; Pikula, S.; Bandorowicz-Pikula, J.; Singhal, S.S.; Srivastava, S.K.; Awasthi, S.; Awasthi, Y.C. Naturally Occurring Human Glutathione S-Transferase GSTP1-1 Isoforms with Isoleucine and Valine in Position 104 Differ in Enzymic Properties. *Eur. J. Biochem.* **1994**, *224*, 893–899. [CrossRef]
41. Johansson, A.-S.; Stenberg, G.; Widersten, M.; Mannervik, B. Structure-Activity Relationships and Thermal Stability of Human Glutathione Transferase P1-1 Governed by the H-Site Residue 105. *J. Mol. Biol.* **1998**, *278*, 687–698. [CrossRef]
42. Hegazy, U.M.; Mannervik, B.; Stenberg, G. Functional Role of the Lock and Key Motif at the Subunit Interface of Glutathione Transferase P1-1. *J. Biol. Chem.* **2004**, *279*, 9586–9596. [CrossRef]
43. Labrou, N.E.; Papageorgiou, A.C.; Pavli, O.; Flemetakis, E. Plant GSTome: Structure and Functional Role in Xenome Network and Plant Stress Response. *Curr. Opin. Biotechnol.* **2015**, *32*, 186–194. [CrossRef] [PubMed]
44. Kolm, R.H.; Danielson, U.H.; Zhang, Y.; Talalay, P.; Mannervik, B. Isothiocyanates as Substrates for Human Glutathione Transferases: Structure-Activity Studies. *Biochem. J.* **1995**, *311*, 453–459. [CrossRef] [PubMed]
45. García-Sáez, I.; Párraga, A.; Phillips, M.F.; Mantle, T.J.; Coll, M. Molecular Structure at 1.8 A of Mouse Liver Class Pi Glutathione S-Transferase Complexed with S-(p-Nitrobenzyl)Glutathione and Other Inhibitors. *J. Mol. Biol.* **1994**, *237*, 298–314. [CrossRef]
46. Jubb, H.C.; Higueruelo, A.P.; Ochoa-Montaño, B.; Pitt, W.R.; Ascher, D.B.; Blundell, T.L. Arpeggio: A Web Server for Calculating and Visualising Interatomic Interactions in Protein Structures. *J. Mol. Biol.* **2017**, *429*, 365–371. [CrossRef] [PubMed]
47. Kyte, J.; Doolittle, R.F. A Simple Method for Displaying the Hydropathic Character of a Protein. *J. Mol. Biol.* **1982**, *157*, 105–132. [CrossRef]
48. Pettersen, E.F.; Goddard, T.D.; Huang, C.C.; Couch, G.S.; Greenblatt, D.M.; Meng, E.C.; Ferrin, T.E. UCSF Chimera: A Visualization System for Exploratory Research and Analysis. *J. Comput. Chem.* **2004**, *25*, 1605–1612. [CrossRef]
49. Yang, Z.; Lasker, K.; Schneidman-Duhovny, D.; Webb, B.; Huang, C.C.; Pettersen, E.F.; Goddard, T.D.; Meng, E.C.; Sali, A.; Ferrin, T.E. UCSF Chimera, MODELLER, and IMP: An Integrated Modeling System. *J. Struct. Biol.* **2012**, *179*, 269–278. [CrossRef]
50. Axarli, I.; Labrou, N.; Petrou, C.; Rassias, N.; Cordopatis, P.; Clonis, Y. Sulphonamide-based bombesin prodrug analogues for glutathione transferase, useful in targeted cancer chemotherapy. *Eur. J. Med. Chem.* **2009**, *44*, 2009–2016. [CrossRef]
51. Emsley, P.; Lohkamp, B.; Scott, W.G.; Cowtan, K. Features and development of Coot. *Acta Crystallogr D Biol Crystallogr.* **2010**, *66*, 486–501. [CrossRef]

biomolecules

MDPI

Commentary

Glutathione-*S*-Transferases as Potential Targets for Modulation of Nitric Oxide-Mediated Vasodilation

Tiffany M. Russell [1] and Des R. Richardson [2,*]

[1] Centre for Cancer Cell Biology and Drug Discovery, Griffith Institute for Drug Discovery, Griffith University, Brisbane 4111, Australia
[2] Department of Pathology and Biological Responses, Graduate School of Medicine, Nagoya University, Nagoya 466-8550, Japan
* Correspondence: d.richardson@griffith.com.au; Tel.: +61-7-3735-7549

Abstract: Glutathione-*S*-transferases (GSTs) are highly promiscuous in terms of their interactions with multiple proteins, leading to various functions. In addition to their classical detoxification roles with multi-drug resistance-related protein-1 (MRP1), more recent studies have indicated the role of GSTs in cellular nitric oxide (NO) metabolism. Vasodilation is classically induced by NO through its interaction with soluble guanylate cyclase. The ability of GSTs to biotransform organic nitrates such as nitroglycerin for NO generation can markedly modulate vasodilation, with this effect being prevented by specific GST inhibitors. Recently, other structurally distinct pro-drugs that generate NO via GST-mediated catalysis have been developed as anti-cancer agents and also indicate the potential of GSTs as suitable targets for pharmaceutical development. Further studies investigating GST biochemistry could enhance our understanding of NO metabolism and lead to the generation of novel and innovative vasodilators for clinical use.

Keywords: glutathione-*S*-transferase; nitroglycerin; nitric oxide; vasodilation

Citation: Russell, T.M.; Richardson, D.R. Glutathione-*S*-Transferases as Potential Targets for Modulation of Nitric Oxide-Mediated Vasodilation. *Biomolecules* **2022**, *12*, 1292. https://doi.org/10.3390/biom12091292

Academic Editor: Bengt Mannervik

Received: 29 August 2022
Accepted: 9 September 2022
Published: 13 September 2022

Publisher's Note: MDPI stays neutral with regard to jurisdictional claims in published maps and institutional affiliations.

1. Introduction

Glutathione-*S*-transferases (GSTs) are a superfamily of phase II detoxification enzymes and ligandins ubiquitously expressed in most living organisms and account for 1% of cellular protein [1,2]. These enzymes are divided into seven classes (α, μ, π, σ, θ, ω, and ξ) that are characterized by sequence similarity and immunological cross-reactivity [3,4]. Cytosolic GSTs are further divided into 16 gene-independent classes distinguished by sequence homology, substrate specificity, inhibitor sensitivity, and immunological properties [3,4].

While GSTs are traditionally associated with detoxification mechanisms due to their ability to conjugate glutathione (GSH) to toxins for excretion, recent advances have explored the role of GSTs in NO metabolism [5–10]. Studies investigating the extensive role of NO in vascular reactivity have identified GSTs as targets for the biotransformation of organic nitrates, including nitroglycerin, that results in vasodilation [11–14]. Intriguingly, there are several existing relationships between GSTs and the regulation of NO metabolism, particularly examining macrophages and tumor cells [8,9,15,16]. This function is related to the rich chemistry of NO coordinating to iron [8,15–20] to form dinitrosyl-dithiol iron complexes (DNICs) that spontaneously form upon the interaction of iron, NO, GSH, or cysteine [6,10,21–24].

These relationships are mediated by: (1) the formation of DNICs [6,10,21–24]; (2) the direct binding of DNICs by GSTP1 to form a stable store of NO [8,9,15,16]; (3) the storage of DNICs by GSTP1 that then leads to a decrease in DNIC transport out of the cell by multi-drug resistance-related protein 1 (MRP1) [8,15]; and (4) the direct association of GSTP1 with inducible nitric oxide synthase (iNOS) to increase its degradation [5] (Figure 1). Overall, GSTP1 acts to bind and store NO, but also inhibits iNOS expression to suppress NO signaling.

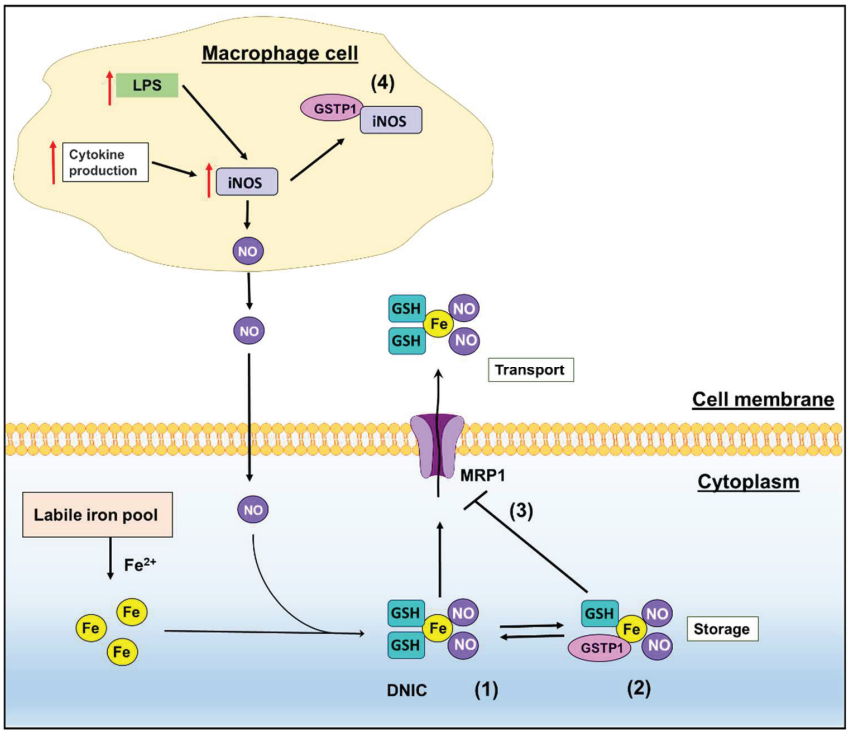

Figure 1. Schematic of the functions of GSTP1 in NO metabolism where: (**1**) NO binds to iron and GSH to generate small molecular weight dinitrosyl-dithiol iron complexes (DNICs); (**2**) DNICs then bind to GSTP1 to lead to a store of NO; (**3**) the binding of DNICs by GSTP1 prevents their transport out of the cell by MRP1; and (**4**) GSTP1 can also bind to inducible nitric oxide synthase (iNOS) that generates intracellular NO.

2. GSTs and Emerging Roles in NO Metabolism

Studies by Cesareo and colleagues reported a crystal structure of a DNIC bound to GSTP1-1 [6]. This interaction with GSTP1-1 markedly increased the half-life of free NO from seconds to 8 h [6,7]. Further studies identified the binding of DNICs to other GST isotypes, namely GSTA1 and GSTM1, which were also able to increase the half-life of NO to approximately 4.5 h [6,7]. Although the function of these GST-DNIC complexes is not well understood, several studies have explored the role of GSTs in DNIC storage and the subsequent transport of DNICs out of cells via the GSH transporter, MRP1 [8,9,15,16].

Lok and colleagues proposed a model in which DNICs behave as a "common currency" for NO transport and storage via MRP1 and GSTP1, respectively, in breast cancer cells and also several macrophage models [8,15]. These studies were based on: previous investigations exploring the interaction of GSTs and DNICs [6]; that MRP1 could transport DNICs in tumor cells [25]; and that GSTs (GSTA1, GSTM1 and GSTP1) protect hepatocytes from the cytotoxic activity of NO [21]. In studies using MCF7 breast cancer cells, a significant decrease in NO-mediated iron release from cells by the GSH transporter, MRP1, was observed in GSTP1-overexpressing MCF7 cells [15]. It was demonstrated that this decreased transport of iron was due to the increased binding of DNICs to GSTP1, and the intrinsic storage of stable NO (as DNICs) by GSTP1 (Figure 1) [15].

Subsequent studies examining activated macrophages demonstrated that silencing Mrp1 resulted in an intracellular accumulation of DNICs, while silencing Gstp1 in these cells augmented the release of iron-59 out of the cell (as DNICs) [8]. Another intriguing GSTP1-NO interaction has been suggested by studies demonstrating the binding of GSTP1

to iNOS [5]. In this later study, GSTP1 was shown to directly interact with the oxygenase domain of iNOS through the GSTP1 G-site domain [5]. The interaction between GSTP1 and iNOS resulted in decreased iNOS dimer levels by the enhanced *S*-nitrosylation of iNOS and its ubiquitination, leading to reduced iNOS stability [5].

3. Nitric Oxide: A Hallmark Vasodilator

A hallmark function of NO is its ability to modulate signaling pathways, which occurs via the binding of NO to the heme prosthetic group of soluble guanylate cyclase (sGC) [26–29]. This NO-sGC interaction produces a heme–iron–nitrosyl complex that can activate the enzyme [22,29]. Activation of sGC results in the conversion of guanosine triphosphate (GMP) into the secondary messenger cyclic guanosine monophosphate (cGMP), which is central to myriad downstream processes, including vasodilation [30–33].

The function of NO in smooth muscle cell relaxation is well-established [34–36]. Endothelial NOS (eNOS) production is highly dependent on calcium and calmodulin (CaM) [37–40]. Increased Ca^{2+} levels enhance the affinity of CaM for eNOS, which promotes the conversion of L-arginine to L-citrulline and the production of NO (Figure 2) [37–40]. The activation of cGMP stimulates the activation of protein kinase G (PKG) and myosin phosphatase, which results in increased calcium release from intracellular stores, inducing smooth muscle relaxation (Figure 2) [40,41]. While no studies have explored the direct relationship between GSTs and NO in vasodilation, there have been multiple reports that indicate a potential link between GSTs and the denitration of vasodilators and organic nitrates for vasorelaxation [11,42–47]. These investigations are described below.

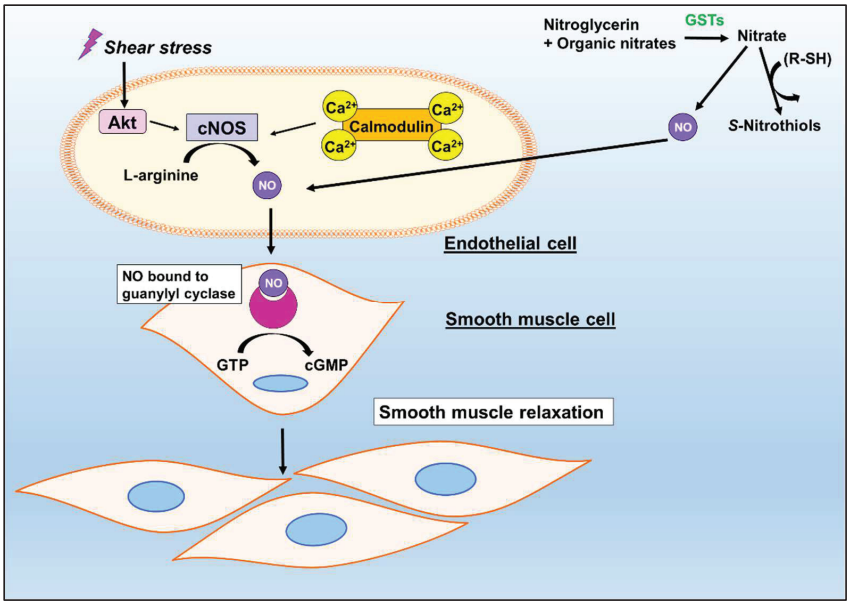

Figure 2. Schematic of the NO and potential GST-mediated regulation of vasorelaxation via sGC activation. Upon activation of constitutive nitric oxide synthases (cNOS; composed of endothelial and neuronal NOS) by calmodulin and calcium, cNOS can catalyze the conversion of L-arginine to L-citrulline to generate NO [37–40]. The production of NO can also result from the breakdown of organic nitrates, such as nitroglycerin [11–14]. NO facilitates the activation of sGC and the subsequent conversion of GTP to cGMP for vasodilation [37–40].

4. Biotransformation and Bioactivation via GSTs

4.1. Biotransformation of Organic Nitrates

Organic nitrates (R–ONO_2) are efficacious pro-drugs that result in NO generation, which promotes vasodilation and decreases blood pressure [48–52]. These drugs have been widely utilized by patients for over a century, although their mechanisms of action are still not completely understood. Early observations regarding the biotransformation of organic nitrates demonstrated that GSH was required for the conversion of the organic nitrates, nitroglycerin and erythritol tetranitrate, into inorganic nitrate (ONO^-) and oxidized GSH (GSSG) [53].

It was identified by Jakoby and colleagues [54] that GSTs catalyze the biotransformation of nitroglycerin, erythritol tetranitrate, isosorbide dinitrate (ISDN), and ethylene glycol dinitrate, to nitrite and GSSG. The mechanism of this GST-catalyzed reaction is thought to involve the nucleophilic attack of the sulfhydryl group of GSH (bound to GST) onto one of the electrophilic nitro groups of nitroglycerin (Figure 3) [55,56]. This reaction produces 1,3-dinitroglycerin and *S*-nitroglutathione ($GSNO_2$), the latter being an unstable intermediate (Figure 3) [55,56]. It is suggested that $GSNO_2$ then non-enzymatically reacts with another GSH molecule to generate GSSG, resulting in nitrite release [55,56]. The nitrite is then converted to NO via nitrite reductases (Figure 3) [57].

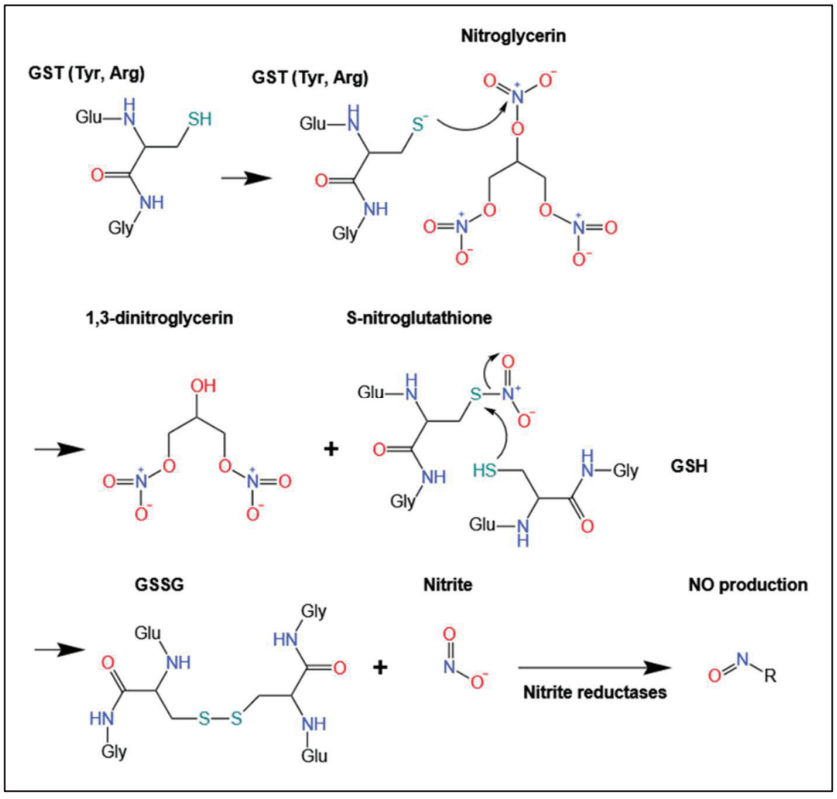

Figure 3. Schematic of the proposed mechanism for the biotransformation of nitroglycerin to form GSSG and nitrate via a mechanism mediated by the binding of GSH to GST. This scheme has been modified from [56].

Notably, the cooperation of tyrosine and arginine residues in GSTs has been proposed to be responsible for the deprotonation of the SH group within GST-bound GSH (Figure 3) [58]. Direct proof of the GST-catalyzed generation of $GSNO_2$ from pharmacologi-

cal organic nitrites, such as nitroglycerin, has yet to be established. However, studies using GST inhibitors demonstrate a direct correlation between GSTs, the organic nitrate-mediated release of NO, and subsequent vasorelaxation [42–47].

4.2. Biotransformation of Other Pro-NO Drugs by GSTs

More recently, other NO-generating agents, such as the diazeniumdiolate pro-NO drugs that are activated by GSH via GSTs, have been studied in terms of developing novel anti-cancer drugs [59–65]. These compounds take selective advantage of the elevated GST levels within tumor cells to induce their anti-cancer activity [59–65]. However, GST-mediated catalysis of NO from the pro-drug, O^2-(2,4-dinitrophenyl) 1-[(4-ethoxycarbonyl) piperazin-1-yl]diazen-1-ium-1,2-diolate (JS-K), has been demonstrated to promote vasodilation, which limits its use for cancer treatment [59,61]. While the structures of these compounds (Figure 4A) are dissimilar to the organic nitrates mentioned above (Figure 3), the mechanism of their GST-mediated biotransformation leading to NO is similar (Figure 4B).

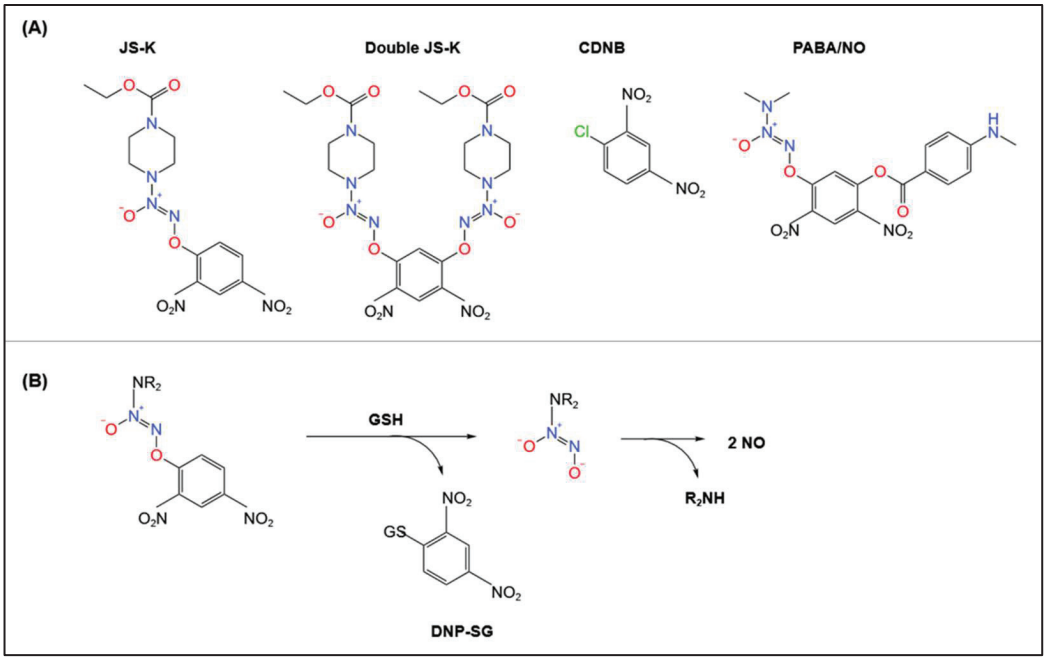

Figure 4. Pro-drugs metabolized by GSTs. (**A**) Line drawings of the chemical structures of common pro-NO drugs metabolized by GSTs. (**B**) Schematic describing the general mechanism of pro-NO drug biotransformation by GSTs.

Common pro-NO drugs include JS-K, 1-chloro-2,4-dinitrobenzene (CDNB), and O^2-{2,4-dinitro-5-[4-(*N*-methylamino)benzoyloxy]phenyl} 1-(*N*,*N*-dimethylamino)diazen-1-ium-1,2-diolate (PABA/NO) (Figure 4A). The general mechanism for the biotransformation of these agents involves a GST-catalyzed nucleophilic aromatic substitution by GSH leading to the common product, *S*-2,4-dinitrophenylglutathione (DNP-SG) (Figure 4B). The diazeniumdiolate anion product then spontaneously decomposes to generate NO.

Interestingly, a second-generation JS-K analog, "double JS-K", has been developed to generate higher concentrations of NO (4 mol NO/mol of compound) and is similarly metabolized by GSTs [66]. Although there are reports that certain pro-NO drugs react with GSH in the absence of GSTs [59,64], enhanced NO generation from JS-K has been observed with increased cellular GST levels [61]. These pro-NO drugs are of interest, as the ability of

GSTs to metabolize these agents, including organic nitrates, may be relevant to developing pharmaceuticals targeted towards NO production, such as new vasodilators.

5. GST Inhibitors Prevent Organic Nitrate-Induced Vasodilation

Several GST isoforms have been characterized in vascular smooth muscle cells, with GSTM1 demonstrating metabolic activity towards organic nitrates [12,13]. An investigation by Yeates and colleagues examined the role of GST inhibitors such as sulphobromophthalein on the spasmolytic activity of nitroglycerin and demonstrated that its dose–activity curve was displaced to the right [43]. It was shown in this study that GST activity within aortic homogenates was suppressed by sulphobromophthalein and that incubation of aortic strips with this inhibitor decreased relaxation induced by the NO-generating compound, *S*-nitroso-*N*-acetyl-penicillamine (SNAP), versus the control [43].

This later study was the first to provide evidence of the role of GSTs in the in vivo activation of organic nitrates. Moreover, these authors proposed a mechanism for the stepwise activation of nitroglycerin and other organic nitrates to *S*-nitrosoglutathione and NO for the relaxation of the aorta [43]. The impact of sulphobromophthalein on nitroglycerin metabolism has also been observed in several other studies [12,45,67].

The effects of sulphobromophthalein and another GST inhibitor, ethacrynic acid, on nitroglycerin metabolism were investigated in rabbit aortic strips [42]. Precontraction of the strips with phenylephrine followed by relaxation with nitroglycerin in the presence of ethacrynic acid resulted in a 32% inhibition of nitroglycerin-induced relaxation [42]. Unlike the previous report of Yeates and associates [43], incubation with sulphobromophthalein did not significantly decrease nitroglycerin activity [42]. To observe the metabolism of nitroglycerin, the dinitrate metabolite of this vasodilator, namely 1,3-dinitroglycerin (Figure 3), was measured within rabbit aortic tissue and was decreased in response to ethacrynic acid [42]. A significant correlation was observed between the ethacrynic acid-induced reduction in nitroglycerin activity and its inhibited metabolism [42]. Furthermore, dose–response curves revealed that ethacrynic acid suppressed nitroglycerin-induced relaxation [42].

The impact of ethacrynic acid on nitroglycerin metabolism was also investigated by Kenkare and Benet in studies using rabbit aortic strips [68]. It was demonstrated that nitroglycerin-induced relaxation and the increased cGMP levels were markedly decreased when strips were pretreated with ethacrynic acid [68]. Collectively, these studies demonstrate that GSTs, which are inhibited by ethacrynic acid, may be crucial in the vascular activation of nitroglycerin that is involved in vasorelaxation.

Impact of GST Inhibitors on the Half-Life of Nitroglycerin

In additional investigations, Benet and colleagues investigated the role of GSTs in 1,3-dinitroglycerin generation from nitroglycerin (Figure 3) in bovine coronary arteries [46]. Arteries were incubated with nitroglycerin for 2 h in the presence of GSH [46]. Under these conditions, nitroglycerin was readily degraded with a half-life of 26 min, with 1,3-dinitroglycerin being the predominant metabolite [46].

Conversely, co-incubation of the arteries with the GST inhibitors, sulphobromophthalein, and ethacrynic acid, decreased the rate of nitroglycerin degradation and formation of 1,3-dinitroglycerin [46]. Sulphobromophthalein and ethacrynic acid treatment resulted in a marked increase in the half-life of nitroglycerin from 26 to 66 min and 84 min, respectively, with a decrease in 1,3-dinitroglycerin generation [46]. The change in nitroglycerin degradation and 1,3-dinitroglycerin production suggested that in bovine coronary arteries, cytosolic GSTs are involved in vascular nitroglycerin metabolism [46].

It is notable that other GST inhibitors such as 6-(7-nitro-2, 1,3-benzoxadiazol-4-ylthio) hexanol (NBDHEX) and ezatiostat HCl (TLK199) have been extensively used in other studies and effectively suppress, primarily, GSTP1 [69,70]. However, sulphobromophthalein, ethacrynic acid, and basilen blue are more frequently used for inhibiting vasodilation [11,12,42,43,45,67,68]. This is because the latter inhibitors are more suited to inhibiting

the interaction of GSTs with organic nitrates and also preferentially target the major GST involved in this biotransformation, namely GSTM1 [11,12,42,43,45,67,68].

6. Role of GST Isoform-Specific Biotransformation on Vasodilator Activity

The results above are supported by a later investigation that purified and characterized rat aortic GSTs and examined their role in the biotransformation of nitroglycerin [45]. The GST isoforms, GSTA (Ya and Yc), GSTM (Yb2), and GSTP (Yp), were detected in the rat aortic cytosol and purified using affinity chromatography and cation- and anion-exchange chromatography [45]. These studies demonstrated the GST Yc and GST Yb2/Yp isozymes could mediate nitroglycerin biotransformation [45].

Interestingly, degradation of nitroglycerin and GST activity was highly sensitive to the GSTM inhibitors, basilen blue and sulphobromophthalein [45]. Furthermore, significant inhibition of GST activity and nitroglycerin biotransformation was observed following the removal of the GSTM Yb2 isozyme from the rat aortic cytosol via immunoprecipitation [45]. This study indicated that GSTs are crucial in the de-nitration of nitroglycerin in rat aortic cytosol and that there was isoform-specific biotransformation by the GSTM Yb2 class [45]. Another study purifying GST isoforms from blood vessels identified five GST forms immunologically related to GSTM within the aorta and heart[12]. Furthermore, the activity of GSTM toward nitroglycerin was inhibited by GST inhibitors [12].

From the above data, it is evident that GSTs, particularly GSTM1, contribute to the biotransformation of nitroglycerin and organic nitrates to produce NO for vasorelaxation. This relationship of GSTs with NO demonstrates that they promote NO-mediated signaling. In contrast, other regulatory effects of GSTs exhibit inhibition of the activity of NO via their ability to directly bind and store NO as DNICs [6,8,15,21].

7. Conclusions and Future Directions

The proposed functions of GSTs have evolved from being solely involved in detoxification to more extensive roles in NO biology and vasodilation. Key observations are the requirement of GSH by GSTs to mediate the biotransformation of organic nitrates, such as nitroglycerin, to lead to NO generation [53]. This includes studies associating GST activity with vasodilation through this biotransformation mechanism [11,12,44–47,49,67,68]. Additionally, GSTs have multiple roles in NO metabolism that include the direct binding of DNICs for storage [8,9,15] and the interaction with the key NO-generating enzyme, iNOS, to promote its degradation [5]. As such, the functional role of GSTs are diverse and appear to bridge seemingly disparate biological processes.

Further studies examining the GSTs and their roles in regulating vasodilation via its interactions with NO could lead to new therapeutic avenues to treat hypertension and other related disorders. In particular, the *GSTM1* null genotype has been associated with an increased risk of blood pressure-related disorders such as preeclampsia and hypertension [71–75]. Investigations exploring the interaction of GSTM1 with NO, especially as DNICs, and the impact on sGC activation would provide novel insights for the treatment of these conditions and potentially advance the development of new vasodilators.

Author Contributions: Conceptualization: T.M.R. and D.R.R.; writing—original draft preparation, T.M.R. and D.R.R.; writing—review and editing, T.M.R. and D.R.R. All authors have read and agreed to the published version of the manuscript.

Funding: T.M.R. thanks the Griffith University, Australian Government Research Training Program (RTP) Stipend Ph.D. Scholarship (2022-2024). D.R.R. thanks the National Health and Medical Research Council of Australia (NHMRC) for a Senior Principal Research Fellowship.

Institutional Review Board Statement: Not applicable.

Informed Consent Statement: Not applicable.

Data Availability Statement: Not applicable.

Acknowledgments: Zhao Deng is kindly thanked for his assistance in preparing Figure 3 and providing appropriate software. Mahan Gholam Azad is thanked for his help with manuscript formatting.

Conflicts of Interest: The authors declare no conflict of interest.

References

1. Morrow, C.S.; Smitherman, P.K.; Townsend, A.J. Combined Expression of Multidrug Resistance Protein (MRP) and Glutathione S-Transferase P1-1 (GSTP1-1) in MCF7 Cells and High Level Resistance to the Cytotoxicities of Ethacrynic Acid but Not Oxazaphosphorines or Cisplatin. *Biochem. Pharmacol.* **1998**, *56*, 1013–1021. [CrossRef]
2. Hayes, J.D.; Pulford, D.J. The Glutathione *S*-Transferase Supergene Family: Regulation of GST and the Contribution of the Isoenzymes to Cancer Chemoprotection and Drug Resistance. *Crit. Rev. Biochem. Mol. Biol.* **1995**, *30*, 445–520. [CrossRef] [PubMed]
3. Mannervik, B.; Board, P.G.; Hayes, J.D.; Listowsky, I.; Pearson, W.R. Nomenclature for Mammalian Soluble Glutathione Transferases. In *Methods in Enzymology*; Sies, H., Packer, L., Eds.; Gluthione Transferases and Gamma-Glutamyl Transpeptidases; Academic Press: Cambridge, MA, USA, 2005; Volume 401, pp. 1–8.
4. Sheehan, D.; Meade, G.; Foley, V.M.; Dowd, C.A. Structure, Function and Evolution of Glutathione Transferases: Implications for Classification of Non-Mammalian Members of an Ancient Enzyme Superfamily. *Biochem. J.* **2001**, *360*, 1–16. [CrossRef] [PubMed]
5. Cao, X.; Kong, X.; Zhou, Y.; Lan, L.; Luo, L.; Yin, Z. Glutathione S-Transferase P1 Suppresses INOS Protein Stability in RAW264.7 Macrophage-like Cells after LPS Stimulation. *Free Radic. Res.* **2015**, *49*, 1438–1448. [CrossRef]
6. Cesareo, E.; Parker, L.J.; Pedersen, J.Z.; Nuccetelli, M.; Mazzetti, A.P.; Pastore, A.; Federici, G.; Caccuri, A.M.; Ricci, G.; Adams, J.J.; et al. Nitrosylation of Human Glutathione Transferase P1-1 with Dinitrosyl Diglutathionyl Iron Complex in Vitro and in Vivo. *J. Biol. Chem.* **2005**, *280*, 42172–42180. [CrossRef]
7. Bocedi, A.; Fabrini, R.; Farrotti, A.; Stella, L.; Ketterman, A.J.; Pedersen, J.Z.; Allocati, N.; Lau, P.C.K.; Grosse, S.; Eltis, L.D.; et al. The Impact of Nitric Oxide Toxicity on the Evolution of the Glutathione Transferase Superfamily: A Proposal for an Evolutionart Driving Force. *J. Biol. Chem.* **2013**, *288*, 24936–24947. [CrossRef]
8. Lok, H.C.; Sahni, S.; Jansson, P.J.; Kovacevic, Z.; Hawkins, C.L.; Richardson, D.R. A Nitric Oxide Storage and Transport System That Protects Activated Macrophages from Endogenous Nitric Oxide Cytotoxicity. *J. Biol. Chem.* **2016**, *291*, 27042–27061. [CrossRef]
9. Lok, H.C.; Sahni, S.; Richardson, V.; Kalinowski, D.S.; Kovacevic, Z.; Lane, D.J.R.; Richardson, D.R. Glutathione S-Transferase and MRP1 Form an Integrated System Involved in the Storage and Transport of Dinitrosyl–Dithiolato Iron Complexes in Cells. *Free Radic. Biol. Med.* **2014**, *75*, 14–29. [CrossRef]
10. Maria, F.D.; Pedersen, J.Z.; Caccuri, A.M.; Antonini, G.; Turella, P.; Stella, L.; Bello, M.L.; Federici, G.; Ricci, G. The Specific Interaction of Dinitrosyl-Diglutathionyl-Iron Complex, a Natural NO Carrier, with the Glutathione Transferase Superfamily: Suggestion for an Evolutionary Pressure in the Direction of the Storage of Nitric Oxide. *J. Biol. Chem.* **2003**, *278*, 42283–42293. [CrossRef]
11. Matsuzaki, T.; Sakanashi, M.; Nakasone, J.; Noguchi, K.; Miyagi, K.; Sakanashi, M.; Kukita, I.; Aniya, Y.; Sakanashi, M. Effects of Glutathione S-Transferase Inhibitors on Nitroglycerin Action in Pig Isolated Coronary Arteries. *Clin. Exp. Pharmacol.* **2002**, *29*, 1091–1095. [CrossRef]
12. Tsuchida, S.; Maki, T.; Sato, K. Purification and Characterization of Glutathione Transferases with an Activity toward Nitroglycerin from Human Aorta and Heart. Multiplicity of the Human Class Mu Forms. *J. Biol. Chem.* **1990**, *265*, 7150–7157. [CrossRef]
13. Kurz, M.A.; Boyer, T.D.; Whalen, R.; Peterson, T.E.; Harrison, D.G. Nitroglycerin Metabolism in Vascular Tissue: Role of Glutathione S-Transferases and Relationship between NO. and NO_2^- Formation. *Biochem. J.* **1993**, *292*, 545–550. [CrossRef]
14. Gorren, A.C.F.; Russwurm, M.; Kollau, A.; Koesling, D.; Schmidt, K.; Mayer, B. Effects of Nitroglycerin/L-Cysteine on Soluble Guanylate Cyclase: Evidence for an Activation/Inactivation Equilibrium Controlled by Nitric Oxide Binding and Haem Oxidation. *Biochem. J.* **2005**, *390*, 625–631. [CrossRef] [PubMed]
15. Lok, H.C.; Rahmanto, Y.S.; Hawkins, C.L.; Kalinowski, D.S.; Morrow, C.S.; Townsend, A.J.; Ponka, P.; Richardson, D.R. Nitric Oxide Storage and Transport in Cells Are Mediated by Glutathione S-Transferase P1-1 and Multidrug Resistance Protein 1 via Dinitrosyl Iron Complexes. *J. Biol. Chem.* **2012**, *287*, 607–618. [CrossRef] [PubMed]
16. Watts, R.N.; Richardson, D.R. Nitrogen Monoxide (NO) and Glucose: Unexpected Links between Energy Metabolism and NO-Mediated Iron Mobilization from Cells. *J. Biol. Chem.* **2001**, *276*, 4724–4732. [CrossRef] [PubMed]
17. Watts, R.N.; Richardson, D.R. Examination of the Mechanism of Action of Nitrogen Monoxide on Iron Uptake from Transferrin. *J. Lab. Clin. Med.* **2000**, *136*, 149–156. [CrossRef] [PubMed]
18. Watts, R.N.; Richardson, D.R. The Mechanism of Nitrogen Monoxide (NO)-Mediated Iron Mobilization from Cells. *Eur. J. Biochem.* **2002**, *269*, 3383–3392. [CrossRef]
19. Richardson, D.; Neumannova, V.; Nagy, E.; Ponka, P. The Effect of Redox-Related Species of Nitrogen Monoxide on Transferrin and Iron Uptake and Cellular Proliferation of Erythroleukemia (K562) Cells. *Blood* **1995**, *86*, 3211–3219. [CrossRef]
20. Richardson, D.R.; Neumannova, V.; Ponka, P. Nitrogen Monoxide Decreases Iron Uptake from Transferrin but Does Not Mobilise Iron from Prelabelled Neoplastic Cells. *Biochim. Biophys. Acta Mol. Cell Res.* **1995**, *1266*, 250–260. [CrossRef]

21. Pedersen, J.Z.; De Maria, F.; Turella, P.; Federici, G.; Mattei, M.; Fabrini, R.; Dawood, K.F.; Massimi, M.; Caccuri, A.M.; Ricci, G. Glutathione Transferases Sequester Toxic Dinitrosyl-Iron Complexes in Cells: A Portection Mechanism against Excess Nitric Oxide. *J. Biol. Chem.* **2007**, *282*, 6364–6371. [CrossRef] [PubMed]
22. Richardson, D.; Ponka, P. The Molecular Mechanisms of the Metabolism and Transport of Iron in Normal and Neoplastic Cells. *Biochim. Biophys. Acta Mol. Cell Res.* **1997**, *1331*, 1–40. [CrossRef]
23. Richardson, D. DNICs and Intracellular Iron: Nitrogen Monoxide (NO)-Mediated Iron Release from Cells Is Linked to NO-Mediated Glutathione Efflux via MRP1. In *Radicals for Life: The Various Forms of Nitric Oxide*; Elsevier Press: Amsterdam, The Netherlands, 2007; pp. 97–118.
24. Hickok, J.R.; Sahni, S.; Shen, H.; Arvind, A.; Antoniou, C.; Fung, L.W.M.; Thomas, D.D. Dinitrosyliron Complexes Are the Most Abundant Nitric Oxide-Derived Cellular Adduct: Biological Parameters of Assembly and Disappearance. *Free Radic. Biol. Med.* **2011**, *51*, 1558–1566. [CrossRef]
25. Watts, R.N.; Hawkins, C.; Ponka, P.; Richardson, D.R. Nitrogen Monoxide (NO)-Mediated Iron Release from Cells Is Linked to NO-Induced Glutathione Efflux via Multidrug Resistance-Associated Protein 1. *Proc. Natl. Acad. Sci. USA* **2006**, *103*, 7670–7675. [CrossRef]
26. Priviero, F.B.M.; Webb, R.C. Heme-Dependent and Independent Soluble Guanylate Cyclase Activators and Vasodilation. *J. Cardiovasc. Pharmacol.* **2010**, *56*, 229–233. [CrossRef]
27. Hwang, T.L.; Wu, C.C.; Teng, C.M. Comparison of Two Soluble Guanylyl Cyclase Inhibitors, Methylene Blue and ODQ, on Sodium Nitroprusside-Induced Relaxation in Guinea-Pig Trachea. *Br. J. Pharmacol.* **1998**, *125*, 1158–1163. [CrossRef]
28. Boerrigter, G.; Costello-Boerrigter, L.C.; Cataliotti, A.; Lapp, H.; Stasch, J.-P.; Burnett, J.C. Targeting Heme-Oxidized Soluble Guanylate Cyclase in Experimental Heart Failure. *Hypertension* **2007**, *49*, 1128–1133. [CrossRef]
29. Watts, R.N.; Ponka, P.; Richardson, D.R. Effects of Nitrogen Monoxide and Carbon Monoxide on Molecular and Cellular Iron Metabolism: Mirror-Image Effector Molecules That Target Iron. *Biochem. J.* **2003**, *369*, 429–440. [CrossRef]
30. Archer, S.L.; Huang, J.M.; Hampl, V.; Nelson, D.P.; Shultz, P.J.; Weir, E.K. Nitric Oxide and CGMP Cause Vasorelaxation by Activation of a Charybdotoxin-Sensitive K Channel by CGMP-Dependent Protein Kinase. *Proc. Natl. Acad. Sci. USA* **1994**, *91*, 7583–7587. [CrossRef]
31. Schmidt, H.H.H.W.; Lohmann, S.M.; Walter, U. The Nitric Oxide and CGMP Signal Transduction System: Regulation and Mechanism of Action. *Biochim. Biophys. Acta Mol. Cell Res.* **1993**, *1178*, 153–175. [CrossRef]
32. Denninger, J.W.; Marletta, M.A. Guanylate Cyclase and the·NO/CGMP Signaling Pathway. *Biochim. Biophys. Acta Mol. Cell Res.* **1999**, *1411*, 334–350. [CrossRef]
33. Schlossmann, J.; Ammendola, A.; Ashman, K.; Zong, X.; Huber, A.; Neubauer, G.; Wang, G.-X.; Allescher, H.-D.; Korth, M.; Wilm, M.; et al. Regulation of Intracellular Calcium by a Signalling Complex of IRAG, IP 3 Receptor and CGMP Kinase Iβ. *Nature* **2000**, *404*, 197–201. [CrossRef]
34. Jurzik, L.; Froh, M.; Straub, R.H.; Schölmerich, J.; Wiest, R. Up-Regulation of NNOS and Associated Increase in Nitrergic Vasodilation in Superior Mesenteric Arteries in Pre-Hepatic Portal Hypertension. *J. Hepatol.* **2005**, *43*, 258–265. [CrossRef]
35. Meredith, I.T.; Currie, K.E.; Anderson, T.J.; Roddy, M.A.; Ganz, P.; Creager, M.A. Postischemic Vasodilation in Human Forearm Is Dependent on Endothelium-Derived Nitric Oxide. *Am. J. Physiol. Heart Circ.* **1996**, *270*, H1435–H1440. [CrossRef]
36. Gilligan, D.M.; Panza, J.A.; Kilcoyne, C.M.; Waclawiw, M.A.; Casino, P.R.; Quyyumi, A.A. Contribution of Endothelium-Derived Nitric Oxide to Exercise-Induced Vasodilation. *Circulation* **1994**, *90*, 2853–2858. [CrossRef]
37. Kuchan, M.J.; Frangos, J.A. Role of Calcium and Calmodulin in Flow-Induced Nitric Oxide Production in Endothelial Cells. *Am. J. Physiol. Cell Physiol.* **1994**, *266*, C628–C636. [CrossRef]
38. Schuh, K.; Uldrijan, S.; Telkamp, M.; Röthlein, N.; Neyses, L. The Plasmamembrane Calmodulin–Dependent Calcium Pump: A Major Regulator of Nitric Oxide Synthase I. *J. Cell Biol.* **2001**, *155*, 201–206. [CrossRef]
39. Jordan, M.L.; Rominski, B.; Jaquins-Gerstl, A.; Geller, D.; Hoffman, R.A. Regulation of Inducible Nitric Oxide Production by Intracellular Calcium. *Surgery* **1995**, *118*, 138–146. [CrossRef]
40. Williams, B.A.; Liu, C.; Deyoung, L.; Brock, G.B.; Sims, S.M. Regulation of Intracellular Ca^{2+} Release in Corpus Cavernosum Smooth Muscle: Synergism between Nitric Oxide and CGMP. *Am. J. Physiol. Cell Physiol.* **2005**, *288*, C650–C658. [CrossRef]
41. Felbel, J.; Trockur, B.; Ecker, T.; Landgraf, W.; Hofmann, F. Regulation of Cytosolic Calcium by CAMP and CGMP in Freshly Isolated Smooth Muscle Cells from Bovine Trachea. *J. Biol. Chem.* **1988**, *263*, 16764–16771. [CrossRef]
42. Lau, D.T.-W.; Benet, L.Z. Effects of Sulfobromophthalein and Ethacrynic Acid on Glyceryl Trinitrate Relaxation. *Biochem. Pharmacol.* **1992**, *43*, 2247–2254. [CrossRef]
43. Yeates, R.A.; Schmid, M.; Leitold, M. Antagonism of Glycerol Trinitrate Activity by an Inhibitor of Glutathione S-Transferase. *Biochem. Pharmacol.* **1989**, *38*, 1749–1753. [CrossRef]
44. Brien, J.F.; McLaughlin, B.E.; Breedon, T.H.; Bennett, B.M.; Nakatsu, K.; Marks, G.S. Biotransformation of Glyceryl Trinitrate Occurs Concurrently with Relaxation of Rabbit Aorta. *J. Pharmacol. Exp. Ther.* **1986**, *237*, 608–614.
45. Nigam, R.; Anderson, D.J.; Lee, S.F.; Bennett, B.M. Isoform-Specific Biotransformation of Glyceryl Trinitrate by Rat Aortic Glutathione S-Transferases. *J. Pharmacol. Exp. Ther.* **1996**, *279*, 1527–1534.
46. Lau, D.T.; Chan, E.K.; Benet, L.Z. Glutathione S-Transferase-Mediated Metabolism of Glyceryl Trinitrate in Subcellular Fractions of Bovine Coronary Arteries. *Pharm. Res.* **1992**, *9*, 1460–1464. [CrossRef]

47. Bennett, B.M.; McDonald, B.J.; Nigam, R.; Craig Simon, W. Biotransformation of Organic Nitrates and Vascular Smooth Muscle Cell Function. *Trends Pharmacol. Sci.* **1994**, *15*, 245–249. [CrossRef]
48. Cederqvist, B.; Persson, M.G.; Gustafsson, L.E. Direct Demonstration of No Formation in Vivo from Organic Nitrites and Nitrates, and Correlation to Effects on Blood Pressure and to in Vitro Effects. *Biochem. Pharmacol.* **1994**, *47*, 1047–1053. [CrossRef]
49. Münzel, T.; Steven, S.; Daiber, A. Organic Nitrates: Update on Mechanisms Underlying Vasodilation, Tolerance and Endothelial Dysfunction. *Vasc. Pharmacol.* **2014**, *63*, 105–113. [CrossRef]
50. França-Silva, M.S.; Balarini, C.M.; Cruz, J.C.; Khan, B.A.; Rampelotto, P.H.; Braga, V.A. Organic Nitrates: Past, Present and Future. *Molecules* **2014**, *19*, 15314–15323. [CrossRef]
51. Kleschyov, A.L.; Oelze, M.; Daiber, A.; Huang, Y.; Mollnau, H.; Schulz, E.; Sydow, K.; Fichtlscherer, B.; Mülsch, A.; Münzel, T. Does Nitric Oxide Mediate the Vasodilator Activity of Nitroglycerin? *Circ. Res.* **2003**, *93*, e104–e112. [CrossRef]
52. Núñez, C.; Víctor, V.M.; Tur, R.; Alvarez-Barrientos, A.; Moncada, S.; Esplugues, J.V.; D'Ocón, P. Discrepancies between Nitroglycerin and NO-Releasing Drugs on Mitochondrial Oxygen Consumption, Vasoactivity, and the Release of NO. *Circ. Res.* **2005**, *97*, 1063–1069. [CrossRef]
53. Heppel, L.A.; Hilmoe, R.J. Metabolism of Inorganic Nitrite and Nitrate Esters: II. The Enzymatic Reduction of Nitroglycerin and Erythritol Tetranitrate by Glutathione. *J. Biol. Chem.* **1950**, *183*, 129–138. [CrossRef]
54. Habig, W.H.; Keen, J.H.; Jakoby, W.B. Glutathione S-Transferase in the Formation of Cyanide from Organic Thiocyanates and as an Organic Nitrate Reductase. *Biochem. Biophys. Res. Commun.* **1975**, *64*, 501–506. [CrossRef]
55. Keen, J.H.; Habig, W.H.; Jakoby, W.B. Mechanism for the Several Activities of the Glutathione S-Transferases. *J. Biol. Chem.* **1976**, *251*, 6183–6188. [CrossRef]
56. Tsikas, D.; Surdacki, A. Biotransformation of Organic Nitrates by Glutathione S-Transferases and Other Enzymes: An Appraisal of the Pioneering Work by William B. Jakoby. *Anal. Biochem.* **2022**, *644*, 113993. [CrossRef]
57. Castiglione, N.; Rinaldo, S.; Giardina, G.; Stelitano, V.; Cutruzzolà, F. Nitrite and Nitrite Reductases: From Molecular Mechanisms to Significance in Human Health and Disease. *Antioxid. Redox Signal.* **2012**, *17*, 684–716. [CrossRef]
58. Angelucci, F.; Baiocco, P.; Brunori, M.; Gourlay, L.; Morea, V.; Bellelli, A. Insights into the Catalytic Mechanism of Glutathione S-Transferase: The Lesson from Schistosoma Haematobium. *Structure* **2005**, *13*, 1241–1246. [CrossRef]
59. Sjödin, B.; Mannervik, B. Role of Human Glutathione Transferases in Biotransformation of the Nitric Oxide Prodrug JS-K. *Sci. Rep.* **2021**, *11*, 20765. [CrossRef]
60. Weyerbrock, A.; Osterberg, N.; Psarras, N.; Baumer, B.; Kogias, E.; Werres, A.; Bette, S.; Saavedra, J.E.; Keefer, L.K.; Papazoglou, A. JS-K, a Glutathione S-Transferase-Activated Nitric Oxide Donor with Antineoplastic Activity in Malignant Gliomas. *Neurosurgery* **2012**, *70*, 497–510. [CrossRef]
61. Liu, Y.; Wang, X.; Li, J.; Tang, J.; Li, B.; Zhang, Y.; Gu, N.; Yang, F. Sphingosine 1-Phosphate Liposomes for Targeted Nitric Oxide Delivery to Mediate Anticancer Effects against Brain Glioma Tumors. *Adv. Mater.* **2021**, *33*, 2101701. [CrossRef]
62. Kaur, I.; Terrazas, M.; Kosak, K.M.; Kern, S.E.; Boucher, K.M.; Shami, P.J. Cellular Distribution Studies of the Nitric Oxide-Generating Antineoplastic Prodrug O^2-(2,4-Dinitrophenyl)1-((4-Ethoxycarbonyl)Piperazin-1-Yl)Diazen-1-Ium-1,2-Diolate Formulated in Pluronic P123 Micelles. *J. Pharm. Pharmacol.* **2013**, *65*, 1329–1336. [CrossRef]
63. Saavedra, J.E.; Srinivasan, A.; Buzard, G.S.; Davies, K.M.; Waterhouse, D.J.; Inami, K.; Wilde, T.C.; Citro, M.L.; Cuellar, M.; Deschamps, J.R.; et al. PABA/NO as an Anticancer Lead: Analogue Synthesis, Structure Revision, Solution Chemistry, Reactivity toward Glutathione, and in Vitro Activity. *J. Med. Chem.* **2006**, *49*, 1157–1164. [CrossRef] [PubMed]
64. Kumar, V.; Hong, S.Y.; Maciag, A.E.; Saavedra, J.E.; Adamson, D.H.; Prud'homme, R.K.; Keefer, L.K.; Chakrapani, H. Stabilization of the Nitric Oxide (NO) Prodrugs and Anticancer Leads, PABA/NO and Double JS-K, through Incorporation into PEG-Protected Nanoparticles. *Mol. Pharm.* **2010**, *7*, 291–298. [CrossRef] [PubMed]
65. Townsend, D.M.; Findlay, V.J.; Fazilev, F.; Ogle, M.; Fraser, J.; Saavedra, J.E.; Ji, X.; Keefer, L.K.; Tew, K.D. A Glutathione S-Transferase π-Activated Prodrug Causes Kinase Activation Concurrent with S-Glutathionylation of Proteins. *Mol. Pharmacol.* **2006**, *69*, 501–508. [CrossRef] [PubMed]
66. Shami, P.J.; Saavedra, J.E.; Bonifant, C.L.; Chu, J.; Udupi, V.; Malaviya, S.; Carr, B.I.; Kar, S.; Wang, M.; Jia, L.; et al. Antitumor Activity of JS-K [O^2-(2,4-Dinitrophenyl) 1-[(4-Ethoxycarbonyl)Piperazin-1-Yl]Diazen-1-Ium-1,2-Diolate] and Related O^2-Aryl Diazeniumdiolates in Vitro and in Vivo. *J. Med. Chem.* **2006**, *49*, 4356–4366. [CrossRef]
67. Nigam, R.; Whiting, T.; Bennett, B.M. Effect of Inhibitors of Glutathione S-Transferase on Glyceryl Trinitrate Activity in Isolated Rat Aorta. *Can. J. Physiol. Pharmacol.* **1993**, *71*, 179–184. [CrossRef]
68. Kenkare, S.R.; Benet, L.Z. Effect of Ethacrynic Acid, a Glutathione-S-Transferase Inhibitor, on Nitroglycerin-Mediated CGMP Elevation and Vasorelaxation of Rabbit Aortic Strips. *Biochem. Pharmacol.* **1993**, *46*, 279–284. [CrossRef]
69. Fulci, C.; Rotili, D.; De Luca, A.; Stella, L.; Morozzo della Rocca, B.; Forgione, M.; Di Paolo, V.; Mai, A.; Falconi, M.; Quintieri, L.; et al. A New Nitrobenzoxadiazole-Based GSTP1-1 Inhibitor with a Previously Unheard of Mechanism of Action and High Stability. *J. Enzyme Inhib. Med. Chem.* **2017**, *32*, 240–247. [CrossRef]
70. Adler, V.; Yin, Z.; Fuchs, S.Y.; Benezra, M.; Rosario, L.; Tew, K.D.; Pincus, M.R.; Sardana, M.; Henderson, C.J.; Wolf, C.R.; et al. Regulation of JNK Signaling by GSTp. *EMBO J.* **1999**, *18*, 1321–1334. [CrossRef]
71. Sandoval-Carrillo, A.; Aguilar-Duran, M.; Vázquez-Alaniz, F.; Castellanos-Juárez, F.X.; Barraza-Salas, M.; Sierra-Campos, E.; Téllez-Valencia, A.; La Llave-León, O.; Salas-Pacheco, J.M. Polymorphisms in the GSTT1 and GSTM1 Genes Are Associated with Increased Risk of Preeclampsia in the Mexican Mestizo Population. *Genet. Mol. Res.* **2014**, *13*, 2160–2165. [CrossRef]

72. Akther, L.; Rahman, M.M.; Bhuiyan, M.E.S.; Hosen, M.B.; Nesa, A.; Kabir, Y. Role of GSTT1 and GSTM1 Gene Polymorphism for Development of Preeclampsia in Bangladeshi Women. *FASEB J.* **2018**, *32*, 538.6. [CrossRef]
73. McBride, M.W.; Carr, F.J.; Graham, D.; Anderson, N.H.; Clark, J.S.; Lee, W.K.; Charchar, F.J.; Brosnan, M.J.; Dominiczak, A.F. Microarray Analysis of Rat Chromosome 2 Congenic Strains. *Hypertension* **2003**, *41*, 847–853. [CrossRef] [PubMed]
74. Gigliotti, J.C.; Tin, A.; Pourafshar, S.; Cechova, S.; Wang, Y.T.; Sung, S.J.; Bodonyi-Kovacs, G.; Cross, J.V.; Yang, G.; Nguyen, N.; et al. GSTM1 Deletion Exaggerates Kidney Injury in Experimental Mouse Models and Confers the Protective Effect of Cruciferous Vegetables in Mice and Humans. *J. Am. Soc. Nephrol.* **2020**, *31*, 102–116. [CrossRef] [PubMed]
75. Eslami, S.; Sahebkar, A. Glutathione-S-Transferase M1 and T1 Null Genotypes Are Associated with Hypertension Risk: A Systematic Review and Meta-Analysis of 12 Studies. *Curr. Hypertens. Rep.* **2014**, *16*, 432. [CrossRef] [PubMed]

biomolecules

MDPI

Article

Reversibility and Low Commitment to Forward Catalysis in the Conjugation of Lipid Alkenals by Glutathione Transferase A4-4

Michele Scian †, Lorela Paço †, Taylor A. Murphree, Laura M. Shireman and William M. Atkins *

Department of Medicinal Chemistry, University of Washington, Seattle, WA 98195-7610, USA
* Correspondence: winky@uw.edu
† These authors contributed equally to this work.

Abstract: High concentrations of electrophilic lipid alkenals formed during oxidative stress are implicated in cytotoxicity and disease. However, low concentrations of alkenals are required to induce antioxidative stress responses. An established clearance pathway for lipid alkenals includes conjugation to glutathione (GSH) via Michael addition, which is catalyzed mainly by glutathione transferase isoform A4 (GSTA4-4). Based on the ability of GSTs to catalyze hydrolysis or *retro*-Michael addition of GSH conjugates, and the antioxidant function of low concentrations of lipid alkenals, we hypothesize that GSTA4-4 contributes a homeostatic role in lipid metabolism. Enzymatic kinetic parameters for *retro*-Michael addition with trans-2-Nonenal (NE) reveal the chemical competence of GSTA4-4 in this putative role. The forward GSTA4-4-catalyzed Michael addition occurs with the rapid exchange of the C2 proton of NE in D_2O as observed by NMR. The isotope exchange was completely dependent on the presence of GSH. The overall commitment to catalysis, or the ratio of first order $k_{cat,f}$ for 'forward' Michael addition to the first order $k_{cat,ex}$ for H/D exchange is remarkably low, approximately 3:1. This behavior is consistent with the possibility that GSTA4-4 is a regulatory enzyme that contributes to steady-state levels of lipid alkenals, rather than a strict 'one way' detoxication enzyme.

Keywords: enzyme detoxication; substrate promiscuity; hydroxynonenal; lipid peroxidation; lipid alkenals; enzyme mechanism; deuterium exchange

Citation: Scian, M.; Paço, L.; Murphree, T.A.; Shireman, L.M.; Atkins, W.M. Reversibility and Low Commitment to Forward Catalysis in the Conjugation of Lipid Alkenals by Glutathione Transferase A4-4. *Biomolecules* **2023**, *13*, 329. https://doi.org/10.3390/biom13020329

Academic Editor: Vicente Rubio

Received: 31 December 2022
Revised: 31 January 2023
Accepted: 6 February 2023
Published: 9 February 2023

1. Introduction

The cytosolic glutathione transferase A4 (GSTA4-4), first characterized in detail by Mannervik and colleagues [1] and Board et al. [2], contributes to the clearance of toxic lipid alkenals formed during oxidative stress. Alkenals of particular interest include 4-hydroxynonenal (HNE), which is a major product of arachidonic acid oxidation, and trans-2-Nonenal (NE) which is derived from the oxidation of omega-7 unsaturated fatty acids. High concentrations of HNE are associated with Alzheimer's disease, Parkinson's disease, aging, diabetes, cardiovascular disease, ferroptosis and other diseases [3–8]. The lipid peroxidation product NE is a constituent of body odor that increases with aging [9,10].

Many studies indicate that lipid alkenals are not solely electrophilic toxins. At low concentrations, lipid alkenals are intracellular 'second messengers' that contribute to homeostasis by managing the expression of antioxidant enzymes [11–16]. Among the canonical glutathione transferases (GSTs), GSTA4-4 is highly efficient at catalyzing the 'Michael addition' (or 'conjugate addition') of lipid alkenals to GSH (Figure 1), and it contributes to their clearance in vivo [17,18]. In comparison, long-chain lipid alkenals are metabolized very slowly by the highly homologous GSTA1-1. GSTA1-1 is extraordinarily substrate promiscuous and is an 'archetypal' detoxication enzyme, but with little activity toward lipid alkenals.

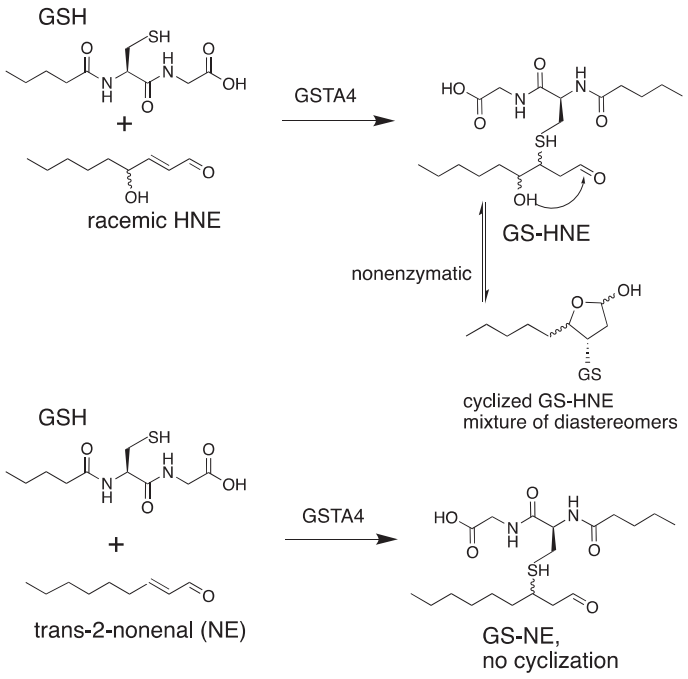

Figure 1. GSTA4-4-catalyzed reaction of lipid alkenals with GSH. The GS-HNE product (**top**) undergoes nonenzymatic cyclization to a mixture of isomers. The GS-NE product (**bottom**) does not cyclize. Curved lines indicate stereochemical heterogeneity.

This striking contrast of GSTA4-4 vs. the substrate promiscuity of GSTA1-1 has been studied in detail and quantified [19–24]. Structural and thermodynamic contributions to the differences in substrate specificity have been identified. Based on the comparison of the subtle differences in the static crystal structures, Mannervik et al. have identified key structural determinants of the specificity of GSTA4-4 and incorporated them into GSTA1-1 to elegantly redesign its activity to metabolize NE [20,21]. Although the two GST isoforms are nearly superimposable in static crystal structures (Figure 2) of the ligand-free enzymes, critical differences in the global dynamics of the proteins and of the C-terminal helix (residues 209–222) have been described [20,22–24]. GSTA4-4 and the redesigned GSTA1-1 are rigid templates with an immobile, ligand-insensitive, C-terminal helix that contributes one side of a long active site [20,25]. In contrast, the C-terminus of GSTA1-1 is highly mobile and adopts ligand-dependent conformations upon binding [20,26–28]. The C-terminus of GSTA1-1 is a mobile 'lid' over the active site. In addition, the C-terminus of GSTA1-1 uniquely exhibits thermodynamic heterogeneity, or 'molten globule' behavior, and its conformational flexibility likely contributes to its substrate promiscuity [29,30]. Structural and dynamic contributions to the substrate selectivity vs. promiscuity of these GSTs are well characterized.

In addition to differences in protein dynamics, the ionization behaviors of active site residues also distinguish the two isoforms. The conserved active site Tyr-9 is mostly protonated at pH 7.4 and hydrogen bonded to the GS^- thiolate in GSTA1-1 [31,32]. The pK_a of Tyr-9 is tuned by active site features to optimize this hydrogen bond [33,34]. In contrast, the highly acidic Tyr-9 of GSTA4-4 is unprotonated and the tyrosinate likely forms hydrogen bonds to a water molecule in GSTA4-4 [20,31], and the same water hydrogen bonds to the protonated GSH. Thus, the protonation states of GSH and Tyr-9 are opposite in GSTA1-1 vs. GSTA4-4. Mannervik et al. have proposed a detailed mechanism for GSTA4-4-dependent Michael addition of GSH to alkenals, based on these considerations [31] (Figure 2).

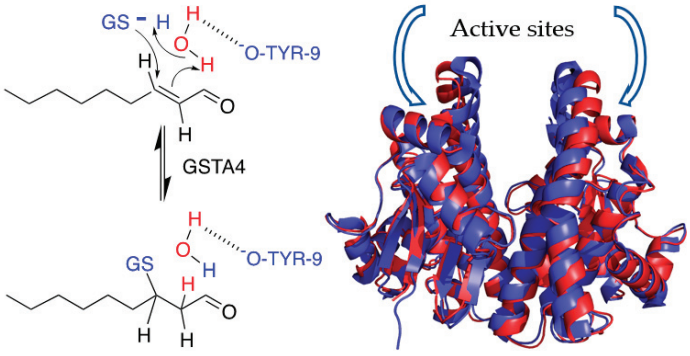

Figure 2. (**Left**): Proposed mechanism for GSH reaction with NE. The active site Tyrosine-9 (Tyr-9) is acidic and remains unprotonated. GSH is initially protonated in contrast to other GSTA isoforms. (**Right**): Superimposition of ligand-free GSTA4-4 (red, PDB1GUL) and GSTA1-1 (blue, PDB1K3L). Each monomer has an active site.

The lack of substrate-dependent conformational change with GSTA4-4 is enigmatic because conformational changes are commonly used by enzymes to achieve substrate specificity [35]. Conformational change after the substrate binding, or 'induced fit,' can increase the flux of substrate to the product by decreasing substrate dissociation and increasing the commitment to catalysis, which is defined qualitatively here as the tendency of enzyme-bound intermediates to partition forward toward the product vs. back to the substrate [35]. Similarly, rapid conformational change after product formation can minimize backward conversion to substrate and facilitate the release of the product to ensure a high commitment to catalysis. In the absence of conformational changes, enzymes do not optimize their directional commitment to catalysis. Based on the apparent lack of conformational change when GSTA4-4 binds ligands, we explored its reversibility with alkenal substrates. Although GSTA4-4 has been reported to catalyze the *retro*-Michael addition with GS-HNE at detectable rates, a detailed kinetic profile has not been reported [36]. Here, we studied the *retro*-Michael addition of GS-NE to understand the enigmatic behavior of GSTA4-4 compared to GSTA1-1. This detailed analysis indicates that GSTA4-4 is relatively inefficient in the forward direction in as much as it has a low commitment to catalysis, despite having high substrate specificity. To the extent that enzyme parameters are tuned by evolutionary pressure for specific functions, the results prompt speculation of a possible role for GSTA4-4 in regenerating lipid alkenals and GSH during extreme oxidative stress, in contrast to its presumed role as a 'one way' detoxication enzyme.

2. Materials and Methods

2.1. Protein Expression and Purification

Human GSTA4-4 and GSTA1-1 were expressed in *E. coli* and purified by affinity chromatography using S-hexylglutathione Sepharose as previously described [37,38]. The purity of the proteins was confirmed by SDS-PAGE. The purified protein solutions were then dialyzed against 100 mM sodium phosphate buffer (NaPi), pH 6.5, to remove GSH. Stock solutions of freshly prepared enzymes were finally buffer exchanged with 100 mM NaPi, pH 6.5, in D_2O and aliquots were stored at −80 °C. To ensure reproducibility, all the reported NMR experiments were conducted on aliquots of the same protein preparations. The following molar extinction coefficients were used to determine the folded protein dimer concentration: GSTA1-1, e_{280} = 46,147 $M^{-1}cm^{-1}$; GSTA4-4, e_{280} = 34,300 $M^{-1}cm^{-1}$. All enzyme concentrations are reported as concentrations of dimeric species.

2.2. UV-Vis Assays for Forward and Reverse Reactions

Reaction velocities for GSTA4-4- and GSTA1-1-catalyzed GSH conjugation to NE were determined in comparable conditions to the ones used in the H/D exchange NMR kinetic assay by monitoring depletion of NE at 224 nm via UV spectroscopy using the extinction coefficient: $\varepsilon_{224\,nm}$ = 19,220 $M^{-1}cm^{-1}$. In the reaction of 20 nM of GSTA4-4 with 20 μM GSH and 200 μM NE in 100 mM KPi, pH 6.76, 2% (v/v) ethanol was monitored for 1 min at 25 °C and the reaction velocity was calculated as the amount of NE depleted over time in the linear range of the reaction (30 s). In the reaction of 5 nM GSTA1-1 with 40 μM GSH and 200 μM NE in 100 mM KPi, pH 6.5, 1% (v/v) ethanol was monitored for 1 min and the reaction velocity was calculated as the amount of NE depleted over time in the first 30 s of the reaction. The dead time of the assay (between initiation and measurement was ~10 s. The $K_{M,\,GSH}$ for GSH (fixed NE, co-substrate), V_{max}, and $k_{cat,f}$ kinetic parameters for the forward reaction of GSTA4-4 with NE were determined by monitoring the depletion of NE at varying concentrations of GSH. A mix of 20 nM GSTA4-4 with 200 μM NE was treated with 20 μM–3 mM of freshly prepared reduced GSH to initiate the reaction in 100 mM KPi, pH 6.7, 5% (v/v) ethanol at 25 °C. Due to the high extinction coefficient of NE, we were limited to using a subsaturating concentration in the reaction mixture to avoid saturating the UV detector. Reaction velocities calculated from the amount of NE depleted in the linear range (10–30 s) of the reaction were corrected for the contribution of the spontaneous reaction in the range of GSH concentrations used and fit to the Michaelis Menten (MM) model of enzyme kinetics to obtain kinetic parameters in GraphPad Prism. The $K_{m,GSNE}$, V_{max}, and $k_{cat,r}$ kinetic parameters for the reverse reaction of GSTA4-4 with NE were determined by monitoring the appearance of NE at 224 nm via UV spectroscopy. GSH, the second product of the reverse reaction, also absorbs at 224 nm but its contribution to absorbance is negligible at the concentrations of GS-NE used. A total of 20 nM of GSTA4-4 was treated with 0.5 μM–200 μM GS-NE in 100 mM KPi, pH 6.7, 5% (v/v) ethanol at 25 °C. The concentrations of GSTA4-4 and GS-NE used were determined from preliminary experiments to allow for the linear formation of NE in the monitored reaction time (~30 s) and an adequate range of GS-NE concentrations. As in the forward direction, the reaction velocities were corrected for the contribution of the spontaneous reaction, and kinetic parameters were obtained by fitting the data to the MM model in the GraphPad Prism.

2.3. GS-NE Synthesis

GS-NE synthesis was initiated by mixing 500 mL of 1 mM NE (97%, Sigma-Aldrich, St. Louis, MO, USA) with 2 mM GSH in 50 mM KPi, pH 7.0, 2% (v/v) DMSO at RT. The reaction was monitored by ^{1}H NMR for 6 h before lowering the pH to 3.0 with 1 M HCl. The reaction mixture was then applied to SPE cartridges (Solid Phase Extraction with Waters Sep-Pak tC18, 6 cc Vac cartridge, 500 mg sorbent) in 25 mL aliquots for bulk separation of reaction mix components. Following the loading of each aliquot, the SPE cartridge was washed with 2 × 5 mL 0.1% FA and 3 × 5 mL H_2O and the GS-NE product was eluted with 1 mL of 70% ACN. At −20 °C the 70% ACN solution forms two phases, where GS-NE is contained in the bottom aqueous layer. The latter was purified by RP-HPLC with UW detection at 254 nm and a Syncronis aQ, 10 × 250 mm, 5 μm C18 column (Thermo Scientific) using a 5–74% mobile phase B gradient for 11.5 min at 4 mL/min (A: H_2O + 0.1% FA; B: ACN + 0.1% FA). The isolated LC fractions were analyzed by NMR (1D; 2D COSY, 2D TOCSY) and MS (direct infusion to Waters Synapt G1) to confirm the formation of pure GS-NE product (Supporting Information, Figures S1–S4).

2.4. LC-Mass Spectrometry

Samples for GST-catalyzed and spontaneous reactions of NE with GSH in the forward and reverse direction were prepared for preliminary determination of kinetic parameters via LC-MS. In the 'forward reaction' samples, 150 or 160 μL of 50 mM KPi, pH 6.5, and 20 μL of 10× reduced GSH solution freshly prepared in the same buffer were mixed with 20 μL of 10× NE stock in 20% ethanol, with or without 10 μL of 20× GST stock solution for a total

reaction volume of 200 μL. The final concentration of GSH was kept constant at 1.5 mM for all 'forward reaction' samples. A total of 20 nM GSTA4-4 or 1 μM GSTA1-1 (Sigma) was used in the GST-catalyzed samples. The final concentration of NE was 0, 20, 50, 100, 200, 500, 750, 1000, or 1500 μM in the GSTA4-4-catalyzed samples and 0, 5, 10, 20, 50, 100, 200, 500, and 750 μM in the GSTA1-1-catalyzed samples. NE concentrations were chosen based on kinetic parameters obtained with both enzymes by the UV assay. In the 'reverse reaction' samples, 20 μL of 10× GS-NE stock solution in 20% ethanol was added to 170 or 180 μL buffer with or without 10 μL of 20× GST stock solution. The final concentration of GS-NE was 0, 5, 10, 20, 50, 100, 200, 500, and 750 μM in the GSTA4-4-catalyzed samples, and 0, 5, 10, 20, 50, 100, 200, 500, 750, and 1000 μM in the GSTA1-1-catalyzed samples. Forward and reverse reaction samples were prepared in duplicate in a well-plate format and all were at 25 °C.

2.5. NMR Assignment of NE

The concentrations of NE (97%, Sigma-Aldrich, St. Louis, MO, USA) and stock solutions in ethanol-d6 were determined by UV-vis as previously reported (e_{225} = 19,220 $M^{-1}cm^{-1}$ and e_{224} = 13,750 $M^{-1}cm^{-1}$, respectively). For assignment purposes, NMR spectra were acquired at a resolution of 32 k points in the time domain (16 k complex) and with 64 accumulations each (sw = 6000 Hz, d1 = 3 s), with sodium 2,2-dimethyl-2-silapentane-5-sulfonate (DSS) as the internal chemical shift reference [39].

2.6. The GSH-Dependence of Deuterium Exchange

Aliquots of GSTA4-4 stock solutions were diluted to 10 μM with 100 mM deuterated NaPi buffer at pH * = 6.66 (purged with Argon for 1 min), where pH * is the reading on a standard electrode where pH * = pD + 0.4 and pD = $-\log [D^+]$. The concentrations were rapidly determined by UV-vis. To appropriate amounts of these solutions, freshly made L-Glutathione (≥98%, Sigma-Aldrich, St. Louis, MO, USA) solutions were added (reduced GSH in 100 mM deuterated NaPi, pH * = 6.66, purged with Argon for 1 min) to a final enzyme concentration of 10 nM and [GSH] = 1.5, 2.5, 5.0, 10 mM (in 600 mL total). Lastly, NE (27.5 mM stock solution in ethanol-d6) to a final concentration of 275 μM was added, immediately before starting the NMR experiment. The co-solvent concentration in each of the NMR samples was kept to 1% *v*/*v*. The contribution of the residual Glutathione present in the enzyme stock solutions was negligible, due to the low protein concentration used for these experiments. A total of 25 individual spectra (256 scans for [GSH] = 1.5 and 2.5 mM, 128 scans for [GSH] = 5.0 and 10.0 mM, 4 k complex points, sw = 6000 Hz, d1 = 1.0 s) were collected with WATERGATE solvent suppression. The dead time, t_0, between mixing and acquisition was around 3–5 min and no pre-acquisition delay between experiments was used. A 1 Hz line-broadening apodization function and zero-filling to 8 k complex points were applied before the Fourier transformation. The C2 proton resonance integrals (normalized to 1 at t_0) were fitted as a function of time to a single exponential decay. All exchange experiments were at 25 °C.

2.7. Equilibrium of GSH, NE and GS-NE by NMR

Aliquots of GSTA4-4 or GSTA1-1 (~235 nM) stock solutions were diluted to ~15 μM with 100 mM NaPi buffer, 10% D_2O, pH * = 6.82 and the concentrations were measured. These solutions were used to prepare the NMR samples (600 mL total) by adding freshly made L-Glutathione stock solutions (reduced GSH in 100 mM NaPi, 10% D_2O, pH * = 6.82) and trans-2-NE (27.5 mM stock solution in ethanol-d6). The final concentrations were as follows: 10 nM enzyme, 1.0 mM GSH, 275 mM NE 1% *v*/*v* ethanol-d6. The mixtures were allowed to react for one hour while monitored by NMR. At equilibrium, more than 85% of the product was formed. To rapidly oxidize the unreacted GSH, 40 mL of a H_2O_2 stock solution ~0.882 M (in 100 mM NaPi buffer, 10% D_2O, pH * = 6.82) was then added at a final concentration of ~55 mM and the *retro*-Michael addition was monitored by NMR. A total of 10 individual spectra were collected for A4-4 (256 scans, 16 k complex points,

sw = 6000 Hz, d1 = 1 s), whereas 30 spectra were collected for A1-1 (256 scans, 16 k complex points, sw = 6000 Hz, d1 = 1 s). WATERGATE solvent suppression and a 30 ms $T1_{rho}$ filter were used. Dead time, t_0, between mixing and acquisition was around 5–10 min and no pre-acquisition delay between experiments was used. A 1 Hz line-broadening apodization function and zero-filling to 32 k complex points were applied before the Fourier transformation.

2.8. Deuterium NMR of NE Recovered from Enzyme Incubation

A 60 mL solution 10 nM GSTA4-4, 0.5 mM NE, 1% v/v CH_3CN, in 100 mM NaPi pH * 6.82 in D_2O were incubated at room temperature for 8 h. The progress of the deuteration reaction was monitored by NMR on a 600 mL aliquot. The mixture was then applied to a centrifugal filter unit (Millipore, 10 kDa MWCO, 50 mL volume) and the filtered was passed, under vacuum, through a disposable C18 column (disposable BAKERBOND Reversed Phase Octadecyl SPE Column, J.T. Baker, 1 mL volume, 100 mg sorbent weight), to immobilize the NE. The C18 column was then washed with 10 × 1 mL H_2O, dried by centrifugation at 3000× g for 10 min and eluted with 350 µL CH_3CN. The eluted was stored at −80 °C. After the elution, the C18 column was washed with 5 mL CH_3CN, 5 mL H_2O and then with 1 mL D_2O to remove the residual H_2O for the next immobilization step. The whole incubation/extraction process was repeated after the addition of a fresh aliquot of GSTA4-4 (to a 10 nM final concentration) and NE (to a 1 mM final concentration) at the extracted solution. The eluted fractions (2 × 350 mL) were pooled together, treated with Na_2SO_4 for 24 h and transferred into an NMR tube. The ^2H NMR spectrum (4096 scans, 2048 complex points, sw = 900 Hz, d1 = 3 s) was collected using the lock channel of a triple resonance, inverse detection probe, and without proton decoupling. The deuterium resonance of CD_3CN (99.96 atom% D, Sigma-Aldrich, St. Louis, MO, USA) was used as internal chemical shift reference and set to 1.94 ppm. A 1 Hz line-broadening apodization function and zero-filling to 4 k complex points were applied before Fourier transformation.

3. Results

To characterize in greater detail the steady state behavior and reaction dynamics of GSTA4-4, we exploited NE as a model substrate. Although HNE is more impactful from a toxicological perspective, its participation in the uncatalyzed approach to equilibrium between ring-closed hemiacetal and ring-opened aldehyde (Figure 1) prohibits analysis of the reaction of interest because the nonenzymatic rates of these reactions are conflated with the enzymatic steps. Therefore, to monitor the reaction dynamics of enzyme-bound states, we focused on NE, which does not cyclize, as a model.

3.1. Steady State Forward and Reverse Reaction

The GSTA4-4-catalyzed forward reaction was monitored by two methods. A previously established method based on UV absorbance at 224 nm has been described and provides a convenient method at varying concentrations of GSH (20 µM–3 mM). The UV method is limited at high concentrations of NE, for which the absorbance saturates the detector. With this method, for variable [GSH] and 200 mM NE, initial velocities in the linear range were plotted against GSH concentration and fit with the Michaelis-Menten equation to yield $K_{M,GSH}$ = 530 µM, $k_{cat,f}$ = 89 s^{-1}, $k_{cat,f}/K_M$ = 0.17 $\mu M^{-1}s^{-1}$ for the forward reaction, where $k_{cat,f}$ and $k_{cat,r}$ refer to forward and reverse reactions. These parameters are in agreement with previously reported values [1]. As noted above, the concentration of NE was not saturating due to high absorbance at 224 nm, so the $k_{cat,f}$ values are expected to be modestly lower than the true value.

To circumvent the limitations of the UV assay with high concentrations of NE, GS-NE formation was also measured by LC-MS with 20 nM GSTA4-4, 1.5 mM GSH, and varying concentrations of NE (20 µM–1.5 mM) in 100 mM KPi, pH 6.5 (Figure 3), resulting in the following kinetic parameters: $K_{M,NE}$ = 195 µM, $k_{cat,f}$ = 184 s^{-1}, $k_{cat,f}/K_{M,NE}$ = 0.95 $\mu M^{-1}s^{-1}$. As expected, the $k_{cat,f}$ value from the LC-MS assay with saturating co-substrate is modestly

higher than the $k_{cat,f}$ from the UV assay with non-saturating co-substrate. The data are summarized in Figure 3. Recovered parameters are in Table 1 and they include a low standard error for the k_{cat} values and modest error in the K_M values. The error in $K_{M,GSH}$ is high for unknown reasons but the recovered value is in line with well-accepted values in the literature.

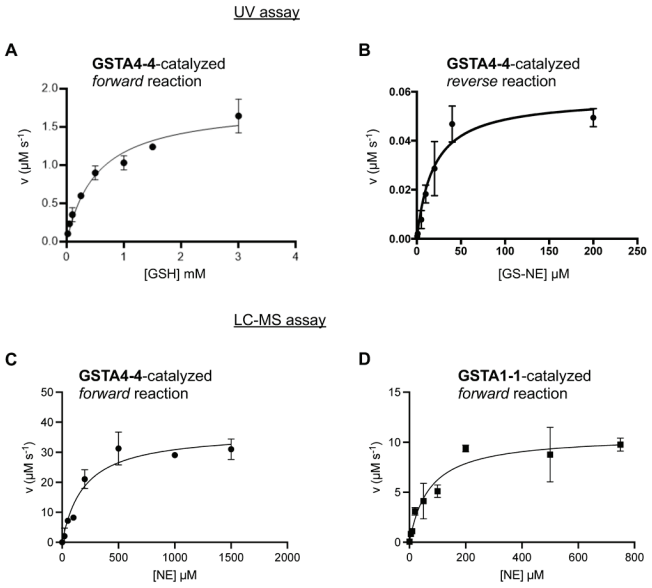

Figure 3. Steady state forward and reverse reactions of GSTA4-4 and forward reaction of GSTA1-1. (**A**): GSTA4-4 activity for the depletion of NE in the 'forward' reaction to yield GS-NE, based on the decrease in UV absorbance. (**B**): GSTA4-4 activity in the 'reverse' direction to form GSH and NE from GS-NE based on the increase in UV absorbance. (**C**): GSTA4-4 activity in the forward reaction based on LC-MS. (**D**): GSTA1-1 activity in the forward reaction based on LC-MS.

Table 1. Kinetic parameters for forward and reverse reactions.

	Forward Reaction					**Reverse Reaction**	
GSTA Isoform (Assay)	**$K_{M,GSH}$ (μM)**	**$K_{M,NE}$ (μM)**	**$k_{cat,f}$ (s^{-1})**	**$k_{cat,f}/K_M$ ($\mu M^{-1}s^{-1}$)**	**$K_{M,GS\text{-}NE}$ (μM)**	**$k_{cat,r}$ (s^{-1})**	**$k_{cat,r}/K_{M,GS\text{-}NE}$ ($\mu M^{-1}s^{-1}$)**
GSTA4-4 (UV)	530 ± 100	NA	89 ± 6	0.17	19 ± 5	1.2 ± 0.1	0.06
GSTA4-4 (LC-MS)	NA	195 ± 49	184 ± 14	0.95	NA	NA	NA
GSTA1-1 (LC-MS)	NA	71 ± 19	0.35 ± 0.1	0.0042	ND	ND	ND

NA, not applicable; the parameters for the reverse reaction were determined only by the UV assay. The K_M for NE ($K_{M,NE}$) and GSH ($K_{M,GSH}$) is reported for the LC-MS and UV assay, respectively. ND, not detected. The GSTA1-1 yields insufficient NE to measure under conditions used for GSTA4-4. All experiments were at 25 °C.

For comparison, kinetic parameters for the GSTA1-1-catalyzed reaction of GSH with NE were obtained by LC-MS in the forward direction with 1 μM GSTA1-1, 1.5 mM GSH and varying concentration of NE (5–750 μM) (Figure 3), resulting in $K_{M,NE}$ = 71 μM, k_{cat} = 0.3 s^{-1}, k_{cat}/K_M = 0.0042 $s^{-1}\mu M^{-1}$. As expected, based on previous results, GSTA1-1 is much less efficient than GSTA4-4 in conjugating NE with GSH.

For the reverse reaction, synthetic GS-NE was prepared and incubated at varying concentrations with GSTA4-4, as described in Methods. For the reverse reaction, the UV assay works well at a low extent of turnover, prior to the generation of high concentrations of NE. The appearance of NE was measured by increased absorbance at 224 nm with 10 nM GSTA4-4 and varying concentrations of GS-NE (0.5–200 μM) in 100 mM KPi, pH 6.7 (Figure 3). It is important to note that we used a mixture of GS-NE diastereomers. For the mixture, the experimentally determined $K_{M,GS\text{-}NE}$ was 19 μM and the $k_{cat,r}$ was 1.2 s^{-1}. The kinetic parameters for the reverse reaction are summarized in Table 1. A striking feature of the reverse reaction with GS-NE is the low K_M. To the extent that K_M can be a surrogate for K_D in some cases, the affinity of GS-NE for GSTA4-4 is much greater than the substrates for the forward reaction, GSH and NE. Interestingly, we observe no product inhibition in the reverse direction, despite the high affinity for GS-NE compared to GSH or NE. In turn, the lack of product inhibition combined with the relatively high reverse rate suggests the possibility of rapid conversion of bound GS-NE to GSH and NE. For the reverse reaction, GSTA1-1 exhibited no detectable reaction at 10 nM enzyme, which was the concentration of GSTA4-4 used for the reverse reaction.

3.2. Solvent Exchange with NE by NMR

Based on our observation and previous literature reports that GSTA4-4 catalyzes the *retro*-Michael addition of GSH with NE, we considered GST-catalyzed solvent deuterium incorporation into NE as a probe of the relative rates of forward and reverse partitioning of an enzyme-bound Michael adduct. The ^{1}H NMR spectrum of NE is shown in Figure 4. When NE was incubated with 10–50 μM GSH and 10 nM GSTA4-4 in D_2O the NMR signal from the C2 proton of NE rapidly decreased. At the same time, the C3 proton changed from a well-resolved doublet of triplets to a poorly resolved multiplet, without any loss in total peak area. Similarly, the aldehydic proton at C1 changed from a doublet to a singlet without the loss of peak area. Changes in the NMR spectrum occurred before any detectable depletion of NE or without detectable formation of GS-adducts in the NMR spectrum indicating that solvent exchange happens on a time scale that is not significantly slower than product, GS-alkenal, formation. These spectral changes did not occur at any detectable level in the absence of GSTA4-4, on the time scale of these experiments. These results are shown in Figure 4 and they suggest that deuterium was incorporated at C2 of the starting substrate NE in an enzyme-mediated process. The results suggest that an initially formed GS-NE adduct with deuterium incorporated from solvent can readily undergo *retro* Michael addition to yield deuterated NE substrate. For comparison, parallel experiments with GSTA1-1 demonstrated no deuterium into NE except at much longer times and in the presence of 1000-fold more enzyme, as shown in Section 3.6.

A critical observation of the data in Figure 4 is the change in peak splitting of H1 and H3 due to ^{2}H-incorporation at C2 without loss of total intensity of H1 or H3, where ^{2}H designates deuterium vs. a proton, ^{1}H. This suggests either the system is at chemical equilibrium prior to reaching isotopic equilibrium, or isotope exchange is much faster than GS-NE production. In fact, under limiting [GSH] conditions, GS-NE is detectable, albeit with low intensity, and the peak areas of the GS-NE protons were monitored. The H1 proton of GS-NE is shifted to the two diastereotopic singlets H′, H″ at 9.56 ppm and 9.58 ppm upon conjugation to GSH (Figure 4C and Supporting Information Figure S1). Based on the NMR, [GS-NE] does not change during the ^{1}H-exchange of NE observed by NMR (5 min dead time). The solvent exchange is not faster than the forward reaction to yield GS-NE. The NMR results report on solvent isotope exchange at equilibrium, as discussed below in Section 3.6.

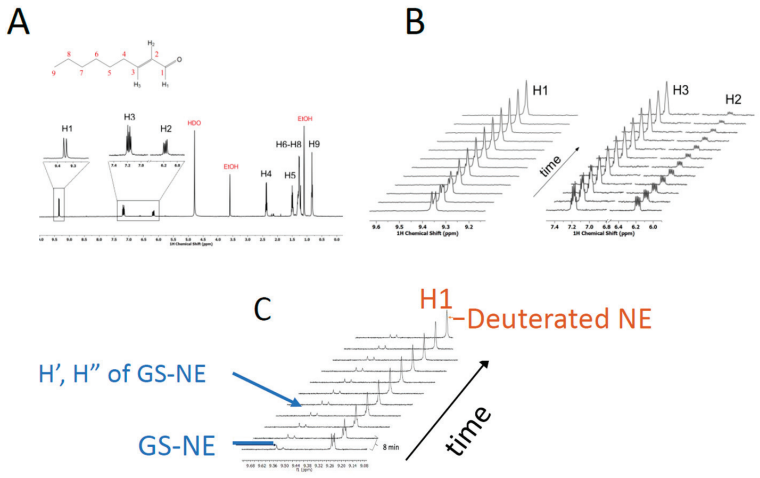

Figure 4. Chemical Structure and ^{1}H-NMR spectrum of NE. (**A**) The structure of NE is shown with carbons or corresponding protons numbered. The ^{1}H-NMR spectrum of NE is shown below its chemical structure. The H1, H2, and H3 protons provide probes of the D_2O exchange at carbon 2, or C2. (**B**) Time-dependent changes in H1, H2, H3 upon incubation with GSTA4-4 in the presence of GSH. (**C**) Time-dependent exchange of ^{1}H of NE to yield deuterated substrate without change in [GS-NE] after the dead time of 4–5 min. The protons H′ and H″ are from GS-NE formed at low concentrations due to limiting [GSH]. For (**B**,**C**), the arrows show the time dependence of the spectra.

3.3. The Site of Deuterium Incorporation from Solvent Exchange

The observed changes in the ^{1}H-NMR spectrum of NE are consistent with the incorporation of deuterium (^{2}H) at C2. To demonstrate directly that the ^{1}H NMR spectral changes were due to the incorporation of deuterium at C2, NE was isolated from incubations with NE, GSH and GSTA4-4 in D_2O buffer and its deuterium NMR spectrum was acquired (Figure S5, Supporting Information). The deuterium spectrum unambiguously confirms that solvent deuterons are incorporated at the C2 position and only at the C2 position. No other protons of NE were exchanged with deuterons.

3.4. Solvent Exchange Requires GSH

To investigate the mechanism of this exchange reaction we measured the rate of exchange at variable [GSH]. Specifically, we aimed to determine whether an initially formed GS-alkenal conjugate was reversibly collapsing into substrates or whether the reversible addition–elimination of water to the alkenal in the active site was the source of deuterium incorporation. When the rate of solvent deuterium incorporation into NE was determined at variable [GSH], there was a dramatic increase in the rates of exchange with increasing [GSH] up to 20 μM (Supporting Information, Figure S6). Above 20 μM [GSH] the rate of deuterium incorporation became too fast to measure by NMR. Notably, in the absence of added GSH, no exchange was detected over the course of 2 h. The exchange of solvent deuterium at C2 of NE was completely dependent on the presence of GSH and GSTA4-4 under the time scales studied here. The obligate presence of GSH in the exchange reaction indicates that the exchange occurs from an intermediate that lies on the reaction coordinate for the formation of GS-alkenal, presumably the [GST•GS-alkenal] intermediate.

3.5. Equilibrium Constant for the Reaction

With the NMR spectra of synthetic GS-NE in hand, the NMR provides a convenient and direct measurement of K_{eq} for the reaction of GSH + NE ⇔ GS-NE. The protons at C1 in the GS-NE (H1′, H1″) are shifted to 9.56 ppm–9.58 ppm and are completely resolved from the H1 of NE. These peaks are assigned as diastereomeric. With 1 mM NE and 2.5 mM

GSH the time-dependent conversion to the equilibrium mixture of GSH, NE, and GS-NE was followed. At equilibrium, the ratio of peak integrals for the H1′ and H″ protons in GS-NE to the peak integral for H1 of NE is:

$$\frac{\text{H1}'_{\text{GS-NEeq}}}{\text{H1}_{\text{NEeq}}} = \frac{[\text{GS}-\text{NE}]_{\text{eq}}}{[\text{NE}]_{\text{eq}}} = 16.7 \pm 5 \quad (1)$$

Based on the 1:1 NE:GSH stoichiometric requirement of the reaction, the K_{eq} = [GS-NE]/[GSH][NE] is calculated to be 10.7 mM^{-1}. With Keq = 10.7, at equilibrium, approximately 94.4% of the material is product GS-NE and only 5.6% is GSH or NE on a molar basis. The propagated error of the measurement is large in terms of the value of K_{eq} but small in terms of the percentages. For example, with a value of $[GS\text{-}NE]_{eq}/[NE]_{eq}$ = 11.7 as the lower limit within the standard error for the experimentally measured ratio, instead of 16.7, the distribution of material is 92.2% GS-NE and 7.8% GSH or NE. The K_{eq} measured by NMR indicates the reaction is highly favored in the forward conjugate addition direction and is thermodynamically highly unfavorable in the reverse elimination direction. The reaction to generate GSH and NE from GS-NE is thermodynamically 'uphill'.

3.6. Estimating Relative Rates of Deuterium Exchange into NE and Formation of GS-NE

The results in Figure 4 demonstrate that the solvent isotope exchange at equilibrium is easily observable. Therefore, to compare the partitioning of the intermediate [GST•GS-NE] complex backwards to form GSH and NE vs. forward to yield GS-NE, we employed a substrate depletion analysis of the ^{1}H-NE (undeuterated NE) under equilibrium conditions using the H1 integrated peak area for the proton at C2. Under these conditions, total NE is not changing but the isotopic composition is changing. The time-dependent decrease in integrated peak area of the C2 NMR peak when the reaction was run in D_2O was fit to a single exponential which yields an empirical first-order rate of ^{1}H-NE depletion or solvent exchange, k_{dep}, which is a fraction of the true $k_{cat,ex}$ for the exchange because the enzyme is not saturated with GSH or NE under conditions that allow for observation by NMR. The exponential behavior and k_{dep} are validated surrogates for the first-order k_{cat} as long as substrate binding is not rate limiting [40]. At 200 μM NE, 20 μM GSH, and 10 nM GST the half-life for NE deuteration was 66.8 min (Figure 5), which corresponds to a k_{dep} for NE of 149.7/min. When normalized to enzyme concentration and saturating [GSH], the $k_{cat,ex}$ for GSTA4-4-dependent deuteration of NE is 69 s^{-1}, which is not much slower than the measured $k_{cat,f}$ for GS-NE formation of 184 s^{-1} determined by the LC-MS assay and even closer to the value determined by the UV assay (Table 1). For comparison, the time-dependent exponential loss of ^{1}H-NE was also determined with GSTA1-1 at 100-fold higher enzyme concentration. The results for both GSTA4-4 and GSTA1-1 are shown in Figure 5 and the recovered rates are summarized in Table 2. Sources of potential error in these initial estimates are described in the Discussion. It is notable, however, that GSTA4-4 exhibits a relatively low ratio of forward partitioning compared to backward exchange compared to the much slower GSTA1-1.

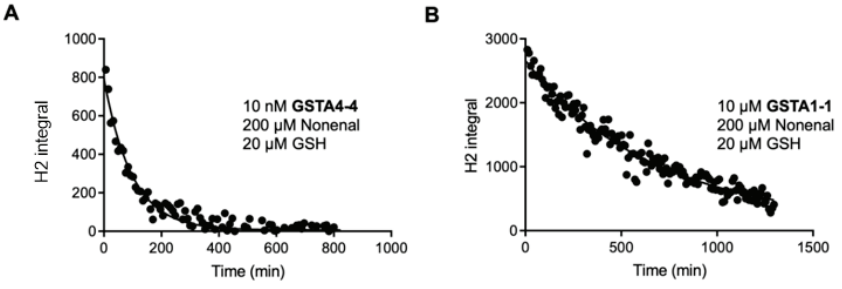

Figure 5. Exponential fits of ^{1}H-NE depletion with GSTA4-4 (**A**) or GSTA1-1 (**B**).

Table 2. Rate of ^{1}H-NE depletion (k_{ex}) and GS-NE formation ($k_{cat,f}$) and for GSTA4-4 and GSTA1-1.

GSTA Isoform	H/D Exchange, k_{ex} (s^{-1})	GS-NE Formation, $k_{cat,f}$ (s^{-1})	Ratio $k_{cat,f}/k_{ex}$
GSTA4-4	63 ± 17	184 ± 14	2.9
GSTA1-1	0.017 ± 0.18	0.35 ± 0.1	20.5

All reactions were at 25 °C.

Concentrations of reagents are shown in each panel. The integrated peak area of the C2 proton (H2) was fit to a single exponential decay. GSTA1-1 exhibits a detectable exchange but is much slower than GSTA4-4.

4. Discussion

The chemical competence of GSTs to catalyze the thermodynamically favored hydrolysis of thioesters or the breakdown of GSH-conjugates has been documented previously [41–45] The mechanistic details of such reverse GST reactions have been explored in a few cases with in vitro chemical probes [41,43]. The potential biological or toxicological effects of toxins delivered to tissues as a result of the breakdown of GSH-conjugates have been demonstrated and discussed [46–48]. For example, the release of methyl isocyanate from its GSH conjugate contributed to the toxicological impact of the 'Bhopal disaster.' In that case, the GSH conjugate provided a vehicle for the transport of methyl isocyanate throughout multiple organs or tissues [49]. In most cases, the nonenzymatic or GST-mediated reversibility of GSH conjugate formation is likely to be deleterious to the organism.

In contrast, the potential advantages of the reversibility of GSTs have not been considered in detail, including the case of the endogenously formed lipid alkenals. The role of GSTA4-4 in regulating HNE levels in cells has been documented based on the 'forward' conjugation to GS-HNE [50,51]. Transfection of cells with GSTA4-4 alters cellular proliferation and oxidative stress responses due to the depletion of HNE. The depletion of HNE apparently leads to altered expression of many other genes related to oxidative stress or cell growth [14,50,51]. Here, we explored the possible contribution of the reversibility of GSTA4-4-catalyzed lipid alkenal conjugation. We hypothesized that GSTA4-4 kinetic behavior could also contribute to the homeostasis of oxidative stress responses by maintaining low concentrations of the lipid alkenals that could possibly activate the NRf2-Keap pathway and by contributing to the regeneration of GSH during oxidative stress. The studies summarized here demonstrate that GSTA4-4 is not evolutionarily optimized as a 'one way' detoxication enzyme to clear lipid alkenals. Instead, enzymatic parameters indicate that GSTA4-4 is an efficient catalyst of *retro*-Michael addition with lipid alkenals and it has a low commitment to catalysis in the forward direction to form GSH adducts. Specifically, the $k_{cat,f}/K_{M,NE}$ and $k_{cat,f}/K_{M,GSH}$ values in the forward direction are only 16-fold and three-fold larger than the $k_{cat,r}/K_{M,GS\text{-}NE}$ in the reverse direction (Table 1). The results from isotope exchange studies demonstrate that GSTA4-4 catalyzes the exchange of solvent deuterium at C2 of NE on time scales that are comparable to the net conversion of GSH and NE to GS-NE. GSTA4-4 is highly reversible due to both a low $K_{M,GS\text{-}NE}$ and rapid conversion of bound GS-NE to GSH and NE. The rapid conversion of bound GS-NE to GSH and NE results in a low commitment to catalysis in the forward direction, as defined in Table 2. It is striking that GSTA1-1 actually has a higher relative commitment to catalysis based on this criterion. Although GSTA1-1 is a very poor catalyst for the metabolism of NE (or HNE) with slow flux in either direction, it has a higher relative flux of enzyme-bound intermediate toward GS-NE than to NE and GSH than GSTA4-4 does.

An accurate estimation of the commitment to catalysis based on NMR and steady-state UV-vis or LC-MS is confounded by stereochemical and kinetic considerations. The requirement for D_2O as a solvent to measure the incorporation of deuterium into NE obviously introduces possible solvent KIEs in both directions. Two types of solvent KIEs could contribute. There could be D_2O KIEs on the physical binding steps, such as the

release or binding of GS-NE, NE and GSH. Effects of D_2O on ligand binding are usually less than 2. Because GSTA4-4 undergoes a minimal conformational change upon binding, and binding is controlled by diffusive properties, solvent isotope effects on binding and dissociation would be negligible [52–54]. There are more likely to be solvent isotope KIEs on the chemical steps in both directions in as much as multiple protons are likely to be involved in bond making or breaking in the transition state(s) for the conjugation–elimination steps of bound ligands, summarized in Figure 1. To determine the magnitude of these solvent isotope effects or the number of protons in flight in the transition states would require proton inventory studies for both forward and reverse reactions [52–54].

In addition to solvent kinetic isotope effects, a primary KIE is also expected in D_2O for the deuterium exchange reaction to produce ^{2}H-NE from GS-NE. Once deuterium is incorporated at C2, a significant primary isotope would be expected to remove it and regenerate NE [52,55]. Thus, the flux of [GST•GS-NE] backwards to [GST•GSH•NE] would be expected to be faster in H_2O than in our experiments with D_2O. The magnitude of primary isotope effects for E2 elimination reactions can vary between 2–8 [56]. If the primary isotope effect were dominant over the solvent isotope effects, the measured partition ratio of forward flux to reverse reaction measured by deuterium exchange could be a significant overestimation and the reverse partitioning of the [GST•GS-NE] intermediate could be much greater in H_2O than observed in our experiments. The magnitude of the primary KIE could, however, be masked (decreased) if the proton removal from C2 in the reverse direction is not stereospecific, and this further complicates any prediction of the expected KIE. The stereochemical course of the conjugation of GSH to the prochiral C3 of NE catalyzed by GSTA4-4 is not defined, in contrast to the reaction with HNE, which occurs at the si face of both (R) and (S) HNE [57].

Finally, secondary deuterium isotope effects on the reverse reaction would also be expected as the rehybridization of C3 from sp3 to sp2 would be faster with deuterium incorporated at C2 [55]. This would yield a faster reverse rate in D_2O than in H_2O and have the opposite effect of the primary isotope effect. However, secondary isotope effects are small (<<2) and this would not be likely to increase the apparent rate significantly. In summary, many experiments with various combinations of isotopic solvent and substrates would be required to precisely measure the partition ratio of the forward reaction to GS-NE vs. the reverse reaction to substrates. However, based on the expected directions and magnitudes of solvent and primary kinetic isotope effects, the estimated ratio of forward-to-reverse flux in Table 2 may be an upper limit to the ratio of $k_{cat,f}/k_{ex}$ in H_2O.

Regardless of the complexity of the kinetics and stereochemical course of the reaction, the results provide the first indication that GSTA4-4 is not specifically evolved to optimize the flux of alkenals to their GSH conjugates. This is particularly apparent in comparison to GSTA1-1, which is a very poor catalyst of the Michael addition and the *retro* Michael addition with NE, but has a higher relative commitment to catalysis in the forward direction once GS-NE is formed on the enzyme. This is a striking difference in light of the much greater specificity of GSTA4-4 for long-chain alkenals and the extreme substrate promiscuity of GSTA1-1. In turn, this raises the interesting speculation that GSTA4-4 is not evolutionarily optimized to clear lipid alkenals, despite its high substrate specificity compared to other canonical cytosolic GSTs. Rather GSTA4-4 might have evolved to balance the clearance of lipid alkenals with the regeneration of GSH and alkenal to maintain Nrf2-dependent oxidative stress responses or regenerate GSH during extreme oxidative stress.

5. Conclusions

Lipid alkenals play dual roles as electrophilic toxins and 'second messengers' that ensure an adequate antioxidant response by activating the Nrf2 transcriptional activator. GSTA4-4 provides a metabolic clearance pathway for lipid alkenals via GSH conjugation, including 2-nonenal (NE). Results presented here with NE reveal that GSTA4-4 efficiently catalyzes the regeneration of GSH and NE from the Michael adduct GS-NE, and the reverse reaction is characterized by remarkably low $K_{M,GS\text{-}NE}$ compared to the K_M values for GSH

or NE in the forward reaction. Furthermore, GSTA4-4 catalyzes the exchange of solvent deuterons from D_2O specifically at C2 of starting NE on a similar time scale as GS-NE formation. This underscores the high degree of reversibility for GSTA4-4 catalyzed Michael addition. The isotope exchange was dependent on the presence of GSH, indicating that exchange occurs from an intermediate formed en route to GS-NE. The results suggest a possible contribution of GSTA4-4 to the homeostasis during oxidative stress by GSTA4-4, which can readily regenerate GSH or lipid alkenal. Restoring GSH and generating low levels of lipid alkenal could provide short-term and long-term benefits during oxidative stress.

Supplementary Materials: The following supporting information can be downloaded at: https://www.mdpi.com/article/10.3390/biom13020329/s1, Figure S1: ^{1}H-NMR Spectra for NE, GSH, GSSG, and GS-NE; Figure S2: 2D COSY Spectrum of synthetic GS-NE; Figure S3: 2D TOCSY spectrum of synthetic GS-NE; Figure S4: Full scan (top) and MS-MS spectra of synthetic GS-NE; Figure S5: Demonstration that deuterium (^{2}H) is exchanged specifically at C2 of NE; Figure S6: H/D exchange of NE requires GSH.

Author Contributions: Conceptualization, W.M.A., L.P. and M.S.; methodology, M.S.,T.A.M., L.P. and L.M.S.; validation, L.P. and M.S.; formal analysis, M.S., L.P., T.A.M., L.M.S. and W.M.A.; data curation, M.S., L.P. and T.A.M.; writing—original draft preparation, M.S., L.P. and W.M.A.; writing—review and editing, M.S., L.P. and W.M.A.; supervision, W.M.A. and M.S.; project administration, W.M.A.; funding acquisition, W.M.A. All authors have read and agreed to the published version of the manuscript.

Funding: This research was funded by The National Institutes of Health Grant GM862284 (WMA).

Institutional Review Board Statement: Not applicable.

Informed Consent Statement: Not applicable.

Data Availability Statement: Not applicable.

Conflicts of Interest: The authors declare no conflict of interest. The funders had no role in the design of the study; in the collection, analyses, or interpretation of data; in the writing of the manuscript; or in the decision to publish the results.

References

1. Hubatsch, I.; Ridderström, M.; Mannervik, B. Human glutathione transferase A4-4: An alpha class enzyme with high catalytic efficiency in the conjugation of 4-hydroxyNE and other genotoxic products of lipid peroxidation. *Biochem. J.* **1998**, *330 Pt 1*, 175–179. [CrossRef] [PubMed]
2. Board, P.G. Identification of cDNAs encoding two human alpha class glutathione transferases (GSTA3 and GSTA4-4) and the heterologous expression of GSTA4-4. *Biochem. J.* **1998**, *330 Pt 2*, 827–831. [CrossRef] [PubMed]
3. Sousa, B.C.; Pitt, A.R.; Spickett, C.M. Chemistry and analysis of HNE and other prominent carbonyl-containing lipid oxidation compounds. *Free. Radic. Biol. Med.* **2017**, *111*, 294–308. [CrossRef] [PubMed]
4. LoPachin, R.M.; Gavin, T.; Petersen, D.R.; Barber, D.S. Molecular Mechanisms of 4-Hydroxy-2-nonenal and Acrolein Toxicity: Nucleophilic Targets and Adduct Formation. *Chem. Res. Toxicol.* **2009**, *22*, 1499–1508. [CrossRef]
5. Csala, M.; Kardon, T.; Legeza, B.; Lizák, B.; Mandl, J.; Margittai, É.; Puskás, F.; Száraz, P.; Szelényi, P.; Bánhegyi, G. On the role of 4-hydroxynonenal in health and disease. *Biochim. Biophys. Acta BBA-Mol. Basis Dis.* **2015**, *1852*, 826–838. [CrossRef]
6. Schaur, R.J.; Siems, W.; Bresgen, N.; Eckl, P.M. 4-Hydroxy-nonenal—A Bioactive Lipid Peroxidation Product. *Biomolecules* **2015**, *5*, 2247–2337. [CrossRef]
7. Forman, H.J.; Fukuto, J.M.; Miller, T.; Zhang, H.; Rinna, A.; Levy, S. The chemistry of cell signaling by reactive oxygen and nitrogen species and 4-hydroxynonenal. *Arch. Biochem. Biophys.* **2008**, *477*, 183–195. [CrossRef]
8. Guéraud, F. 4-Hydroxynonenal metabolites and adducts in pre-carcinogenic conditions and cancer. *Free. Radic. Biol. Med.* **2017**, *111*, 196–208. [CrossRef]
9. Ishino, K.; Wakita, C.; Shibata, T.; Toyokuni, S.; Machida, S.; Matsuda, S.; Matsuda, T.; Uchida, K. Lipid Peroxidation Generates Body Odor Component trans-2-Nonenal Covalently Bound to Protein in Vivo. *J. Biol. Chem.* **2010**, *285*, 15302–15313. [CrossRef]
10. Saito, K.; Tokorodani, Y.; Sakamoto, C.; Kataoka, H. Headspace Solid-Phase Microextraction/Gas Chromatography–Mass Spectrometry for the Determination of 2-Nonenal and Its Application to Body Odor Analysis. *Molecules* **2021**, *26*, 5739. [CrossRef]
11. Wójcik, P.; Gęgotek, A.; Žarković, N.; Skrzydlewska, E. Oxidative Stress and Lipid Mediators Modulate Immune Cell Functions in Autoimmune Diseases. *Int. J. Mol. Sci.* **2021**, *22*, 723. [CrossRef]
12. Gasparovic, A.C.; Milkovic, L.; Sunjic, S.B.; Zarkovic, N. Cancer growth regulation by 4-hydroxynonenal. *Free. Radic. Biol. Med.* **2017**, *111*, 226–234. [CrossRef]

13. Noguchi, N. Role of Oxidative Stress in Adaptive Responses in Special Reference to Atherogenesis. *J. Clin. Biochem. Nutr.* **2008**, *43*, 131–138. [CrossRef]
14. Awasthi, Y.C.; Ramana, K.V.; Chaudhary, P.; Srivastava, S.K.; Awasthi, S. Regulatory roles of glutathione-S-transferases and 4-hydroxynonenal in stress-mediated signaling and toxicity. *Free. Radic. Biol. Med.* **2017**, *111*, 235–243. [CrossRef]
15. Wu, R.P.; Hayashi, T.; Cottam, H.B.; Jin, G.; Yao, S.; Wu, C.C.N.; Rosenbach, M.D.; Corr, M.; Schwab, R.B.; Carson, D.A. Nrf2 responses and the therapeutic selectivity of electrophilic compounds in chronic lymphocytic leukemia. *Proc. Natl. Acad. Sci. USA* **2010**, *107*, 7479–7484. [CrossRef]
16. Gerhäuser, C.; Klimo, K.; Hümmer, W.; Hölzer, J.; Petermann, A.; Garreta-Rufas, A.; Böhmer, F.-D.; Schreier, P. Identification of 3-hydroxy-β-damascone and related carotenoid-derived aroma compounds as novel potent inducers of Nrf2-mediated phase 2 response with concomitant anti-inflammatory activity. *Mol. Nutr. Food Res.* **2009**, *53*, 1237–1244. [CrossRef]
17. Mol, M.; Regazzoni, L.; Altomare, A.; Degani, G.; Carini, M.; Vistoli, G.; Aldini, G. Enzymatic and non-enzymatic detoxification of 4-hydroxynonenal: Methodological aspects and biological consequences. *Free. Radic. Biol. Med.* **2017**, *111*, 328–344. [CrossRef]
18. Hartley, D.P.; A Ruth, J.; Petersen, D.R. The Hepatocellular Metabolism of 4-Hydroxynonenal by Alcohol Dehydrogenase, Aldehyde Dehydrogenase, and Glutathione S-Transferase. *Arch. Biochem. Biophys.* **1995**, *316*, 197–205. [CrossRef]
19. Nath, A.; Atkins, W.M. A quantitative index of substrate promiscuity. *Biochemistry.* **2008**, *47*, 157–166. [CrossRef]
20. Bruns, C.M.; Hubatsch, I.; Ridderström, M.; Mannervik, B.; Tainer, J. Human glutathione transferase A4-4 crystal structures and mutagenesis reveal the basis of high catalytic efficiency with toxic lipid peroxidation products. *J. Mol. Biol.* **1999**, *288*, 427–439. [CrossRef]
21. Nilsson, L.O.; Gustafsson, A.; Mannervik, B. Redesign of substrate-selectivity determining modules of glutathione transferase A1–1 installs high catalytic efficiency with toxic alkenal products of lipid peroxidation. *Proc. Natl. Acad. Sci. USA* **2000**, *97*, 9408–9412. [CrossRef] [PubMed]
22. Hou, L.; Honaker, M.T.; Shireman, L.M.; Balogh, L.M.; Roberts, A.G.; Ng, K.-C.; Nath, A.; Atkins, W.M. Functional Promiscuity Correlates with Conformational Heterogeneity in A-class Glutathione S-Transferases. *J. Biol. Chem.* **2007**, *282*, 23264–23274. [CrossRef] [PubMed]
23. Ibarra, C.A.; Chowdhury, P.; Petrich, J.W.; Atkins, W.M. The Anomalous pK of Tyr-9 in Glutathione S-Transferase A1-1 Catalyzes Product Release. *J. Biol. Chem.* **2003**, *278*, 19257–19265. [CrossRef] [PubMed]
24. Grahn, E.; Novotny, M.; Jakobsson, E.; Gustafsson, A.; Grehn, L.; Olin, B.; Madsen, D.; Wahlberg, M.; Mannervik, B.; Kleywegt, G.J. New crystal structures of human glutathione transferase A1-1 shed light on glutathione binding and the conformation of the C-terminal helix. *Acta Crystallogr. Sect. D Biol. Crystallogr.* **2006**, *62 Pt 2*, 197–207. [CrossRef] [PubMed]
25. Balogh, L.M.; Le Trong, I.; Kripps, K.A.; Tars, K.; Stenkamp, R.E.; Mannervik, B.; Atkins, W.M. Structural Analysis of a Glutathione Transferase A1-1 Mutant Tailored for High Catalytic Efficiency with Toxic Alkenals. *Biochemistry* **2009**, *48*, 7698–7704. [CrossRef]
26. Zhan, Y.; Rule, G.S. Glutathione induces helical formation in the carboxy terminus of human glutathione transferase A1-1. *Biochemistry.* **2004**, *43*, 7244–7254. [CrossRef]
27. Sinning, I.; Kleywegt, G.J.; Cowan, S.W.; Reinemer, P.; Dirr, H.; Huber, R.; Gilliland, G.L.; Armstrong, R.N.; Ji, X.; Board, P.G.; et al. Structure Determination and Refinement of Human Alpha Class Glutathione Transferase A1-1, and a Comparison with the Mu and Pi Class Enzymes. *J. Mol. Biol.* **1993**, *232*, 192–212. [CrossRef]
28. Adman, E.T.; Le Trong, I.; Stenkamp, R.E.; Nieslanik, B.S.; Dietze, E.C.; Tai, G.; Ibarra, C.; Atkins, W.M. Localization of the C-terminus of rat glutathione S-transferase A1-1: Crystal structure of mutants W21F and W21F/F220Y. *Proteins Struct. Funct. Bioinform.* **2000**, *42*, 192–200. [CrossRef]
29. Honaker, M.T.; Acchione, M.; Zhang, W.; Mannervik, B.; Atkins, W.M. Enzymatic Detoxication, Conformational Selection, and the Role of Molten Globule Active Sites. *J. Biol. Chem.* **2013**, *288*, 18599–18611. [CrossRef]
30. Honaker, M.; Acchione, M.; Sumida, J.P.; Atkins, W.M. Ensemble perspective for catalytic promiscuity: Calorimetric analysis of the active site conformational landscape of a detoxification enzyme. *J. Biol. Chem.* **2011**, *286*, 42770–42776. [CrossRef]
31. Hubatsch, I.; Mannervik, B. A Highly Acidic Tyrosine 9 and a Normally Titrating Tyrosine 212 Contribute to the Catalytic Mechanism of Human Glutathione Transferase A4-4. *Biochem. Biophys. Res. Commun.* **2001**, *280*, 878–882. [CrossRef]
32. Atkins, W.M.; Wang, R.W.; Bird, A.W.; Newton, D.J.; Lu, A.Y. The catalytic mechanism of glutathione S-transferase (GST). Spectroscopic determination of the pKa of Tyr-9 in rat alpha 1-1 GST. *J. Biol. Chem.* **1993**, *268*, 19188–19191. [CrossRef]
33. Gustafsson, A.; Etahadieh, M.; Jemth, P.; Mannervik, B. The C-terminal region of human glutathione transferase A1-1 affects the rate of glutathione binding and the ionization of the active-site Tyr9. *Biochemistry* **1999**, *38*, 16268–16275. [CrossRef]
34. Dietze, E.C.; Ibarra, C.; Dabrowski, M.J.; Bird, A.; Atkins, W.M. Rational modulation of the catalytic activity of A1-1 glutathione S-transferase: Evidence for incorporation of an on-face (pi...HO-Ar) hydrogen bond at tyrosine-9. *Biochemistry* **1996**, *35*, 11938–11944. [CrossRef]
35. Johnson, K.A. Role of induced fit in enzyme specificity: A molecular forward/reverse switch. *J. Biol. Chem.* **2008**, *283*, 26297–26301. [CrossRef]
36. Alary, J.; Fernandez, Y.; Debrauwer, L.; Perdu, E.; Guéraud, F. Identification of Intermediate Pathways of 4-HydroxyNE Metabolism in the Rat. *Chem. Res. Toxicol.* **2003**, *16*, 320–327. [CrossRef]
37. Habig, W.H.; Pabst, M.J.; Jakoby, W.B. Glutathione S-Transferases: THE FIRST ENZYMATIC STEP IN MERCAPTURIC ACID FORMATION. *J. Biol. Chem.* **1974**, *249*, 7130–7139. [CrossRef]

38. Stenberg, G.; Bjo¨rnestedt, R.; Mannervik, B. Heterologous expression of recombinant human glutathione transferase A1-1 from a hepatoma cell line. *Protein Expr. Purif.* **1992**, *3*, 80–84. [CrossRef]
39. Piotto, M.; Saudek, V.; Sklenar, V. Gradient-tailored excitation for single-quantum NMR spectroscopy of aqueous solutions. *J. Biomol. NMR* **1992**, *2*, 661–665. [CrossRef]
40. Nath, A.; Atkins, W.M. A Theoretical Validation of the Substrate Depletion Approach to Determining Kinetic Parameters. *Drug Metab. Dispos.* **2006**, *34*, 1433–1435. [CrossRef]
41. Dietze, E.C.; Grillo, M.P.; Kalhorn, T.; Nieslanik, B.S.; Jochheim, C.M.; Atkins, W.M. Thiol ester hydrolysis catalyzed by glutathione S-transferase A1-1. *Biochemistry* **1998**, *37*, 14948–14957. [CrossRef] [PubMed]
42. Meyer, D.J.; Crease, D.J.; Ketterer, B. Forward and reverse catalysis and product sequestration by human glutathione S-transferases in the reaction of GSH with dietary aralkyl isothiocyanates. *Biochem. J.* **1995**, *306 Pt 2*, 565–569. [CrossRef] [PubMed]
43. Chen, J.; Armstrong, R.N. Stereoselective catalysis of a *retro*-Michael reaction by class mu glutathione transferases. Consequences for the internal distribution of products in the active site. *Chem. Res. Toxicol.* **1995**, *8*, 580–585. [CrossRef] [PubMed]
44. Ibarra, C.; Grillo, M.P.; Bello, M.L.; Nucettelli, M.; Bammler, T.K.; Atkins, W.M. Exploration of in vitro pro-drug activation and futile cycling by glutathione S-transferases: Thiol ester hydrolysis and inhibitor maturation. *Arch. Biochem. Biophys.* **2003**, *414*, 303–311. [CrossRef]
45. Zhang, Y.; Kolm, R.; Mannervik, B.; Talalay, P. Reversible Conjugation of Isothiocyanates with Glutathione Catalyzed by Human Glutathione Transferases. *Biochem. Biophys. Res. Commun.* **1995**, *206*, 748–755. [CrossRef]
46. Slatter, J.G.; Rashed, M.S.; Pearson, P.G.; Han, D.H.; Baillie, T.A. Biotransformation of methyl isocyanate in the rat. Evidence for glutathione conjugation as a major pathway of metabolism and implications for isocyanate-mediated toxicities. *Chem. Res. Toxicol.* **1991**, *4*, 157–161. [CrossRef]
47. Baillie, T.A.; Kassahun, K. Reversibility in glutathione-conjugate formation. *Adv. Pharmacol.* **1994**, *27*, 163–181. [CrossRef]
48. Pearson, P.G.; Slatter, J.; Rashed, M.S.; Han, D.-H.; Grillo, M.P.; Baillie, T.A. S-(N-Methylcarbamoyl)glutathione: A reactive S-linked metabolite of methyl isocyanate. *Biochem. Biophys. Res. Commun.* **1990**, *166*, 245–250. [CrossRef] [PubMed]
49. Varma, D.R.; Guest, I. The Bhopal accident and methyl isocyanate toxicity. *J. Toxicol. Environ. Health* **1993**, *40*, 513–529. [CrossRef]
50. Awasthi, Y.C.; Yang, Y.; Tiwari, N.K.; Patrick, B.; Sharma, A.; Li, J.; Awasthi, S. Regulation of 4-hydroxynonenal-mediated signaling by glutathione S-transferases. *Free. Radic. Biol. Med.* **2004**, *37*, 607–619. [CrossRef]
51. Awasthi, Y.C.; Ansari, G.A.; Awasthi, S. Regulation of 4-hydroxynonenal mediated signaling by glutathione S-transferases. *Methods Enzymol.* **2005**, *401*, 379–407. [CrossRef] [PubMed]
52. Fitzpatrick, P.F. Combining solvent isotope effects with substrate isotope effects in mechanistic studies of alcohol and amine oxidation by enzymes. *Biochim. Biophys. Acta* **2015**, *1854*, 1746–1755. [CrossRef]
53. Fernandez, P.L.; Murkin, A.S. Inverse Solvent Isotope Effects in Enzyme-Catalyzed Reactions. *Molecules* **2020**, *25*, 1933. [CrossRef]
54. Schowen, K.B.; Schowen, R.L. Solvent isotope effects of enzyme systems. *Methods Enzymol.* **1982**, *87*, 551–606.
55. Spies, M.A.; Toney, M.D. Intrinsic Primary and Secondary Hydrogen Kinetic Isotope Effects for Alanine Racemase from Global Analysis of Progress Curves. *J. Am. Chem. Soc.* **2007**, *129*, 10678–10685. [CrossRef]
56. Saunders, W.H., Jr.; Edison, D.H. Mechanisms of Elimination Reactions. IV. Deuterium Isotope Effects in E2 Reactions of Some 2-Phenylethyl Derivatives. *J. Am. Chem. Soc.* **1960**, *82*, 138–145. [CrossRef]
57. Balogh, L.M.; Le Trong, I.; Kripps, K.A.; Shireman, L.M.; Stenkamp, R.E.; Zhang, W.; Mannervik, B.; Atkins, W.M. Substrate specificity combined with stereopromiscuity in glutathione transferase A4-4-dependent metabolism of 4-hydroxyNE. *Biochemistry* **2010**, *9*, 1541–1548. [CrossRef]

biomolecules

MDPI

Review

Role of Insect and Mammal Glutathione Transferases in Chemoperception

Mathieu Schwartz [1], Valentin Boichot [1], Stéphane Fraichard [1], Mariam Muradova [1], Patrick Senet [2], Adrien Nicolai [2], Frederic Lirussi [3,4,5], Mathilde Bas [1], Francis Canon [1], Jean-Marie Heydel [1] and Fabrice Neiers [1,*]

[1] Laboratory: Flavour Perception: Molecular Mechanims (Flavours), INRAE, CNRS, Institut Agro, Université de Bourgogne Franche-Comté, 21000 Dijon, France
[2] Laboratoire Interdisciplinaire Carnot de Bourgogne, UMR 6303 CNRS, Université de Bourgogne Franche-Comté, 21078 Dijon, France
[3] UMR 1231, Lipides Nutrition Cancer, INSERM, 21000 Dijon, France
[4] UFR des Sciences de Santé, Université de Bourgogne Franche-Comté, 25000 Besançon, France
[5] Plateforme PACE, Laboratoire de Pharmacologie-Toxicologie, Centre Hospitalo-Universitaire Besançon, 25000 Besançon, France
* Correspondence: fabrice.neiers@u-bourgogne.fr

Abstract: Glutathione transferases (GSTs) are ubiquitous key enzymes with different activities as transferases or isomerases. As key detoxifying enzymes, GSTs are expressed in the chemosensory organs. They fulfill an essential protective role because the chemosensory organs are located in the main entry paths of exogenous compounds within the body. In addition to this protective function, they modulate the perception process by metabolizing exogenous molecules, including tastants and odorants. Chemosensory detection involves the interaction of chemosensory molecules with receptors. GST contributes to signal termination by metabolizing these molecules. By reducing the concentration of chemosensory molecules before receptor binding, GST modulates receptor activation and, therefore, the perception of these molecules. The balance of chemoperception by GSTs has been shown in insects as well as in mammals, although their chemosensory systems are not evolutionarily connected. This review will provide knowledge supporting the involvement of GSTs in chemoperception, describing their localization in these systems as well as their enzymatic capacity toward odorants, sapid molecules, and pheromones in insects and mammals. Their different roles in chemosensory organs will be discussed in light of the evolutionary advantage of the coupling of the detoxification system and chemosensory system through GSTs.

Keywords: insects; glutathione transferase; olfaction; taste; chemosensory organs; detoxification; evolution; flavor

Citation: Schwartz, M.; Boichot, V.; Fraichard, S.; Muradova, M.; Senet, P.; Nicolai, A.; Lirussi, F.; Bas, M.; Canon, F.; Heydel, J.-M.; et al. Role of Insect and Mammal Glutathione Transferases in Chemoperception. *Biomolecules* **2023**, *13*, 322. https://doi.org/10.3390/biom13020322

Academic Editors: Bengt Mannervik and Nurhayat Tabanca

Received: 14 December 2022
Revised: 1 February 2023
Accepted: 6 February 2023
Published: 8 February 2023

1. Introduction

Evolution shapes all living organisms to perceive chemicals, enabling them to detect nutritive compounds and avoid toxic compounds. Although chemical detection supports several biological functions related to chemical communication in animals, the primary function of this ancient sense was most likely to find nutritive molecules. According to the Red Queen hypothesis [1], it can be hypothesized that the appearance of detoxification systems results from developments in defensive systems, such as the synthesis of toxic compounds. In response to this new pressure of selection, predators have evolved and developed defensive mechanisms capable of taking in toxic xenobiotics. In this context, the extension of the organism's detoxifying capacity should have also enabled species to extend their food sources due to their new capacity to metabolize xenobiotic compounds within these food sources. Xenobiotics are molecules that are not used as building blocks for biological macromolecules and also do not provide energy. Glutathione transferases (GSTs; EC 2.5.1.18), originally discovered as detoxification enzymes [2,3], are one of the key

enzymes involved in the metabolization of endogenous and exogenous molecules. GSTs are found in most living organisms, including insects and mammals. Xenobiotic molecules include chemicals naturally present in food sources as well as molecules produced industrially as pollutants and pesticides. Most flavor molecules can also be considered xenobiotics, regulated by GSTs and other detoxifying enzymes through the xenobiotic detoxifying network [4,5], such as glutathione transferases (GSTs; EC 2.5.1.18). GSTs, originally discovered as detoxication enzymes [2,3], are found in most living organisms, including insects and mammals. The best known function of GST is to catalyze the conjugation of reduced glutathione (GSH) to xenobiotic electrophilic centers, resulting in an increase in the hydrophilicity of xenobiotic compounds and thereby facilitating their elimination from the body. This function is shared by two entirely distinct superfamilies of enzymes [6], one microsomal (membrane-associated eicosanoid and glutathione metabolism, also called MAPEG), and the other soluble, also called canonical. These two superfamilies are not evolutionarily related and are found both in mammals and insects; moreover, in general, the number of microsomal GSTs is much lower than that of canonical GSTs. A third type of GST can be considered: mitochondrial Kappa GST [7]. Both kappa and canonical GSTs present a thioredoxin-like domain recognizing the GSH motif but are differently organized in the overall fold, suggesting their parallel evolution from a thiol-disulfide oxidoreductase progenitor [8]. Kappa GSTs are found in prokaryotes and eukaryotes, including mammals, but not in insects. However, Kappa GSTs have been identified in other arthropods and crustaceans [7,9]. For example, Acari, *Ixodes scapularis*, presents two Kappa GSTs involved in glutathione conjugation, and canonical GSTs also catalyze peroxide reduction [10], dehydrochlorination [11], and isomerization [12,13]. Moreover, they may trap substrates in the absence of enzymatic activity, which enables the sequestration of toxic compounds; this function is called ligandin [14]. Canonical GSTs are subdivided into classes, designated by the names of the Greek letters—Alpha, Delta, Epsilon, etc.—abbreviated as Roman capitals A, D, E, etc. Class members are distinguished by Arabic numerals [15]. GST members exhibit their own distinct tissue-specific expression patterns, suggesting that they have different functions. This differential pattern of expression is observed both in mammals [16] and insects [17]. It is not surprising that GSTs are preferentially expressed in insect detoxification organs, such as the fat body, midgut, or epidermis [18], and in the mammalian liver [19]. Chemosensory organs are exposed to the external environment and, thus, to xenobiotics. Consequently, GST expression is also observed in these organs, which represent specific places in the animal body. The detoxifying system can advantageously protect the chemosensory system, and additionally or as a result of its activity, it modulates chemosensory detection. The molecular organization of the chemosensory organs has been well described in both mammals and insects (the main laboratory models are rodents and *Drosophila*). In this review, we detail the knowledge supporting the involvement of GSTs in chemoperception, describing their localization in these systems as well as their enzymatic capacity toward odorants, sapid molecules, and pheromones in insects and mammals.

2. The Involvement of GSTs in Mammalian Chemoperception

2.1. Chemoperception in Mammals

Chemoperception in mammals involves three components: olfaction, taste, and trigeminal sensations [20,21]. Olfaction is a fundamental sense that enables animals to locate their food and their sexual partners and to warn of danger, which is also of great importance for their well-being through the hedonic tone of food. In mammals, olfaction is assured by the olfactory system located in the nasal cavity. Odorant compounds are small, volatile chemicals, generally of a hydrophobic nature, that enter the body through the nostrils and solubilize within the nasal mucus. Odorants bind to olfactory receptors (ORs) located on the olfactory receptor neurons (ORNs) present in the main olfactory epithelium. Indeed, in addition to the olfactory epithelium, mammals have several accessory olfactory organs, such as the vomeronasal organ, the septal organ of Masera, and the Grueneberg ganglion, which all contain ORNs. These organs exhibit overlapping functions with the main ol-

factory system, but their specificities are not fully characterized. Each olfactory receptor neuron expresses only one type of OR [22]. ORNs are connected to the olfactory bulb, where the olfactory signal is processed and further transmitted to higher brain regions. This organization transforms a chemical signal into an electrical signal thanks to an efficient combinatorial code of odors permitted by the high diversity of olfactory receptors (380 for humans) [23].

In contrast to olfaction, which is important for various functions such as food search and enjoyment, reproduction, and survival, the sense of taste in mammals is exclusively devoted to the evaluation of food quality and is closely related to feeding behavior [24]. Taste compounds are divided into five qualities, namely, sweet (sugars), bitter (various compounds of organic or inorganic nature), sour (acidic compounds), salty (ionic inorganic compounds such as Na^+), and umami (amino acids). In mammals, taste sensations result from the activation of taste receptors by taste compounds. Taste receptor cells assemble at the surface of the tongue or palate into small structures called "taste buds", composed of approximately 100 cells. These taste buds are found in epithelial structures called "papillae", classified into different types and present different structures and locations at the tongue surface. Papillae include fungiform, circumvallate, and foliate papillae. Taste receptor cells are linked by afferent nerves to the geniculate and petrosal ganglions, which mediate taste signals to the brain stem. Taste receptors from the T1R and T2R families are part of the class C and class A GPCR families, respectively [25]. They assemble through different functional homo- or heterodimers for T1Rs that are able to detect sweet (T1R2 + T1R3) and umami (T1R1 + T1R3) compounds. Monomeric T2Rs enable the detection of bitter molecules. Two other families of receptors have been proposed for the detection of sourness (PKD2L1) and saltiness (ENaC) [24].

In addition to the five qualities of taste, a few studies have evidenced a sixth sensation, which is more of a modulation of some of the basic tastes, namely the kokumi taste [26]. Kokumi means "rich taste" in Japanese and is associated with the reinforcement of umami, sweetness, and saltiness due to the presence of kokumi compounds. Kokumi compounds include both nonpeptide compounds and peptide compounds such as gamma-glutamyl peptides such as glutathione [27]. Kokumi compounds have been proposed to activate the calcium-sensing receptor (CaSR) to elicit the kokumi sensation [28]. Kokumi is an increasingly studied topic of research with great potential for flavor enhancement and food product development [26].

In addition to olfaction and taste, a third chemosensory sensation is related to the trigeminal system and enables the detection of trigeminal compounds such as astringent plant polyphenols, compounds present in foods eliciting a sensation of cooling (menthol) or burning (capsaicin), or carbonated drinks containing CO_2 that trigger a prickly sensation [21]. Trigeminal compounds mainly stimulate transient receptor potential (TRP) channels present in sensory neurons of the oral mucosa, which convert chemical signals into electric activity. The identification of astringent compounds may either involve mechanoreceptors detecting changes in the friction forces at the surface of the oral mucosae or the transmembrane mucin MUC1, as recently proposed by our group [29].

Olfaction, taste, and trigeminal sensations can be modulated by the metabolic activities present in the vicinity of the chemosensory receptors [30]. This metabolism involves enzymes such as glutathione transferases (GSTs). These have shown to be linked to both olfaction and taste perception, as explained in the following section.

2.2. Roles of GSTs in Mammalian Chemoperception

Many drug-metabolizing enzymes are present in the nasal cavity, within the nasal epithelium and mucus [31,32], as well as in the oral cavity, within the saliva and the oral mucosa [33,34]. These enzymes assure the protection of the epithelia and, notably, the olfactory receptor neurons from damage provoked by xenobiotics entering the nasal (or oral) cavity. In addition to their role in detoxification, some of these enzymes handle flavor molecules, thus producing flavor metabolites in the oronasal sphere [35–38]. All these

enzymes, in addition to proteins able to bind flavor compounds such as odorant-binding proteins (OBPs), have an impact on both the quality and quantity of flavor compounds that activate chemoreceptors [30]. These molecular mechanisms have been named "perireceptor events" because they occur in the environment surrounding the chemoreceptors. In the context of mammalian olfaction, a body of evidence indicates that glutathione transferase is an important perireceptor enzyme acting on odorant detection modulation. Additionally, pioneering studies have started to investigate the potential role of glutathione transferases in taste perception. Both of these aspects are treated in this part of the review. Among the seven canonical mammalian GSTs identified thus far (alpha, mu, theta, pi, omega, sigma, and zeta [15]), alpha, mu, and pi classes of GSTs are common [39] among mammals [40].

In 1992, Ben-Arie and coworkers showed that the olfactory epithelium is the extrahepatic tissue in a rat model that exhibits the highest glutathione transfer activity with the chemical substrate chlorodinitrobenzene (CDNB), thus showing the strong expression of GSTs and suggesting a potential role in olfaction [41]. All GST classes were shown to be expressed in chemosensory organs in different mammalian species (Table 1). Glutathione transferase of the mu class was demonstrated in the rat nasal mucus and olfactory epithelium [4], supporting a previous study already showing GST expression in rat chemosensory mucosae [42]. Additionally, in the same study, the ability of recombinant rat GSTM2 to catalyze the transfer of glutathione to various odorant compounds, including aldehydes, ketones, and epoxides, was shown. Using a competition assay, GSTM2 was also found to be able to bind a large variety of odorants, most likely due to its ligandin properties [4]. Similar results were obtained for human GSTA1 and GSTP1, which are two GSTs that play roles in glutathione and ligand transfer for many odorous molecules and are expressed in the human respiratory epithelium [43]. Immunohistochemistry experiments showed the localization of human GSTs in ciliated cells (at the surface of the epithelium from the human olfactory vicinity), thus facilitating the entry of odorants into the epithelium. Furthermore, the first X-ray structure of a GST bound to a metabolized odorant enabled a fine analysis of its active site and its capacity to specifically recognize odorant molecules [43]. The crystal structure of human GSTA1 bound to the metabolite glutathionyl-dihydrocinnamaldehyde was analyzed and revealed the ability of the hydrophobic site of GSTA1 to strongly adapt to small hydrophobic volatile compounds. This property facilitates the binding of cinnamaldehyde and promotes the formation of the glutathione conjugate through a nucleophilic substitution, suppressing the carbon double bond of cinnamaldehyde [43].

GST expression levels were also shown to be associated with olfactory dysfunction. Zinc deficiency is linked to olfactory and gustatory dysfunction in mammals [44,45]. Interestingly, in rats, zinc deficiency is associated with a reduction in GST mRNA in some cell types of the olfactory epithelium (supporting cells [46]).

The involvement of GSTs in odorant metabolism has become increasingly documented; however, less evidence is available concerning the significance of these molecular mechanisms in odorant perception. In this context, experiments with a rabbit model enabled us to reveal some clues on the role of GSTs in odorant signal termination. It was shown that the mammary pheromone, corresponding to the compound 2-methylbut-2-enal (2MB2), triggers the grasping of the mother rabbit mammae. Newborn rabbits are blind, and suckling-related behavior allows them to survive despite the short time that allows the mother to feed them [47]. This chemically triggered behavior is critical for pups, which are constrained to finding nipples within the five minutes of daily nursing. It has been shown that the mammary pheromone is metabolized to a glutathione conjugate in the olfactory epithelium of newborn rabbits, in accordance with a high early expression of glutathione transferases in this tissue [48]. Furthermore, it has been shown that this metabolism is also present in the nasal mucus of newborn rabbits due to the presence of glutathione transferases in this biological fluid based on proteomic analysis [49]. Additionally, the deregulation of this metabolism by in vivo washing of the nasal mucus, thus diminishing the glutathione conjugation of 2MB2, led to increased sensitivity of the behavior response in newborns exposed to the mammary pheromone. Similar results were obtained when the 2MB2 metabolism

was reduced due to competition with another odorant substrate catalyzed by the same enzyme [50]. Decreasing the glutathione conjugation of the mammary pheromone allowed us to record behavioral responses with concentrations of mammary pheromone that were usually inactive. Glutathione conjugation to the mammary pheromone modifies its structure and thus terminates the odorant signal. This metabolization thus enables the newborn rabbit to remain responsive to the mammary pheromone by reinitializing the chemical signal. Rabbit GSTs catalyze glutathione conjugation with 2MB2 but can ensure the role of odorant signal termination for a wide range of other odorant compounds in mammals, including humans.

In addition to the nasal cavity, GSTs are expressed in the oral cavity, particularly in taste bud cells [51]. In rats, GSTM and GSTP were found to be expressed in both circumvallate and foliate papillae. The expression seems to be GST member-dependent; GSTA is not found in these papillae. Moreover, the results obtained in human and rat olfactory epithelia show differences with regard to the type of GST expressed in this tissue depending on the species, highlighting differences in their expression in chemosensory tissue between mammalian species [4,43]. GST was also found to be expressed in mammalian saliva, including human saliva [52]. Glutathione is found at a concentration of approximately 1 g/L in human saliva [53], enabling the GSH saturation of GSTP, the main human salivary GST, and then allowing it to catalyze glutathione conjugation at the maximal rate. Additionally, this salivary expression was shown to be modulated in humans in association with food behavior. Indeed, increased GST expression in response to specific diets, such as those rich in broccoli or coffee, was observed [52,54]. Recently, a study explored a possible link between GST expression in saliva and bitter taste perception [55]. GSTA1 and GSTP1 were identified in a cohort of 104 people, all of whom expressed the 2 GSTs in saliva. Additionally, people exhibiting ageusia or dysgeusia, included in this study, showed significantly lower salivary GSTA1 levels than those in the saliva of the control group, suggesting possible relationships between salivary GST levels and taste function. In the same study, GSTA1 and GSTP1 interacted with various bitter compounds, including flavonoids and isothiocyanates. This last family of compounds is metabolized within the saliva [55]. The X-ray structures obtained between GSTs and isothiocyanates showed that different binding sites exist, whether the interactions imply glutathione conjugation (binding in the active site) or covalent adduction to an exposed cysteine in the GSTA1 ligand site.

All these elements suggest the involvement of GSTs in mammalian taste perception, in addition to olfaction. In addition, the level of expression of GST is correlated with disorders related to both taste and smell.

Table 1. Location and classes of GSTs within the mammal's chemosensory organs.

Mammal Species	Location	GST Classes	Ref.
Canis lupus familiaris	Saliva	Alpha, Mu, and Omega	[56]
Equus caballus	Saliva	Pi	[57]
Homo sapiens	Olfactory mucus	Alpha and Pi	[58,59]
	Olfactory epithelium	Alpha, Mu, and Pi	[43]
	Saliva	Alpha, Kappa, Mu Omega, Theta, and Pi	[60,61]
Mus musculus	Sensory cilia	Alpha, Kappa, Mu, Omega, Tau, and Zeta	[62]
	Saliva	Omega	[63]
Oryctolagus cuniculus	Olfactory mucus	Alpha, Mu, and Pi	[49]
Ovis aries	Saliva	Alpha	[57]
Rattus norvegicus	Sensory cilia	Alpha and Mu	[64]
	Olfactory epithelium	Alpha, Mu, and Pi	[4,41]
	Olfactory mucus	Alpha, Mu, and Pi	[4]

3. The Involvement of GSTs in Insect Chemoperception

3.1. Chemoperception in Insects

Insects constitute the largest class of living animal species. Due to their small size, they have developed multiple mechanisms to limit toxic xenobiotic effects, including the enhancement of metabolic detoxification [65,66], which reduces penetration through the cuticle, or behavioral avoidance [67]. Insects can taste through many parts of their body. The proboscis organs used for feeding and sucking allow insects to taste food during ingestion before it reaches the digestive system. In addition to the proboscis, insects are able to detect tastants with their legs, wings, and ovipositor organs. Consequently, due to their small size compared with food, they are generally already in contact with it before ingesting it, making it advantageous to taste it with their legs before eating or with the ovipositor organ before laying eggs. Although the taste systems of mammals and insects evolved independently, they enable the detection of similar qualities, including sweet, salty, and bitter stimuli. Insects are able to detect carbonation as a taste modality through gustatory neurons [68], similar to mammals, through carbonic anhydrase IV, which produces protons that activate a proton-gated channel [69]. Interestingly, carbonation detection is also possible in both mammals and insects through the olfactory system [69]. Insects have gustatory sensory neurons that mediate the recognition of water [70]; to date, it has not been established whether other animals can taste the water. In mammals, taste receptors are not hosted by neurons. Neurons are in contact with the taste cells that carry gustatory receptors and are located in taste buds. In insects, gustatory receptors are directly carried by gustatory neurons, in contrast to vertebrate gustatory neurons, which are housed in cells that are indirectly in contact with neurons. Gustatory neurons are housed within the hundreds of gustatory sensilla distributed on the surface of the different sensory organs except the proboscis, which also includes internal sensilla [71].

In insects, the equivalent of the mammalian nose is the antenna and the maxillary palps. Although they do not exhibit any evolutionary relationship with mammals, olfaction is also supported by olfactory neurons in insects. Indeed, the olfactory sensilla cover the distal segment of the antenna, and the maxillary palps host the olfactory neurons. Dendrites of olfactory neurons that express olfactory neurons are located in the sensilla lymph within the sensilla. Odor molecules pass through pores or slits in the sensillum cuticle and enter the sensillum lymph [72]. Insect olfactory receptors are not homologs of vertebrate olfactory receptors [73], suggesting different evolutionary origins compared with those found in vertebrates. Consequently, although the organizational features of the olfactory systems of vertebrates and insects appear very similar, these structures may not share a common evolutionary heritage [74].

Insect GRs and ORs, which are membrane proteins, do not show any homology to those of vertebrates [75,76] and consequently do not belong to the GPCR family. However, both GRs and ORs evolved from an ancestral protein, and in addition to sharing the same sequence identity, they share the same inverted transmembrane topology as vertebrate olfactory GPCRs. The expansion of genes coding for the insect GR and OR has occurred only in insects [77]. In contrast to the monomeric ORs of vertebrates, insect ORs form heteromers with a conserved OR receptor also called Orco (i.e., the OR coreceptor). One specific OR is expressed in each insect olfactory neuron in addition to Orco, as in vertebrate olfactory neurons, where one specific OR is expressed in each olfactory neuron. It is unclear whether insect GRs can function alone as multimers or with other insect GRs due to the observation that multiple GR genes are expressed in a single GR neuron [78].

Even if the chemosensory systems in insects and mammals present similar biological organizations, they do not share any evolutionary links. However, in both chemosensory systems, glutathione transferases from the same common ancestor are expressed, most likely sharing similar physiological roles.

3.2. Roles of GSTs in Insect Chemoperception

In addition to the Omega, Sigma, Theta, and Zeta GST classes found in insects and shared with mammals, two other classes are observed: Delta and Epsilon GSTs. Delta GSTs are found in insects and are observed in a more general manner in arthropods, such as crustaceans [9]. Epsilon GSTs appear more specific to insects and were hypothesized to be insect-specific [79]. The numbers of Delta and Epsilon GSTs are variable from one insect species to another, mostly due to duplication events that occur in each insect species (Table 2). This gene-coding GST duplication might be associated with functional differentiation during insect evolution and is related to environmental adaptation. Gene duplication followed by sequence divergence is a key process during evolution, allowing the creation of novel gene functions [80]. Interactions of insects with plants, and especially plant chemicals and their adaptations to them, appear to be the most likely major driving force in herbivorous insect evolution [81]. Plant molecules can be toxic to insects, and consequently, GSTs and detoxifying enzymes are essential for insect survival. GSTs detoxify a broad range of plant molecules, generally with an overlap of GSTs for the same substrate [82–84]. Signatures of a positive selection of Delta GSTs suggest that they may have evolved under positive selection in the herbivorous [85] lineage after the transition of insects to herbivory > 350 Ma [86]. This adaptation phenomenon can be rapid; indeed, anthropological pressure toward insects for insecticide resistance has been suggested to promote *Musca domestica gst* gene amplification [87,88]. The main classes of GST diversification appear to be the Epsilon and Delta classes in various insects, such as *Anopheles gambiae*, *Drosophilia melanogaster*, or *Tribolium castaneum* [79,89]. In this context, it is not surprising to observe numerous insect adaptations toward insecticides [90,91] due to the Delta and Epsilon GSTs in the role of *A. gambiae* GSTE1 and GSTE2 in the DDT resistance [92]. The chemical resistance promoted by GSTs involves various chemicals, such as pyrethroids or neonicotinoids and 2,2-dichlorovinyl dimethylphosphate for *Diaphorina citri* [93] and *Rynochophorus phoenicis*, respectively [94]. In contrast, *Apis mellifera*, known to be highly sensitive to insecticides, presents only one Delta GST (including two isoforms) and no Epsilon GST. It is not excluded that some GSTs resulting from functional differentiation appear with different functions not related at all to xenobiotic metabolism, such as GSTE14 in *D. melanogaster*, which is involved in ecdysone biosynthesis [13,95,96]. Additionally, GSTs formed during the diversification process can also be specific in metabolizing some molecules without a functional overlap from other GSTs within the same insect species. For example, the deletion of epsilon and omega GSTs in the Asian gypsy moth, *Lymantria dispar*, affected its adaptability to salicin and rutin produced by its host, the poplar tree [97].

Table 2. Number of identified canonical GSTs in different insect species.

Order	Insect Species	Cytosolic							Total	Ref.
		Delta	Epsilon	Omega	Sigma	Theta	Zeta	Unclassified		
Coleoptera	*Lasioderma serricorne*	1	0	0	1	1	0	0	3	[98]
	Agrilus planipennis	5	9	0	2	0	0	0	16	[98]
	Anoplophora glabripennis	10	10	2	4	2	0	0	28	[99]
	Rhaphuma horsfieldi	5	8	3	2	1	1	0	20	[98]
	Xylotrechus quadripes	5	7	2	2	1	1	0	18	[98]
	Diabrotica virgifera	3	11	1	0	2	0	0	17	[98]
	Leptinotarsa Decemlineata	6	11	7	6	2	1	0	33	[100]
	Phyllotreta striolata	5	6	2	6	1	1	2	23	[101]
	Dendroctonus armandi	0	4	1	2	1	0	0	8	[102]
	Dendroctonus ponderosae	6	12	2	5	2	1	0	28	[103]

Table 2. *Cont.*

Order	Insect Species	Cytosolic							Total	Ref.
	Lissorhoptrus oryzophilus	3	7	2	8	1	1	2	24	[98]
	Sitophilus oryzae	2	12	3	6	2	1	0	26	[104]
	Aethina tumida	3	19	1	7	1	5	7	43	[105]
	Oryctes borbonicus	4	5	3	15	3	1	0	31	[106]
	Onthophagus taurus	4	7	3	1	4	0	0	19	[98]
	Nicrophorus vespilloides	8	6	0	1	3	0	0	18	[98]
	Asbolus verrucosus	3	14	2	2	1	0	0	22	[98]
	Tribolium castaneum	3	19	3	7	1	1	2	36	[79]
	Tenebrio molitor	2	13	1	5	1	1	2	25	[107]
Diptera	*Chironomus riparius*	3	1	1	4	1	1	2	13	[108]
	Aedes aegypti	8	8	1	1	4	1	3	26	[109]
	Anopheles gambiae	17	8	1	1	2	1	2	32	[79]
	Culex quinquefasciatus	14	10	1	1	6	0	3	35	[110, 111]
	Drosophila melanogaster	11	14	4	1	4	2	1	37	[79]
	Bactrocera dorsalis	9	5	3	1	3	3	1	25	[112]
	Ceratitis capitata	7	14	1	1	3	2	1	29	[113]
Hemiptera	*Bemisia tabaci*	14	0	1	6	0	2	0	23	[114]
	Orius laevigatus	1	0	2	16	1	1	0	21	[115]
	Acyrthosiphon pisum	16	1	2	6	2	0	3	30	[79]
	Myzus persicae	8	0	0	8	2	0	0	18	[116]
	Laodelphax striatellus	1	1	1	3	1	1	0	8	[117]
	Nilaparvata lugens	2	1	1	3	1	1	0	9	[118, 119]
	Supraphorura furcifera	2	1	1	1	1	1	0	7	[119]
	Rhodnius prolixus	1	0	1	7	4	1	0	14	[120]
	Diaphorina citri	2	2	0	3	0	0	1	8	[114]
Hymenoptera	*Apis mellifera*	2	0	2	4	1	1	1	11	[79]
	Bombus impatiens	5	0	2	4	1	1	0	13	[121]
	Bombus terrestris	5	0	2	4	1	1	0	13	[121]
	Meteorus pulchricornis	4	0	3	7	0	1	0	15	[122]
	Nasonia vitripennis	5	0	2	8	3	1	0	19	[123]
	Pteromalus puparum	5	0	2	8	3	1	0	19	[124]
Lepidoptera	*Bombyx mori*	4	8	4	2	1	2	2	23	[125]
	Cnaphalocrocis medinalis	4	9	3	5	0	2	2	25	[107]
	Heortia vitessoides	3	2	3	3	1	2	2	16	[126]
	Spodoptera litura	5	21	3	7	1	2	3	42	[127]
	Danaus plexippus	3	6	3	5	1	3	2	23	[98]
	Pieris rapae	3	3	4	4	1	2	0	17	[128]
	Plutella xylostella	5	5	5	2	1	2	2	22	[129]
	Manduca sexta	6	9	4	2	1	2	1	25	[98]

Table 2. *Cont.*

Order	Insect Species	Cytosolic							Total	Ref.
	Cydia pomonella	4	3	2	1	1	1	1	13	[130]
Orthoptera	*Locusta migratoria*	10	0	3	12	2	1	0	28	[131]
Phthiraptera	*Pediculus humanus*	4	0	1	4	1	1	0	11	[132]
Psocoptera	*Liposcelis entomophila*	17	0	1	13	3	1	0	35	[133]

As shown in vertebrate chemosensory organs, GSTs are also expressed in insect chemosensory organs (Table 3). This expression is advantageous to protect these sensitive organs where neurons are directly exposed to xenobiotics. GSTs were shown to be expressed in the antennae of various orders of insect species, such as the dipteran *D. melanogaster* [17,134], various lepidopteran species [107,130,135–139] such as *Manduca sexta* [140] or *Spodoptera littoralis* [141], and in the Coleoptera antennae of *Agrilus planipennis* [142] or *Dendroctonus valens* [143]. Table 3 shows the diversity of insect species expressing GSTs within their sensory organs. Although a limited number of studies have analyzed GST expression, GSTs appear to be ubiquitously expressed in antennae. To support this hypothesis, GST expression in two particular insect species can be highlighted. The only Delta GST found in *A. melifera* is expressed in its antennae [144]. Ticks have a unique chemosensory organ presumed to function similarly to insect antennae, the fore-tarsal Haller's organ. GSTs were found to be expressed in this organ of the dog tick, *Dermacentor variabilis* [145]. As in mammals, GSTs were proposed to protect the chemosensory organs so they could participate in odorant clearance and consequently signal termination. Antennal GSTs were shown to be active toward the model substrate CDNB (1-chloro-2,4-dinitrobenzene); for example, most antennal *Drosophila* GSTs [146,147]. The ability to conjugate CDNB was also observed for the antennal-specific GST identified in *Bombyx mori* [137]. The selective pressure to conserve efficient odorant clearance is crucial for flying insects, which need to reinitiate odorant perception as quickly as possible to follow the odorant volute. The detection of odorant food sources can be diversified, probably involving different GSTs. However, pheromone detection can also involve more specialized GSTs, as shown for an antenna-specific Delta GST found in *Manducta sexta*. This GST was shown to metabolize *trans*-2-hexenal, a plant-derived green leaf aldehyde known to stimulate the olfactory system of *M. sexta*. This GST was proposed to be involved in the signal termination of a complex mixture of aldehyde molecules forming the sex pheromone bouquet [140]. A delta GST found in the antennae of *Grapholita molesta* shows high activity toward a sex pheromone component, (*Z*)-8-dodecenyl alcohol [148]. The role of GST in sex pheromone detection is also supported by the differential expression of GST depending on the insect sex. For example, antennal-specific genes of a GST belonging to the Delta class were significantly more highly expressed in male *Helicoverpa armigera* antennae compared with females [139]. Despite all the different studies, to the best of the authors' knowledge, the cellular localization of GSTs within the olfactory sensilla is not known to date. Moreover, expression within the sensory lymph, where the olfactory neurons are located, has not been validated experimentally. The same question about localization exists for insect gustatory sensilla. GSTs have been identified in diverse taste organs, such as the labellum, in insects belonging to the dipteran and lepidopteran orders (Table 3); however, the cell types and localization within the lymph of gustatory sensilla are not shown. Food containing bitter molecules such as glucosinolates and isothiocyanates led to GST overexpression in aphids in a general manner [149]. Additionally, other results have shown the same regulation in chemosensory organs. Isothiocyanates were shown to increase the expression of GST Delta in *Drosophila* labellum [5]. This modulation can be hypothesized to affect food habits. The results showed that the loss of bitter taste receptors observed in *D. suzukii* in comparison to *D. melanogaster* was proposed to contribute to the evolutionary shift in oviposition preference between the two species [150], knowing that ovipositor organs are taste-sensitive. In the same study, the

taste difference between these two *Drosophila* species showed an associated differential expression of xenobiotic metabolism enzymes, including delta and epsilon GSTs. Again, this observation supports a direct link between these enzymes and the taste biochemistry in insects.

Table 3. Identification of GSTs in the chemosensory organs of various insect species.

Order	Insect Species	Location	GST Classes	Ref.
Coleoptera	*Agrilus planipennis*	Antennae	Delta	[142]
	Dendroctonus valens	Antennae	Not indicated	[143]
	Phyllotreta striolata	Antennae	Delta and Epsilon	[101]
Diptera	*Aedes albopictus*	Antennae/maxillary palps	Not indicated	[151]
	Drosophila melanogaster	Antennae/maxillary palps/labellum	Delta, Epsilon, Omega, Sigma, Theta, and Zeta	[5,17,134]
Hymenoptera	*Apis melifera*	Antennae	Delta	[144]
Ixodida	*Dermacentor variabilis*	Haller's organ	Epsilon and Mu	[145]
Lepidoptera	*Bombyx Mori*	Antennae	Delta	[137]
	Chilo suppressalis	Antennae	Delta, Epsilon, Omega, Sigma, Theta, and Zeta	[136]
	Cydia pomonella	Antennae	Delta, Epsilon, Omega, Sigma, Theta, and Zeta	[130]
	Epiphyas postvittana	Antennae	Delta, Epsilon, Omega, Sigma, and Theta	[152]
	Grapholita molesta	Antennae	Delta	[148]
	Helicoverpa armigera	Antenna	Delta	[139]
	Heortia vitessoides	Antennae	Delta and Epsilon	[126]
	Manduca sexta	Antennae	Delta	[140]
	Papilio xuthus	Antennae, labella, and tarsi	Delta	[153]
	Plodia interpunctella	Antennae	Delta, Epsilon, Omega, Sigma, Theta, and Zeta	[154]
	Spodoptera littoralis	Antennae	Delta, Epsilon, Omega, Sigma, Theta, and Zeta	[141,155]

4. Discussion

GST appears to be a main actor in the mammalian and insect detoxifying systems. In insects, Delta and Epsilon GST diversification were shown to be associated with chemical resistance toward numerous molecules found naturally in plants, such as isothiocyanates, or resulting from human activity, such as pesticides. Interestingly, GSTs were found to be involved in the metabolism of similar molecules both in mammals and insects after the separation of these lineages [156]. Isothiocyanate molecules found in terrestrial plants were shown to modulate GST expression in mammals and insects [5,54,157]. These observations support the idea that GST gene diversification offers advantageous opportunities during evolution to build functional chemosensory systems to face molecular diversification in plant molecules. It may also have offered some species better adaptability to their environment, although this advantage is less important for species with a more specific ecological niche, such as *Apis melifera*. Interestingly, both olfactory and gustatory organs appeared independently in mammals and insects during their evolution and present an analogous organization as the chemosensory neurons wearing membrane olfactory receptors. In both cases, the receptors evolved from a different membrane protein ancestor, whereas the GSTs found in these two systems evolved from the same ancestral GST (homologous). In the

insect lineage, GSTs of the Delta class have been found in almost all studies analyzing the contents of the antennae, indicating the importance of this class in the olfactory organs.

Crustaceans and insects share Delta and Epsilon GSTs, indicating their appearance before the separation of the lineages and consequently before the evolutionary elaboration of their olfactory systems, which did not share the same protein actors [158]. This observation supports that these specific GST classes did not appear to support the physiology of the chemosensory organs, and it is more likely that different members of existing classes of GSTs were randomly used in the chemosensory organs, highlighting the versatility of GSTs. One of the main biological functions of chemosensory GSTs is the protection of the chemosensory organs where neurons are exposed. The lifespan of olfactory neurons in rodents is approximately 40 days [159], although xenobiotic metabolism enzymes already contribute to extending this life; thus, neurons must continuously be replenished. In this context, it is not surprising to find numerous GST members as key players in xenobiotic metabolism in both mammalian and insect chemosensory systems (Table 3). In addition to chemoprotection, GSTs modulate their perception when these xenobiotic molecules are perceived by decreasing the xenobiotic concentration. This metabolic activity can also be involved in the termination of the signal if the metabolites are no longer perceived, or in the perception of a new signal if the metabolite is perceived by other chemoreceptors (Figure 1). To date, GSTs have only been shown to be involved in signal termination in mammals (rabbits) and insects. Due to the increased steric hindrance after glutathione conjugation, it is more likely that the chance of molecules binding receptors will decrease. However, it is not excluded that, after GST catalysis, those molecules can be perceived differently. Other GST activities, such as glutathione conjugation, are more susceptible to generating molecules that can be perceived, including isomerization activity. Indeed, chemosensory receptors are known to be stereospecific. Additionally, the ligandin capacity of GSTs has been proposed to help the diffusion of hydrophobic molecules as odorants in hydrophilic olfactory mucus surrounding the olfactory receptors [4]. A similar role in the sensillary lymph surrounding the insect olfactory receptors is not excluded if GSTs are expressed within the lymph. GST localization in sensilla lymphs is only supported by the observation of a signal peptide in some insect GSTs that are expressed in sensilla [141]. Interestingly, an increase in diffusion can also be proposed for all chemosensory molecules as a consequence of glutathione conjugation, as suggested for bitter molecules [55]. After glutathione conjugation, molecules are more hydrophilic. Thus, if it does not impact the ability of the molecules to bind to their receptors or their affinity ranges, they are most likely rapidly perceived.

To conclude, numerous questions about GSTs and their function in the chemosensory system remain open. For instance, their roles in trigeminal perception have never been studied to date in any organism. Numerous GST members are produced in bacteria, opening questions regarding their role in both mammalian and insect chemoperception in view of recent advances showing the potential roles of bacterial enzymes in human chemosensory perception [160,161] and insect chemoperception [162]. GST functions in chemosensory perception seem to be conserved in non-evolutionarily related chemosensory systems. Thus, the knowledge obtained from experimental data in one lineage should be tested in other lineages to enhance the understanding of their functions.

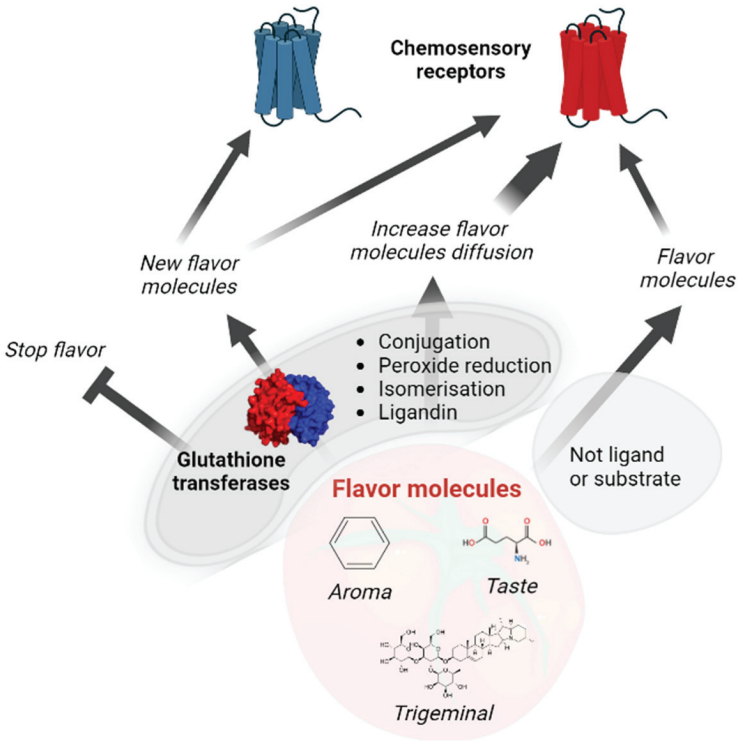

Figure 1. Role of glutathione transferases in chemosensory modulation.

Author Contributions: M.S. and F.N. wrote the manuscript, V.B., S.F., M.M., P.S., A.N., F.L., M.B., F.C. and J.-M.H. reviewed and edited the manuscript. All authors have read and agreed to the published version of the manuscript.

Funding: The authors received funding for this work: F.N., Agence Nationale de la Recherche grant number ANR-16-CE21-0004-01 (https://anr.fr). J.-M.H., ANR-18-CE92-0018-01, M.S., ANR-22-CE21-0001, F.C. ANR-20-CE21-0002.

Institutional Review Board Statement: Not applicable.

Informed Consent Statement: Not applicable.

Data Availability Statement: All data are available in the manuscript.

Conflicts of Interest: The authors declare no conflict of interest.

References

1. Van Valen, L. A new evolutionary law. *Evol. Theory* **1973**, *1*, 1–30.
2. Booth, J.; Boyland, E.; Sims, P. An enzyme from rat liver catalysing conjugations with glutathione. *Biochem. J.* **1961**, *79*, 516–524. [CrossRef] [PubMed]
3. Mannervik, B. Five decades with glutathione and the GSTome. *J. Biol. Chem.* **2012**, *287*, 6072–6083. [CrossRef]
4. Heydel, J.M.; Menetrier, F.; Belloir, C.; Canon, F.; Faure, P.; Lirussi, F.; Chavanne, E.; Saliou, J.M.; Artur, Y.; Canivenc-Lavier, M.C.; et al. Characterization of rat glutathione transferases in olfactory epithelium and mucus. *PLoS ONE* **2019**, *14*, e0220259. [CrossRef]
5. Gonzalez, D.; Fraichard, S.; Grassein, P.; Delarue, P.; Senet, P.; Nicolai, A.; Chavanne, E.; Mucher, E.; Artur, Y.; Ferveur, J.F.; et al. Characterization of a Drosophila glutathione transferase involved in isothiocyanate detoxification. *Insect Biochem. Mol. Biol.* **2018**, *95*, 33–43. [CrossRef]
6. Hayes, J.D.; Strange, R.C. Glutathione S-transferase polymorphisms and their biological consequences. *Pharmacology* **2000**, *61*, 154–166. [CrossRef]
7. Morel, F.; Aninat, C. The glutathione transferase kappa family. *Drug Metab. Rev.* **2011**, *43*, 281–291. [CrossRef]

8. Ladner, J.E.; Parsons, J.F.; Rife, C.L.; Gilliland, G.L.; Armstrong, R.N. Parallel evolutionary pathways for glutathione transferases: Structure and mechanism of the mitochondrial class kappa enzyme rGSTK1-1. *Biochemistry* **2004**, *43*, 352–361. [CrossRef]
9. Roncalli, V.; Cieslak, M.C.; Passamaneck, Y.; Christie, A.E.; Lenz, P.H. Glutathione S-Transferase (GST) Gene Diversity in the Crustacean Calanus finmarchicus–Contributors to Cellular Detoxification. *PLoS ONE* **2015**, *10*, e0123322. [CrossRef]
10. Hurst, R.; Bao, Y.; Jemth, P.; Mannervik, B.; Williamson, G. Phospholipid hydroperoxide glutathione peroxidase activity of human glutathione transferases. *Biochem. J.* **1998**, *332 Pt 1*, 97–100. [CrossRef]
11. Clark, A.G.; Shamaan, N.A. Evidence that DDT-dehydrochlorinase from the house fly is a glutathione S-transferase. *Pestic. Biochem. Physiol.* **1984**, *22*, 249–261. [CrossRef]
12. Johansson, A.S.; Mannervik, B. Human glutathione transferase A3-3, a highly efficient catalyst of double-bond isomerization in the biosynthetic pathway of steroid hormones. *J. Biol. Chem.* **2001**, *276*, 33061–33065. [CrossRef]
13. Škerlová, J.; Lindström, H.; Gonis, E.; Sjödin, B.; Neiers, F.; Stenmark, P.; Mannervik, B. Structure and steroid isomerase activity of Drosophila glutathione transferase E14 essential for ecdysteroid biosynthesis. *FEBS Lett.* **2019**, *594*, 1187–1195. [CrossRef]
14. Kamisaka, K.; Gatmaitan, Z.; Moore, C.L.; Arias, I.M. Ligandin Reverses Bilirubin Inhibition of Liver Mitochondrial Respiration In Vitro. *Pediatr. Res.* **1975**, *9*, 903–905.
15. Mannervik, B.; Board, P.G.; Hayes, J.D.; Listowsky, I.; Pearson, W.R. Nomenclature for mammalian soluble glutathione transferases. *Methods Enzymol.* **2005**, *401*, 1–8. [CrossRef]
16. Sherratt, P.J.; Hayes, J.D. *9 Glutathione S-Transferases*; Costas, I., Ed.; John Wiley and Sons: Hoboken, NJ, USA, 2001. [CrossRef]
17. Gonis, E.; Fraichard, S.; Chertemps, T.; Hecker, A.; Schwartz, M.; Canon, F.; Neiers, F. Expression Patterns of Drosophila Melanogaster Glutathione Transferases. *Insects* **2022**, *13*, 612. [CrossRef]
18. Huang, Y.; Xu, Z.; Lin, X.; Feng, Q.; Zheng, S. Structure and expression of glutathione S-transferase genes from the midgut of the Common cutworm, Spodoptera litura (Noctuidae) and their response to xenobiotic compounds and bacteria. *J. Insect Physiol.* **2011**, *57*, 1033–1044. [CrossRef]
19. Knight, T.R.; Choudhuri, S.; Klaassen, C.D. Constitutive mRNA expression of various glutathione S-transferase isoforms in different tissues of mice. *Toxicol. Sci.* **2007**, *100*, 513–524. [CrossRef]
20. Sullivan, S.L. Mammalian chemosensory receptors. *Neuroreport* **2002**, *13*, A9–A17. [CrossRef]
21. Filiou, R.P.; Lepore, F.; Bryant, B.; Lundstrom, J.N.; Frasnelli, J. Perception of trigeminal mixtures. *Chem. Senses* **2015**, *40*, 61–69. [CrossRef]
22. Su, C.Y.; Menuz, K.; Carlson, J.R. Olfactory perception: Receptors, cells, and circuits. *Cell* **2009**, *139*, 45–59. [CrossRef] [PubMed]
23. Malnic, B.; Hirono, J.; Sato, T.; Buck, L.B. Combinatorial receptor codes for odors. *Cell* **1999**, *96*, 713–723. [CrossRef] [PubMed]
24. Yarmolinsky, D.A.; Zuker, C.S.; Ryba, N.J. Common sense about taste: From mammals to insects. *Cell* **2009**, *139*, 234–244. [CrossRef] [PubMed]
25. Ahmad, R.; Dalziel, J.E. G Protein-Coupled Receptors in Taste Physiology and Pharmacology. *Front. Pharmacol.* **2020**, *11*, 587664. [CrossRef]
26. Li, Q.; Zhang, L.; Lametsch, R. Current progress in kokumi-active peptides, evaluation and preparation methods: A review. *Crit. Rev. Food Sci. Nutr.* **2022**, *62*, 1230–1241. [CrossRef]
27. Toelstede, S.; Hofmann, T. Kokumi-active glutamyl peptides in cheeses and their biogeneration by Penicillium roquefortii. *J. Agric. Food Chem.* **2009**, *57*, 3738–3748. [CrossRef]
28. Maruyama, Y.; Yasuda, R.; Kuroda, M.; Eto, Y. Kokumi substances, enhancers of basic tastes, induce responses in calcium-sensing receptor expressing taste cells. *PLoS ONE* **2012**, *7*, e34489. [CrossRef]
29. Canon, F.; Belloir, C.; Bourillot, E.; Brignot, H.; Briand, L.; Feron, G.; Lesniewska, E.; Nivet, C.; Septier, C.; Schwartz, M.; et al. Perspectives on Astringency Sensation: An Alternative Hypothesis on the Molecular Origin of Astringency. *J. Agric. Food Chem.* **2021**, *69*, 3822–3826. [CrossRef]
30. Boichot, V.; Muradova, M.; Nivet, C.; Proskura, A.; Heydel, J.M.; Canivenc-Lavier, M.C.; Canon, F.; Neiers, F.; Schwartz, M. The role of perirecetor events in flavor perception. *Front. Food Sci. Technol.* **2022**, *2*, 989291. [CrossRef]
31. Sarkar, M.A. Drug metabolism in the nasal mucosa. *Pharm. Res.* **1992**, *9*, 1–9. [CrossRef]
32. Heydel, J.M.; Faure, P.; Neiers, F. Nasal odorant metabolism: Enzymes, activity and function in olfaction. *Drug Metab. Rev.* **2019**, *51*, 224–245. [CrossRef]
33. Mallery, S.R.; Budendorf, D.E.; Larsen, M.P.; Pei, P.; Tong, M.; Holpuch, A.S.; Larsen, P.E.; Stoner, G.D.; Fields, H.W.; Chan, K.K.; et al. Effects of human oral mucosal tissue, saliva, and oral microflora on intraoral metabolism and bioactivation of black raspberry anthocyanins. *Cancer Prev. Res.* **2011**, *4*, 1209–1221. [CrossRef]
34. Schwartz, M.; Neiers, F.; Charles, J.P.; Heydel, J.M.; Munoz-Gonzalez, C.; Feron, G.; Canon, F. Oral enzymatic detoxification system: Insights obtained from proteome analysis to understand its potential impact on aroma metabolization. *Compr. Rev. Food Sci. Food Saf.* **2021**, *20*, 5516–5547. [CrossRef]
35. Canon, F.; Neiers, F.; Guichard, E. Saliva and Flavor Perception: Perspectives. *J. Agric. Food Chem.* **2018**, *66*, 7873–7879. [CrossRef]
36. Munoz-Gonzalez, C.; Brule, M.; Martin, C.; Feron, G.; Canon, F. Molecular mechanisms of aroma persistence: From noncovalent interactions between aroma compounds and the oral mucosa to metabolization of aroma compounds by saliva and oral cells. *Food Chem.* **2022**, *373*, 131467. [CrossRef]

37. Robert-Hazotte, A.; Faure, P.; Menetrier, F.; Folia, M.; Schwartz, M.; Le Quere, J.L.; Neiers, F.; Thomas-Danguin, T.; Heydel, J.M. Nasal Odorant Competitive Metabolism Is Involved in the Human Olfactory Process. *J. Agric. Food Chem.* **2022**, *70*, 8385–8394. [CrossRef]
38. Ployon, S.; Brule, M.; Andriot, I.; Morzel, M.; Canon, F. Understanding retention and metabolization of aroma compounds using an in vitro model of oral mucosa. *Food Chem.* **2020**, *318*, 126468. [CrossRef]
39. Mannervik, B.; Alin, P.; Guthenberg, C.; Jensson, H.; Tahir, M.K.; Warholm, M.; Jornvall, H. Identification of three classes of cytosolic glutathione transferase common to several mammalian species: Correlation between structural data and enzymatic properties. *Proc. Natl. Acad. Sci. USA* **1985**, *82*, 7202–7206. [CrossRef]
40. Sheehan, D.; Meade, G.; Foley, V.M.; Dowd, C.A. Structure, function and evolution of glutathione transferases: Implications for classification of non-mammalian members of an ancient enzyme superfamily. *Biochem. J.* **2001**, *360*, 1–16. [CrossRef]
41. Ben-Arie, N.; Khen, M.; Lancet, D. Glutathione S-transferases in rat olfactory epithelium: Purification, molecular properties and odorant biotransformation. *Biochem. J.* **1993**, *292 Pt 2*, 379–384. [CrossRef]
42. Krishna, N.S.; Getchell, T.V.; Getchell, M.L. Differential expression of alpha, mu, and pi classes of glutathione S-transferases in chemosensory mucosae of rats during development. *Cell Tissue Res.* **1994**, *275*, 435–450. [CrossRef] [PubMed]
43. Schwartz, M.; Menetrier, F.; Heydel, J.M.; Chavanne, E.; Faure, P.; Labrousse, M.; Lirussi, F.; Canon, F.; Mannervik, B.; Briand, L.; et al. Interactions Between Odorants and Glutathione Transferases in the Human Olfactory Cleft. *Chem. Senses* **2020**, *45*, 645–654. [CrossRef] [PubMed]
44. Toyoshima, K.; Tandler, B. Dividing type II cell in rabbit taste bud. *Anat Rec.* **1986**, *214*, 161–164. [CrossRef] [PubMed]
45. Russell, R.M.; Cox, M.E.; Solomons, N. Zinc and the special senses. *Ann. Intern. Med.* **1983**, *99*, 227–239. [CrossRef] [PubMed]
46. Kudo, H.; Doi, Y.; Nishino, T.; Nara, S.; Hamasaki, K.; Fujimoto, S. Dietary zinc deficiency decreases glutathione S-transferase expression in the rat olfactory epithelium. *J. Nutr.* **2000**, *130*, 38–44. [CrossRef]
47. Schaal, B.; Coureaud, G.; Langlois, D.; Ginies, C.; Semon, E.; Perrier, G. Chemical and behavioural characterization of the rabbit mammary pheromone. *Nature* **2003**, *424*, 68–72. [CrossRef]
48. Legendre, A.; Faure, P.; Tiesset, H.; Potin, C.; Jakob, I.; Sicard, G.; Schaal, B.; Artur, Y.; Coureaud, G.; Heydel, J.M. When the nose must remain responsive: Glutathione conjugation of the mammary pheromone in the newborn rabbit. *Chem. Senses* **2014**, *39*, 425–437. [CrossRef]
49. Robert-Hazotte, A.; Faure, P.; Neiers, F.; Potin, C.; Artur, Y.; Coureaud, G.; Heydel, J.M. Nasal mucus glutathione transferase activity and impact on olfactory perception and neonatal behavior. *Sci. Rep.* **2019**, *9*, 3104. [CrossRef]
50. Hanser, H.I.; Faure, P.; Robert-Hazotte, A.; Artur, Y.; Duchamp-Viret, P.; Coureaud, G.; Heydel, J.M. Odorant-odorant metabolic interaction, a novel actor in olfactory perception and behavioral responsiveness. *Sci. Rep.* **2017**, *7*, 10219. [CrossRef]
51. Nishino, T.; Kudo, H.; Doi, Y.; Maeda, M.; Hamasaki, K.; Morita, M.; Fujimoto, S. Immunocytochemistry of glutathione S-transferase in taste bud cells of rat circumvallate and foliate papillae. *Chem. Senses* **2001**, *26*, 179–188. [CrossRef]
52. Fabrini, R.; Bocedi, A.; Camerini, S.; Fusetti, M.; Ottaviani, F.; Passali, F.M.; Topazio, D.; Iavarone, F.; Francia, I.; Castagnola, M.; et al. Inactivation of human salivary glutathione transferase P1-1 by hypothiocyanite: A post-translational control system in search of a role. *PLoS ONE* **2014**, *9*, e112797. [CrossRef]
53. Derindag, G.; Akgul, H.M.; Kiziltunc, A.; Ozkan, H.I.; Kiziltunc Ozmen, H.; Akgul, N. Evaluation of saliva glutathione, glutathione peroxidase, and malondialdehyde levels in head-neck radiotherapy patients. *Turk J. Med. Sci.* **2021**, *51*, 644–649. [CrossRef]
54. Sreerama, L.; Hedge, M.W.; Sladek, N.E. Identification of a class 3 aldehyde dehydrogenase in human saliva and increased levels of this enzyme, glutathione S-transferases, and DT-diaphorase in the saliva of subjects who continually ingest large quantities of coffee or broccoli. *Clin. Cancer Res.* **1995**, *1*, 1153–1163.
55. Schwartz, M.; Brignot, H.; Feron, G.; Hummel, T.; Zhu, Y.; von Koskull, D.; Heydel, J.M.; Lirussi, F.; Canon, F.; Neiers, F. Role of human salivary enzymes in bitter taste perception. *Food Chem.* **2022**, *386*, 132798. [CrossRef]
56. Franco-Martinez, L.; Gelemanovic, A.; Horvatic, A.; Contreras-Aguilar, M.D.; Dabrowski, R.; Mrljak, V.; Ceron, J.J.; Martinez-Subiela, S.; Tvarijonaviciute, A. Changes in Serum and Salivary Proteins in Canine Mammary Tumors. *Animals* **2020**, *10*, 741. [CrossRef]
57. de Sousa-Pereira, P.; Cova, M.; Abrantes, J.; Ferreira, R.; Trindade, F.; Barros, A.; Gomes, P.; Colaco, B.; Amado, F.; Esteves, P.J.; et al. Cross-species comparison of mammalian saliva using an LC-MALDI based proteomic approach. *Proteomics* **2015**, *15*, 1598–1607. [CrossRef]
58. Debat, H.; Eloit, C.; Blon, F.; Sarazin, B.; Henry, C.; Huet, J.C.; Trotier, D.; Pernollet, J.C. Identification of human olfactory cleft mucus proteins using proteomic analysis. *J. Proteome Res.* **2007**, *6*, 1985–1996. [CrossRef]
59. Yoshikawa, K.; Wang, H.; Jaen, C.; Haneoka, M.; Saito, N.; Nakamura, J.; Adappa, N.D.; Cohen, N.A.; Dalton, P. The human olfactory cleft mucus proteome and its age-related changes. *Sci. Rep.* **2018**, *8*, 17170. [CrossRef]
60. Pappa, E.; Vastardis, H.; Mermelekas, G.; Gerasimidi-Vazeou, A.; Zoidakis, J.; Vougas, K. Saliva Proteomics Analysis Offers Insights on Type 1 Diabetes Pathology in a Pediatric Population. *Front. Physiol.* **2018**, *9*, 444. [CrossRef]
61. Grassl, N.; Kulak, N.A.; Pichler, G.; Geyer, P.E.; Jung, J.; Schubert, S.; Sinitcyn, P.; Cox, J.; Mann, M. Ultra-deep and quantitative saliva proteome reveals dynamics of the oral microbiome. *Genome Med.* **2016**, *8*, 44. [CrossRef]
62. Kuhlmann, K.; Tschapek, A.; Wiese, H.; Eisenacher, M.; Meyer, H.E.; Hatt, H.H.; Oeljeklaus, S.; Warscheid, B. The membrane proteome of sensory cilia to the depth of olfactory receptors. *Mol. Cell Proteom.* **2014**, *13*, 1828–1843. [CrossRef] [PubMed]

63. Murphy, S.; Zweyer, M.; Mundegar, R.R.; Swandulla, D.; Ohlendieck, K. Dataset on the comparative proteomic profiling of mouse saliva and serum from wild type versus the dystrophic mdx-4cv mouse model of dystrophinopathy. *Data Brief* **2018**, *21*, 1236–1245. [CrossRef] [PubMed]
64. Mayer, U.; Ungerer, N.; Klimmeck, D.; Warnken, U.; Schnolzer, M.; Frings, S.; Mohrlen, F. Proteomic analysis of a membrane preparation from rat olfactory sensory cilia. *Chem. Senses* **2008**, *33*, 145–162. [CrossRef] [PubMed]
65. Nauen, R.; Bass, C.; Feyereisen, R.; Vontas, J. The Role of Cytochrome P450s in Insect Toxicology and Resistance. *Annu. Rev. Entomol.* **2022**, *67*, 105–124. [CrossRef] [PubMed]
66. Pavlidi, N.; Vontas, J.; Van Leeuwen, T. The role of glutathione S-transferases (GSTs) in insecticide resistance in crop pests and disease vectors. *Curr. Opin. Insect Sci.* **2018**, *27*, 97–102. [CrossRef]
67. Zalucki, M.P.; Furlong, M.J. Behavior as a mechanism of insecticide resistance: Evaluation of the evidence. *Curr. Opin. Insect Sci.* **2017**, *21*, 19–25. [CrossRef]
68. Fischler, W.; Kong, P.; Marella, S.; Scott, K. The detection of carbonation by the Drosophila gustatory system. *Nature* **2007**, *448*, 1054–1057. [CrossRef]
69. Scott, K. Out of thin air: Sensory detection of oxygen and carbon dioxide. *Neuron* **2011**, *69*, 194–202. [CrossRef]
70. Cameron, P.; Hiroi, M.; Ngai, J.; Scott, K. The molecular basis for water taste in Drosophila. *Nature* **2010**, *465*, 91–95. [CrossRef]
71. Falk, R.; Bleiser-Avivi, N.; Atidia, J. Labellar taste organs of Drosophila melanogaster. *J. Morphol.* **1976**, *150*, 327–341. [CrossRef]
72. Steinbrecht, R.A. Structure and function of insect olfactory sensilla. *Ciba Found Symp.* **1996**, *200*, 158–174; discussion 157–174. [CrossRef]
73. Benton, R.; Sachse, S.; Michnick, S.W.; Vosshall, L.B. Atypical membrane topology and heteromeric function of Drosophila odorant receptors in vivo. *PLoS Biol.* **2006**, *4*, e20. [CrossRef]
74. Strausfeld, N.J.; Hildebrand, J.G. Olfactory systems: Common design, uncommon origins? *Curr. Opin. Neurobiol.* **1999**, *9*, 634–639. [CrossRef]
75. Clyne, P.J.; Warr, C.G.; Carlson, J.R. Candidate taste receptors in Drosophila. *Science* **2000**, *287*, 1830–1834. [CrossRef]
76. Vosshall, L.B.; Amrein, H.; Morozov, P.S.; Rzhetsky, A.; Axel, R. A spatial map of olfactory receptor expression in the Drosophila antenna. *Cell* **1999**, *96*, 725–736. [CrossRef]
77. Isono, K.; Morita, H. Molecular and cellular designs of insect taste receptor system. *Front. Cell Neurosci.* **2010**, *4*, 20. [CrossRef]
78. Sanchez-Gracia, A.; Vieira, F.G.; Rozas, J. Molecular evolution of the major chemosensory gene families in insects. *Heredity* **2009**, *103*, 208–216. [CrossRef]
79. Shi, H.; Pei, L.; Gu, S.; Zhu, S.; Wang, Y.; Zhang, Y.; Li, B. Glutathione S-transferase (GST) genes in the red flour beetle, Tribolium castaneum, and comparative analysis with five additional insects. *Genomics* **2012**, *100*, 327–335. [CrossRef]
80. Ohno, S. *Evolution by Gene Duplication*; Allen & Unwin; Springer: London, UK; New York, NY, USA, 1970; p. xv. 160p.
81. Mitter, C.; Farrell, B.; Wiegmann, B. The phylogenetic study of adaptive zones: Has phytophagy promoted insect diversification? *Am. Nat.* **1988**, *132*, 107–128. [CrossRef]
82. Saruta, F.; Yamada, N.; Yamamoto, K. Functional Analysis of an Epsilon-Class Glutathione S-Transferase From Nilaparvata lugens (Hemiptera: Delphacidae). *J. Insect Sci.* **2019**, *19*, 14. [CrossRef]
83. Yang, J.; Kong, X.D.; Zhu-Salzman, K.; Qin, Q.M.; Cai, Q.N. The Key Glutathione S-Transferase Family Genes Involved in the Detoxification of Rice Gramine in Brown Planthopper Nilaparvata lugens. *Insects* **2021**, *12*, 1055. [CrossRef] [PubMed]
84. Zou, X.; Xu, Z.; Zou, H.; Liu, J.; Chen, S.; Feng, Q.; Zheng, S. Glutathione S-transferase SlGSTE1 in Spodoptera litura may be associated with feeding adaptation of host plants. *Insect Biochem. Mol. Biol.* **2016**, *70*, 32–43. [CrossRef] [PubMed]
85. Gloss, A.D.; Vassao, D.G.; Hailey, A.L.; Nelson Dittrich, A.C.; Schramm, K.; Reichelt, M.; Rast, T.J.; Weichsel, A.; Cravens, M.G.; Gershenzon, J.; et al. Evolution in an ancient detoxification pathway is coupled with a transition to herbivory in the drosophilidae. *Mol. Biol. Evol.* **2014**, *31*, 2441–2456. [CrossRef] [PubMed]
86. Labandeira, C.C. Early history of Arthropod and vascular plant associations. *Annu. Rev. Earth Planet. Sci.* **1998**, *26*, 329–377. [CrossRef]
87. Syvanen, M.; Zhou, Z.; Wharton, J.; Goldsbury, C.; Clark, A. Heterogeneity of the glutathione transferase genes encoding enzymes responsible for insecticide degradation in the housefly. *J. Mol. Evol.* **1996**, *43*, 236–240. [CrossRef]
88. Wang, J.Y.; McCommas, S.; Syvanen, M. Molecular cloning of a glutathione S-transferase overproduced in an insecticide-resistant strain of the housefly (Musca domestica). *Mol. Gen. Genet. MGG* **1991**, *227*, 260–266. [CrossRef]
89. Paton, M.G.; Karunaratne, S.H.; Giakoumaki, E.; Roberts, N.; Hemingway, J. Quantitative analysis of gene amplification in insecticide-resistant Culex mosquitoes. *Biochem. J.* **2000**, *346 Pt 1*, 17–24. [CrossRef]
90. Yamamoto, K.; Higashiura, A.; Hirowatari, A.; Yamada, N.; Tsubota, T.; Sezutsu, H.; Nakagawa, A. Characterisation of a diazinon-metabolising glutathione S-transferase in the silkworm Bombyx mori by X-ray crystallography and genome editing analysis. *Sci. Rep.* **2018**, *8*, 16835. [CrossRef]
91. Yamamoto, K.; Ichinose, H.; Aso, Y.; Banno, Y.; Kimura, M.; Nakashima, T. Molecular characterization of an insecticide-induced novel glutathione transferase in silkworm. *Biochim. Biophys. Acta* **2011**, *1810*, 420–426. [CrossRef]
92. Ortelli, F.; Rossiter, L.C.; Vontas, J.; Ranson, H.; Hemingway, J. Heterologous expression of four glutathione transferase genes genetically linked to a major insecticide-resistance locus from the malaria vector Anopheles gambiae. *Biochem. J.* **2003**, *373*, 957–963. [CrossRef]

93. Yu, X.; Killiny, N. RNA interference of two glutathione S-transferase genes, Diaphorina citri DcGSTe2 and DcGSTd1, increases the susceptibility of Asian citrus psyllid (Hemiptera: Liviidae) to the pesticides fenpropathrin and thiamethoxam. *Pest Manag. Sci.* **2018**, *74*, 638–647. [CrossRef]
94. Bamidele, O.S.; Ajele, J.O.; Olajuyigbe, F.M.; Gaber, Y. An evaluation of glutathione transferase associated with Dichlorvos degradation in African palm weevil (Rynchophorus phoenicis) larva. *Cogent Biol.* **2017**, *3*, 1286764. [CrossRef]
95. Chanut-Delalande, H.; Hashimoto, Y.; Pelissier-Monier, A.; Spokony, R.; Dib, A.; Kondo, T.; Bohere, J.; Niimi, K.; Latapie, Y.; Inagaki, S.; et al. Pri peptides are mediators of ecdysone for the temporal control of development. *Nat. Cell Biol.* **2014**, *16*, 1035–1044. [CrossRef]
96. Enya, S.; Ameku, T.; Igarashi, F.; Iga, M.; Kataoka, H.; Shinoda, T.; Niwa, R. A Halloween gene noppera-bo encodes a glutathione S-transferase essential for ecdysteroid biosynthesis via regulating the behaviour of cholesterol in Drosophila. *Sci. Rep.* **2014**, *4*, 6586. [CrossRef]
97. Ma, J.; Sun, L.; Zhao, H.; Wang, Z.; Zou, L.; Cao, C. Functional identification and characterization of GST genes in the Asian gypsy moth in response to poplar secondary metabolites. *Pestic. Biochem. Physiol.* **2021**, *176*, 104860. [CrossRef]
98. Zhao, Y.J.; Wang, Z.Q.; Zhu, J.Y.; Liu, N.Y. Identification and characterization of detoxification genes in two cerambycid beetles, Rhaphuma horsfieldi and Xylotrechus quadripes (Coleoptera: Cerambycidae: Clytini). *Comp. Biochem. Physiol. B Biochem. Mol. Biol.* **2020**, *243–244*, 110431. [CrossRef]
99. McKenna, D.D.; Scully, E.D.; Pauchet, Y.; Hoover, K.; Kirsch, R.; Geib, S.M.; Mitchell, R.F.; Waterhouse, R.M.; Ahn, S.J.; Arsala, D.; et al. Genome of the Asian longhorned beetle (Anoplophora glabripennis), a globally significant invasive species, reveals key functional and evolutionary innovations at the beetle-plant interface. *Genome Biol.* **2016**, *17*, 227. [CrossRef]
100. Schoville, S.D.; Chen, Y.H.; Andersson, M.N.; Benoit, J.B.; Bhandari, A.; Bowsher, J.H.; Brevik, K.; Cappelle, K.; Chen, M.M.; Childers, A.K.; et al. A model species for agricultural pest genomics: The genome of the Colorado potato beetle, Leptinotarsa decemlineata (Coleoptera: Chrysomelidae). *Sci. Rep.* **2018**, *8*, 1931. [CrossRef]
101. Wu, Z.; Bin, S.; He, H.; Wang, Z.; Li, M.; Lin, J. Differential Expression Analysis of Chemoreception Genes in the Striped Flea Beetle Phyllotreta striolata Using a Transcriptomic Approach. *PLoS ONE* **2016**, *11*, e0153067. [CrossRef]
102. Dai, L.; Ma, J.; Ma, M.; Zhang, H.; Shi, Q.; Zhang, R.; Chen, H. Characterisation of GST genes from the Chinese white pine beetle Dendroctonus armandi (Curculionidae: Scolytinae) and their response to host chemical defence. *Pest Manag. Sci.* **2016**, *72*, 816–827. [CrossRef]
103. Keeling, C.I.; Yuen, M.M.; Liao, N.Y.; Docking, T.R.; Chan, S.K.; Taylor, G.A.; Palmquist, D.L.; Jackman, S.D.; Nguyen, A.; Li, M.; et al. Draft genome of the mountain pine beetle, Dendroctonus ponderosae Hopkins, a major forest pest. *Genome Biol.* **2013**, *14*, R27. [CrossRef] [PubMed]
104. Hu, F.; Ye, K.; Tu, X.F.; Lu, Y.J.; Thakur, K.; Jiang, L.; Wei, Z.J. Identification and expression profiles of twenty-six glutathione S-transferase genes from rice weevil, Sitophilus oryzae (Coleoptera: Curculionidae). *Int. J. Biol. Macromol.* **2018**, *120*, 1063–1071. [CrossRef] [PubMed]
105. Evans, J.D.; McKenna, D.; Scully, E.; Cook, S.C.; Dainat, B.; Egekwu, N.; Grubbs, N.; Lopez, D.; Lorenzen, M.D.; Reyna, S.M.; et al. Genome of the small hive beetle (Aethina tumida, Coleoptera: Nitidulidae), a worldwide parasite of social bee colonies, provides insights into detoxification and herbivory. *Gigascience* **2018**, *7*, giy138. [CrossRef] [PubMed]
106. Meyer, J.M.; Markov, G.V.; Baskaran, P.; Herrmann, M.; Sommer, R.J.; Rodelsperger, C. Draft Genome of the Scarab Beetle Oryctes borbonicus on La Reunion Island. *Genome Biol. Evol.* **2016**, *8*, 2093–2105. [CrossRef]
107. Liu, S.; Rao, X.J.; Li, M.Y.; Feng, M.F.; He, M.Z.; Li, S.G. Glutathione s-transferase genes in the rice leaffolder, cnaphalocrocis medinalis (Lepidoptera: Pyralidae): Identification and expression profiles. *Arch Insect Biochem. Physiol.* **2015**, *90*, 1–13. [CrossRef]
108. Nair, P.M.; Choi, J. Identification, characterization and expression profiles of Chironomus riparius glutathione S-transferase (GST) genes in response to cadmium and silver nanoparticles exposure. *Aquat. Toxicol.* **2011**, *101*, 550–560. [CrossRef]
109. Strode, C.; Wondji, C.S.; David, J.P.; Hawkes, N.J.; Lumjuan, N.; Nelson, D.R.; Drane, D.R.; Karunaratne, S.H.; Hemingway, J.; Black, W.C.t.; et al. Genomic analysis of detoxification genes in the mosquito Aedes aegypti. *Insect Biochem. Mol. Biol.* **2008**, *38*, 113–123. [CrossRef]
110. Yan, L.; Yang, P.; Jiang, F.; Cui, N.; Ma, E.; Qiao, C.; Cui, F. Transcriptomic and phylogenetic analysis of Culex pipiens quinquefasciatus for three detoxification gene families. *BMC Genom.* **2012**, *13*, 609. [CrossRef]
111. Niranjan Reddy, B.P.; Prasad, G.B.; Raghavendra, K. In silico characterization and comparative genomic analysis of the Culex quinquefasciatus glutathione S-transferase (GST) supergene family. *Parasitol. Res.* **2011**, *109*, 1165–1177. [CrossRef]
112. Hu, F.; Dou, W.; Wang, J.J.; Jia, F.X.; Wang, J.J. Multiple glutathione S-transferase genes: Identification and expression in oriental fruit fly, Bactrocera dorsalis. *Pest Manag. Sci.* **2014**, *70*, 295–303. [CrossRef]
113. Papanicolaou, A.; Schetelig, M.F.; Arensburger, P.; Atkinson, P.W.; Benoit, J.B.; Bourtzis, K.; Castanera, P.; Cavanaugh, J.P.; Chao, H.; Childers, C.; et al. The whole genome sequence of the Mediterranean fruit fly, Ceratitis capitata (Wiedemann), reveals insights into the biology and adaptive evolution of a highly invasive pest species. *Genome Biol.* **2016**, *17*, 192. [CrossRef]
114. Aidlin Harari, O.; Santos-Garcia, D.; Musseri, M.; Moshitzky, P.; Patel, M.; Visendi, P.; Seal, S.; Sertchook, R.; Malka, O.; Morin, S. Molecular Evolution of the Glutathione S-Transferase Family in the Bemisia tabaci Species Complex. *Genome Biol. Evol.* **2020**, *12*, 3857–3872. [CrossRef]

115. Bailey, E.; Field, L.; Rawlings, C.; King, R.; Mohareb, F.; Pak, K.H.; Hughes, D.; Williamson, M.; Ganko, E.; Buer, B.; et al. A scaffold-level genome assembly of a minute pirate bug, Orius laevigatus (Hemiptera: Anthocoridae), and a comparative analysis of insecticide resistance-related gene families with hemipteran crop pests. *BMC Genom.* **2022**, *23*, 45. [CrossRef]
116. Ramsey, J.S.; Rider, D.S.; Walsh, T.K.; De Vos, M.; Gordon, K.H.; Ponnala, L.; Macmil, S.L.; Roe, B.A.; Jander, G. Comparative analysis of detoxification enzymes in Acyrthosiphon pisum and Myzus persicae. *Insect Mol. Biol.* **2010**, *19* (Suppl. S2), 155–164. [CrossRef]
117. Zhou, W.W.; Li, X.W.; Quan, Y.H.; Cheng, J.; Zhang, C.X.; Gurr, G.; Zhu, Z.R. Identification and expression profiles of nine glutathione S-transferase genes from the important rice phloem sap-sucker and virus vector Laodelphax striatellus (Fallen) (Hemiptera: Delphacidae). *Pest Manag. Sci.* **2012**, *68*, 1296–1305. [CrossRef]
118. Xue, J.; Zhou, X.; Zhang, C.X.; Yu, L.L.; Fan, H.W.; Wang, Z.; Xu, H.J.; Xi, Y.; Zhu, Z.R.; Zhou, W.W.; et al. Genomes of the rice pest brown planthopper and its endosymbionts reveal complex complementary contributions for host adaptation. *Genome Biol.* **2014**, *15*, 521. [CrossRef]
119. Zhou, W.W.; Liang, Q.M.; Xu, Y.; Gurr, G.M.; Bao, Y.Y.; Zhou, X.P.; Zhang, C.X.; Cheng, J.; Zhu, Z.R. Genomic insights into the glutathione S-transferase gene family of two rice planthoppers, Nilaparvata lugens (Stal) and Sogatella furcifera (Horvath) (Hemiptera: Delphacidae). *PLoS ONE* **2013**, *8*, e56604. [CrossRef]
120. Schama, R.; Pedrini, N.; Juarez, M.P.; Nelson, D.R.; Torres, A.Q.; Valle, D.; Mesquita, R.D. Rhodnius prolixus supergene families of enzymes potentially associated with insecticide resistance. *Insect Biochem. Mol. Biol.* **2016**, *69*, 91–104. [CrossRef]
121. Sadd, B.M.; Barribeau, S.M.; Bloch, G.; de Graaf, D.C.; Dearden, P.; Elsik, C.G.; Gadau, J.; Grimmelikhuijzen, C.J.; Hasselmann, M.; Lozier, J.D.; et al. The genomes of two key bumblebee species with primitive eusocial organization. *Genome Biol.* **2015**, *16*, 76. [CrossRef]
122. Zhang, X.R.; Zhang, J.Q.; Shao, Y.Y.; Xing, X.R.; Wang, J.; Liu, Z.X.; Li, Y.J.; Ofori, A.D.; Tu, Q.B.; Wang, J.; et al. Identification of glutathione-S-transferase genes by transcriptome analysis in Meteorus pulchricornis (Hymenoptera: Braconidae) and their expression patterns under stress of phoxim and cypermethrin. *Comp. Biochem. Physiol. Part D Genom. Proteom.* **2019**, *31*, 100607. [CrossRef]
123. Oakeshott, J.G.; Johnson, R.M.; Berenbaum, M.R.; Ranson, H.; Cristino, A.S.; Claudianos, C. Metabolic enzymes associated with xenobiotic and chemosensory responses in Nasonia vitripennis. *Insect Mol. Biol.* **2010**, *19* (Suppl. S1), 147–163. [CrossRef] [PubMed]
124. Xu, G.; Teng, Z.W.; Gu, G.X.; Guo, L.; Wang, F.; Xiao, S.; Wang, J.L.; Wang, B.B.; Fang, Q.; Wang, F.; et al. Genomic and transcriptomic analyses of glutathione S-transferases in an endoparasitoid wasp, Pteromalus puparum. *Arch. Insect Biochem. Physiol.* **2020**, *103*, e21634. [CrossRef] [PubMed]
125. Yu, Q.; Lu, C.; Li, B.; Fang, S.; Zuo, W.; Dai, F.; Zhang, Z.; Xiang, Z. Identification, genomic organization and expression pattern of glutathione S-transferase in the silkworm, Bombyx mori. *Insect Biochem. Mol. Biol.* **2008**, *38*, 1158–1164. [CrossRef]
126. Cheng, J.; Wang, C.Y.; Lyu, Z.H.; Lin, T. Multiple Glutathione S-Transferase Genes in Heortia vitessoides (Lepidoptera: Crambidae): Identification and Expression Patterns. *J. Insect Sci.* **2018**, *18*, 23. [CrossRef]
127. Cheng, T.; Wu, J.; Wu, Y.; Chilukuri, R.V.; Huang, L.; Yamamoto, K.; Feng, L.; Li, W.; Chen, Z.; Guo, H.; et al. Genomic adaptation to polyphagy and insecticides in a major East Asian noctuid pest. *Nat. Ecol. Evol.* **2017**, *1*, 1747–1756. [CrossRef]
128. Liu, S.; Zhang, Y.X.; Wang, W.L.; Zhang, B.X.; Li, S.G. Identification and characterisation of seventeen glutathione S-transferase genes from the cabbage white butterfly Pieris rapae. *Pestic. Biochem. Physiol.* **2017**, *143*, 102–110. [CrossRef]
129. You, Y.; Xie, M.; Ren, N.; Cheng, X.; Li, J.; Ma, X.; Zou, M.; Vasseur, L.; Gurr, G.M.; You, M. Characterization and expression profiling of glutathione S-transferases in the diamondback moth, Plutella xylostella (L.). *BMC Genom.* **2015**, *16*, 152. [CrossRef]
130. Huang, X.L.; Fan, D.S.; Liu, L.; Feng, J.N. Identification and characterization of glutathione S-transferase genes in the antennae of codling moth (Lepidoptera: Tortricidae). *Ann. Entomol. Soc. Am.* **2017**, *110*, 409–416. [CrossRef]
131. Wang, X.; Fang, X.; Yang, P.; Jiang, X.; Jiang, F.; Zhao, D.; Li, B.; Cui, F.; Wei, J.; Ma, C.; et al. The locust genome provides insight into swarm formation and long-distance flight. *Nat. Commun.* **2014**, *5*, 2957. [CrossRef]
132. Kirkness, E.F.; Haas, B.J.; Sun, W.; Braig, H.R.; Perotti, M.A.; Clark, J.M.; Lee, S.H.; Robertson, H.M.; Kennedy, R.C.; Elhaik, E.; et al. Genome sequences of the human body louse and its primary endosymbiont provide insights into the permanent parasitic lifestyle. *Proc. Natl. Acad. Sci. USA* **2010**, *107*, 12168–12173. [CrossRef]
133. Wei, D.D.; Chen, E.H.; Ding, T.B.; Chen, S.C.; Dou, W.; Wang, J.J. De novo assembly, gene annotation, and marker discovery in stored-product pest Liposcelis entomophila (Enderlein) using transcriptome sequences. *PLoS ONE* **2013**, *8*, e80046. [CrossRef]
134. Younus, F.; Chertemps, T.; Pearce, S.L.; Pandey, G.; Bozzolan, F.; Coppin, C.W.; Russell, R.J.; Maibeche-Coisne, M.; Oakeshott, J.G. Identification of candidate odorant degrading gene/enzyme systems in the antennal transcriptome of Drosophila melanogaster. *Insect Biochem. Mol. Biol.* **2014**, *53*, 30–43. [CrossRef]
135. Corcoran, J.A.; Jordan, M.D.; Thrimawithana, A.H.; Crowhurst, R.N.; Newcomb, R.D. The Peripheral Olfactory Repertoire of the Lightbrown Apple Moth, Epiphyas postvittana. *PLoS ONE* **2015**, *10*, e0128596. [CrossRef]
136. Liu, S.; Gong, Z.J.; Rao, X.J.; Li, M.Y.; Li, S.G. Identification of Putative Carboxylesterase and Glutathione S-transferase Genes from the Antennae of the Chilo suppressalis (Lepidoptera: Pyralidae). *J. Insect Sci.* **2015**, *15*, 103. [CrossRef]
137. Tan, X.; Hu, X.M.; Zhong, X.W.; Chen, Q.M.; Xia, Q.Y.; Zhao, P. Antenna-specific glutathione S-transferase in male silkmoth Bombyx mori. *Int. J. Mol. Sci.* **2014**, *15*, 7429–7443. [CrossRef]

138. Leal, W.S.; Ishida, Y.; Pelletier, J.; Xu, W.; Rayo, J.; Xu, X.; Ames, J.B. Olfactory proteins mediating chemical communication in the navel orangeworm moth, Amyelois transitella. *PLoS ONE* **2009**, *4*, e7235. [CrossRef]
139. Wang, G.R.; Guo, Y.Y.; Wu, K.M. Cloning of a cDNA fragment of an antenna-specific gene in *Helicoverpa armigera*. *Chin. J. Agric. Biotechnol.* **2002**, *1*, 37–43. [CrossRef]
140. Rogers, M.E.; Jani, M.K.; Vogt, R.G. An olfactory-specific glutathione-S-transferase in the sphinx moth Manduca sexta. *J. Exp. Biol.* **1999**, *202*, 1625–1637. [CrossRef]
141. Durand, N.; Pottier, M.A.; Siaussat, D.; Bozzolan, F.; Maibeche, M.; Chertemps, T. Glutathione-S-Transferases in the Olfactory Organ of the Noctuid Moth Spodoptera littoralis, Diversity and Conservation of Chemosensory Clades. *Front. Physiol.* **2018**, *9*, 1283. [CrossRef]
142. Mamidala, P.; Wijeratne, A.J.; Wijeratne, S.; Poland, T.; Qazi, S.S.; Doucet, D.; Cusson, M.; Beliveau, C.; Mittapalli, O. Identification of odor-processing genes in the emerald ash borer, Agrilus planipennis. *PLoS ONE* **2013**, *8*, e56555. [CrossRef]
143. Gu, X.C.; Zhang, Y.N.; Kang, K.; Dong, S.L.; Zhang, L.W. Antennal Transcriptome Analysis of Odorant Reception Genes in the Red Turpentine Beetle (RTB), Dendroctonus valens. *PLoS ONE* **2015**, *10*, e0125159. [CrossRef] [PubMed]
144. Nie, H.; Xu, S.; Xie, C.; Geng, H.; Zhao, Y.; Li, J.; Huang, W.F.; Lin, Y.; Li, Z.; Su, S. Comparative transcriptome analysis of Apis mellifera antennae of workers performing different tasks. *Mol. Genet Genom.* **2018**, *293*, 237–248. [CrossRef]
145. Carr, A.L.; Mitchell, R.D., III; Dhammi, A.; Bissinger, B.W.; Sonenshine, D.E.; Roe, R.M. Tick Haller's Organ, a New Paradigm for Arthropod Olfaction: How Ticks Differ from Insects. *Int. J. Mol. Sci.* **2017**, *18*, 1563. [CrossRef] [PubMed]
146. Saisawang, C.; Ketterman, A.J. Micro-plasticity of genomes as illustrated by the evolution of glutathione transferases in 12 Drosophila species. *PLoS ONE* **2014**, *9*, e109518. [CrossRef] [PubMed]
147. Sawicki, R.; Singh, S.P.; Mondal, A.K.; Benes, H.; Zimniak, P. Cloning, expression and biochemical characterization of one Epsilon-class (GST-3) and ten Delta-class (GST-1) glutathione S-transferases from Drosophila melanogaster, and identification of additional nine members of the Epsilon class. *Biochem. J.* **2003**, *370*, 661–669. [CrossRef]
148. Li, G.W.; Chen, X.L.; Xu, X.L.; Wu, J.X. Degradation of sex pheromone and plant volatile components by an antennal glutathione S-transferase in the oriental fruit moth, Grapholita molesta Busck (Lepidoptera: Tortricidae). *Arch Insect Biochem.Physiol.* **2018**, *99*, e21512. [CrossRef]
149. Francis, F.; Vanhaelen, N.; Haubruge, E. Glutathione S-transferases in the adaptation to plant secondary metabolites in the Myzus persicae aphid. *Arch Insect Biochem. Physiol.* **2005**, *58*, 166–174. [CrossRef]
150. Dweck, H.K.; Talross, G.J.; Wang, W.; Carlson, J.R. Evolutionary shifts in taste coding in the fruit pest Drosophila suzukii. *Elife* **2021**, *10*, e64317. [CrossRef]
151. Lombardo, F.; Salvemini, M.; Fiorillo, C.; Nolan, T.; Zwiebel, L.J.; Ribeiro, J.M.; Arca, B. Deciphering the olfactory repertoire of the tiger mosquito Aedes albopictus. *BMC Genom.* **2017**, *18*, 770. [CrossRef]
152. Jordan, M.D.; Stanley, D.; Marshall, S.D.; De Silva, D.; Crowhurst, R.N.; Gleave, A.P.; Greenwood, D.R.; Newcomb, R.D. Expressed sequence tags and proteomics of antennae from the tortricid moth, Epiphyas postvittana. *Insect Mol. Biol.* **2008**, *17*, 361–373. [CrossRef]
153. Ono, H.; Ozaki, K.; Yoshikawa, H. Identification of cytochrome P450 and glutathione-S-transferase genes preferentially expressed in chemosensory organs of the swallowtail butterfly, Papilio xuthus L. *Insect Biochem. Mol. Biol.* **2005**, *35*, 837–846. [CrossRef]
154. Liu, H.; Tang, Y.; Wang, Q.; Shi, H.; Yin, J.; Li, C. Identification and Characterization of an Antennae-Specific Glutathione S-Transferase From the Indian Meal Moth. *Front. Physiol.* **2021**, *12*, 727619. [CrossRef]
155. Legeai, F.; Malpel, S.; Montagne, N.; Monsempes, C.; Cousserans, F.; Merlin, C.; Francois, M.C.; Maibeche-Coisne, M.; Gavory, F.; Poulain, J.; et al. An Expressed Sequence Tag collection from the male antennae of the Noctuid moth Spodoptera littoralis: A resource for olfactory and pheromone detection research. *BMC Genom.* **2011**, *12*, 86. [CrossRef]
156. Agerbirk, N.; Olsen, C.E. Glucosinolate structures in evolution. *Phytochemistry* **2012**, *77*, 16–45. [CrossRef]
157. Kolm, R.H.; Danielson, U.H.; Zhang, Y.; Talalay, P.; Mannervik, B. Isothiocyanates as substrates for human glutathione transferases: Structure-activity studies. *Biochem. J.* **1995**, *311 Pt 2*, 453–459. [CrossRef]
158. Harzsch, S.; Krieger, J. Crustacean olfactory systems: A comparative review and a crustacean perspective on olfaction in insects. *Prog. Neurobiol.* **2018**, *161*, 23–60. [CrossRef]
159. Graziadei, P.P.; Graziadei, G.A. Neurogenesis and neuron regeneration in the olfactory system of mammals. I. Morphological aspects of differentiation and structural organization of the olfactory sensory neurons. *J. Neurocytol.* **1979**, *8*, 1–18. [CrossRef]
160. Neiers, F.; Gourrat, K.; Canon, F.; Schwartz, M. Metabolism of Cysteine Conjugates and Production of Flavor Sulfur Compounds by a Carbon-Sulfur Lyase from the Oral Anaerobe Fusobacterium nucleatum. *J. Agric. Food Chem.* **2022**, *70*, 9969–9979. [CrossRef]
161. Schwartz, M.; Canon, F.; Feron, G.; Neiers, F.; Gamero, A. Impact of Oral Microbiota on Flavor Perception: From Food Processing to In-Mouth Metabolization. *Foods* **2021**, *10*, 2006. [CrossRef]
162. Ai, S.; Zhang, Y.; Chen, Y.; Zhang, T.; Zhong, G.; Yi, X. Insect-Microorganism Interaction Has Implicates on Insect Olfactory Systems. *Insects* **2022**, *13*, 1084. [CrossRef]

biomolecules

MDPI

Article

Biochemical and Structural Characterization of Chi-Class Glutathione Transferases: A Snapshot on the Glutathione Transferase Encoded by *sll0067* Gene in the Cyanobacterium *Synechocystis* sp. Strain PCC 6803

Eva Mocchetti [1,†], Laura Morette [2,†], Guillermo Mulliert [1], Sandrine Mathiot [1], Benoît Guillot [1], François Dehez [3], Franck Chauvat [4], Corinne Cassier-Chauvat [4], Céline Brochier-Armanet [5], Claude Didierjean [1,*] and Arnaud Hecker [2,*]

[1] Université de Lorraine, CNRS, CRM2, F-54000 Nancy, France
[2] Université de Lorraine, INRAE, IAM, F-54000 Nancy, France
[3] Université de Lorraine, CNRS, LPCT, F-54000 Nancy, France
[4] Université Paris-Saclay, CEA, CNRS, Institute for Integrative Biology of the Cell (I2BC), F-91190 Gif-sur-Yvette, France
[5] Université de Lyon 1, CNRS, LBBE, F-69622 Villeurbanne, France
* Correspondence: claude.didierjean@univ-lorraine.fr (C.D.); arnaud.hecker@univ-lorraine.fr (A.H.)
† These authors contributed equally to this work.

Citation: Mocchetti, E.; Morette, L.; Mulliert, G.; Mathiot, S.; Guillot, B.; Dehez, F.; Chauvat, F.; Cassier-Chauvat, C.; Brochier-Armanet, C.; Didierjean, C.; et al. Biochemical and Structural Characterization of Chi-Class Glutathione Transferases: A Snapshot on the Glutathione Transferase Encoded by *sll0067* Gene in the Cyanobacterium *Synechocystis* sp. Strain PCC 6803. *Biomolecules* **2022**, *12*, 1466. https://doi.org/10.3390/biom12101466

Academic Editor: Bengt Mannervik

Received: 4 August 2022
Accepted: 5 October 2022
Published: 13 October 2022

Abstract: Glutathione transferases (GSTs) constitute a widespread superfamily of enzymes notably involved in detoxification processes and/or in specialized metabolism. In the cyanobacterium *Synechocsytis* sp. PCC 6803, SynGSTC1, a chi-class GST (GSTC), is thought to participate in the detoxification process of methylglyoxal, a toxic by-product of cellular metabolism. A comparative genomic analysis showed that GSTCs were present in all orders of cyanobacteria with the exception of the basal order Gloeobacterales. These enzymes were also detected in some marine and freshwater noncyanobacterial bacteria, probably as a result of horizontal gene transfer events. GSTCs were shorter of about 30 residues compared to most cytosolic GSTs and had a well-conserved SRAS motif in the active site (^{10}SRAS^{13} in SynGSTC1). The crystal structure of SynGSTC1 in complex with glutathione adopted the canonical GST fold with a very open active site because the α4 and α5 helices were exceptionally short. A transferred multipolar electron-density analysis allowed a fine description of the solved structure. Unexpectedly, Ser10 did not have an electrostatic influence on glutathione as usually observed in serinyl-GSTs. The S10A variant was only slightly less efficient than the wild-type and molecular dynamics simulations suggested that S10 was a stabilizer of the protein backbone rather than an anchor site for glutathione.

Keywords: glutathione transferase; glutathione; cyanobacteria; *Synechocystis* sp. PCC 6803; crystallography; biochemistry; phylogeny

1. Introduction

Glutathione transferases (GSTs) constitute a widespread superfamily of enzymes playing crucial roles in the cell notably in detoxification processes and in specialized secondary metabolism by catalyzing three major kinds of reactions. These include catalytic reactions where glutathione (GSH) is consumed (GSH-conjugation), reactions where GSH is not consumed (isomerization and dehalogenation) and reactions where GSH is oxidized (thiol-transferase and reduction activities) [1]. At the structural level, canonical GSTs are mainly dimeric proteins, and each subunit adopts a conserved fold composed of an N-terminal thioredoxin (TRX) domain linked to an all α-helical C-terminal domain. The active site of the enzyme is located in a cleft at the interface between both domains and contains a GSH-binding site (G site) and a hydrophobic-substrate binding site (H site). Depending

on their primary sequence conservation, GSTs were classified into classes designated by a Greek letter. GSTs with a sequence identity greater than 40% belong to the same class, whereas proteins of different classes share less than 25% sequence identity [2]. GSTs were further distinguished into four catalytic types, tyrosine (TyrGSTs), serine (SerGSTs), cysteine (CysGSTs) and atypical (AtyGSTs), depending on an assumed important residue for catalysis [3]. The tyrosine, serine and cysteine residues have a conserved position in the structures. The tyrosine residue is located at the C-terminal end of the first strand (β1). The serine and cysteine residues have the same position at the N-terminal end of the first helix (α1). AtyGSTs do not have a specific residue at a conserved position. In CysGSTs, the cysteine residue has a reactant role according to the enzyme mechanism ontology [4], since it forms a covalent bond with the substrate during the catalytic act. The important residue of the others (TyrGSTs, SerGSTs and AtyGSTs) has a spectator role in enhancing the nucleophilicity of the glutathione thiolate group, and the mutation of this residue does not abolish the activity. Through noncatalytic properties, so-called ligandins, hitherto underestimated compared to the other documented roles of GSTs, many GSTs also participate in the binding and transport of small heterocyclic ligands [5,6].

GSTs have been extensively investigated in animals and plants because of their great relevance to human health and agriculture [7–9]. In contrast, studies in bacteria remain scarce, especially in the cyanobacterial phylum that encompasses oxygenic photosynthetic prokaryotes considered to be the ancestors of chloroplasts. It has been speculated that cyanobacteria may be the first organisms to harbored GSTs [10]. Greek letters have been used for eight classes of GSTs from bacteria: beta, chi, eta, nu, rho, theta, xi and zeta [11,12]. Other classes exist that often have specific functions such as LigE, LigF and LigG involved in lignin degradation in soil bacteria [13,14].

The chi class is thought to be specific of cyanobacteria and three isoforms (TeGSTC1 from *Thermosynechococcus elongatus* BP-1, SeGSTC1 from *Synechococcus elongatus* PCC 6301 and SynGSTC1 from *Synechocystis* sp. PCC 6803) have been characterized biochemically [10,15,16]. A preliminary crystallographic study has been reported for TeGSTC1 and SeGSTC1 [17]. All the three isoforms (TeGSTC1, SeGSTC1 and SynGSTC1) exhibit similar activities. They efficiently catalyze the addition of GSH on various isothiocyanates and show moderate activities toward other classical substrates such as chlorodinitrobenzene [10,15,16]. Interestingly, we recently showed that SynGSTC1 is involved in the detoxification of methylglyoxal, a toxic by-product of the cellular metabolism [15]. Despite a shorter sequence length compared to other GSTs, homology modelling combined with secondary structure prediction suggested that chi GSTs (GSTCs) adopt the fold of canonical GSTs. Their amino acid sequences show two motifs usually found in GSTs. The motif I, which contains an invariant cis-proline residue as well as a βββα structure essential for the stabilization of the γ-glutamyl moiety of GSH, is the most conserved region in all of the GSTs [18]. Motif II, in turn, contains a very well conserved aspartic acid important for fold stability [19]. Recently, a conserved tyrosine residue located at the fifth position of the N-terminus of GSTCs has been proposed as the catalytic residue [20]. To better characterize the chi class of GSTs, it was necessary to obtain an experimental three-dimensional model. Therefore, we determined the first crystal structure of a chi-class GST (SynGSTC1), performed a robust phylogenetic study and completed the biochemical data by testing new substrates and modulating the active site residues by site-directed mutagenesis.

2. Materials and Methods

2.1. Cloning, Mutagenesis, Expression and Purification

SynGSTC1 (Sll0067) encoding sequence was amplified by PCR from *Synechocystis* sp. PCC 6803 genomic DNA as template using specific forward and reverse primers containing *Nde*I and *Xho*I restriction sites, respectively (Table S1). The amplified sequence was subsequently digested and cloned in *E. coli* expression vector pET-26b between *Nde*I and *Xho*I restriction sites allowing the fusion of a His-tag at the C-terminal part of SynGSTC1 as previously described [15]. Various catalytic mutants (S10T, S10A, S10C and R11A) were generated

by site-directed mutagenesis using the QuikChange site-directed mutagenesis kit (Agilent Technologies) and specific mutagenic primers listed in Table S1. The sequences have been confirmed by DNA sequencing.

The expression of recombinant SynGSTC1 and variants were performed at 37 °C using *E. coli* Rosetta2 (DE3) pLysS expression strain (Novagen) transformed with appropriate plasmid in LB medium supplemented with kanamycin (50 μg/mL) and chloramphenicol (34 μg/mL). When the cell culture reached an $OD_{600\ nm}$ of 0.7–0.8, the expression of the SynGSTC1 (or S10T or S10A or S10C or R11A) recombinant protein was induced with 0.1 mM isopropyl β-D-1-thio-galactopyranoside (IPTG) for 4 h at 37 °C. Cells were then harvested by centrifugation, resuspended in a 30 mM Tris-HCl buffer (pH 8.0) supplemented with 200 mM NaCl (lysis buffer) and stored at −20 °C until use. After the lysis of the cells by sonication, the resulting cell extract was centrifuged at 40,000× *g* for 20 min at 4 °C to remove cellular debris and aggregated proteins. After the addition of 10 mM imidazole, SynGSTC1 was purified from the soluble extract by gravity-flow chromatography on a nickel nitrilotriacetate (Ni-NTA) agarose resin (Qiagen, Hilden Germany). After a washing step with lysis buffer containing 20 mM imidazole, recombinant SynGSTC1 was eluted using lysis buffer supplemented with 250 mM imidazole. The fractions of interest were pooled, concentrated by ultrafiltration, subjected to a size exclusion chromatography using a Superdex^{TM}200 16/600 column connected to an ÄKTA-Purifier^{TM} device (Cytiva) and eluted with lysis buffer. The purified recombinant protein was concentrated and finally stored at −20 °C. The concentration of SynGSTC1 recombinant protein was determined at 280 nm using a theoretical molar absorption coefficient of 28,420 $M^{-1}{\cdot}cm^{-1}$.

2.2. Crystallization, X-ray Data Collection, Processing and Refinement

A first screening of 288 crystallization conditions was carried out at the CRM2 crystallogenesis platform (University of Lorraine) with an Oryx 8 crystallogenesis robot (Douglas Instruments Ltd, Hungerford, UK). Crystals were optimized manually at 4 °C by the microbatch-under-oil method. Solutions of SynGSTC1 ant the variants contained 30–40 $mg{\cdot}mL^{-1}$ protein in 30 mM Tris buffer (pH 8.0) supplemented with 200 mM NaCl, 1 mM Tris(2-carboxyethyl)phosphine (TCEP) and 10 mM glutathione. SynGSTC1 was crystallized by mixing 1 μL of protein with 1 μL of solution consisting of 16% (*w/v*) PEG 8000, 40 mM potassium phosphate monobasic and 20% (*w/v*) glycerol (condition no. 32, Wizard™ Classic Crystallization Screen III, Rigaku, Tokyo, Japan).

Preliminary X-ray diffraction experiments were carried out in-house on an Agilent SuperNova diffractometer (Rigaku Oxford Diffraction) equipped with a CCD detector. Data collections were carried out at the ESRF, on beamline FIP BM07 (ESRF, Grenoble, France) and (PX1 and PX2, SOLEIL, Gif-Sur-Yvette, France). Data sets were indexed and integrated with XDS [21], and scaled and merged with Aimless [22] from the CCP4 suite [23]. The structure of SynGSTC1 was solved by molecular replacement using *MoRDa* [24] with the coordinates of a GST from *Rhodobacter sphaeroides* (PDB entry 3LSZ) as the search model. Structures of SynGSTC1 and its variants were refined with *BUSTER* [25] and manually improved with *Coot* [26]. The validation of all structures was performed with the PDB validation service (http://validate.wwpdb.org, accessed on 30 September 2022). The coordinates and structure factors have been deposited in the Protein Data Bank (PDB entries 8AI8, 8AI9, 8AIB). Crystal data, diffraction and refinement statistics are shown in Table 1.

Table 1. Statistics of X-ray diffraction data collection and model refinement.

	Wild-Type	**S10T**	**R11A**
Data Collection			
Diffraction source	ESRF-BM07	ESRF-BM07	ESRF-BM07
Detector	Pilatus 6M	Pilatus 6M	Pilatus 6M
Wavelength (Å)	0.97951	0.97951	0.97951

Table 1. *Cont.*

	Wild-Type	**S10T**	**R11A**
Space Group	$P4_32_12$	$P4_32_12$	$P4_32_12$
Unit-cell *a*; *c* (Å)	92.5; 193.6	92.9; 193.6	92.2; 193.1
Resolution Range (Å)	48.4 1.7 (1.73 1.70)	48.4 1.7 (1.73 1.70)	46.1 2.2 (2.27 2.20)
Tot. no. of meas. int.	1,200,217 (41158)	1,244,521 (62,785)	503,802 (22,268)
Unique reflections	92,986 (4529)	93,931 (4590)	39,298 (2006)
Average redundancy	13 (9)	13.2 (14)	13 (11)
Mean I/σ (I)	24.8 (1.8)	17.0 (2.0)	18.4 (2.4)
Completeness (%)	100.0 (99.6)	100.0 (100.0)	91.3 (55.5)
R_{merge}	0.056 (1.097)	0.084 (1.52)	0.097 (1.039)
R_{meas}	0.061 (1.168)	0.087 (1.59)	0.100 (1.142)
$CC_{1/2}$	1.00 (0.83)	1.00 (0.84)	1.00 (0.85)
Wilson *B*-factor (Å^2)	29.6	28.6	41.5
Refinement			
Resolution Range (Å)	24.8 1.7	24.2 1.7	31.3 2.2
No. of reflections	92839	93783	39248
R_{work}/R_{free}	0.204/0.221	0.206/0.221	0.215/0.242
Corr *Fo-Fc*/*Fo-Fc*$_{free}$	0.938/0.936	0.940/0.939	0.907/0.888
Total number of atoms	3469	3500	3253
Average *B*-factor (Å^2)	34.0	32.5	44.0
Model quality			
RMSZ Bond lengths	0.41	0.42	0.42
RMSZ Bond angles	0.54	0.56	0.56
Ramachandran fav. (%)	98	98	98
Ramachandran all. (%)	2	2	2
Rotamer outliers (%)	0	0	1
Clashscore	1	1	1
PDB entry	8AI8	8AI9	8AIB

$R_{merge} = \sum_{hkl} \sum_i |I_i(hkl) - I(hkl)| / \sum_{hkl} \sum_i I_i(hkl)$. $R_{meas} = \sum_{hkl} \{N(hkl)/[N(hkl)-1]\}^{1/2} \sum_i |I_i(hkl) - I(hkl)| / \sum_{hkl} \sum_i I_i(hkl)$. $CC_{1/2}$ is the correlation coefficient of the mean intensities between two random half-sets of data. $R_{work} = \sum_{hkl} ||F_{obs}| - |F_{calc}|| / \sum_{hkl} |F_{obs}|$. In total, 5% of reflections were selected for R_{free} calculation. RMSZ: root mean square *Z*-score. The MolProbity clashscore is the number of serious clashes per 1000 atoms. Values in parentheses are for highest resolution shell.

2.3. Structure Analysis Based on Electron Density Distribution

To calculate the electrostatic interaction energies between residues of SynGSTC1 active site and the glutathione ligand, the electron charge density of the complex based on the Hansen and Coppens multipolar model [27] was determined (method detailed in Supplementary Materials). The electron density parameters for the SynGSTC1-GSH complex were transferred from the ELMAM2 database2, which provides parameters averaged over experimental peptide electron densities from ultra-high resolution X-ray scattering data [28]. In addition, polarization effects due to the environment were estimated in the transferred electron density using the procedure described recently by Leduc et al. [29] and implemented in *MoProViewer* software (version 0.1.1302) [30]. The electrostatic interaction energy

(E_{tot}^{elec}) between the glutathione ligand and the SynGSTC1 active site residues was computed using *Charger*, which is a fast and analytical electrostatic energy calculation tool [31] also implemented in *MoProViewer*. E_{tot}^{elec} includes two terms, the electrostatic interaction permanent energy E_{perm}^{elec} and the polarization contribution E_{pol}^{elec} (hence $E_{tot}^{elec} = E_{perm}^{elec} + E_{pol}^{elec}$). The *MoProViewer* database transfer tool enables an automatic parameter transfer on the structure with appropriate formal charge assignment (+1e for arginine and lysine, −1e for aspartate and glutamate, 0 for others). The His38 and His61 of SynGSTC1 were protonated on the Nε atom and the formal charge of glutathione was set to −1e. The procedure is detailed in the Supplementary Materials.

2.4. Molecular Dynamics Simulation

The Molecular Dynamics simulations presented in this study were based on the crystallographic structure of SynGSTC1 in complex with GSH. This system was immersed in a cubic simulation cell of length equal to 73 Å filled by a solvent of 9881 water molecules with 150 mM NaCl. The simulations were performed using *NAMD 3.0* [32] with the CHARMM36 [33] force field for proteins and the TIP3P water model [34]. The parameters for the GSH ligand were generated by the CHARMM general force field (CGenFF) [35]. Long-range electrostatic forces were evaluated using the particle mesh Ewald algorithm with a grid spacing of 1.0 Å. A smoothed 12.0 Å spherical cutoff was applied to truncate the short-range van der Waals and electrostatic interactions. The temperature was maintained at 300 K thanks to the Langevin thermostat and the pressure at 1 atm thanks to the Langevin piston method. Covalent bonds involving hydrogen atoms were restrained to their equilibrium length by the Rattle algorithm [36] and the water molecules were constrained to their equilibrium geometry using the Settle algorithm [37]. In addition, a mass-repartitioning scheme was used to integrate the equations of motion with a time step of 4 fs, according to Hopkins et al. [38]. A smooth equilibration, along which the positions of the heavy atoms of the protein were restrained harmonically, was carried out during 8 ns before a non-restrained long equilibration of 100 ns. Then, the SynGSTC1-GSH complex was probed in production runs including a long simulation of 500 ns and five independent shorter simulations of 100 ns. These trajectories were visualized and analyzed using *VMD* [39]. These simulations were aimed at exploring the stability of the interactions between the glutathione and the active site as well as the flexibility of the protein interdomain linker.

2.5. Enzymatic Assays

The GSH-conjugation activity was assayed at 25 °C toward 1-chloro-2,4-dinitrobenzene (CDNB), benzyl-isothiocyanate (BITC), 2-phenetyl-isothiocyanate (PITC) or p-nitrophenyl butyrate (PNP-butyrate). The reactions were performed in 500 µL of 30 mM Tris-HCl (pH 8.0) and 1 mM EDTA for CDNB and PNP-butyrate and 100 mM phosphate buffer (pH 6.5) for ITC derivatives in the presence of various concentrations of CDNB (0–4000 µM), BITC (0–1000 µM), PITC (0–1000 µM) or PNP-butyrate (0–2000 µM) at a fixed saturating GSH concentration. Peroxidase and thiol-transferase activities were assayed at 25 °C toward cumene hydroperoxide (CuOOH) and 2-hydroxyethyl disulfide (HED) in a NADPH-coupled spectrophotometric method by following the absorbance at 340 nm. The reactions were carried out in 500 µL of 30 mM Tris-HCl (pH 8.0) containing 200 µM NADPH, 0.5 unit of yeast glutathione reductase and various concentrations of HED (0–500 µM) or CuOOH (0–3000 µM) at a fixed GSH concentration. The optimum pH of the wild-type enzyme and its variants was determined against PITC using 100 mM sodium citrate, phosphate, or borate buffers at pH ranging from 4.0 to 11.0. GSH-conjugation activity was determined as described above.

For all activity assays, the recombinant protein, used at a concentration (3 µM) within the linear response range of the enzyme, was added after 2 min of preincubation and the variation of absorbance monitored using a Cary 50 spectrophotometer. The activity recorded without enzymes was subtracted and three independent experiments were performed at each substrate concentration. The kinetic parameters, apparent K_m (Michaelis

constant) and $ksoftware_{cat}$ (turnover number) were determined by fitting the data to the nonlinear regression Michaelis–Menten model in *GraphPad Prism* (version 8, GraphPad Software, Inc., San Diego, CA, USA). The k_{cat} values were expressed as μmol of substrate oxidized per second per μmol of enzyme (i.e., the turnover number in s^{-1}) using specific molar absorption coefficients of 9600 $M^{-1}{\cdot}cm^{-1}$ at 340 nm for CDNB, 9250 $M^{-1}{\cdot}cm^{-1}$ at 274 nm for BITC, 8890 $M^{-1}{\cdot}cm^{-1}$ at 274 nm for PITC, 17700 $M^{-1}{\cdot}cm^{-1}$ at 412 nm for PNP-butyrate and 6220 $M^{-1}{\cdot}cm^{-1}$ at 340 nm for NADPH.

2.6. Phylogenetic Analysis

In total, 222 proteomes of the Cyanobacteria/Melainabacteria group were retrieved from the RefSeq database of the NCBI. These corresponded to 208 proteomes of Cyanobacteria labelled as RefSeq "reference proteomes" or from type strains, and 14 proteomes from noncyanobacterial lineages (i.e., Margulisbacteria, Melainabacteria, Gastranaerophilales) classified in the Cyanobacteria/Melainabacteria group (Table S2). The sequences of the 53 ribosomal protein families (rprots) were retrieved from the 222 proteomes using the riboDB database [40] (Table S3). The corresponding protein sequences were aligned using *MAFFT v7.453* with the accurate option L-INS-I [41]. The resulting multiple alignments were trimmed with *BMGE v1.2* using the BLOSUM30 substitution matrix [42]. The multiple alignments of the 52 rprots present in more than 30% of the 222 analyzed proteomes were combined to build a large supermatrix (222 sequences, 6430 amino acid positions) and used to build a phylogeny using the maximum likelihood method. The tree was inferred with *IQ-TREE* (multicore version 2.2.0 COVID-edition, June 2022) with the LG + C20 + F + R4 evolutionary model [43]. The branch robustness of the inferred tree was computed with the ultrafast bootstrap procedure implemented in *IQ-TREE* (1000 replicates). The resulting tree was rooted using the 14 noncyanobacterial sequences.

The 222 studied proteomes were queried with *BLASTP* using the GSTC1 sequence from the *Synechocystis* sp. PCC 6803 strain (RefSeq protein Id WP_010873500.1, locus tag SGL_RS13850) as seed. The 924 GST sequences displaying an E-value lower than 10^{-3} were retrieved and aligned using *MAFFT* with the auto option. A total of 54 partial sequences were discarded from the analysis. A survey of the nr database at the NCBI identified 11 sequences of GSTC in noncyanobacterial bacteria. These 11 sequences were added to the cyanobacterial GSTC sequences. The 881 GSTC sequences were realigned with *MAFFT* with the L-INS-I option and trimmed using *BMGE* with the BLOSUM30 substitution matrix. The 104 kept amino acid positions were used to infer a phylogeny using *FastTree v2* [44] with 20 rate categories of sites, the gamma optimization option, and the Le and Gascuel model [45]. The branch robustness of the inferred tree was estimated using the Shimodaira Hasegawa test (resampling the site likelihoods 1000 times). Finally, a phylogenetic analysis of the 147 cyanobacterial GSTC sequences was performed using FastTree and the same parameters (147 sequences, 110 amino acid positions).

The trees were drawn using *iToL v6.5.8* [46].

3. Results and Discussion

3.1. Crystal Structure of SynGSTC1

In this study, the crystal structure of the glutathione transferase chi1 from *Synechocystis* sp. PCC 6803 (SynGSTC1) in complex with GSH is presented. We also solved the structures of two variants (S10T and R11A variants in complex with GSH) which did not show significant differences from the wild-type. The protein samples were cocrystallized with an excess of GSH (10:1) in the presence of TCEP to avoid oxidation of the GSH thiol group into sulfenic acid. SynGSTC1 crystallized in space group $P4_32_12$ with two polypeptide chains in the asymmetric unit. They formed a two-fold dimer that had a globular shape with molecular dimensions of approximately 55 Å× 55 Å × 45 Å (Figure 1). The dimer buried 1710 $Å^2$ of surface area for each monomer and was tightly stabilized by ten hydrogen bonds and six salt bridges (Table S4). At the core, a four-helix bundle consisting of the α3 and α4 helices of the two monomers buried aliphatic residues (L70 and L94 of chains A and B).

This interaction pattern was complemented by a lock-and-key motif where the F49 residue fitted into a low-polar cavity of the adjacent subunit (W92, F95, L117, L121) (Figure 1).

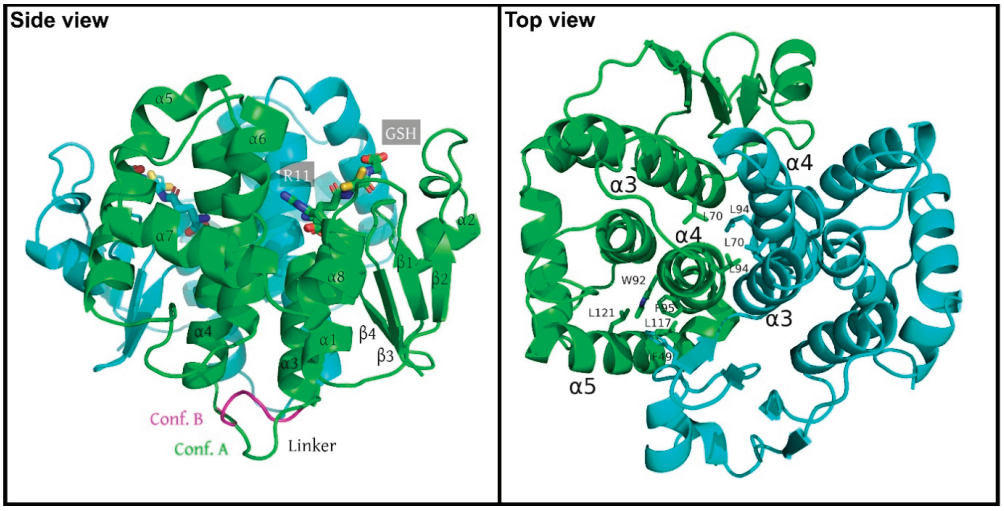

Figure 1. Crystal structure of the SynGSTC1 dimer, left, and rotated 90°, right. The monomers A and B are shown in ribbon mode and colored green and blue, respectively. (**Left**), side view. The secondary structures of the monomer A are labelled. In each monomer, the side chain of residue R11 and the glutathione molecules are labelled and highlighted as sticks. Both conformations of the linker are shown in monomer A. (**Right**), top view. The figure highlights the hydrophobic patches on SynGSTC1 dimer interface. L70 and L94 of both monomers are buried in the center of the dimer. This interaction pattern is complemented by a lock-and-key motif where the F49 residue (blue) fits into a low-polar cavity of the adjacent subunit (W92, F95, L117, L121) (green). The symmetry related lock-and-key motif is not shown for clarity.

Both subunits were very similar structures and could be superimposed within 0.33 Å root-mean-square deviation over 181 α-carbon atoms. The SynGSTC1 protomer adopted the conserved GST fold that was subdivided into two domains for clarity (N-terminal domain β1α1β2α2β3β4α3 and C-terminal domain α4α5α6α7α8). As mentioned in the introduction, the chain length of GSTCs (approximately 180 residues) was significantly shorter by at least 20 residues compared to most canonical GSTs [47]. The α4–α5 hairpin pattern was significantly shortened (roughly 10 residues) and the angle between these two helices (~42°) was twice that usually observed (Figure 2). This "missing" region made the active site of SynGSTC1 very open, with no clear pocket for the hydrophobic substrate (H-site). Both motifs I (47–71) and II (129–147) played their expected structural roles. In motif I, the V52–P53 peptide bond was cis, and V52 formed the typical antiparallel β-sheet-like interaction with the cysteine moiety of GSH. Motif II contained the Ncap sequence ^{137}SVVD^{140} where the side chains of the serine and aspartic acid residues contributed to the stabilization of the α6 helix [19]. The linker (^{76}ASTIPAD^{82}) between the N- and C-terminal domains was peculiar because it had no aliphatic or aromatic residue wedged between these two domains as usually observed [48,49]. The consequence was an interdomain linker without a unique conformation. The quality of the electron density allowed the building of two major conformations (Figures 1 and S1). To investigate this property, we performed molecular dynamics simulations of the SynGSTC1-GSH complex in an aqueous environment. The simulation revealed a protein very stable with the linker as one of the most mobile regions. The time-evolution of the φ and ψ torsion angles of the linker residues revealed transitions between two main conformations during the trajectory

(Figure S2). Interestingly, these two conformations corresponded to those observed in the crystal structure.

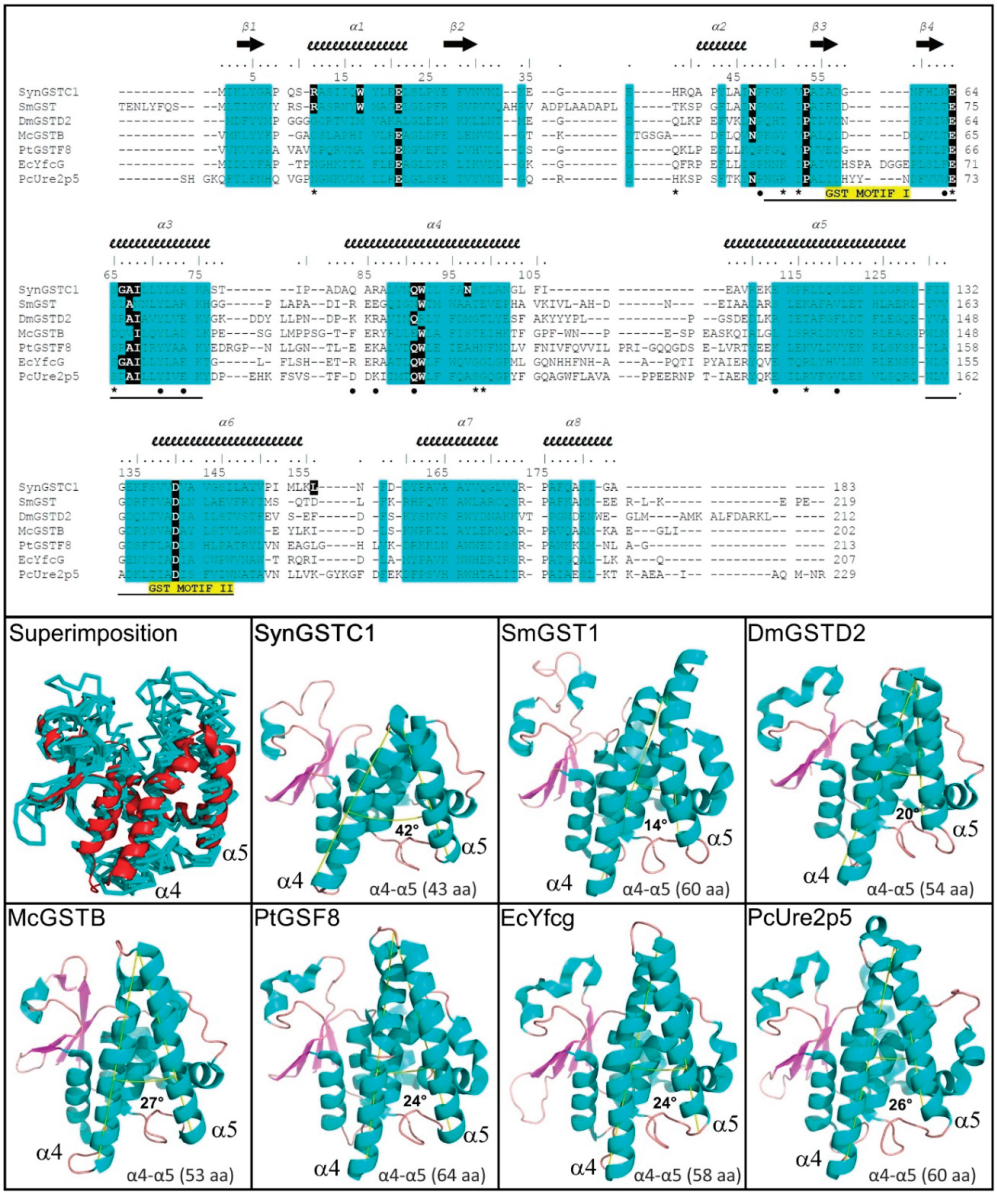

Figure 2. Comparison of SynGSTC1 with structural homologs. The top figure shows a structure-based sequence alignment, and the bottom figures highlight that SynGSTC1 has the shortest α4–α5 hairpin and the highest angle between α4 and α5 helices. Crystal structure and sequences can be found at the Protein Data Bank (http://www.rcsb.org, accessed on 30 September 2022): SynGSTC1, this study, PDB ENTRY 8AI8; SmGST, GST from *Sinorhizobium meliloti* 2011, PDB entry 4NHW; DmGSTD2, GST delta 2

from *Drosophila melanogaster*, PDB entry 5F0G; McGSTB, GST beta from *Methylococcus capsulatus* str. Bath, PDB entry 3UAP; PtGSTF8, GST phi 8 from *Populus trichocarpa*, PDB entry 5F07; EcYfcG, GST nu from *Escherichia coli* K-12, PDB entry 5HFK; PcUre2p5, Ure2p 5 from *Phanerodontia chrysosporium*, PDB entry 4F0C. The characteristics of the top figure are as follows: secondary structures are labelled and shown using arrows (β-strands) and squiggles (helices); common regions, i.e., regions with no gaps and with pairwise residue distances less than 4 Å are highlighted in blue; the invariant residues in the GST chi class are in bold type, coloured white and highlighted in black; residues that participates in dimer stabilization of SynGSTC1 via strong polar interactions are marked with •; residues involved in binding glutathione (G-site) in SynGSTC1 are marked with *. The characteristics of the bottom figures are as follows: the models are shown in the cartoon or ribbon modes; the α4 and α5 helices are labelled; the first figure shows a superimposition of the seven structures where SynGSTC1 is colored red and the others cyan; in the other figures, the estimated angle between α4 and α5 helices is provided as well as the number of amino acids in the α4–α5 hairpin; the angles were calculated using the *AngleBetweenHelices* script (https://pymolwiki.org/index.php/AngleBetweenHelices, accessed on 30 September 2022) implemented in *PyMol Molecular Graphics System* (Version 2.0 Schrödinger, LLC, New York, NY, USA).

3.2. Structural Comparison

A search for the structural homologs using the Dali server (http://ekhidna2.biocenter.helsinki.fi/dali/, accessed on 30 September 2022) ranked proteobacterial nu GSTs and fungal GSTs from the Ure2p class at the top of the list [50]. The other hits included proteobacterial beta GSTs, insect delta GSTs, an unclassified proteobacterial GST and plant phi GSTs. To better depict the proximities of these structures, an additional multiple structural alignment was performed using the mTM-align server (https://yanglab.nankai.edu.cn/mTM-align/, accessed on 30 September 2022) [51] (Figure 2). The resulting dendrogram based on the pairwise alignment scores (Figure S3) showed a distribution of the proteins into two clades, one of which containing SynGSTC1 and the unclassified proteobacterial GST (GST SMc00097 from *Sinorhizobium meliloti* 2011, PDB entry 4nhw). The latter had therefore the most similar structure to SynGSTC1. SMc00097 had one of the structural attributes of SynGSTC1, namely a SRAS motif at the beginning of the α1 helix in its active site (see below) (Figure 2). The first serine residue adopted the same orientation and did not participate in the stabilization of GSH while the arginine residue did (Figure S4). The closeness between SynGSTC1 and SMc00097 could be explained in a more comprehensive way by a domain-by-domain comparison. Indeed, the overall structures (i.e., both the N-ter and C-ter domains) of SynGSTC1 and SMc0097 overlapped well (Table S5). The proximity of SynGSTC1 with other hits (nu, beta, delta and phi GSTs) was rather due to the good overlap of N-terminal domains.

3.3. Active Site Structure and Its Analysis Using Transferred Multipolar Electron-Density

The active site contained GSH tightly bound to the G-site by numerous polar interactions (respectively, six, two and three for the γ-Glu, Cys and Gly moieties) (Figure 3). The GSH Cys moiety adopted two rotamers (**m**, $\chi_1 = -52^\circ$ and **t**, $\chi_1 = 172^\circ$) exposing the GSH thiol group towards the solvent (Figure 1). The three regular rotamers (**p**, **m**, and **t**) of the glutathione cysteine moiety were accessible during the molecular dynamics simulations with the frequencies of 0.35, 0.42 and 0.16, respectively (Figure S5). The crystal structure did not reveal a strong polar interaction between the sulfur atom of GSH and the enzyme. The smallest distance was 3.8 Å with the amide group of R11. The Y5 residue, recently proposed as a catalytic residue [20], was far too distant to stabilize the GSH-thiolate group during catalysis as the Y5 hydroxyl group was 17 Å away from the GSH sulfur-atom. Based on the sequence analysis of SynGSTC1, we could have thought that S10 played an important role in catalysis. Indeed, this serine residue belongs to the ^{10}SRAS^{13} motif, which is related to the CXXC active-site motif of thioredoxin [52]. The equivalent serine residue in Ser-GSTs (see introduction) is almost always found hydrogen-bonded to the GSH thiol group while this is not the case in SynGSTC1 [53,54]. Indeed, the OG atom invariably retained the same orientation in all structures (wild-type and variants), and was hydrogen bonded to the main chains of A7 and A12. This interaction network remained stable throughout most of

the molecular dynamics simulations showing that S10 was important for the stabilization of the protein backbone. Whatever its conformation, this serine residue never formed a strong interaction with the GSH thiol group during the simulation (Figure S6).

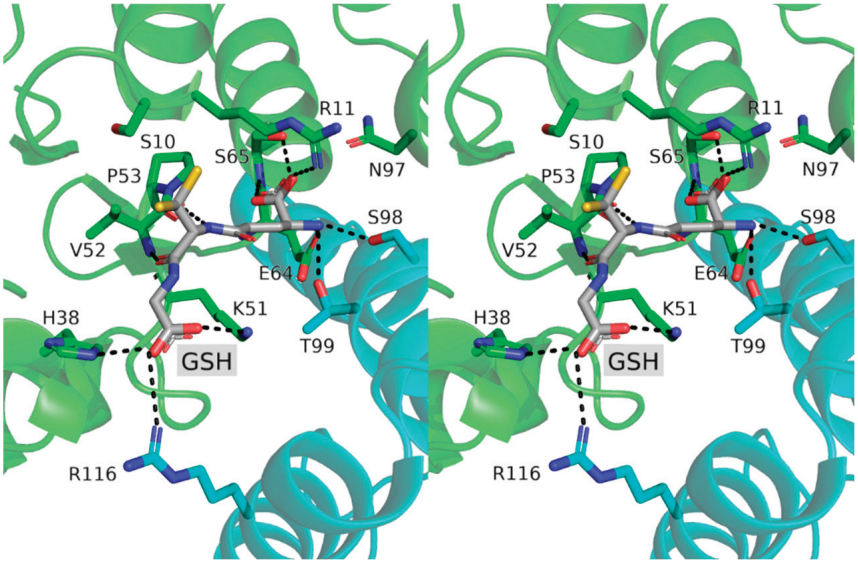

Figure 3. Stereoview of the glutathione binding site of SynGSTC1. The monomers A and B are shown in cartoon mode and colored green and blue, respectively. GSH and residues around it are shown as sticks and labelled. Numbering of residues is according to sequence of SynGSTC1. Strong intermolecular interactions are shown as dashed sticks.

The description of the interactions between a ligand and a protein is most often summarized by the list of residues involved, without quantifying the importance of each. We developed recently a fast and analytical procedure to estimate the electrostatic contribution of each residue to the ligand binding, based on a continuous distribution of electron density of experimental origin [31]. This method implemented in *MoProViewer* [30] was applied on SynGSTC1 in complex with GSH where the contributions of eleven residues were evaluated (distance cutoff of 3.5 Å away from GSH). This included eight residues from one chain (S10, R11, L33, H38, K51, V52, E64, S65 and N97) and three from the other (S98, T99 and R116). *MoproSuite* calculates electrostatic interaction energies E_{tot}^{elec} that are divided into two contributions: a permanent electrostatic interaction term, E_{perm}^{elec}, and a polarization one, E_{pol}^{elec}, which can be interpreted as a molecular recognition term and an adaptation term, respectively (Figure 4, Table S6). By definition, the polarization term is negative and makes the total interaction energy more favorable for all the active site residues and especially for charged residues [29]. We performed the calculations for the two GSH thiol orientations observed in the crystal structure. The orientation of the thiol group did not affect notably the GSH binding, from an electrostatic and dipolar-induction point of view (Table S6). Thus, the following analysis did not depend on the GSH conformation.

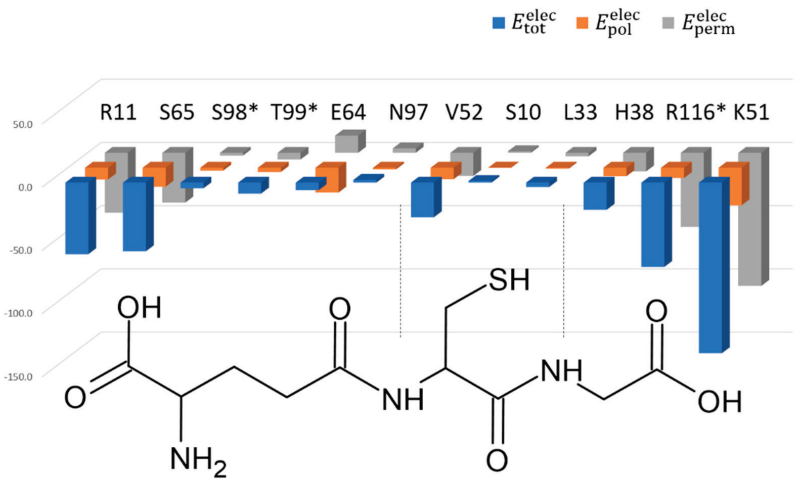

Figure 4. Permanent, polarization and total electrostatic interaction energies. The permanent $E_{\text{perm}}^{\text{elec}}$, polarization $E_{\text{pol}}^{\text{elec}}$ and total $E_{\text{tot}}^{\text{elec}}$ electrostatic interaction energies between the glutathione ligand and twelve residues of the SynGSTC1 active site are presented in kcal/mol. $E_{\text{perm}}^{\text{elec}}$ is computed using the electron density model transferred on the glutathione and the protein atoms, whereas E_{tot}^{elec} is obtained after the electron density polarization procedure. Finally, $E_{\text{pol}}^{\text{elec}}$ is computed using $E_{\text{pol}}^{\text{elec}} = E_{tot}^{elec} - E_{\text{perm}}^{\text{elec}}$, and represents the polarization contribution to the total electrostatic interaction energy. The reported energy values have been averaged over the two conformations of the glutathione (A and B) observed in the crystal structure and over the two monomers. The GSH formula has been added to highlight the proximity of the residues to the GSH moieties. The residues marked with a star (*) in the figure are not from the same monomer as glutathione. The numerical values of these energies and the associated standard deviations are available in the Supplementary Materials.

The permanent interaction energy $E_{\text{perm}}^{\text{elec}}$ pictures the electrostatic complementarity between the GSH chemical groups and the residues lining the binding site. GSH was assumed to bear three charges: a zwitterionic γ-glutamic acid moiety and a terminal glycine carboxylate group. The SynGSTC1 residues with the largest contributions were R11, K51, R116, which formed salt bridges with the GSH negative charges (Figure 3, Table S6). As an example, the energy values $E_{\text{tot}}^{\text{elec}}$, $E_{\text{perm}}^{\text{elec}}$ and $E_{\text{pol}}^{\text{elec}}$ obtained for R11 were -56.6 kcal·mol^{-1}, -47.3 kcal·mol^{-1} and -9.3 kcal·mol^{-1}, respectively. S65 showed the most favorable $E_{\text{perm}}^{\text{elec}}$ among the uncharged residues ($E_{\text{perm}}^{\text{elec}} = -39.3$ kcal·mol^{-1}), and its contribution was close to those of R11 and R116 when the dipolar induction is included ($E_{\text{tot}}^{\text{elec}} = -54.3$ kcal·mol^{-1}). This serine residue was double-hydrogen-bonded to the γ-Glu carboxylate group. This interaction pattern, well conserved in GSTs, is ensured either by a serine residue or a threonine residue [55]. The negatively charged E64 residue was an interesting case because it had an unfavorable $E_{\text{perm}}^{\text{elec}}$ (13.6 kcal·mol^{-1}) that underwent a significant dipolar induction ($E_{\text{pol}}^{\text{elec}} = -19.7$ kcal·mol^{-1}) to interact with the positively charged N-terminal amine group of GSH ($E_{\text{tot}}^{\text{elec}} = -6.0$ kcal·mol^{-1}, Figure 4, Table S6). The major contributors for the GSH γ-Glu moiety, $E_{\text{perm}}^{\text{elec}}$ speaking, were therefore R11 via its guanidium group and S65 via its amide and hydroxyl groups (Figure 3). This showed that the site where the zwitterionic fragment of GSH was located was an electrophilic site. This property is verified in the crystallographic structures of glutathione-free GSTs because they often contain a negative ion in this site such as chloride, acetate or formate ions [56]. In addition, this electrophilic site was found to be catalytically important as it hosts the γ-Glu carboxylate group which is presumed to decrease the pKa of the GSH thiol group [57]. The glycine part of GSH was surrounded by the two positively charged

K51 and R116 residues, and by the lateral chain of H38 residue. These residues tightly stabilized the GSH C-terminal carboxylate group (Figures 3 and 4). Finally, the GSH Cys part was strongly stabilized by a single residue (V52) via two main-chain–main-chain hydrogen bonds (Figure 3). This twofold contribution was significantly lower compared to that of S65 probably because the V52-GSH interaction did not involve charged groups. The S10 residue, which was assumed to be the catalytic residue interacting with the thiol group, presented an unfavorable electrostatic interaction energy and did not contribute to the GSH stabilization ($E_{tot}^{elec} = 1.3$ kcal·mol^{-1}, Table S6). It also showed an almost zero polarization energy so this residue was not affected by the binding of the glutathione. This correlated well with the fact that the crystal structure of SynGSTC1 revealed no intermolecular interaction between S10 and GSH. The side chain of the "main" tyrosine residue of TyrGSTs (Tyrosine type GSTs) was always observed interacting with the thiol group of GSH in the crystal structures. The "main" serine residue of SerGSTs plays the same role in most known structures. We evaluated the electrostatic contribution of residues to GSH binding in a TyrGST (and a SerGST) containing a putative hydrogen bond between the tyrosine (serine) residue and GSH (Table S6). In both cases, the important residue (tyrosine or serine) provided a stabilizing effect on the ligand ($E_{tot}^{elec} = -12$ kcal·mol^{-1} and $E_{tot}^{elec} = -7.3$ kcal·mol^{-1}, respectively, Table S6). However, this contribution was never predominant. The main anchor points remained the positively charged residues that stabilized the terminal carboxylate groups of GSH.

3.4. Biochemical Characterization of SynGSTC1 and Variants

We recently detected an activity for SynGSTC1 toward methylglyoxal as substrate and also tested glutathione transferase reactions namely aromatic substitution, and addition using, respectively, 1-chloro-2,4-dinitrobenzene (CDNB) and isothiocyanates (ITCs) as substrates [15]. In addition to these activities, we tested here the ability of SynGSTC1 to conjugate GSH on 4-nitrophenyl butyrate (PNP-butyrate) by transacylation and to reduce hydroperoxide toward cumene hydroperoxide (CuOOH). The measured activities (k_{cat}/K_m), respectively of 49.0 ± 1.7 M^{-1}.s^{-1} for PNP-butyrate and 604.6 ± 37.7 M^{-1}·s^{-1} for CuOOH are similar to the one measured toward CDNB 112.5 ± 14.2 M^{-1}·s^{-1}. These activities remain significantly lower than those measured with ITCs ($6.7 \times 10^5 \pm 0.2 \times 10^5$ M^{-1}·s^{-1} and $5.7 \times 10^5 \pm 0.2 \times 10^5$ M^{-1}·s^{-1} for PITC and BITC, respectively) due to a higher affinity of the enzyme for PITC and BITC (31.4 ± 3.5 and 82.0 ± 10.0 µM, respectively) associated to a higher turn-over number (21.0 ± 0.5 s^{-1} and 45.0 ± 1.6 s^{-1}, respectively) (Table S7).

We also investigated the structure–activity relationships of SynGSTC1 by targeting the first two residues of the ^{10}SRAS^{13} motif, S10 being suspected to activate glutathione as in Ser-GSTs and R11 because of its ubiquity in GSTCs (see below in Section 3.5). The kinetic constants and the effect of pH on activities toward PITC were determined for S10T, S10A, S10C and R11A variants (Table 2 and Figure S7). The optimal pH of SynGSTC1 WT (7.4 units) was in the same range as usually observed for GSTs [57]. The substitution of S10 by a threonine residue slightly decreased the optimal pH of the enzyme (6.9 vs. 7.4 for WT) and the catalytic efficiency (k_{cat}/K_m) of the protein (2.1×10^5 M^{-1}·s^{-1} for S10T vs. 3.7×10^5 M^{-1}·s^{-1} for WT). This result was consistent with the crystal structure of S10T which was superimposable to the wild-type (Figure S8). The bulkier threonine side chain did not impair GSH binding. Indeed, the GSH apparent affinity (K_m) was not altered in the S10T variant (Table 2). Furthermore, a sequence analysis of GSTCs (see below in Section 3.5) showed either a serine or a threonine as the first residue of the active site motif (^{10}SRAS^{13} in SynGSTC1). S10A remained effective even though the decrease was greater than for S10T, being divided by 10 and 1.2 in S10A and S10T, respectively, compared to WT. All the kinetic parameters were affected roughly similarly. The crystal structure of SynGSTC1 did not show interaction between S10 and GSH. Instead, S10 was rather involved in stabilizing the β1-α1 loop in the close vicinity of the G-site (see above in Section 3.3) suggesting that the S10A substitution most likely disrupted the integrity of the active site. This resulted in a degradation of the catalytic constants and a moderate increase of the

catalysis optimal pH (shift of 0.4 unit compared to WT). The R11A substitution also did not fully abolish the activity of the enzyme even though it decreased significantly (divided by a factor close to 250 as compared to WT). R11 formed a salt bridge with the N-terminal carboxylate group of GSH in the crystal structure (see above in Section 3.3). This interaction did not seem to be essential for the catalysis because the GSH apparent affinity in R11A was not much more degraded than in S10A (four and five times higher in S10A and R11A variants, respectively, compared to WT). The electrostatic influence of R11 on the catalytic process was, however, clear since the catalytic rate was 75 times lower in R11A compared to WT. This was accompanied by a significant one-unit increase in optimal pH suggesting a higher GSH-thiol pKa in the R11A variant than in the WT enzyme. These variations appeared small compared to those observed in eta GSTH1-1 from *Agrobacterium tumefaciens*, which harbored an arginine residue at the same position as in SynGSTC1. Indeed, the R34A mutation in AtuGSTH1-1 had a detrimental effect on the catalytic constant, which dropped by at least a factor of 5000 [58]. Finally, the substitution of S10 by a cysteine residue, had the same global effect as the S10A mutation (2.9×10^4 $M^{-1} \cdot s^{-1}$ for S10C vs. 3.6×10^4 for S10A). Unlike the WT protein and other variants, the S10C enzyme was also active (k_{cat}/K_m of $3.36 \times 10^3 \pm 0.08 \times 10^3$ $M^{-1} \cdot s^{-1}$) with HED, a substrate commonly used to characterize Grxs and cysteinyl-GSTs, indicating that this variant acquired a significant thiol-transferase activity.

Table 2. Kinetic parameters of SynGSTC1 toward model substrates.

	PITC	GSH	HED
k_{cat} (s^{-1})			
WT	12.6 ± 0.2		ND
S10T	7.2 ± 0.1		ND
S10A	2.60 ± 0.05		ND
S10C	1.19 ± 0.02		0.0111 ± 0.0002
R11A	0.170 ± 0.003		ND
K_m (μM)			
WT	33.8 ± 2.5	135.2 ± 7.9	ND
S10T	33.6 ± 2.6	$142{,}8 \pm 14.6$	ND
S10A	89.7 ± 6.4	528.4 ± 33.0	ND
S10C	33.0 ± 3.0	2149 ± 123	3.3 ± 0.4
R11A	108.4 ± 6.0	719.2 ± 58.2	ND
k_{cat}/K_m ($M^{-1} \cdot s^{-1}$)			
WT	$3.73 \times 10^5 \pm 0.06 \times 10^5$		ND
S10T	$2.14 \times 10^5 \pm 0.04 \times 10^5$		ND
S10A	$2.89 \times 10^4 \pm 0.06 \times 10^4$		ND
S10C	$3.60 \times 10^4 \pm 0.06 \times 10^4$		$3.36 \times 10^3 \pm 0.08 \times 10^3$
R11A	$1.53 \times 10^3 \pm 0.02 \times 10^3$		ND

The apparent K_m values of SynGSTC1 wild-type and variants (S10T, S10A, S10C and R11A) were determined by varying substrate concentrations at a fixed saturating GSH concentration. The apparent K_m and k_{cat} values were calculated with *Prism 8* software using the Michaelis–Menten equation as nonlinear regression model. Results are means ± S.D. ($n = 3$).

3.5. Comparative Genomic Analysis

A similarity-based survey of 222 reference proteomes of the Cyanobacteria/Melainabacteria group led to the identification of 870 full-length GSTC1 homologues (BLASTP E-value cutoff 10^{-3}). The phylogenetic analysis of these sequences led to a large tree (Figure S9). According to this tree, the glutathione transferase chi1 from *Synechocystis* sp. PCC 6803 (SynGSTC1) belonged to a large group of 147 sequences displaying a SRAS motif or related motifs (Figures S9 and S10 and Table S8). These 147 GSTC protein sequences displayed more than 35% of sequence identity and were largely distributed in Cyanobacteria, being present in 144 of the 208 analyzed cyanobacterial proteomes (Figures 5 and S11 for high-quality version). In contrast, they were absent in the noncyanobacterial members of the Cyanobacteria/Melainabacteria group. More precisely, they were present in all cyanobacterial orders excepted Gloeobacterales, the oldest branching extant group of cyanobacteria [59].

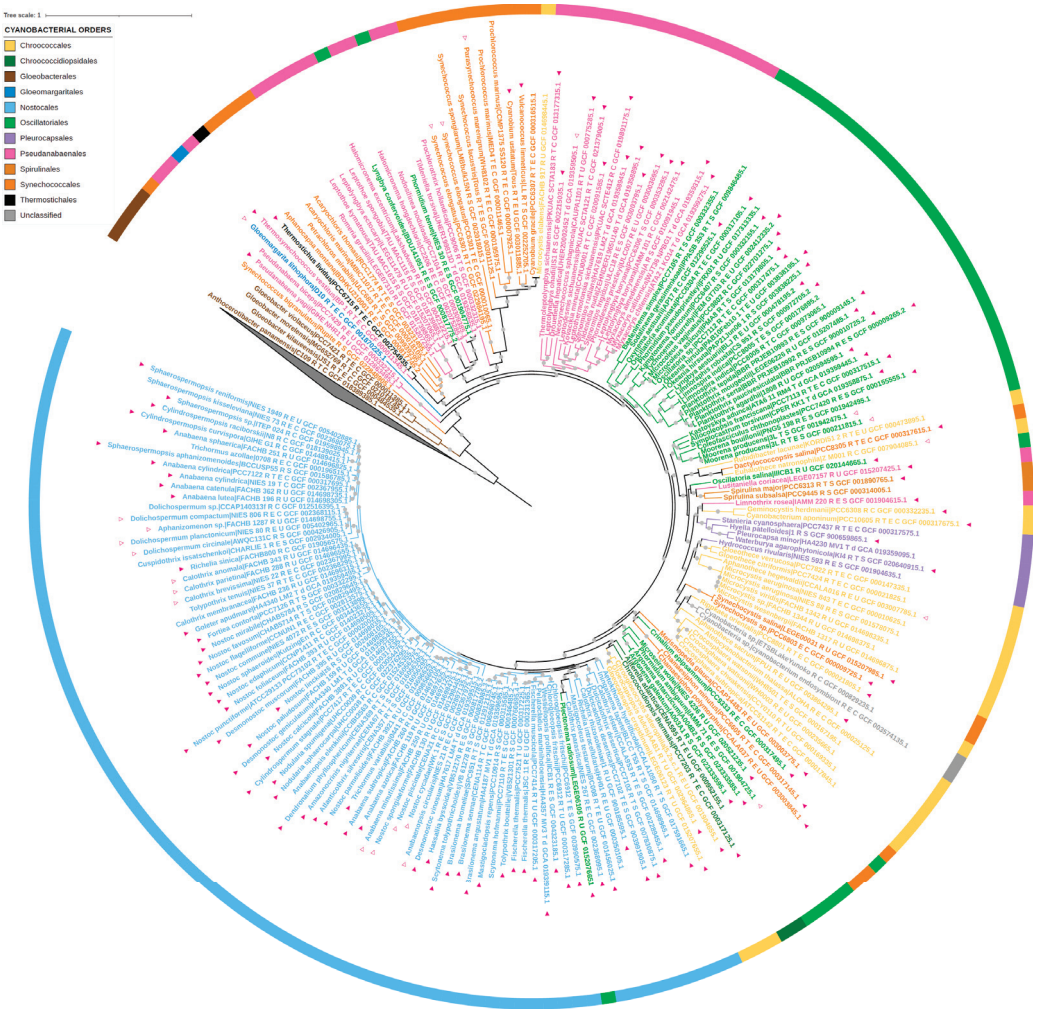

Figure 5. Phylogeny of the 222 proteomes of Cyanobacteria/Melainabacteria group considered in this study. The tree was inferred with *IQ-TREE* using the 52 rprots sequences present in more than 70% of the 222 proteomes (6430 amino acid sites, LG + C20 + F + R4 evolutionary model). The scale bar corresponds to the average number of substitutions per site. Gray circles correspond to ultrafast bootstrap values >90% (1000 replicates). The taxonomy of each proteome is indicated: Gloeobacterales (brown), Synechococcales (orange), Pseudanabaenales (pink), Gloeomargaritales (dark blue), Thermostichales (black), Oscillatoriales (light green), Chroococcales (yellow), Pleurocapsales (purple), Chroococcidiopsidales (dark green), Nostocales (light blue), and unclassified (gray). The 122 GSTC protein sequences harboring the SRAS motif are indicated with filled triangles, while the 25 GSTC sequences harboring variants of the SRAS motif are indicated with empty triangles. All the motifs are described in the Supplementary Table S8. The phylogeny of these 147 GSTC sequences is shown as Figure S10. A high-quality pdf version of the tree is provided as Figure S11 in the online Supplementary Materials.

To go further, we inferred the phylogeny of the 147 sequences displaying the SRAS motif (or related motifs) (Table S9). As expected, due to the restricted number of amino acid positions retained after the alignment trimming, branch supports were overall low

(Figure S10). Despite this global lack of support, the resulting tree showed clearly that sequences harboring the SRAS motif and sequences harboring related motifs were mixed on the tree, indicating that the canonical SRAS motif was lost several times independently during the diversification of GSTCs. Furthermore, the topology of the tree also showed some inconsistencies with the phylogeny of species (Figures 5 and S10). For instance, some Chroococcales sequences emerged within Nostocales (Figure S10), indicating that the evolutionary history of GSTCs harboring the SRAS (or related motifs) was impacted by horizontal gene transfers (HGTs) (Figure S10). Interestingly, these HGTs also contributed to spread GSTC1 outside of Cyanobacteria, since homologues were found in a few non-cyanobacterial bacteria (Figure S9). Most of them were marine and freshwater bacteria and some were recently closely related to cyanobacteria as Planctomycetaceae bacterium TMED241. Indeed, it was found that this bacterium contains a circadian clock kaiABC operon, which is typically found in cyanobacteria [60].

The majority of the 147 GSTC sequences had a length of less than 190 amino acids (Table S10). A dozen had longer sequences because they contained extensions at the N-terminus and/or between the secondary structures. All GSTCs had a reduced C-ter domain with a shortening of helices α4 and α5 as observed in the crystal structure of SynGSTC1. The SRAS motif (^{10}SRAS^{13} in SynGSTC1) was well conserved. The arginine residue was invariant, the first position was replaced in a few cases by a threonine residue and the last two positions were a bit more variable. Surprisingly other residues involved in the structural attributes of SynGSTC1 were not conserved such as the patch of leucine residues (L70 and L94) in the core of the dimer, or the key residue of the lock and key motif (F49), or quaternary contributors to the stabilization of GSH (S98, T99, R116) (Figure 2). The sequence alignment revealed the conservation of 13 residues, most of which were located in the N-terminal domain (eight residues) and more precisely in the domain I (six residues) (Tables S8 and S9). The N-ter domain is generally better conserved than the C-ter domain because it contains an extended part of the active site [2]. In one subunit, the set of conserved residues was not centered on the active site but rather on the center of gravity of the monomer. The residues were distributed almost homogeneously around this center and most of them were located at a distance of less than 10 Å from it (Figure S12). This distribution was consistent with what is usually observed in proteins, namely that the most conserved positions tend to be situated in the core of the protein or on functional surfaces [61]. While the structural role of these conserved residues is obvious, it is difficult to identify those that form the signature of GSTs chi and most of them have be shown conserved in a class of GSTs. Only N97 seemed specific to the GST chi class; it most likely contributed electrostatically to the active site, as it was located near the γ-Glu moiety of GSH and close to the guanidinium group of the SRAS motif (Table S9).

4. Conclusions

This study increased the knowledge on the biochemical characteristic acquired on the chi class of GSTs (GSTCs) and detailed for the first time the structural attributes of this GST class, specific to cyanobacteria. These short-sequence GSTs (~180 aa) had a three-dimensional structure with a very open active site because the α4 and α5 helices were significantly shorter than those usually observed. The glutathione substrate was tightly bound to the enzyme with its reactive center exposed to the solvent. The transfer of multipolar density parameters from small peptides to SynGSTC1 permitted the gradation of residues involved in GSH stabilization. The two carboxylate groups of GSH were the two chemical groups that best adhered to the protein.

GSTCs contained a SRAS conserved motif at the N-terminus of the α1 helix indicating that they belonged to the SerGST group because the first residue of the motif was a serine residue. However, this serine residue was not directly involved in the catalytic act as assumed in SerGSTs [9]. The SRAS motif appeared to constrain the conformation of the serine side chain towards the interior of the protein and not towards the thiol group of GSH. S10 (in SynGSTC1) had a weak and unfavorable electrostatic influence on GSH and its

mutation did not drastically alter the catalytic properties of the enzyme. The denomination TyrGST, CysGST, SerGST and AtyGST (tyrosine type GST, . . . , Atypical GST) has the advantage of simplifying the confusing and cumbersome Greek letter classification. It is relevant in the case of TyrGSTs from a phylogenetic point of view [1]. It is also appropriate in the case of CysGSTs because the cysteine residue is covalently bound to the substrate in one step of the catalytic mechanism [62]. The disadvantage of the residue-based naming is its stigmatization on one residue that may not have a strong link to the activity of the enzyme as is the case for SynGSTC1.

Supplementary Materials: The following supporting information can be downloaded at: https://www.mdpi.com/article/10.3390/biom12101466/s1; Table S1. List of the PCR and mutagenic primers used in this study; Table S2. List of the 222 studied proteomes; Table S3. List of the 53 ribosomal protein families present in bacteria according to riboDB database; Table S4. Strong intersubunit contacts in SynGSTC1; Table S5. Comparison of SynGSTC1 with its structural homologs; Table S6. Permanent, polarization and total electrostatic interaction energies in the active sites of SynGSTC1, of Epsilon 2 GST from *Anopheles Gambiae* (AgGSTE2) and of Alpha 1 GST from chicken (GgGSTA1); Table S7. Kinetic parameters of SynGSTC1 toward model substrates; Table S8. List of the 147 full-length protein sequences displaying a SRAS motif (or a related motif) identified in the 222 proteomes of Cyanobacteria/Melainabacteria group; Table S9. Invariant amino acid residues in the GST Chi Class; Table S10. Multiple sequence alignment of the 147 GSTCs (displaying a SRAS motif or a related motif) identified in the 222 proteomes of Cyanobacteria/Melainabacteria group; Figure S1. Stereoviews of the 2mFo-DFc map of the SynGSTC1 inter-domain linker; Figure S2. Φ and Ψ torsion angles for the inter-domain linker residues in SynGSTC1 during the simulation; Figure S3. Structure-based phylogenetic tree of SynGSTC1 with structural homologs; Figure S4. Stereoview of the comparison of the SRAS motif in SynGSTC1 and in GST SMc00097 from *Sinorhizobium meliloti* 2011; Figure S5. N-Cα-Cβ-Sγ torsion angle of glutathione during molecular dynamics simulation of SynGSTC1; Figure S6. Interatomic distances (Å) between γ-oxygen atom of Ser10 and selected atoms during molecular dynamics simulation of SynGSTC1; Figure S7. Optimal reaction pH of SynGSTC1 and variants S10T, S10A, S10C and R11A; Figure S8. Structural comparison of the active site of SynGSTC1 WT with S10T and R11A variants; Figure S9. Phylogeny of the 870 GST sequences identified in the 222 studied proteomes of the Cyanobacteria / Melainabacteria group and the 11 GSTC-related sequences identified in noncyanobacterial bacteria; Figure S10. Phylogeny of the 147 cyanobacterial GST1 sequences harboring the SRAS motif or related motifs; Figure S11. Phylogeny of the 222 proteomes of Cyanobacteria/Melainabacteria group considered in this study (high quality version of the tree provided in Figure 5); Figure S12. Stereoview of the invariant amino acid residues in the GST Chi Class and WebLogos of aligned GSTCs from cyanobacteria. References [63–68] are cited in Supplementary Materials.

Author Contributions: Conceptualization, C.D. and A.H.; formal analysis, E.M., L.M., G.M., B.G., C.B.-A., C.D. and A.H.; funding acquisition, C.D. and A.H.; methodology, E.M., L.M., S.M., B.G. and A.H.; supervision, B.G., F.D., C.D. and A.H.; writing—original draft, E.M., C.D. and A.H.; writing—review and editing, E.M., G.M., B.G., F.C., C.C.-C., C.B.-A., C.D. and A.H. All authors have read and agreed to the published version of the manuscript.

Funding: This work was supported by a grant from "Agence Nationale pour la Recherche" as part of the "Investissements d'Avenir" program (ANR-11-LABX-0002-01 and ANR-17-CE20-0008-01). This work was supported by the "Institut Jean Barriol".

Institutional Review Board Statement: Not relevant for this study.

Informed Consent Statement: Not relevant for this study.

Data Availability Statement: PDB data (8AI8, 8AI9 and 8AIB) are made freely available by the wwPDB (https://www.wwpdb.org/ (accessed on 30 September 2022)).

Acknowledgments: We thank LabEx ARBRE and Région Grand Est for funding LM's PhD thesis. The authors appreciated the access to the "Plateforme de mesures de diffraction X" of the Université de Lorraine. We acknowledge SOLEIL (Gif Sur Yvette, France) and ESRF (Grenoble, France) for providing synchrotron radiation facilities, and we thank the staffs of PROXIMA-1, PROXIMA-2 and BM07 beamlines for assistance.

Conflicts of Interest: The authors declare no conflict of interest. The funders had no role in the design of the study; in the collection, analyses, or interpretation of data; in the writing of the manuscript, or in the decision to publish the results.

Abbreviations

GST: glutathione transferase; GSTC, chi-class GST; SynGSTC1, GSTC1 from *Synechocystis* sp. PCC 6803; rmsd, root-mean-square deviation; ESRF, European Synchrotron Radiation Facility; PDB, Protein Data Bank; WT, wild-type.

References

1. Mashiyama, S.T.; Malabanan, M.M.; Akiva, E.; Bhosle, R.; Branch, M.C.; Hillerich, B.; Jagessar, K.; Kim, J.; Patskovsky, Y.; Seidel, R.D.; et al. Large-scale determination of sequence, structure, and function relationships in cytosolic glutathione transferases across the biosphere. *PLoS Biol.* **2014**, *12*, e1001843. [CrossRef]
2. Allocati, N.; Federici, L.; Masulli, M.; Di Ilio, C. Glutathione transferases in bacteria. *FEBS J.* **2009**, *276*, 58–75. [CrossRef] [PubMed]
3. Ma, X.-X.; Jiang, Y.-L.; He, Y.-X.; Bao, R.; Chen, Y.; Zhou, C.-Z. Structures of yeast glutathione-S-transferase Gtt2 reveal a new catalytic type of GST family. *EMBO Rep.* **2009**, *10*, 1320–1326. [CrossRef] [PubMed]
4. Ribeiro, A.J.M.; Tyzack, J.D.; Borkakoti, N.; Holliday, G.L.; Thornton, J.M. A global analysis of function and conservation of catalytic residues in enzymes. *J. Biol. Chem.* **2020**, *295*, 314–324. [CrossRef]
5. Perrot, T.; Schwartz, M.; Saiag, F.; Salzet, G.; Dumarçay, S.; Favier, F.; Gérardin, P.; Girardet, J.-M.; Sormani, R.; Morel-Rouhier, M.; et al. Fungal Glutathione Transferases as Tools to Explore the Chemical Diversity of Amazonian Wood Extractives. *ACS Sustain. Chem. Eng.* **2018**, *6*, 13078–13085. [CrossRef]
6. Schwartz, M.; Perrot, T.; Aubert, E.; Dumarçay, S.; Favier, F.; Gerardin, P.; Morel-Rouhier, M.; Mulliert, G.; Saiag, F.; Didierjean, C.; et al. Molecular recognition of wood polyphenols by phase II detoxification enzymes of the white rot *Trametes versicolor*. *Sci. Rep.* **2018**, *8*, 8472. [CrossRef]
7. Allocati, N.; Masulli, M.; Di Ilio, C.; Federici, L. Glutathione transferases: Substrates, inihibitors and pro-drugs in cancer and neurodegenerative diseases. *Oncogenesis* **2018**, *7*, 8. [CrossRef] [PubMed]
8. Nianiou-Obeidat, I.; Madesis, P.; Kissoudis, C.; Voulgari, G.; Chronopoulou, E.; Tsaftaris, A.; Labrou, N.E. Plant glutathione transferase-mediated stress tolerance: Functions and biotechnological applications. *Plant Cell Rep.* **2017**, *36*, 791–805. [CrossRef]
9. Sylvestre-Gonon, E.; Law, S.R.; Schwartz, M.; Robe, K.; Keech, O.; Didierjean, C.; Dubos, C.; Rouhier, N.; Hecker, A. Functional, Structural and Biochemical Features of Plant Serinyl-Glutathione Transferases. *Front. Plant Sci.* **2019**, *10*, 608. [CrossRef]
10. Wiktelius, E.; Stenberg, G. Novel class of glutathione transferases from cyanobacteria exhibit high catalytic activities towards naturally occurring isothiocyanates. *Biochem. J.* **2007**, *406*, 115–123. [CrossRef]
11. Shehu, D.; Abdullahi, N.; Alias, Z. Cytosolic Glutathione S-transferase in Bacteria: A Review. *Pol. J. Environ. Stud.* **2019**, *28*, 515–528. [CrossRef]
12. Meux, E.; Prosper, P.; Ngadin, A.; Didierjean, C.; Morel, M.; Dumarçay, S.; Lamant, T.; Jacquot, J.-P.; Favier, F.; Gelhaye, E. Glutathione Transferases of *Phanerochaete chrysosporium*: S-Glutathionyl-p-hydroquinone Reductase Belongs to a New Structural Class. *J. Biol. Chem.* **2011**, *286*, 9162–9173. [CrossRef] [PubMed]
13. Masai, E.; Ichimura, A.; Sato, Y.; Miyauchi, K.; Katayama, Y.; Fukuda, M. Roles of the enantioselective glutathione S-transferases in cleavage of beta-aryl ether. *J. Bacteriol.* **2003**, *185*, 1768–1775. [CrossRef] [PubMed]
14. Meux, E.; Prosper, P.; Masai, E.; Mulliert, G.; Dumarçay, S.; Morel, M.; Didierjean, C.; Gelhaye, E.; Favier, F. *Sphingobium* sp. SYK-6 LigG involved in lignin degradation is structurally and biochemically related to the glutathione transferase omega class. *FEBS Lett.* **2012**, *586*, 3944–3950. [CrossRef] [PubMed]
15. Kammerscheit, X.; Hecker, A.; Rouhier, N.; Chauvat, F.; Cassier-Chauvat, C. Methylglyoxal Detoxification Revisited: Role of Glutathione Transferase in Model Cyanobacterium *Synechocystis* sp. Strain PCC 6803. *mBio* **2020**, *11*, e00882-20. [CrossRef]
16. Pandey, T.; Singh, S.K.; Chhetri, G.; Tripathi, T.; Singh, A.K. Characterization of a Highly pH Stable Chi-Class Glutathione S-Transferase from *Synechocystis* PCC 6803. *PLoS ONE* **2015**, *10*, e0126811. [CrossRef]
17. Feil, S.C.; Tang, J.; Hansen, G.; Gorman, M.A.; Wiktelius, E.; Stenberg, G.; Parker, M.W. Crystallization and preliminary X-ray analysis of glutathione transferases from cyanobacteria. *Acta Crystallogr. Sect. F Crystallogr. Commun.* **2009**, *65*, 475–477. [CrossRef]
18. Allocati, N.; Casalone, E.; Masulli, M.; Ceccarelli, I.; Carletti, E.; Parker, M.W.; Di Ilio, C. Functional analysis of the evolutionarily conserved proline 53 residue in *Proteus mirabilis* glutathione transferase B1-1. *FEBS Lett.* **1999**, *445*, 347–350. [CrossRef]
19. Dragani, B.; Stenberg, G.; Melino, S.; Petruzzelli, R.; Mannervik, B.; Aceto, A. The Conserved N-capping Box in the Hydrophobic Core of Glutathione S-Transferase P1-1 Is Essential for Refolding. Identification of A buried and Conserved Hydrogen Bond Important for Protein Stability. *J. Biol. Chem.* **1997**, *272*, 25518–25523. [CrossRef]
20. ShylajaNaciyar, M.; Karthick, L.; Prakasam, P.A.; Deviram, G.; Uma, L.; Prabaharan, D.; Saha, S.K. Diversity of Glutathione S-Transferases (GSTs) in Cyanobacteria with Reference to Their Structures, Substrate Recognition and Catalytic Functions. *Microorganisms* **2020**, *8*, 712. [CrossRef]
21. Kabsch, W. XDS. *Acta Crystallogr. Sect. D Biol. Crystallogr.* **2010**, *66*, 125–132. [CrossRef] [PubMed]

22. Evans, P.R.; Murshudov, G.N. How good are my data and what is the resolution? *Acta Crystallogr. Sect. D Biol. Crystallogr.* **2013**, *69*, 1204–1214. [CrossRef] [PubMed]
23. Winn, M.D.; Ballard, C.C.; Cowtan, K.D.; Dodson, E.J.; Emsley, P.; Evans, P.R.; Keegan, R.M.; Krissinel, E.B.; Leslie, A.G.W.; McCoy, A.; et al. Overview of the CCP4 suite and current developments. *Acta Crystallogr. Sect. D Biol. Crystallogr.* **2011**, *67*, 235–242. [CrossRef] [PubMed]
24. Vagin, A.; Lebedev, A. *MoRDa*, an automatic molecular replacement pipeline. *Acta Crystallogr. Sect. A Found. Adv.* **2015**, *71*, s19. [CrossRef]
25. Smart, O.S.; Womack, T.O.; Flensburg, C.; Keller, P.; Paciorek, W.; Sharff, A.; Vonrhein, C.; Bricogne, G. Exploiting structure similarity in refinement: Automated NCS and target-structure restraints in BUSTER. *Acta Crystallogr. Sect. D Biol. Crystallogr.* **2012**, *68*, 368–380. [CrossRef]
26. Emsley, P.; Lohkamp, B.; Scott, W.G.; Cowtan, K. Features and development of Coot. *Acta Crystallogr. Sect. D Biol. Crystallogr.* **2010**, *66*, 486–501. [CrossRef] [PubMed]
27. Hansen, N.K.; Coppens, P. Testing aspherical atom refinements on small-molecule data sets. *Acta Crystallogr. Sect. A Found. Adv.* **1978**, *34*, 909–921. [CrossRef]
28. Domagala, S.; Fournier, B.; Liebschner, D.; Guillot, B.; Jelsch, C. An improved experimental databank of transferable multipolar atom models—ELMAM2. Construction details and applications. *Acta Crystallogr. Sect. A Found. Adv.* **2012**, *68*, 337–351. [CrossRef]
29. Leduc, T.; Aubert, E.; Espinosa, E.; Jelsch, C.; Iordache, C.; Guillot, B. Polarization of Electron Density Databases of Transferable Multipolar Atoms. *J. Phys. Chem.* **2019**, *123*, 7156–7170. [CrossRef]
30. Guillot, B.; Enrique, E.; Huder, L.; Jelsch, C. MoProViewer: A tool to study proteins from a charge density science perspective. *Acta Crystallogr. Sect. A Found. Adv.* **2014**, *70*, C279. [CrossRef]
31. Vuković, V.; Leduc, T.; Jelić-Matošević, Z.; Didierjean, C.; Favier, F.; Guillot, B.; Jelsch, C. A rush to explore protein–ligand electrostatic interaction energy with Charger. *Acta Crystallogr. Sect. D Biol. Crystallogr.* **2021**, *77*, 1292–1304. [CrossRef] [PubMed]
32. Phillips, J.C.; Hardy, D.J.; Maia, J.D.C.; Stone, J.E.; Ribeiro, J.V.; Bernardi, R.C.; Buch, R.; Fiorin, G.; Hénin, J.; Jiang, W.; et al. Scalable molecular dynamics on CPU and GPU architectures with NAMD. *J. Chem. Phys.* **2020**, *153*, 044130. [CrossRef] [PubMed]
33. Brooks, B.R.; Brooks, C.L., III; Mackerell, A.D., Jr.; Nilsson, L.; Petrella, R.J.; Roux, B.; Won, Y.; Archontis, G.; Bartels, C.; Boresch, S.; et al. CHARMM: The biomolecular simulation program. *J. Comput. Chem.* **2009**, *30*, 1545–1614. [CrossRef]
34. Jorgensen, W.L.; Chandrasekhar, J.; Madura, J.D.; Impey, R.W.; Klein, M.L. Comparison of simple potential functions for simulating liquid water. *J. Chem. Phys.* **1983**, *79*, 926–935. [CrossRef]
35. Vanommeslaeghe, K.; Hatcher, E.; Acharya, C.; Kundu, S.; Zhong, S.; Shim, J.; Darian, E.; Guvench, O.; Lopes, P.; Vorobyov, I.; et al. CHARMM general force field: A force field for drug-like molecules compatible with the CHARMM all-atom additive biological force fields. *J. Comput. Chem.* **2010**, *31*, 671–690. [CrossRef] [PubMed]
36. Andersen, H.C. Rattle: A "velocity" version of the shake algorithm for molecular dynamics calculations. *J. Comput. Phys.* **1983**, *52*, 24–34. [CrossRef]
37. Miyamoto, S.; Kollman, P.A. Settle: An analytical version of the SHAKE and RATTLE algorithm for rigid water models. *J. Comput. Chem.* **1992**, *13*, 952–962. [CrossRef]
38. Hopkins, C.W.; Le Grand, S.; Walker, R.C.; Roitberg, A.E. Long-Time-Step Molecular Dynamics through Hydrogen Mass Repartitioning. *J. Chem. Theory Comput.* **2015**, *11*, 1864–1874. [CrossRef]
39. Humphrey, W.; Dalke, A.; Schulten, K. VMD: Visual molecular dynamics. *J. Mol. Graph.* **1996**, *14*, 33–38. [CrossRef]
40. Jauffrit, F.; Penel, S.; Delmotte, S.; Rey, C.; de Vienne, D.M.; Gouy, M.; Charrier, J.P.; Flandrois, J.P.; Brochier-Armanet, C. RiboDB Database: A Comprehensive Resource for Prokaryotic Systematics. *Mol. Biol. Evol.* **2016**, *33*, 2170–2172. [CrossRef]
41. Katoh, K.; Standley, D.M. MAFFT multiple sequence alignment software version 7: Improvements in performance and usability. *Mol. Biol. Evol.* **2013**, *30*, 772–780. [CrossRef] [PubMed]
42. Criscuolo, A.; Gribaldo, S. BMGE (Block Mapping and Gathering with Entropy): A new software for selection of phylogenetic informative regions from multiple sequence alignments. *BMC Evol. Biol.* **2010**, *10*, 210. [CrossRef] [PubMed]
43. Minh, B.Q.; Schmidt, H.A.; Chernomor, O.; Schrempf, D.; Woodhams, M.D.; von Haeseler, A.; Lanfear, R. IQ-TREE 2: New Models and Efficient Methods for Phylogenetic Inference in the Genomic Era. *Mol. Biol. Evol.* **2020**, *37*, 1530–1534. [CrossRef] [PubMed]
44. Price, M.N.; Dehal, P.S.; Arkin, A.P. FastTree 2–approximately maximum-likelihood trees for large alignments. *PLoS ONE* **2010**, *5*, e9490. [CrossRef]
45. Le, S.Q.; Gascuel, O. An improved general amino acid replacement matrix. *Mol. Biol. Evol.* **2008**, *25*, 1307–1320. [CrossRef]
46. Letunic, I.; Bork, P. Interactive Tree Of Life (iTOL) v5: An online tool for phylogenetic tree display and annotation. *Nucleic Acids Res.* **2021**, *49*, W293–W296. [CrossRef]
47. Hayes, J.D.; Flanagan, J.U.; Jowsey, I.R. Glutathione transferases. *Annu. Rev. Pharmacol. Toxicol.* **2005**, *45*, 51–88. [CrossRef]
48. Polekhina, G.; Board, P.G.; Blackburn, A.C.; Parker, M.W. Crystal structure of maleylacetoacetate isomerase/glutathione transferase zeta reveals the molecular basis for its remarkable catalytic promiscuity. *Biochemistry* **2001**, *40*, 1567–1576. [CrossRef]
49. Wilce, M.C.J.; Parker, M.W. Structure and function of glutathione S-transferasese. *Biochim. Biophys. Acta Prot. Struct. Mol. Enzymol.* **1994**, *1205*, 1–18. [CrossRef]
50. Holm, L.; Laakso, L.M. Dali server update. *Nucleic Acids Res.* **2016**, *44*, W351–W355. [CrossRef]
51. Dong, R.; Pan, S.; Peng, Z.; Zhang, Y.; Yang, J. mTM-align: A server for fast protein structure database search and multiple protein structure alignment. *Nucleic Acids Res.* **2018**, *46*, W380–W386. [CrossRef]

52. Jacquot, J.P.; Gelhaye, E.; Rouhier, N.; Corbier, C.; Didierjean, C.; Aubry, A. Thioredoxins and related proteins in photosynthetic organisms: Molecular basis for thiol dependent regulation. *Biochem. Pharmacol.* **2002**, *64*, 1065–1069. [CrossRef]
53. Dixon, D.P.; Edwards, R. Glutathione Transferases. *Arabidop. Book* **2010**, *8*, e0131. [CrossRef]
54. Pegeot, H.; Koh, C.S.; Petre, B.; Mathiot, S.; Duplessis, S.; Hecker, A.; Didierjean, C.; Rouhier, N. The poplar Phi class glutathione transferase: Expression, activity and structure of GSTF1. *Front. Plant. Sci.* **2014**, *5*, 712. [CrossRef]
55. Sheehan, D.; Meade, G.; Foley, V.M.; Dowd, C.A. Structure, function and evolution of glutathione transferases: Implications for classification of non-mammalian members of an ancient enzyme superfamily. *Biochem. J.* **2001**, *360*, 1–16. [CrossRef]
56. Sylvestre-Gonon, E.; Morette, L.; Viloria, M.; Mathiot, S.; Boutilliat, A.; Favier, F.; Rouhier, N.; Didierjean, C.; Hecker, A. Biochemical and structural insights on the poplar tau glutathione transferase GSTU19 and 20 paralogs binding flavonoids. *Front. Mol. Biosci.* **2022**, *9*, 9585866. [CrossRef] [PubMed]
57. Dourado, D.F.; Fernandes, P.A.; Mannervik, B.; Ramos, M.J. Glutathione transferase: New model for glutathione activation. *Chemistry* **2008**, *14*, 9591–9598. [CrossRef]
58. Skopelitou, K.; Dhavala, P.; Papageorgiou, A.C.; Labrou, N.E. A glutathione transferase from *Agrobacterium tumefaciens* reveals a novel class of bacterial GST superfamily. *PLoS ONE* **2012**, *7*, e34263. [CrossRef]
59. Moreira, D.; Tavera, R.; Benzerara, K.; Skouri-Panet, F.; Couradeau, E.; Gerard, E.; Fonta, C.L.; Novelo, E.; Zivanovic, Y.; Lopez-Garcia, P. Description of *Gloeomargarita lithophora* gen. nov., sp. nov., a thylakoid-bearing, basal-branching cyanobacterium with intracellular carbonates, and proposal for *Gloeomargaritales* ord. nov. *Int. J. Syst. Evol. Microbiol.* **2017**, *67*, 653–658. [CrossRef]
60. Dvornyk, V.; Mei, Q. Evolution of *kaiA*, a key circadian gene of cyanobacteria. *Sci. Rep.* **2021**, *11*, 9995. [CrossRef]
61. Halabi, N.; Rivoire, O.; Leibler, S.; Ranganathan, R. Protein sectors: Evolutionary units of three-dimensional structure. *Cell* **2009**, *138*, 774–786. [CrossRef] [PubMed]
62. Board, P.G.; Coggan, M.; Chelvanayagam, G.; Easteal, S.; Jermiin, L.S.; Schulte, G.K.; Danley, D.E.; Hoth, L.R.; Griffor, M.C.; Kamath, A.V.; et al. Identification, characterization, and crystal structure of the omega class glutathione transferases. *J. Biol. Chem.* **2000**, *275*, 24798–24806. [CrossRef]
63. Williams, C.J.; Headd, J.J.; Moriarty, N.W.; Prisant, M.G.; Videau, L.L.; Deis, L.N.; Verma, V.; Keedy, D.A.; Hintze, B.J.; Chen, V.B.; et al. MolProbity: More and better reference data for improved all-atom structure validation. *Protein Sci.* **2018**, *27*, 293–315. [CrossRef] [PubMed]
64. DeLano, W.L. Pymol: An open-source molecular graphics tool. CCP4 Newsl. *Protein Crystallogr.* **2002**, *40*, 82–92.
65. Roret, T.; Thuillier, A.; Favier, F.; Gelhaye, E.; Didierjean, C.; Morel-Rouhier, M. Evolutionary divergence of Ure2pA glutathione transferases in wood degrading fungi. *Fungal Genet. Biol.* **2015**, *83*, 103–112. [CrossRef] [PubMed]
66. Aceto, A.; Dragani, B.; Melino, S.; Allocati, N.; Masulli, M.; Ilio, C.D.; Petruzzelli, R. Identification of an N-capping box that affects the α6-helix propensity in glutathione S-transferase superfamily proteins: A role for an invariant aspartic residue. *Biochem. J.* **1997**, *322*, 229–234. [CrossRef]
67. Dirr, H.; Reinemer, P.; Huber, R. X-ray crystal structures of cytosolic glutathione Stransferases: Implications for protein architecture, substrate recognition and catalytic function. *Eur. J. Biochem.* **1994**, *220*, 645–661. [CrossRef] [PubMed]
68. Crooks, G.E.; Hon, G.; Chandonia, J.M.; Brenner, S.E. WebLogo: A sequence logo generator. *Genome Res.* **2004**, *14*, 1188–1190. [CrossRef]

biomolecules

MDPI

Article

Conservation of Glutathione Transferase mRNA and Protein Sequences Similar to Human and Horse Alpha Class GST A3-3 across Dog, Goat, and Opossum Species

Shawna M. Hubert [1,2], Paul B. Samollow [3], Helena Lindström [4], Bengt Mannervik [4,*] and Nancy H. Ing [1,5]

[1] Department of Animal Science, Texas A&M AgriLife Research, Texas A&M University, College Station, TX 77843-2471, USA; smhubert@mdanderson.org (S.M.H.); n-ing@tamu.edu (N.H.I.)
[2] Department of Thoracic Head & Neck Medical Oncology, University of Texas M.D. Anderson Cancer Center, Houston, TX 77030-4000, USA
[3] Department of Veterinary Integrative Biosciences, School of Veterinary Medicine and Biosciences, Texas A&M University, College Station, TX 77843-2471, USA; psamollow@tamu.edu
[4] Department of Biochemistry and Biophysics, Arrhenius Laboratories, Stockholm University, SE-10691 Stockholm, Sweden; helenesemail@yahoo.com
[5] Faculty of Biotechnology, Texas A&M University, College Station, TX 77843-2128, USA
* Correspondence: bengt.mannervik@dbb.su.se; Tel.: +46-(0)70-425-0849

Abstract: The glutathione transferase A3-3 (GST A3-3) homodimeric enzyme is the most efficient enzyme that catalyzes isomerization of the precursors of testosterone, estradiol, and progesterone in the gonads of humans and horses. However, the presence of GST A3-3 orthologs with equally high ketosteroid isomerase activity has not been verified in other mammalian species, even though pig and cattle homologs have been cloned and studied. Identifying *GSTA3* genes is a challenge because of multiple *GSTA* gene duplications (e.g., 12 in the human genome); consequently, the *GSTA3* gene is not annotated in most genomes. To improve our understanding of *GSTA3* gene products and their functions across diverse mammalian species, we cloned homologs of the horse and human *GSTA3* mRNAs from the testes of a dog, goat, and gray short-tailed opossum, the genomes of which all currently lack *GSTA3* gene annotations. The resultant novel *GSTA3* mRNA and inferred protein sequences had a high level of conservation with human *GSTA3* mRNA and protein sequences (≥70% and ≥64% identities, respectively). Sequence conservation was also apparent for the 12 residues of the "H-site" in the 222 amino acid GSTA3 protein that is known to interact with the steroid substrates. Modeling predicted that the dog GSTA3-3 may be a more active ketosteroid isomerase than the corresponding goat or opossum enzymes. However, expression of the *GSTA3* gene was higher in liver than in other dog tissue. Our results improve understanding of the active sites of mammalian GST A3-3 enzymes, inhibitors of which might be useful for reducing steroidogenesis for medical purposes, such as fertility control or treatment of steroid-dependent diseases.

Keywords: estrogen; glutathione transferase A3-3 (GST A3-3); steroidogenesis; testes; testosterone; progesterone

Citation: Hubert, S.M.; Samollow, P.B.; Lindström, H.; Mannervik, B.; Ing, N.H. Conservation of Glutathione Transferase mRNA and Protein Sequences Similar to Human and Horse Alpha Class GST A3-3 across Dog, Goat, and Opossum Species. *Biomolecules* **2023**, *13*, 1420. https://doi.org/10.3390/biom13091420

Academic Editor: Ajoy Basak

Received: 3 August 2023
Revised: 29 August 2023
Accepted: 13 September 2023
Published: 20 September 2023

1. Introduction

It is widely appreciated that reproduction of vertebrate animal species centers around sex steroid production by the gonads. While driven by peptide hormones from the hypothalamic/pituitary axis, production of testosterone by the Leydig cells of the testis and estradiol and progesterone by the granulosa cells and corpora lutea of the ovary are required for successful production of offspring [1–3]. Testosterone, estradiol, and progesterone act in reproductive tissues by binding to specific receptors which regulate the coordinated expression of genes important to male and female reproduction [4,5].

Testosterone, estradiol, and progesterone are produced from cholesterol by a series of enzymatic modifications [6,7]. This reaction sequence differs among species: rodents utilize

the Δ^4 pathway, whereas humans and other larger mammals utilize the Δ^5 pathway [7]. The biosynthetic pathway for testosterone in human and horse testes involves the alpha class glutathione transferase A3-3 (GST (Abbreviations used: GST glutathione transferase; Δ5-AD delta-5 androstenedione; SF1 steroidogenic factor 1; RT reverse transcription; PCR polymerase chain reaction; cDNA complementary DNA) A3-3) as a ketosteroid isomerase that acts as a homodimer to convert Δ^5-androstene-3,17-dione (Δ^5-AD) to Δ^4-androstene-3,17-dione, the immediate precursor of testosterone [8–16]. The human GST A3-3 enzyme is 230 times more efficient at this isomerization than the hydroxy-Δ^5-steroid dehydrogenase, 3β-hydroxysteroid delta-isomerase 2 (HSD3B2), the enzyme to which this activity previously had been attributed [2]. Estradiol synthesis is likewise dependent upon GSTA3-3 in humans and horses because testosterone is further converted to estradiol by aromatase [7]. GST A3-3 also participates in the synthesis of progesterone in female mammals utilizing the Δ^5 pathway by isomerizing Δ^5-pregnene-3,20-dione to Δ^4-pregnene-3,20-dione (i.e., progesterone).

The *GSTA* class of genes is best characterized in humans. It is represented by 12 genes and pseudogenes with almost indistinguishable sequences. These arose from gene duplications and, in humans, are clustered in a 282 kbp region on chromosome 6 [17]. Because of the redundancy of GSTA genes, the *GSTA3* genes are inexactly identified, if identified at all, in the current annotations of the genomes of most mammals. This gap in knowledge limits studies of *GSTA3* gene expression because standard *GSTA3* mRNA and protein detection reagents crossreact with other four gene products in the GSTA family, which are ubiquitously expressed [11].

Inhibitors of the GST A3-3 homodimeric enzyme and factors that decrease *GSTA3* gene expression inhibit the synthesis of sex steroid hormones. In extracts of the steroidogenic JEG-3 cell line of placental origin, two specific inhibitors of GSTA3-3 (ethacrynic acid and tributyltin acetate) decreased isomerization of Δ^5-AD with very low half maximal inhibitory concentrations (IC_{50}) values of 2.5 μM and 0.09 μM, respectively [18]. In addition, transfection of this cell line with either of two different small, interfering RNAs decreased progesterone synthesis by 22% to 30%. In stallions treated with dexamethasone, a glucocorticoid drug used to treat inflammation, testicular levels of *GSTA3* mRNAs decreased by 50% at 12 h post-injection, concurrent with a 94% reduction in serum testosterone [19,20]. In stallion testes and cultured Leydig cells, dexamethasone also decreased concentrations of steroidogenic factor 1 (*SF1* or *NR5A1*) mRNA [21]. In a human genome-wide study of the genes regulated by SF1 protein, chromatin immunoprecipitation determined that the SF1 protein bound to the *GSTA3* promoter to up-regulate the gene [13]. Notably, the SF1 transcription factor up-regulates the expression of several gene products involved in steroidogenesis [2]. These data indicate that there are reagents and pathways by which *GSTA3* gene expression and steroidogenesis can be altered in vivo. This could be useful for reducing steroidogenesis for fertility control or other medical purposes, such as reducing tumor growth in advanced prostate cancer [22].

The equine and common marmoset GST A3-3 enzymes are structurally similar to the human enzyme, and they match or exceed the very high steroid isomerase activity of the latter [15,23]. Remarkably, the phylogenetically more closely related GSTA3 homologs from the gonads of domestic pigs (*Sus scrofa*) and cattle (*Bos taurus*) yielded enzymes that differed greatly as ketosteroid isomerases [10,24]. For reasons yet to be determined, the pig enzyme was highly active and showed 70-fold higher activity than the cow enzyme [15].

In the current work, *GSTA3* mRNA was cloned from the testes of the dog and goat (eutherian mammals), and gray short-tailed opossum (metatherian mammal). The purposes were (1) to compare mRNA and protein sequences with the human and horse counterparts to search for more highly active ketosteroid isomerases, (2) to generate GSTA3-specific reagents for future studies of the regulation of *GSTA3* genes, and (3) to understand the scope of the GSTA3-3 function in steroidogenesis across a range of mammalian species in which reproduction is important to humans. Information from these additional mammalian

species will expand our knowledge of GSTA3 structure and function across a considerably broader phylogenetic range than has previously been examined (Figure 1).

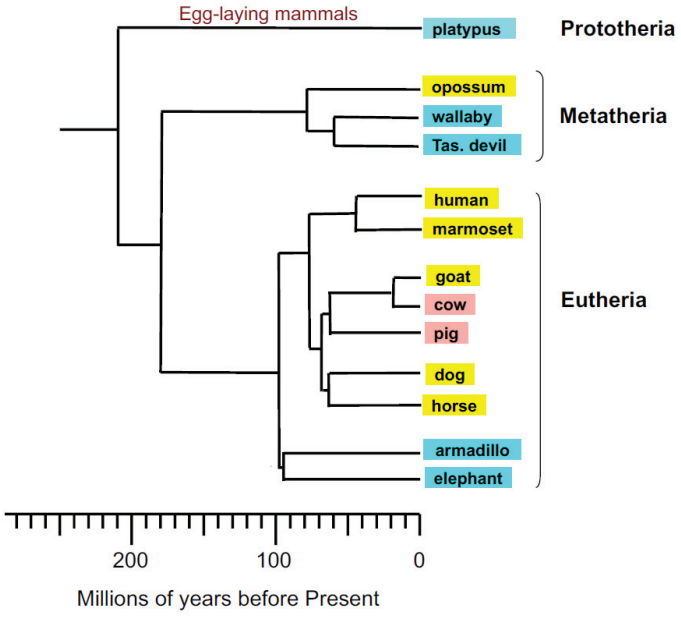

Figure 1. Phylogenetic relationships of among mammalian species used in this study (adapted from [25,26] with refinements from WJ Murphy, personal communication). Species investigated in this report and those used as references are highlighted in yellow; additional species with reported GSTA ketosteroid isomerase data are shown in pink; species included for phylogenetic context only are shown in blue.

2. Materials and Methods

2.1. Materials

The chemical reagents were from Sigma-Aldrich (St. Louis, MO, USA) unless otherwise noted.

2.2. Methods

2.2.1. Testis Tissue Samples and RNA Preparation

All animal procedures were approved by the Texas A&M University Institutional Animal Care and Use Committee. Adult testes used in this study were obtained from Texas A&M University-owned research animals; specifically, from a large-breed hound (*Canis lupus familiaris*), a goat (*Capra hircus),* and a gray short-tailed opossum (*Monodelphis domestica*). Additional tissues (adrenal gland, liver, small intestine, ovary, ovary with follicles, spleen, heart, skeletal muscle, kidney, uterus, mammary gland, cerebrum, and hypothalamus) were collected from two female large-breed hounds.

Total cellular RNA was extracted from each testis with the Tripure reagent (Sigma-Aldrich; St. Louis, MO, USA) protocol. The concentration and purity of the RNA were assessed using a Nanodrop spectrophotometer.

2.2.2. Reverse Transcription

Reverse transcription reactions (25 µL) for the production of cDNA were run with each RNA sample (500 ng) using random octamer primers (312 ng), dT_{20} primers (625 ng), dNTPs, DTT, first strand buffer, Superasin and Superscript II Reverse Transcriptase (RT), following the manufacturer's instructions (ThermoFisher Scientific; Waltham, MA, USA).

The RT reactions incubated in an air incubator at 42 °C for three hours. The RT enzyme was inactivated by incubating at 70 °C for 15 min.

2.2.3. Cloning GSTA3 cDNAs into the Vector pCR2.1

Nested PCR was utilized to selectively amplify the *GSTA3* mRNA targets to increase the sensitivity and fidelity of amplification. Primers (Table 1) were designed from BLAST analyses with human and horse *GSTA3* mRNA sequences (GenBank accession numbers NM_000847.1 and KC512384.1, respectively) to identify related dog, goat, and opossum sequences for cloning cDNAs into the general use vector pCR2.1 (TA Cloning Kit; ThermoFisher Scientific). The primers were synthesized by Integrated DNA Technologies (Skokie, IL, USA). PCR reactions (50 µL) were performed with Ex Taq enzyme (Takara Bio Inc.; Mountain View, CA, USA) in a GeneAmp PCR System 9600 (PerkinElmer; Norwalk, CT, USA). Primary PCR reactions (50 µL) were set up with outside primers and 1 µL of the appropriate RT reaction. Cycling parameters were 30 cycles of 94 °C for 15 s, 45 °C annealing for 30 s, and 72 °C for one minute, followed by a one-time hold at 72 °C for five minutes. Secondary PCR reactions (50 µL) were set up with inside primers and 5 µL of the primary PCR reactions as a cDNA template source instead of using the RT reaction. Cycling parameters were maintained for the secondary PCR. The PCR products were run out on both a 1% agarose gel and a 0.8% low melting temperature agarose gel. Ethidium bromide staining of DNA bands was visualized under UV light. This procedure confirmed the presence of the intended PCR products of 670 to 700 base pairs in all of the secondary PCR reactions.

Table 1. PCR primer sequences (5′-3′) for TA cloning GSTA3 cDNAs into pCR2.1.

Species	Primer Set	Orientation	Sequence
Dog	Outside	Sense	GGAGACCTGCATCATGGCAGTGAAGCCCATG
		Antisense	AGGAGATTGGCCCTGCATGTGCT
	Inside	Sense	ATGGCGGGGAAGCCCAAGCTTCACTACTTCAATGG
		Antisense	CTGGGCATCCATTCCTGTTCAGTTAATCCT
Goat	Outside	Sense	GGAGACTGCATCATGGCAGTGAAGCCCATG
		Antisense	TCAAATTTGTCCCAAACAGCCCC
	Inside	Sense	ATGGCAGGGAAGCCCATTCTTCACTATTTCAATGG
		Antisense	CCCCGCCAGCCGCCAGCTTTATTAAAACTT
Opossum	Outside	Sense	GGAGACTGCCATCATGGCAGTGAAGCCCATG
		Antisense	TGTGTTTAAGAAACACAGAGTCA
	Inside	Sense	GGTAAAGAAGATATTCAAGGTTGATGA
		Antisense	TCATCAACCTTGAATATCTTCTTTACC

GSTA3 cDNA bands were cut from the 0.8% low melting temperature agarose gels and melted at 70 °C for 10 min. Ligation of the cDNA inserts to pCR2.1 was performed according to the kit manufacturer's instructions (TA Cloning kit; ThermoFisher). These ligation reactions were then utilized in transformation of *E. coli* competent cells. After incubation in SOC broth for 1 h at 37 °C, transformations were plated on LB-ampicillin agar containing isopropyl β-D-1-thiogalactopyranoside and 5-bromo-4-chloro-3-indolyl-β-D-galactopyranoside for blue-white colony selection. Plates were incubated overnight at 37 °C. Selected white colonies were cultured overnight in LB-ampicillin broth and plasmid DNA was purified using the Qiagen QIAprep Spin Kit (Germantown, MD, USA). *GSTA3* cDNAs were released from the pCR2.1 plasmids by digestion with EcoRI before being analyzed by gel electrophoresis. Plasmid samples that demonstrated the expected 670 to 700 base pair bands were sequenced.

2.2.4. Sequencing and Structure Analyses

The *GSTA3* cDNAs inserts in the pCR2.1 vectors were amplified by PCR through the use of Big-Dye mix (Applied Biosystems, ThermoFisher Scientific) using the M13 forward and M13 reverse primers (5′-TGTAAAACGACGGCCAGT-3′ and 5′-CAGGAAACAGCTATGAC-3′, respectively). After PCR amplification, G-50 spin columns were used to remove unincorporated nucleotides. Samples were sequenced at the Texas A&M University Gene Technologies Laboratory on a PRISM 3100 Genetic Analyzer mix (Applied Biosystems, ThermoFisher Scientific). Each sequence was then compared to the NCBI GenBank database records for the human and horse *GSTA3* mRNA sequences (GenBank accession numbers NM_000847.1 and KC512384.1, respectively). The basic local alignment search tool (BLAST) on the NCBI website was also utilized to check for alignments to reference mRNA sequences of other species. For each species, the sequence with the highest identity to the NCBI *GSTA3* mRNA reference sequences was translated to its amino acid sequence through the use of the ExPASy translate tool (https://web.expasy.org/translate/ (accessed on 28 August 2023)). Sequence validation of *GSTA3* mRNAs and proteins was obtained by locating the five amino acid residues that have been identified as key to the activity of the human GST A3-3 enzyme [9,26]. Following this analysis, *GSTA3* mRNA sequences were submitted to NCBI GenBank. Accession numbers for these sequences are given in the Results and Discussion section. Sequence alignments were made with Clustal Omega [27].

Homology modeling of the 3-D structures of the novel GST A3-3 proteins was made using the program MODELLER [28] (version 10.4, University of California San Franscisco, CA, USA) which calculates a model based on the known structure of a homologous protein. The template used was the crystal structure of human GST A3-3 with glutathione and Δ^4-androstene-3,17-dione bound in the active site (PDB code 2vcv). The model of dog GST A3-3, shown in Section 3.4, had the following scores: GA341:1.00; zDOPE: −1.80; Estimated RMSD: 0.894; Estimated Overlap (3.5 Å): 0.950. The structure was depicted in Chimera 1.17.1 [29].

2.2.5. Cloning GSTA3 cDNA in the Bacterial Expression Vector pET-21a(+)

Another set of optimized primers was created for cloning into the bacterial expression vector pET-21a(+) (EMD Millipore; Billerica, MA, USA). For directional in-frame cloning into pET-21a(+), the EcoRI (GAATTC) and XhoI (CTCGAG) restriction sites were added to the 5′ ends of the inside sense and antisense primers, respectively (Table 2). Nested PCR was performed as described in Section 2.2.3. Secondary PCR samples along with the pET-21a(+) vector were digested with EcoRI and XhoI endonucleases. cDNA and plasmid vector DNA purified by electrophoresis on an 0.8% LMT agarose gel were ligated. After transformation, colony growth in broth, and plasmid mini-preparation, the plasmid cDNAs were sequenced with the T7 promoter and the T7 terminator primers (5′-TAATACGACTCACTATAG-3′ and 5′-GCTAGTTATTGCTCAGCGG-3′, respectively). Sequence analysis was as described in Section 2.2.4, and included confirming in-frame insertion of the sense strand sequence into the pET-21a(+) vector for protein expression in bacteria.

2.2.6. Quantitative Reverse Transcription-PCR

Reverse transcription for the 13 female dog tissues and the male testis was performed as described in 2.2.2 except that only 100 ng of RNA was used. Real time PCR was performed in triplicate with 1 µL of 4-fold diluted cDNA, Power SYBR Green PCR Master Mix (Applied Biosystems; Foster City, CA, USA) and GSTA3-specific primers: Sense ACATCCACCTGGTTGAACTTCTCTACT; Antisense CTGGTTTTCAGGGCCTTCAG. The 96-well plates were run on an ABI 7900HT Fast Real Time PCR System for an initial denaturation of 95 °C for 15 s, then 40 cycles of 95 °C denaturation for 15 s and 60 °C annealing and extension for one minute. This was followed by a 20 min dissociation curve to assess the single PCR product's melting temperature. The Cts were averaged for each tissue. Linear values were generated by 2ˆ-("tissue X" Ct- Highest Ct). Linear values presented are relative to the lowest expressor (uterus) set at 1.0.

Table 2. PCR primer sequences (5′–3′) for cloning GSTA3 cDNAs into pET-21a+. Lowercase letters designate the restriction enzyme sites.

Species	Primer Set	Orientation	Sequence
Dog	Outside	Sense	CCAGAGACTACCATGGCGGGGAAGCCCAAG
		Antisense	TCTCAGGAGATTGGCCCTGCATG
	Inside	Sense	gcgaattcATGGCGGGGAAGCCCAAGCTTCACTACTTCAATGG
		Antisense	cgctcgagCTGGGCATCCATTCCTGTTCAGTTAATCCT
Goat	Outside	Sense	AGAACTGCTATTATGGCAGGGAAGCCCAT
		Antisense	TCAAATTTGTCCCAGACAGCCC
	Inside	Sense	gcgaattcATGGCAGGGAAGCCCATTCTTCACTATTTCAATGG
		Antisense	cgctcgagCCCCGCCAGCCGCCAGCTTTATTAAAACTT
Opossum	Outside	Sense	GAATGGAAGATCATGTCTGGGAAGCCCAT
		Antisense	TTGCATTACTTAGAACTCTTCCTGAATATTCAGCT
	Inside	Sense	gcgaattcGGTAAAGAAGATATTCAAGGTTGATGA
		Antisense	cgctcgagTCATCAACCTTGAATATCTTCTTTACC

3. Results

3.1. Alignment of the Cloned GSTA3 mRNA Sequences to Those of Human and Horse GSTA3 mRNAs

Figure 2 shows the alignments of the newly cloned dog, goat, and gray short-tailed opossum *GSTA3* mRNA sequences to the known *GSTA3* mRNA sequences of human (GenBank accession number NM_000847.4), marmoset (XM_002746649), and horse (KC512384.1). As expected, there is a high degree of conservation of the GSTA3 mRNA sequence across all species. The GenBank accession numbers of the newly cloned *GSTA3* cDNAs are KJ766127 (dog), KM578828 (goat), and KP686394 (gray short-tailed opossum). The overall percentages of identical residues at each position were compared pairwise between each *GSTA3* mRNA, and are presented in Table 3. Residue identities declined approximately as expected according to the phylogenetic relationships among the species examined. Compared to the human *GSTA3* mRNA, for example, the marmoset *GSTA3* mRNA has the highest sequence identity to that of the human, with 94% identical bases. The new dog and goat GSTA3 sequences had similar identities to each other and to human and horse GSTA3 mRNA sequences. The *GSTA3* mRNA of the gray short-tailed opossum, the only metatherian representative, showed greater divergence, with identities to the *GSTA3* mRNAs of the five eutherian species examined ranging from 68% to 71% identical bases.

Table 3. The percentages of identical nucleotides at each position between GSTA3 mRNAs of different mammalian species.

	Human	Marmoset	Dog	Horse	Goat	Opossum
Human	100	94	88	85	84	70
Marmoset	94	100	86	86	85	70
Dog	88	86	100	87	87	71
Horse	85	86	87	100	85	70
Goat	84	85	87	85	100	68
Opossum	70	70	71	70	68	100

```
Human       ATGGCAGGGAAGCCCAAGCTTCACTACTTCAATGGACGGGGCAGAATGGAGCCCATCCGG   60
Horse       ATGGCAGTGAAGCCCATGCTTCACTACTTCAATGGACGAGGCCGGATGGAGCCTATCCGG   60
Marmoset    ATGGCCGGGAAGCCCAAGCTTCACTACTTCAATGCACGGGGCAGAATGGAGCCCATCCGG   60
Dog         ATGGCAGTGAAGCCCATGCTTCACTACTTCAATGGACGAGGCAGAATGGAGTCCATCCGG   60
Goat        ATGGCAGGGAAGCCCATTCTTCACTATTTCAATGGACGCGGCAGAATGGAGTGCATTCGG   60
Opossum     ATGGCAGTGAAGCCCATGCTTCACTACTTCAATGGAAGAGGCAGAATGGAATCAGTGCGC   60
            ***** * ********  ******** ******* * * *** * *****     * **

Human       TGGCTCTTGGCTGCAGCTGGAGTGGAGTTTGAAGAGAAATTTATAGGATCTGCAGAAGAT   120
Horse       TGGCTCCTGGCTGCTGCGGGAGTCGAGTTTGAAGAGACATTTATAGACACTCCAGAAGAC   120
Marmoset    TGGCTCTTGGCTGCAGCTGGAGTGGAGTTTGAAGAGCAATTTCTAGAATCTGCAGAAGAT   120
Dog         TGGCTCCTGGCTTCAGCTGGAGTAGAGTTTGAAGAGAAATTTATAAATACTCCAGAAGAC   120
Goat        TGGCTCCTGGCTGCGGCTGGAGTGGAGTTTGAAGAAAAATTTATAGAAAAACCAGAAGGC   120
Opossum     TGGCTCTTGGCAGCTGCTGGAGTCGAGTTTGAAGAAAAGATATTAAAATCAGCTGAAGAT   120
            ****** ****  * ** ***** ***********     *  **       * ****

Human       TTGGGAAAGTTAAGAAATGATGGGAGTTTGATGTTCCAGCAAGTACCAATGGTTGAGATT   180
Horse       TTTGAAAAGCTAAAAAATGATGGGAGTTTGATGTTCCAGCAAGTGCCAATGGTCGAAATT   180
Marmoset    TTGGAAAAGTTAAAAAATGATGGGTATTTAATGTTCCAGCAAGTGCCAATGGTTGAGATT   180
Dog         TTGGATAAATTAAAAAATGATGGAAGTCTGATGTTCCAGCAAGTGCCAATGGTGGAAATT   180
Goat        TTGGATAAGTTAAAAAATGATGGGAGTTTGATGTTCCAGCAAGTGCCAATGGCTGAAATT   180
Opossum     TTTGAAAATTTAGTTAAGGGTGGAAACCTGATGTATCAACAAGTGCCAATGGTTGAAATT   180
            ** *  **  **   ** * ***     * ****  ** ***** *******  ** ***


Human       GATGGGATGAAGTTGGTACAGACCAGAGCCATTCTCAACTACATTGCCAGCAAATACAAC   240
Horse       GATGGGATGAAGCTGGTGCAGAGCAGAGCCATTCTCAACTATGTTGCCGCCAAACACAAC   240
Marmoset    GATGGGATGAAGCTGGTGCAGAGCAGAGCCATTCTCAACTACATTGCCAGCAAATATGAT   240
Dog         GATGGAATGAAGCTGGTACAGACCAGAGCCATTCTCAACTACATTGCCACCAAATACAAC   240
Goat        GATGGGATGAAGCTGGTGCAGACCAGAGCCATTCTCAACTACATTGCCGCCAAACACAAC   240
Opossum     GATGGACTGAACCTGGTACAAACCAGAGCCATCCTGAAGTATATAGCTGCCAAATACAAC   240
            *****  ****  **** ** * ********* ** ** **  * **   **** *  *

Human       CTCTACGGGAAAGACATAAAGGAGAGAGCCCTAATTGATATGTATACAGAAGGTATGGCA   300
Horse       CTCTATGGGAAAGACATCAAGGAGAGAGCCCTGATTGATATGTACATAGAAGGTGTGGCA   300
Marmoset    CTCTATGGGAAAGACATAAAGGAGAGAGCCCTGATTGATATGTATACAGAAGGTATGGCA   300
Dog         CTCTATGGGAAAGACATAAAGGAGAGAGCTCTGATAGATATGTACACAGAAGGTATAGTA   300
Goat        CTCTACGGGAAAGACATGAAGGAGAGAGCCCTGATTGATATGTACTCAGAGGGTGTGGCA   300
Opossum     TTGTATGGGAAGGACCTGAAGGAGAAAGCTCTGATTGACATGTATGTGGAAGGGATGAGA   300
             * ** ***** *** * ******* *** ** ** ** *****    ** **  *   *

Human       GATTTGAATGAAATGATCCTTCTTCTGCCCTTATGTCGACCTGAGGAAAAAGATGCCAAG   360
Horse       GATTTGAATGAAATGATCCTGCTTTTACCCATAACCCCACCTGCTGAAAAAGATGCTAAG   360
Marmoset    GATTTGTATGAAATGATCCTTCTTCTGCCCTTATGCCGACCTGAGGAAAAAGACACCAAG   360
Dog         GATTTGAATGAAATGATCATGGTTTTGCCTCTATGCCCACCTGATCAAAAAGATGCCAAG   360
Goat        GATTTGGGTGAAATGATCATGCATTTGCCACTGTGCCCACCTGCTGAAAAAGACGCCAAG   360
Opossum     GATCTGAATGAAATGATCATGTACTACCCACTGTGTTATCCTGGAGAAGAGGAAAAGAAC   360
            *** **  ********** *       **  *       ****   ** * **    **
```

Figure 2. *Cont.*

```
Human         ATTGCCTTGATCAAAGAGAAAACAAAAAGTCGCTATTTCCCTGCCTTCGAAAAAGTGTTA   420
Horse         ATTATGCTGATCAAAGACAGAACAACAAATCGTTATTTGCCTGCGTTTGAAAAAGTGTTA   420
Marmoset      ATTGCCTTGATCCAAGAGAAAACAAAAAATCGCTATTTCCCTGCCTTCGAAAAAGTGTTA   420
Dog           ATTACTCTGATCAGAGAGAGAACAACAGATCGTTATCTCCCCGTGTTTGAAAAAGTGTTA   420
Goat          CTGACCCTAATCCGAGAAAAGACAACAAACCGTTATCTCCCTGCATTTGAAAATGTGCTG   420
Opossum       CTCAACTTCATCCTGGAGAGAGCCACTGAAAGATTCTTCCCAGTGTATGAGAAGGCTTTA   420
                *     * ***   ** *   * *       * *   * ** *  *  ** ** *   *

Human         CAGAGCCATGGACAAGACTACCTTGTTGGCAACAAGCTGAGCCGGGCTGACATTAGCCTG   480
Horse         AAGAGCCACGGAGAAGACTATCTGGTTGGAAACAGGCTGAGCAGGGCTGACATCCACCTG   480
Marmoset      AAGAGCCACGAACAAGACTACCTTGTTGGCAACAAGCTGAGCCGGGCTGACATTCAGCTG   480
Dog           AAGAGCCATGGACAAGACTACCTTGTTGGCAACAAGCTGAGCAGGGCTGACATTCACCTG   480
Goat          AAGAGCCACGGACAAGACTACCTGGTGGGCAACAAGCTGAGCAGGGCTGACATCCACCTG   480
Opossum       AAAAGTCATGGGAAAAATTATCTTGTTGGCAACCAGATGAGCTGGGCAGATATACAGCTG   480
                * ** ** *   ** * ** ** ** ** ***  * ***** **** ** **    ***

Human         GTGGAACTTCTCTACTATGTGGAAGAGCTTGACTCCAGCCTTATCTCCAACTTCCCTCTG   540
Horse         GTGGAACTTCTCTACCTTGTTGAAGAGCTTGACCCCAGCCTTCTGACCAACTTCCCTCTG   540
Marmoset      GTGGAACTTCTCTACTTTGTGGAAGAGCTTGACCCCAGCCTTATCTCCAGCTTCCCTCTG   540
Dog           GTTGAACTTCTCTACTATGTGGAAGAGCTTGACTCCAGCCTTCTGGCCAACTTCCCTCTG   540
Goat          GTTGAACTTCTCTACTATGTGGAAGAGCTGGACCCTAGCCTTTTGGCCAGCTTCCCTCTG   540
Opossum       TTTGAAGCCATCCTAATGGTTGAAGAATTAAAGTCGGATATTCTCTCTGCATTCCCTAAA   540
                * ***    **       ** *****  *  *  *     ** *  *    ******

Human         CTGAAGGCCCTGAAAACCAGAATCAGCAACCTGCCCACGGTGAAGAAGTTTCTACAGCCT   600
Horse         CTGAAGGCCCTGAAAGCCAGAATCAGCAACCTGCCCACCGTGAAGAAGTTTCTGCAGCCT   600
Marmoset      CTGCAGGCCCTGAAAACCAGAATCAGCAACCTGCCCACGCTGAAGAAGTTTCTGCAGCCT   600
Dog           CTGAAGGCCCTGAAAACCAGAGTCAGCAATCTCCCCACCGTGAAGAAGTTTCTGCAGCCT   600
Goat          CTGAAGGCCCTAAAAGCCAGAGTCAGCAATCTCCCGGCCGTGAAGAAGTTTCTGCAGCCC   600
Opossum       CTGCAGGAGTTCAAAGCTAGAATGAGCAAACTCCCCAGCATTCAGAAATTCCTTCAGCCT   600
              *** ***   * *** * *** * ***** ** **     *  **** ** ** *****

Human         GGCAGCCCAAGGAAGCCTCCCGCAGATGCAAAAGCTTTAGAAGAAGCCAGAAAGATTTTC   660
Horse         GGTGGGGCGAGGAAGCCTCCAGGGGATGAGAAATCTGTAGAAAAGTCAAGGAAGATTTTC   660
Marmoset      GGCAGCCCAAGGAAGCCTCCTACAAATGCGAAATCTGTAGAAGAAGCAAGGAAGATTTTC   660
Dog           GGCAGCCCAAGGAAGCCTCCCTTGGATGAGAAAAGTTTAGAGCAAGCGAAGAAGATTTTC   660
Goat          GGTAGCCAGAGGAAGCCTCCCACGGACGAGAAAAAAATAGAAGAAGCCAGGAGGGCTTTC   660
Opossum       GGCAGTCAAAGAAAAGCAAAAATGGATGGCAAAAATCTTGCAGAGGCAAAGAAGATATTC   660
              **  *    ** **  *        * *  ***    * *   *  * *  * *   ***

Human         AGGTTTTAA---          669
Horse         AAGTTTTGA---          669
Marmoset      AAGTTTTAA---          669
Dog           AGGATTAACTGA          672
Goat          AAGTTTTAA             669
Opossum       AAGTTTGAATGA          672
```

Figure 2. Aligned nucleotide sequences of the coding regions of *GSTA3* mRNAs from selected species including those from three reference species: Human (*Homo sapiens;* NM_000847.4), horse (*Equus caballus;* KC512384.1), and marmoset (*Callithrix jacchus*; XM_002746649), and those cloned from testes and sequenced in the present study: dog (*Canis lupus familiaris;* KJ651954), goat (*Capra hircus;* KM578828), and opossum (*Monodelphis domestica;* KM977823). Start and stop codons are identified in bold green and red type, respectively, and codons for the critical H-site (steroid binding) amino acids are highlighted. Asterisks under the alignment indicate conserved nucleotides across all six species.

3.2. Alignment of the Predicted GSTA3 Protein Sequences from Six Mammals

The amino acid sequences of the GSTA3 proteins were inferred from the cloned *GSTA3* mRNA sequences. They are aligned with the human and horse GSTA3 protein sequences (GenBank accession numbers NP_000838.3 and AGK36275.1, respectively) in Figure 3.

One-hundred ten (110) of the 222 total amino acid positions (50%) had identical residues across the GSTA3 proteins of all six species. Similarly, 56 positions (25%) had highly similar residues and 11 positions had less similar residues (5%) within the six species' GSTA3 proteins. The rest of the residue positions (44 or 20%) were not similar across all six GSTA3 proteins. The conservation of amino acid residues between GSTA3 proteins of different species appears to be fairly consistent across the length of the proteins. The percentage of identical amino acids in the various positions was calculated between pairs of aligned GSTA3 protein sequences of all species (Table 4). The degrees of conservation of the new dog and goat GSTA3 protein sequences to each other and to human, marmoset, and horse GSTA3 proteins were similar. The opossum GSTA3 protein exhibited weaker conservation compared to the GSTA3 proteins of the eutherian species.

```
Human          MAGKPKLHYFNGRGRMEPIRWLLAAAGVEFEEKFIGSAEDLGKLRNDGSLMFQQVPMVEI   60
Horse          MAVKPMLHYFNGRGRMEPIRWLLAAAGVEFEETFIDTPEDFEKLKNDGSLMFQQVPMVEI   60
Marmoset       MAGKPKLHYFNARGRMEPIRWLLAAAGVEFEEQFLESAEDLEKLKNDGYLMFQQVPMVEI   60
Dog            MAVKPMLHYFNGRGRMESIRWLLASAGVEFEEKFINTPEDLDKLKNDGSLMFQQVPMVEI   60
Goat           MAGKPILHYFNGRGRMECIRWLLAAAGVEFEEKFIEKPEGLDKLKNDGSLMFQQVPMAEI   60
Opossum        MAVKPMLHYFNGRGRMESVRWLLAAAGVEFEEKILKSAEDFENLVKGGNLMYQQVPMVEI   60
               ** ** *****.***** :*****:******* :: . *.: :* :.* **:*****.**

Human          DGMKLVQTRAILNYIASKYNLYGKDIKERALIDMYTEGMADLNEMILLLPLCRPEEKDAK   120
Horse          DGMKLVQSRAILNYVAAKHNLYGKDIKERALIDMYIEGVADLNEMILLLPITPPAEKDAK   120
Marmoset       DGMKLVQSRAILNYIASKYDLYGKDIKERALIDMYTEGMADLYEMILLLPLCRPEEKDTK   120
Dog            DGMKLVQTRAILNYIATKYNLYGKDIKERALIDMYTEGIVDLNEMIMVLPLCPPDQKDAK   120
Goat           DGMKLVQTRAILNYIAAKHNLYGKDMKERALIDMYSEGVADLGEMIMHLPLCPPAEKDAK   120
Opossum        DGLNLVQTRAILKYIAAKYNLYGKDLKEKALIDMYVEGMRDLNEMIMYYPLCYPGEEEKN   120
               **:***:****:*:*:*::*****:**:****** **: ** ***:  *:  * ::: :

Human          IALIKEKTKSRYFPAFEKVLQSHGQDYLVGNKLSRADISLVELLYYVEELDSSLISNFPL   180
Horse          IMLIKDRTTNRYLPAFEKVLKSHGEDYLVGNRLSRADIHLVELLYLVEELDPSLLTNFPL   180
Marmoset       IALIQEKTKNRYFPAFEKVLKSHEQDYLVGNKLSRADIQLVELLYFVEELDPSLISSFPL   180
Dog            ITLIRERTTDRYLPVFEKVLKSHGQDYLVGNKLSRADIHLVELLYYVEELDSSLLANFPL   180
Goat           LTLIREKTTNRYLPAFENVLKSHGQDYLVGNKLSRADIHLVELLYYVEELDPSLLASFPL   180
Opossum        LNFILERATERFFPVYEKALKSHGKNYLVGNQMSWADIQLFEAILMVEELKSDILSAFPK   180
               : :* ::::..*::*.:*:.*:** ::******::* *** *.* :  ****. .::: **

Human          LKALKTRISNLPTVKKFLQPGSPRKPPADAKALEEARKIFRF-   222
Horse          LKALKARISNLPTVKKFLQPGGARKPPGDEKSVEKSRKIFKF-   222
Marmoset       LQALKTRISNLPTLKKFLQPGSPRKPPTNAKSVEEARKIFKF-   222
Dog            LKALKTRVSNLPTVKKFLQPGSPRKPPLDEKSLEQAKKIFRIN  223
Goat           LKALKARVSNLPAVKKFLQPGSQRKPPTDEKKIEEARRAFKF-   222
Opossum        LQEFKARMSKLPSIQKFLQPGSQRKAKMDGKNLAEAKKIFKFD  223
               *: :*:*:*:**:::******. **   : * : :::: *::
```

Figure 3. Aligned amino acid sequences for GSTA3 of all six species investigated including those used as references (translations of GenBank sequences in Figure 2). The critical amino acids for steroid isomerase activity of the human enzyme are highlighted. Symbols below the alignment: "*" identical residues, ":" similar residues, "." conservation of residues with weakly similar properties in all six species GSTA3 proteins.

Table 4. The percentages of identical amino acids at each position between GSTA3 proteins of different mammalian species.

	Human	Marmoset	Dog	Horse	Goat	Opossum
Human	100	88	85	81	81	64
Marmoset	88	100	79	82	79	63
Dog	85	79	100	81	83	62
Horse	81	82	81	100	82	61
Goat	81	79	83	82	100	62
Opossum	64	63	62	61	62	100

3.3. Conservation of Amino Acids Critical for Steroid Isomerase Activity and Binding of the Cofactor Glutathione

H-site residues for steroid binding, as well as G-site residues for glutathione binding, occur throughout the length of the GSTA3 primary structure (Figure 3). The G-site residues for binding the cofactor glutathione in human GSTA3 are Tyr9, Arg15, Arg45, Gln54, Val55, Pro56, Gln67, Thr68, Asp101, Arg131, and Phe220 [15]. Compared to human proteins, the G-site residues were identical or conservatively changed among the GSTA3 proteins of the five other species we examined, with the exception of Arg45 or Lys45, replaced by Ile45 in the opossum enzyme (Figure 3). Most of the H-site residues are nearly identical across all of the species. The five critical amino acids were defined as having high ketosteroid isomerase activity in the human GSTA3-3 homodimeric enzyme, compared to the low activity of human GST A2-2 [9], and are marked with "*" in Table 5 column 1. These are identical or similar to the human GST A3-3 residues in the three new sequences, with the exception of more bulky residues in position 208. Table 5 shows the H-site residues in the GSTA enzymes expressed in pig ("GST A2-2" in [10]) and bovine ("GST A1-1" in [24]) steroidogenic tissues and comparisons against the ketosteroid isomerase activities of equine and human GSTA3-3 enzymes [15]. (The pig enzyme was the second porcine GST characterized and was therefore named GST A2-2 in spite of being the functional equivalent of human GST A3-3 [10]). Both pig GSTA2-2 and bovine GSTA1-1 enzymes are similar to the dog, goat, and opossum enzymes in having more bulky residues at position 208 than do the human and equine GSTA3-3 enzymes. This may be part of the reason that the pig and bovine enzymes show 27% and 0.38% of the equine GST A3-3 activity with the substrate Δ^5-androstene-3,17-dione, respectively [10]. The divergent residues in position 108 of the dog, goat, and opossum GST A3-3 and the bovine GST A1-1 proteins are probably also relevant to isomerase activities based on the modeled structure.

Table 5. Conservation of H-site residues involved in steroid isomerization across GSTA3 proteins of different mammalian species. The residues marked by "*" in column 1 were experimentally determined to be critical for the steroid isomerase activity of the human GSTA3 protein [9]. Identical amino acids at human GSTA3 residue positions are highlighted. Pig and cattle data are from [10,24] and GenBank accession numbers NP_999015.2 and NP_001071617.1, respectively.

Residue	Human	Marmoset	Horse	Dog	Goat	Opossum	Pig	Cattle
10 *	F	F	F	F	F	F	F	F
12 *	G	A	G	G	G	G	G	G
14	G	G	G	G	G	G	G	G
107	L	L	L	M	M	M	L	M
108	L	L	L	V	H	Y	L	H
110	P	P	P	P	P	P	P	P
111 *	L	L	L	L	L	L	L	L
208 *	A	T	G	L	T	M	T	T
213	L	V	V	L	I	L	L	I
216 *	A	A	S	A	A	V	A	A
220	F	F	F	F	F	F	F	F
222	F	F	F	I	F	V	F	F

3.4. Modeling the Structures of the Newly Described GST A3 Sequences

The crystal structure of human GST A3-3 in complex with Δ^4-androstene-3,17-dione has been determined [30] and was used to model the structures of the homologous novel GST proteins. All GST A3-3 proteins appear to fold in a similar manner, and could possibly accommodate the steroid substrate in a productive binding mode without major clashes with the H-site residues. The dog GST model shows the most favorable interactions with the steroid. The high-activity human and equine GST A3-3 enzymes have smaller residues in position 208, Ala208 and Gly208, respectively (Table 5). The modeled opossum GST A3-3 enzyme indicates that its Met208 clashes with the steroid, unless the overlap can be avoided by a rotation of the Met sidechain. The goat GST A3-3 has Thr208 in this highly variable

position, and this residue is smaller than Leu208 in the dog enzyme. It is noteworthy that all H-site residues of goat GST A3-3 are identical with those of the cattle enzyme (Table 5). The latter has been expressed and displays a very low steroid isomerase activity [24], possibly indicating low activity for the goat enzyme as well. On the basis of the modeling using the high-activity human GST A3-3 in complex with androstenedione [30], the dog GST A3-3 appears as the most likely one to have steroid isomerase activity of the three new enzymes (Figure 4). In comparing the H-site residues of the human GST A3-3 to the corresponding dog residues, all but four are identical between the two proteins. Ala208 in the human enzyme is replaced by the larger Leu208 in the dog enzyme, which may interfere with the D-ring of the steroid substrate. The highly active horse GST A3-3 features the smallest residue Gly208 (Table 5). The replacement of Leu108 by Val108 is presumably without consequence, since the sidechain points away from the steroid. Substitutions of Leu107 by Met107 and the C-terminal Phe222 by Ile222 are probably compatible with the binding of the steroid substrate since the sidechains are flexible. In summary, the nature of residue 208 may hamper the activity of the dog enzyme in the steroid isomerase reaction.

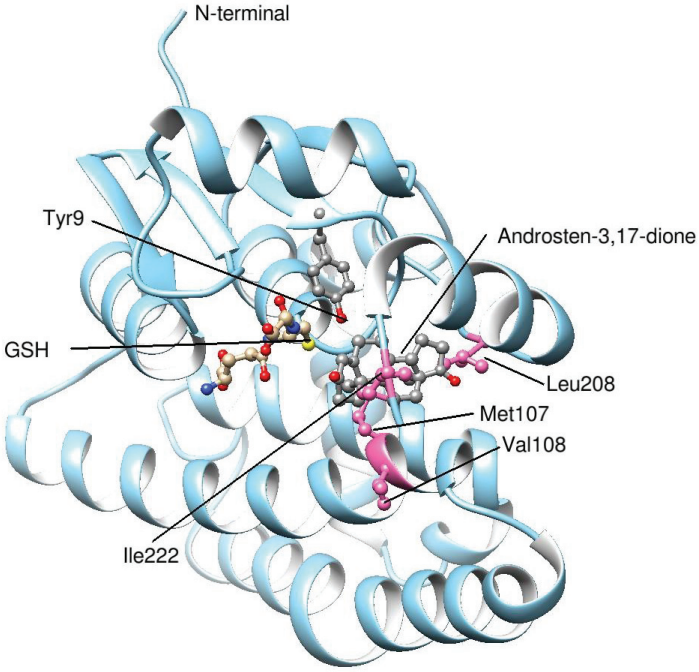

Figure 4. The dog GST A3-3 modeled with Δ^4-androsten-3,17-dione bound in the active site. A homology structure of the dog enzyme was built in the program MODELLER (version 10.4, University of California San Franscisco, CA, USA) and depicted in Chimera 1.17.1 (version 1.17.1, University of California San Franscisco, CA, USA) based on the 85% amino acid sequence identity with the template human GST A3-3. The ligands glutathione and androsten-3,17-dione of the crystal structure of human GST A3-3 (PDB code 2vcv) are superpositioned in corresponding binding sites and the same binding modes in the model of the dog enzyme. In the model the sulfur of glutathione and the oxygen of Tyr9 implicated in the catalytic mechanism of steroid isomerization emerged adjacent to the scissile bonds of C4 and C6 in the androsten-3,17-dione. The four residues in the dog GST A3-3 differing from the corresponding H-site residues in the human enzyme are rendered in pink; the conserved H-site residues were overlapping in the two proteins.

3.5. Expression of Dog GSTA3 mRNA in Dog Tissues

Quantitative reverse transcription-PCR was used to measure the expression of the GSTA3 gene in 14 tissues from adult dogs. The highest expression was found in the liver, which was six-fold greater than levels in testes (Figure 5). The GSTA3 mRNA concentrations in testis were four-fold higher than in the adrenal gland and ovaries. Small intestine and skeletal muscle had GSTA3 gene expression levels similar to gonads. This expression pattern of the dog GSTA3 is quite different than expression in horse tissues, which had the highest levels in testis and adrenal gland, which were four-fold greater than in liver [15].

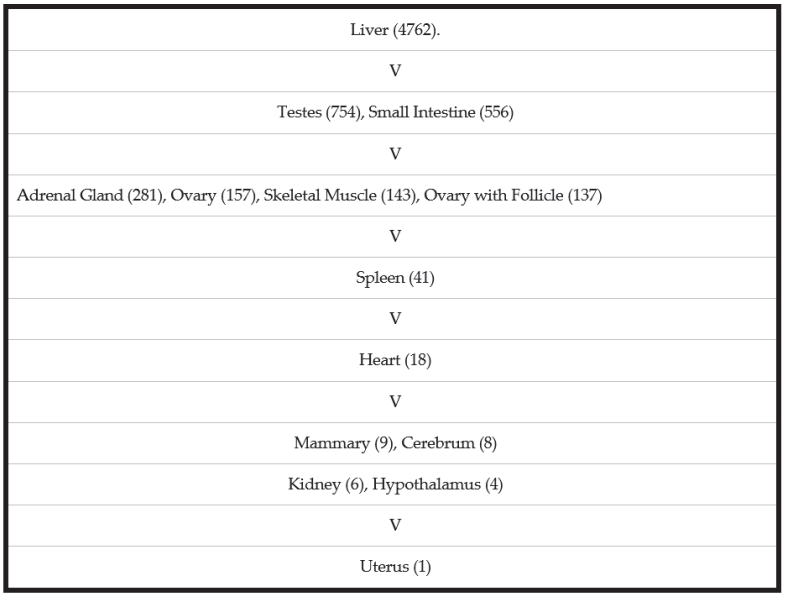

Figure 5. GSTA3 mRNA levels in canine tissues measured by real time quantitative polymerase chain reaction. The lowest value was set to 1.0 with all other values relative to that in order to rank the tissues based on their concentrations. "V" designates a 4-fold or more difference between tissue values above and below.

4. Discussion

Complementary DNA were cloned from *GSTA3* mRNAs in testes from the dog, goat, and gray short-tailed opossum. Given that the sequences of the *GSTA1, GSTA2*, and *GSTA3* mRNAs are highly conserved [10], cloning of *GSTA3* mRNA was difficult, even from testes, which has a distinctively high level of *GSTA3* gene expression [15]. The PCR primers used here were designed to have their 3′ ends bind to codons or untranslated sequences that are unique to the *GSTA3* mRNA. Interestingly, there are no reagents for nucleic acid hybridization or antibody immunodetection that can distinguish *GSTA3* gene products from those of *GSTA1* and *GSTA2* genes, both of which are ubiquitously expressed. The *GSTA3* mRNA can only be specifically amplified using PCR primers, such as those designed here and previously [11,19]. For example, to localize *GSTA3* gene expression to Leydig cells within horse testes, we developed an in situ reverse transcription-PCR protocol that was specific for *GSTA3* mRNA [19].

The human GSTA3-3 homodimeric enzyme has well characterized catalytic efficiency with substrates Δ^5—androstene-3,17-dione and Δ^5—pregnene-3,20-dione, which is second only to the equine GSTA3 enzyme of the six GSTA proteins that have been characterized at the time of this writing [15]. The H-site residues of the GSTA3 proteins are critical for positioning the steroid substrate to undergo the ketosteroid isomerization. The amino acids required for that activity were initially determined experimentally for human GSTA3-3 [9,24].

The human and horse GSTA3 proteins have very high conservation of H-site residues (Table 5). These differ from related GSTA enzymes, such as human GSTA2-2, which have very little activity [15]. When activity data become available for the dog, goat, and opossum enzymes, we may be able to relate enzymatic activity differences to specific amino acids or combinations of them. It will also be instructive to compare the steroid isomerase activities of the newly cloned GSTA3-3 enzymes with those of the bovine [24] and pig [10] cognates of the human GSTA3-3, of which, in particular, the bovine enzyme has significantly lower steroid isomerase activities than the human and horse GSTA3-3 enzymes [15].

As a recently discovered enzyme in steroid hormone biosynthesis, the GSTA3-3 enzyme and its corresponding mRNA sequence lack extensive functional data across species. The mechanism of GSTA3-3 action, and regulation of the *GSTA3* gene, must be more fully characterized in order to better understand the roles they play in steroid hormone biosynthesis and the possible implications of impairment of the enzyme's function. Our work contributes to this objective through identification of the *GSTA3* mRNA coding sequences in multiple species, as well as provision of *GSTA3* clones in the expression vector pET-21a(+), which can deliver GST A3-3 proteins to be evaluated for their activities as steroid isomerases. Evaluation of these enzymes will enable quantitative comparisons of the steroid isomerase activities among the species investigated, and enable further investigation of the effects of endogenous compounds, such as follicle-stimulating hormone, luteinizing hormone, testosterone, estradiol, and glucocorticoids, as well as pharmaceuticals such as phenobarbital or dexamethasone, on expression of the enzyme. For instance, expression of the *GSTA3* gene was down-regulated along with testosterone synthesis in testes of stallions treated with dexamethasone [19,20], whereas in cultured porcine Sertoli cells, follicle-stimulating hormone, testosterone, and estradiol increased *GSTA* gene expression [31]. In addition, inhibitors of the GSTA3-3 enzyme have been identified that may be medically useful for reducing fertility or progression of steroid-dependent diseases [15]. These include the GST A3-3 enzyme inhibitors ethacrynic acid or tributyltin [32], or the small interfering RNAs that reduce *GSTA3* gene expression [18].

5. Conclusions

The three new *GSTA3* mRNA and protein sequences we report extend our comparative knowledge of the GST A3-3 enzymes of diverse mammalian species. Moreover, the information and reagents we have generated will help to facilitate future studies to characterize the GST A3-3 enzymes more generally. In addition, they may augment studies of the regulation of the expression of *GSTA3* genes in steroidogenic and other tissues. Mechanistic data of this kind can enable development of new approaches for manipulating GSTA3-3 enzyme activities in vivo for medical purposes. These could include inducing fertility interruptions in animal species important to humans or developing novel pharmacological treatments for steroid-dependent diseases in humans and other animals. It is essential that the new treatments that are prescribed are both effective and specific. It is, therefore, crucial that researchers continue to investigate steroidogenesis and its regulation in order to generate more complete mechanistic knowledge.

Author Contributions: S.M.H., P.B.S., B.M. and N.H.I. contributed to the conceptualization of the study. S.M.H., P.B.S., H.L., B.M. and N.H.I. contributed to methodology and validation. B.M. and N.H.I. supervised. S.M.H., H.L., B.M. and N.H.I. prepared the original draft. All authors edited and revised the manuscript. All authors have read and agreed to the published version of the manuscript.

Funding: Bengt Mannervik was supported by the Swedish Research Council (grant 2015-04222). The Resource for Biocomputing, Visualization, and Informatics at the University of California, San Francisco was supported by NIGMS P41-GM103311. The APC was funded by Stockholm University.

Institutional Review Board Statement: All animal procedures were approved by the Texas A&M University Institutional Animal Care and Use Committee. Approval code and date: 2009-0209 and 2014-0214.

Data Availability Statement: Experimental data are available from the authors upon request.

Acknowledgments: The authors acknowledge the assistance of John Edwards with tissue collection and helpful discussions with William J. Murphy for the creation of Figure 1.

Conflicts of Interest: The authors declare no conflict of interest.

References

1. Diemern, T.; Hales, D.B.; Weidner, W. Immune-endocrine interactions and Leydig cell function: The role of cytokines. *Andrologia* **2003**, *35*, 55–63. [CrossRef]
2. Payne, A.H.; Hales, D.B. Overview of steroidogenic enzymes in the pathway from cholesterol to active steroid hormones. *Endocr. Rev.* **2004**, *25*, 947–970. [CrossRef]
3. Herrera-Luna, C.V.; Budik, S.; Aurich, C. Gene expression of ACTH, glucocorticoid receptors, 11BHSD enzymes, LH-, FSH-, GH receptors and aromatase in equine epididymal and testicular tissue. *Reprod. Dom. Anim.* **2012**, *47*, 928–935. [CrossRef]
4. Ing, N.H. Steroid hormones regulate gene expression posttranscriptionally by altering the stabilities of messenger RNAs. *Biol. Reprod.* **2005**, *72*, 1290–1296. [CrossRef]
5. Lonard, D.M.; O'Malley, B.W. Nuclear receptor coregulators: Modulators of pathology and therapeutic targets. *Nat. Rev. Endocrinol.* **2012**, *8*, 598–604. [CrossRef]
6. Agular, B.M.; Vinggaard, A.M.; Vind, C. Regulation by dexamethasone of the 3β-hydroxysteroid dehydrogenase activity in adult rat Leydig cells. *J. Steroid Biochem. Mol. Biol.* **1992**, *43*, 565–571. [CrossRef]
7. Conley, A.J.; Bird, I.M. The role of cytochrome P450 17α-hydroxylase and 3ß-hydroxysteroid dehydrogenase in the integration of gonadal and adrenal steroidogenesis via the Δ5 and Δ4 pathways of steroidogenesis in mammals. *Biol. Reprod.* **1997**, *56*, 789–799. [CrossRef]
8. Johansson, A.-S.; Mannervik, B. Human glutathione transferase A3-3, a highly efficient catalyst of double-bond isomerization in the biosynthetic pathway of steroid hormones. *J. Biol. Chem.* **2001**, *276*, 33061–33065. [CrossRef]
9. Johansson, A.-S.; Mannervik, B. Active-site residues governing high steroid isomerase activity in human glutathione transferase A3-3. *J. Biol. Chem.* **2002**, *277*, 16648–16654. [CrossRef]
10. Fedulova, N.; Raffalli-Mathieu, F.; Mannervik, B. Porcine glutathione transferase Alpha 2-2 is a human GST A3-3 analogue catalyzing steroid double-bond isomerization. *J. Biochem.* **2010**, *431*, 159–167. [CrossRef]
11. Larsson, E.; Mannervik, B.; Raffalli-Mathieu, F. Quantitative and selective polymerase chain reaction analysis of highly similar human alpha-class glutathione transferases. *Anal. Biochem.* **2011**, *412*, 96–101. [CrossRef] [PubMed]
12. Calvaresi, M.; Stenta, M.; Garavelli, M.; Altoe, P.; Bottoni, A. Computational evidence for the catalytic mechanism of human glutathione transferase A3-3: A QM/MM investigation. *ACS Catal.* **2012**, *2*, 280–286. [CrossRef]
13. Matsumura, T.; Imamichi, Y.; Mizutani, T.; Ju, Y.; Yazawa, T.; Kawabe, S.; Kanno, M.; Ayabe, T.; Katsumata, N.; Fukami, M.; et al. Human glutathione transferase A (GSTA) family genes are regulated by steroidogenic factor 1 (SF-1) and are involved in steroidogenesis. *FASEB J.* **2013**, *27*, 3198–3208. [CrossRef] [PubMed]
14. Dourado, D.F.A.R.; Fernandes, P.A.; Mannervik, B.; Ramos, M.J. Isomerization of Δ^5-androstene-3,17-dione into Δ^4-androstene-3, 17-dione catalyzed by human glutathione transferase A3-3: A computational study identifies a dual role for glutathione. *J. Phys. Chem. A* **2014**, *31*, 5790–5800. [CrossRef]
15. Lindström, H.; Peer, S.M.; Ing, N.H.; Mannervik, B. Characterization of equine GST A3-3 as a steroid isomerase. *J. Steroid Biochem. Mol. Biol.* **2018**, *178*, 117–128. [CrossRef]
16. Mannervik, B.; Ismail, A.; Lindström, H.; Sjödin, B.; Ing, N.H. Glutathione transferases as efficient ketosteroid isomerases. *Front. Mol. Biosci.* **2021**, *8*, 765970. [CrossRef]
17. Islam, M.Q.; Platz, A.; Szpirer, J.; Szpirer, C.; Levan, G.; Mannervik, B. Chromosomal localization of human glutathione transferase genes of classes Alpha, Mu and Pi. *Hum. Genet.* **1989**, *82*, 338–342. [CrossRef]
18. Raffalli-Mathieu, F.; Orre, C.; Stridsberg, M.; Edalat, M.; Mannervik, B. Targeting human glutathione transferase A3-3 attenuates progesterone production in human steroidogenic cells. *Biochem. J.* **2008**, *414*, 103–109. [CrossRef]
19. Ing, N.H.; Forrest, D.W.; Riggs, P.K.; Loux, S.; Love, C.C.; Brinsko, S.P.; Varner, D.D.; Welsh, T.H., Jr. Dexamethasone acutely down-regulates genes involved in steroidogenesis in stallion testes. *J. Steroid Biochem. Mol. Biol.* **2014**, *143*, 451–459. [CrossRef]
20. Ing, N.; Brinsko, S.; Curley, K.; Forrest, D.; Love, C.; Hinrichs, K.; Vogelsang, M.; Varner, D.; Welsh, T. Dexamethasone acutely regulates endocrine parameters in stallions and subsequently affects gene expression in testicular germ cells. *Anim. Reprod. Sci.* **2015**, *152*, 47–54. [CrossRef]
21. Valdez, R.; Cavinder, C.A.; Varner, D.D.; Welsh, T.W.; Vogelsang, M.M.; Ing, N.H. Dexamethasone downregulates expression of several genes encoding orphan nuclear receptors that are important to steroidogenesis in stallion testes. *J. Biochem. Mol. Toxicol.* **2019**, *33*, e22309. [CrossRef] [PubMed]
22. Shiota, M.; Endo, S.; Blas, L.; Fujimoto, N.; Eto, M. Steroidogenesis in castration-resistant prostate cancer. *Urologic Oncol.* **2023**, *41*, 240–251. [CrossRef]
23. Ismail, A.; Sawmi, J.; Mannervik, B. Marmoset glutathione transferases with ketosteroid isomerase activity. *Biochem. Biophys. Rep.* **2021**, *27*, 101078. [CrossRef]

24. Raffalli-Mathieu, F.; Persson, D.; Mannervik, B. Differences between bovine and human steroid double-bond isomerase activities of Alpha-class glutathione transferases selectively expressed in steroidogenic tissues. *Biochim. Biophys. Acta* **2007**, *1770*, 130–136. [CrossRef] [PubMed]
25. Murphy, W.J.; Foley, N.M.; Bredmeyer, K.R.; Gatesy, J.; Springer, M.S. Phylogenetics and the genetic architecture of the placental mammal radiation. *Annu. Rev. Anim. Biosci.* **2021**, *9*, 29–53. [CrossRef] [PubMed]
26. Kumar, S.; Suleski, M.; Craig, J.M.; Kasprowicz, A.E.; Sanderford, M.; Li, M.; Stecher, G.; Hedges, S.B. TimeTree 5: An expanded resource for species divergence times. *Mol. Biol. Evol.* **2022**, *39*, msac174. [CrossRef] [PubMed]
27. Madeira, F.; Pearce, M.; Tivey, A.R.N.; Basutkar, P.; Lee, J.; Edbali, O.; Madhusoodanan, N.; Kolesnikov, A.; Lopez, R. Search and sequence analysis tools services from EMBL-EBI in 2022. *Nucleic Acids Res.* **2022**, *50*, W267–W279. [CrossRef]
28. Webb, B.; Sali, A. Comparative protein structure modeling using MODELLER. *Curr. Protoc. Bioinform.* **2016**, *54*, 5.6.1–5.6.37. [CrossRef]
29. Pettersen, E.F.; Goddard, T.D.; Huang, C.C.; Couch, G.S.; Greenblatt, D.M.; Meng, E.C.; Ferrin, T.E. UCSF Chimera—A visualization system for exploratory research and analysis. *J. Comput. Chem.* **2004**, *25*, 1605–1612. [CrossRef]
30. Tars, K.; Olin, B.; Mannervik, B. Structural basis for featuring of steroid isomerase activity in Alpha class glutathione transferases. *J. Mol. Biol.* **2010**, *397*, 332–340. [CrossRef]
31. Benbrahim-Tallaa, L.; Tabone, E.; Tosser-Klopp, G.; Hatey, F.; Benamed, M. Glutathione transferase alpha expressed in porcine Sertoli cells is under the control of follicle-stimulating hormone and testosterone. *Biol. Reprod.* **2002**, *66*, 1734–1742. [CrossRef] [PubMed]
32. Škerlová, J.; Ismail, A.; Lindström, H.; Sjödin, B.; Mannervik, B.; Stenmark, P. Structural and functional analysis of the inhibition of equine glutathione transferase A3-3 by organotin endocrine disrupting pollutants. *Environ. Pollut.* **2021**, *268*, 115960. [CrossRef] [PubMed]

biomolecules

MDPI

Article

Potent GST Ketosteroid Isomerase Activity Relevant to Ecdysteroidogenesis in the Malaria Vector *Anopheles gambiae*

Yaman Musdal [1,2], Aram Ismail [1], Birgitta Sjödin [1] and Bengt Mannervik [1,3,*]

[1] Department of Biochemistry and Biophysics, Stockholm University, SE-10691 Stockholm, Sweden; ymusdal@gmail.com (Y.M.); aram.ismail@dbb.su.se (A.I.); birgitta.sjodin@dbb.su.se (B.S.)
[2] Department of Pediatric Genetics, Faculty of Medicine, Hacettepe University, 06230 Ankara, Turkey
[3] Department of Chemistry, Scripps Research, La Jolla, CA 92037, USA
* Correspondence: bengt.mannervik@dbb.su.se; Tel.: +46-(0)70-425-0849

Abstract: Nobo is a glutathione transferase (GST) crucially contributing to ecdysteroid biosynthesis in insects of the orders *Diptera* and *Lepidoptera*. Ecdysone is a vital steroid hormone in insects, which governs larval molting and metamorphosis, and the suppression of its synthesis has potential as a novel approach to insect growth regulation and combatting vectors of disease. In general, GSTs catalyze detoxication, whereas the specific function of Nobo in ecdysteroidogenesis is unknown. We report that Nobo from the malaria-spreading mosquito *Anopheles gambiae* is a highly efficient ketosteroid isomerase catalyzing double-bond isomerization in the steroids 5-androsten-3,17-dione and 5-pregnen-3,20-dione. These mammalian ketosteroids are unknown in mosquitoes, but the discovered prominent catalytic activity of these compounds suggests that the unknown Nobo substrate in insects has a ketosteroid functionality. Aminoacid residue Asp111 in Nobo is essential for activity with the steroids, but not for conventional GST substrates. Further characterization of Nobo may guide the development of new insecticides to prevent malaria.

Keywords: Nobo; *Anopheles gambiae* GSTE8; malaria; ketosteroids; ecdysteroidogenesis

Citation: Musdal, Y.; Ismail, A.; Sjödin, B.; Mannervik, B. Potent GST Ketosteroid Isomerase Activity Relevant to Ecdysteroidogenesis in the Malaria Vector *Anopheles gambiae*. *Biomolecules* **2023**, *13*, 976. https://doi.org/10.3390/biom13060976

Academic Editor: Vladimir N. Uversky

Received: 3 May 2023
Revised: 3 June 2023
Accepted: 9 June 2023
Published: 11 June 2023

1. Introduction

The glutathione transferase (GST) enzyme Nobo is essential to the biosynthesis of the molting hormone ecdysone in the mosquito *Anopheles gambiae*. The mosquito is a prominent vector of *Plasmodium falciparum*, the parasite causing malaria, and several hundred thousand people die from malaria every year. The disease is spread by bites of parasite-carrying mosquitoes, thereby threatening billions of people in >100 countries world-wide. Transmission of the infectious agent is generally prevented by control of the vector by insecticides, mosquito nets, and the elimination of breeding sites [1]. However, the spread of insecticide resistance has led to general agreement that malaria control is in urgent need of novel agents [2].

The proliferation of mosquitoes is critically dependent on the steroid hormone ecdysone, and the GST enzyme called Nobo (encoded by the gene *Noppera-bo*) was first discovered in the fruit fly *Drosophila melanogaster* to be essential for ecdysteroid biosynthesis [3,4]. Nobo is expressed abundantly in the major ecdysone-producing tissues, primarily in the prothoracic gland, but also in the testis and the ovary [4,5]. Nobo knockout *D. melanogaster* presents with embryonic lethality and a naked cuticle structure—phenotypes typical for mutants showing embryonic ecdysteroid deficiency. Furthermore, Nobo knockdown larvae displayed lowered titers of the ultimate hormone 20-hydroxyecdysone. A corresponding Nobo GST has also been discovered in the mosquitoes *Aedes aegypti* and *Culex quinquefasciatus* [4], which, like *An. gambiae*, are important vectors of infectious diseases.

A flavonoid inhibitor of Nobo from *Ae. aegypti* was recently demonstrated to have larvicidal activity, thus supporting the notion that Nobo inhibitors could find use as novel insecticides [6]. Notably, Nobo is present only in dipteran and lepidopteran insects and not

in other life forms including humans [4]. From this perspective, the enzyme is a perfect new target for new preventative and selective insecticides, avoiding collateral toxicity to honeybees and other valuable biological species. In spite of its demonstrated importance for ecdysteroid biosynthesis, the biochemical function of Nobo is unknown. We have initiated investigations of Nobo from the mosquito *An. gambiae*, the major vector of the pathogen *P. falciparum*. A better understanding of the enzymatic properties can form the basis of the discovery and design of potent and selective Nobo inhibitors for use in combating the malaria vector.

2. Materials and Methods

2.1. Materials

The steroids 5-androsten-3,17-dione and 5-pregnen-3,20-dione were purchased from Steraloids Inc. (Newport, RI, USA). All other chemicals were obtained from Sigma-Aldrich (St. Louis, MO, USA).

2.2. Methods

2.2.1. Extracting Plasmid DNA from Filters

DNA coding for Nobo protein XP_319963.1 from *An. gambiae* str. PEST (also known as the enzyme GSTE8) was synthesized by ATUM (Newark, CA, USA). The synthetic gene encodes the same protein sequence as the natural gene AGAP009190-PA located on chromosome 3R. However, alternative codons promoting high-level expression in *Escherichia coli* were used in the synthesis according to ATUM's proprietary algorithms. The gene was ligated into the pD444-SR expression plasmid and delivered on a GF/C glass microfiber filter. Site-specific single-point mutants of Nobo were similarly produced by ATUM via total chemical synthesis of the corresponding genes. The DNA was extracted with 100 µL 10 mM Tris-HCl, pH 7.5, and centrifuged for 1 min at 10,000× g, yielding 90 µL containing the extracted DNA at a concentration of 20 ng/µL.

2.2.2. Transformation of Bacteria

E. coli BL21 (DE3) cells were transformed with 2 µL (40 ng) of the extracted DNA. The cells were kept on ice for 30 min before being heat shocked in a 42 °C water bath for 45 s and then put on ice for 2 min. LB broth (250 µL) was added and the bacteria were grown at 37 °C with shaking for 45 min. The transformed cells were plated on agar with ampicillin (50 µg/mL) and incubated overnight at 37 °C.

2.2.3. Expression and Purification of Recombinant GSTs

An overnight culture was prepared from a colony of transformed bacteria suspended in 50 mL LB medium containing ampicillin (50 µg/mL) and incubated overnight at 37 °C with 200 rpm shaking. A flask of 500 mL expression medium 2 × TY (8 g bacto-tryptone, 5 g yeast extract, 2.5 g NaCl, and 25 mg ampicillin) was inoculated with 5 mL overnight culture and grown at 37 °C, 200 rpm. When OD_{600} reached 0.4, enzyme expression was induced with 0.2 mM isopropyl β-D-1-thiogalactopyranoside and the bacteria were further grown for 3 h at 37 °C. The culture was then centrifuged for 7 min at 7000× *g*. The bacterial pellet was mixed with 10 mL lysis buffer (20 mM sodium phosphate, 20 mM imidazole, 0.5 M NaCl pH 7.4, 0.2 mg/mL lysozyme, and one complete mini tablet of protease inhibitor cocktail) and incubated for 1 h. Finally, the cells were disrupted by sonication and the lysate was centrifuged for 30 min at 27,000× *g*.

The expressed GSTs contained an N-terminal hexahistidine tag, enabling their purification by immobilized metal affinity chromatography (IMAC) using a Ni-IMAC column (GE Healthcare, Uppsala, Sweden). The supernatant fraction from the centrifugation was loaded onto the column equilibrated with binding buffer (20 mM sodium phosphate, 20 mM imidazole, 0.5 M NaCl, pH 7.4), and the column was rinsed with the binding buffer to remove unbound material. An elution buffer (20 mM sodium phosphate, 500 mM NaCl, 250 mM imidazole, pH 7.4) was used to release GST from the column. The eluted

GST was dialyzed two times against 10 mM Tris-HCl, pH 7.8, 1 mM EDTA, and 0.2 mM tris(2-carboxyethyl)phosphine. SDS-PAGE (sodium dodecyl sulfate-polyacrylamide gel electrophoresis) verified the purity of the dialyzed enzyme.

2.2.4. Kinetic Experiments

Enzyme activities were determined with a selection of standard GST substrates [7]. Measurements were performed spectrophotometrically at 30 °C as described in detail previously, including the wavelengths and extinction coefficients used to determine reaction rates [8,9]. However, the assay systems were supplemented with 0.1% (*w/v*) bovine serum albumin, which gave more reproducible measurements. It should be noted that due to limitations of solubility, 5-AD was tested at 0.10 mM, whereas 5-PD was limited to 0.010 mM in the determination of specific activities. The inhibition experiments were performed in 96-well plates at pH 7.5 in 0.1 M sodium phosphate buffer with 1.0 mM DCNB, 5.0 mM glutathione, and 17β-estradiol dissolved in ethanol (5% final concentration in the assay system). Kinetic data were evaluated by nonlinear regression analysis using GraphPad Prism 9.

3. Results

A gene encoding the 217 amino acid sequence of Nobo from *An. gambiae* (also named AgaGSTE8) was synthesized and ligated into a plasmid for expression in *Escherichia coli*. The enzyme purified by Ni-IMAC was estimated as >95% homogeneous by SDS-PAGE. Gel filtration verified the purity of Nobo and showed the molecular mass of approximately 50 kDa expected for a dimeric GST protein.

The catalytic activity of the purified enzyme was assayed with standard GST substrates [10]: two aryl halides, 1-chloro-2,4-dinitribenzene (CDNB) and 1,2-dichloro-4- nitrobenzene (DCNB); cumene hydroperoxide (CuOOH); and two isothiocyanates, phenethyl isothiocyanate (PEITC) and allyl isothiocyanate (AITC). The specific activities with these conventional substrates varied between 0.4 and 25 μmol/min per mg protein in the range common to many GST enzymes (Table 1).

Table 1. Specific activities (μmol/min per mg) of Nobo from *An. gambiae* with alternative GST substrates. Initial reaction rates at 30 °C were determined spectrophotometrically by published procedures. The values are based on triplicate measurements.

Substrate	WT	D111N	S9A	H40N	R116A
CDNB	24.7 ± 3.4	26.2 ± 4.8	1.8 ± 0.2	14.0 ± 0.5	3.3 ± 0.1
DCNB	16.4 ± 1.9	14.7 ± 0.5	0.49 ± 0.03	5.0 ± 0.1	2.34 ± 0.02
CuOOH	5.0 ± 0.5	3.8 ± 0.4	0.05 ± 0.01	0.9 ± 0.1	0.16 ± 0.02
Allyl-ITC	3.3 ± 0.4	3.4 ± 0.5	0.2 ± 0.1	2.7 ± 0.3	2.0 ± 0.2
Phenethyl-ITC	0.4 ± 0.1	1.2 ± 0.3	0.04 ± 0.01	0.34 ± 0.02	0.1 ± 0.04
5-AD	245 ± 8	0.8 ± 0.1	16.0 ± 2.0	69.3 ± 3.7	48.1 ± 1.2
5-PD	49.7 ± 6.1	0.6 ± 0.2	5.3 ± 0.5	23.7 ± 4.1	14.7 ± 1.4

Remarkably, the double-bond isomerase activity with 5-androsten-3,17-dione (5-AD) was 245 μmol/min per mg, significantly higher than the specific activity with any other substrate (Table 1). Similar efficient ketosteroid isomerase catalysis was demonstrated with the alternative steroid substrate 5-pregnen-3,20-dione (5-PD) measured at a 10-fold lower concentration (Table 1). Glutathione was an essential cofactor, although not consumed in the steroid reactions, as earlier demonstrated for mammalian GSTs [11]. Previous studies have identified high double-bond isomerase activity in human [12] and equine GST A3-3 [8], indicating the involvement of GST A3-3 in steroid hormone biosynthesis [13]. A steady-state kinetic analysis of Nobo with 5-AD as the varied substrate determined kcat as 291 ± 6 s^{-1} and kcat/Km as (6.9 ± 0.3) × 10^6 $M^{-1}s^{-1}$.

Modeling of the *An. gambiae* Nobo protein was performed using the homology with the crystal structures of Nobo from *Ae. aegypti* (PDB ID: 7EBW) as well as from *D. melanogaster* (PDB ID: 6KEP). The *An. gambiae* models were highly similar even though the template

sequences between themselves were only 41% identical. The similarities were particularly prominent in the regions of protein secondary structure and in the location of the cofactor glutathione. The second ligand, desmethylglycitein (4′,6,7-trihydroxyisoflavone) in 7EBW and 17β-estradiol in 6KEP, is a polycyclic molecule occupying essentially the same position in the protein structure, juxtaposed to the bound glutathione. Figure 1 shows the *An. gambiae* model derived from 6KEP with the two ligands 17β-estradiol and glutathione superpositioned from the template structure.

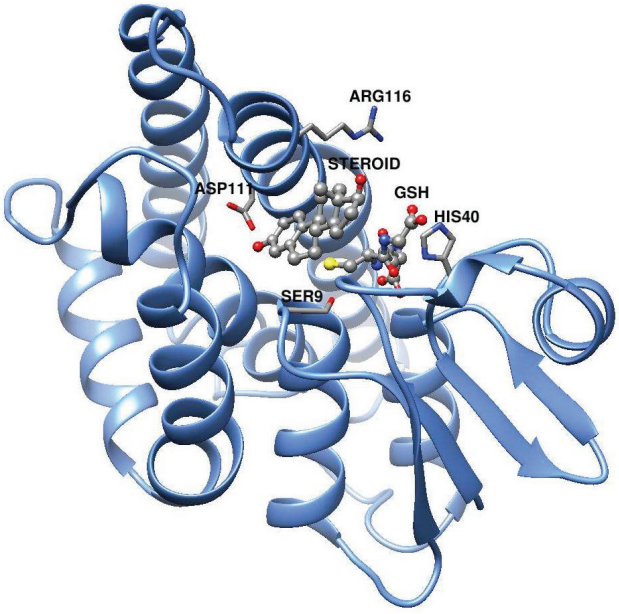

Figure 1. Model of *Anopheles gambiae* Nobo subunit. The structure is based on PDB ID: 6KEP, which is not shown in the picture except for the two ligands 17β-estradiol (steroid) and glutathione (GSH) rendered as ball-and-stick models and colored according to element. The steroid substrates 5-AD and 5-PD have a similar size and overall shape as 17β-estradiol, such that they presumably bind to the same site in Nobo. The functional enzyme is a structural dimer composed of two identical subunits.

Examination of the *An. gambiae* Nobo model suggested four residues of possible importance for catalytic activity: Ser9, His40, Asp111, and Arg116. The following single-point mutants of the enzyme were therefore synthesized: D111N, S9A, H40N, and R116A. In D111N, the acidic Asp is replaced with the isosteric but uncharged Asn, and in H40N His is similarly changed to Asn, which cannot act as an acid–base catalyst. The substitution S9A removes the hydroxyl group of Ser, supposedly forming a hydrogen bond to the sulfur of glutathione bound to the active site [6]. In R116A, removal of the positively charged guanidinium group of Arg prevents the formation of an ionic bond with a carboxyl group of glutathione. All mutant proteins expressed appeared properly folded and the purified mutant enzymes were tested with the alternative substrates (Table 1).

Notably, the D111N mutation did not markedly change the specific activities with the conventional GST substrates. However, the ketosteroid isomerase activity was dramatically diminished by two orders of magnitude with both 5-AD and 5-PD. The mutation S9A decreased the activity with most substrates by 10- to 20-fold, but 100-fold with CuOOH (Table 1). The mutations H40N and R116A clearly reduced the activities with the ketosteroids, aryl halides, and with CuOOH, but had only a small effect on the isothiocyanate reactions.

In previous studies on Nobo from *D. melanogaster* and *Ae. aegypti*, 17β-estradiol was found to be an inhibitor of the enzyme, demonstrating an affinity for steroids [6,14].The Nobo

from *An. gambiae* was likewise inhibited by estradiol with an IC_{50} value 0.17 ± 0.03 μM (Figure 2). Notably, the D111N mutant was significantly less sensitive to the inhibitor, showing an IC_{50} value of 15.5 ± 6.0 μM.

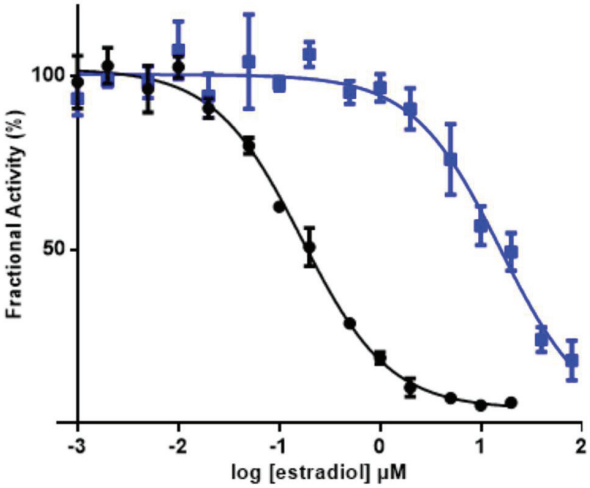

Figure 2. Inhibition of Nobo from *An. gambiae* with 17β−estradiol. Comparison of wild-type (black dots) with mutant Asp111Asn (blue squares) enzyme using 1 mM DCNB and 5 mM glutathione as substrates and varied 17βestradiol concentrations at pH 7.5. Measurements were carried out in triplicate at 30 °C.

Nobo Is an Efficient Ketosteroid Isomerase

The bacterial ketosteroid isomerase is among the most efficient of all enzymes known, with a specific activity of the *Pseudomonas testosterone* enzyme reported as 45,300 μmol/min per mg and the catalytic efficiency kcat/Km 1.58 × 10^8 $M^{-1}s^{-1}$ [15], approaching the diffusion limit of enzyme reactions [16]. The corresponding values for *An. gambiae* Nobo, 245 μmol/min per mg and 6.9 × 10^6 $M^{-1}s^{-1}$, are significantly lower, but the mosquito enzyme still qualifies for the upper echelon of highly active enzymes [17]. The requisite in Nobo for the obligatory glutathione in the active site may limit the catalytic turnover as compared with the bacterial ketosteroid isomerase, which is lacking a cofactor. The steroids 5-AD and 5-PD, shown to be excellent substrates of Nobo, are not intermediates in insect ecdysteroidogenesis, but by mechanistic analogy their efficient isomerization suggests that the enzyme catalyzes a similar reaction in the "black box" of ecdysone biosynthesis [18]. The finding that glutathione is required for ecdysteroidogenesis [19] lends further support to the notion that the glutathione-dependent Nobo fulfills a catalytic role in the biological context.

The modeling of *An. gambiae* Nobo based on the crystal structures of the homologous enzymes from *Ae. aegypti* and *D. melanogaster* demonstrates that 5-AD (or 5-PD) can fit in an active site pocket apparently reaching the carboxyl group of Asp111 (Figure 1). A corresponding carboxylate (Asp113 in *D. melanogaster* and Glu113 in *Ae. aegypti*) is considered a salient and conserved signature feature of all 21 identified Nobo GSTs in *Diptera* and *Lepidoptera* [14]. In the *D. melanogaster* Nobo, binding of 17β-estradiol occurs via its 3-hydroxyl group to Asp113 in the conserved site [14], but binding affinity is lost upon the mutation of Asp113 into Ala, which eliminates the carboxylate responsible for hydrogen bonding. Our demonstration that the D111N mutation in *An. gambiae* Nobo causes a 100-fold loss of affinity for 17β-estradiol as indicated by the increased IC50 indicates a corresponding interaction with the inhibitor (Figure 2). We propose that Asp111 makes a similar bond to the 3-keto group of the ketosteroid substrate, thereby promoting the formation of a dienolate intermediate (Figure 3). The thiolate group of glutathione

bound to Nobo is stabilized by hydrogen bonding to Ser9, like in other GSTs featuring Ser in the active site [20]. The activated thiolate close to the steroid in the active site could serve as a base and abstract a proton from the C4 position, as previously shown in the mammalian GST A3-3 [21].

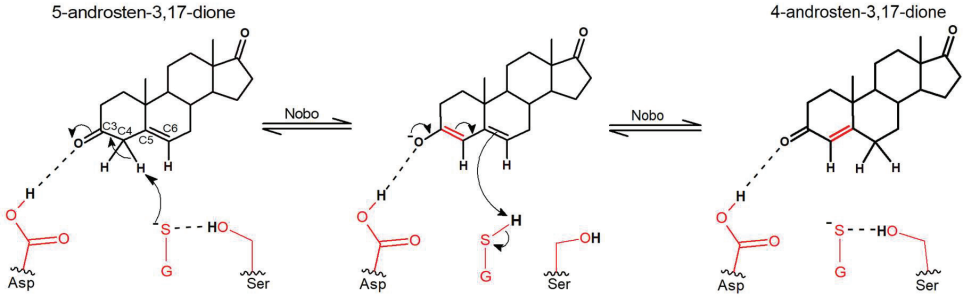

Figure 3. Proposed reaction mechanism of Nobo from *An. gambiae* in the double-bond isomerization of 5-androsten-3,17-dione. Asp111 in a steroid-binding pocket is polarizing the carbonyl group in the C3 position of the substrate. Ser9 is stabilizing the thiolate of glutathione (GSH), which serves as a base abstracting a proton from the C4 position.

The reaction is then completed by addition of a proton to C6 in the steroid. The substantial loss of ketosteroid isomerase activity effected by mutations D111N and S9A in *An. gambiae* Nobo are consistent with these proposed functions of the active-site residues (Table 1). The modeled structure indicates that His40 could contribute to the binding of glutathione by interacting with the C-terminal carboxylate group of the tripeptide. Arg116 is located at the other side of the same carboxylate and near the orifice of the proposed binding site of the steroid substrate, and like His40 is distant from the residues directly involved in catalysis. Thus, the H40N and R116A mutations remote from the site of chemical transitions in the steroid substrate only modestly diminish the catalytic activity.

Our proposed mechanism for Nobo in the steroid double-bond isomerization is similar to the bacterial ketosteroid isomerase reaction by invoking a carboxylate, which polarizes C=O in position C3 of the steroid substrate [22]. Like in the mammalian GSTs with steroid isomerase activity [23], the glutathione thiolate in Nobo serves as the base attacking the C4 hydrogen. In other respects, the enzymes differ in functional groups even though they catalyze the same isomerization reaction. The primary structures of the Nobo proteins and the mammalian GSTs segregate into widely separated evolutionary clades [14], and neither of them shows any structural relationship to the bacterial ketosteroid isomerase.

4. Discussion

Every year more than half a million people die of malaria and other diseases whose pathogenic agents are spread by mosquito bites. The most severe form of human malaria is caused by *P. falciparum*, which is transmitted by mosquitoes of the *Anopheles* genus, and the disease is endemic in 76 countries. The transmission of pathogens is largely prevented by controlling vector populations by spraying insecticides, the use of impregnated mosquito nets, and the elimination of breeding sites. Malaria control relies heavily on insecticides via indoor residual spraying and long-lasting insecticidal bed nets targeting the principal African vector *An. gambiae*. However, both resistance and climate change threaten to reverse the progress made by insecticidal mosquito control in recent years. Disappointingly, the WHO reports that resistance of the *Anopheles* vectors has emerged against the four main insecticide classes used for mosquito control, i.e., pyrethroids, organochlorines, carbamates, and organophosphates [1]. Malaria vectors are able to resist the actions of insecticides due to various resistance mechanisms, including target site mutations, cuticular modification, and metabolic inactivation. The latter occurs by the selection of mosquitoes with upregulated

or more efficient endogenous insecticide detoxifying enzymes. Obviously, novel means to combat the *Anopheles* vectors transmitting the deadly pathogen are in urgent demand [24].

GSTs are ubiquitous and abundant proteins performing a wide range of enzymatic and non-enzymatic functions [25]. In insects, GSTs form an important detoxication system comprising numerous enzymes involved in the metabolism of a wide range of foreign and endogenous compounds [26]. GSTs play an essential role in insect herbivory through the detoxification of deterrent and toxic plant allelochemicals. Research on GSTs in insects was initially motivated by their plausible involvement in insecticide resistance [27], since elevated GST activity had been detected in strains of insects that are resistant to organophosphates and organochlorines [28]. Insect GSTs have been divided into six classes of cytosolic enzymes: Delta, Epsilon, Omega, Sigma, Theta, and Zeta [29]. In addition, membrane-bound insect GSTs exist, similar to mammalian MAPEG proteins [30]. Members of the Delta- and Epsilon-class GSTs have been associated with the detoxication of various chemicals, including DDT, an insecticide used in indoor residual spraying. The *An. gambiae* GST Nobo in the present investigation (also called GSTE8 [2]) belongs to the Epsilon class and its orthologs in *D. melanogaster* and *Ae. aegypti* are designated GSTE14 and GSTE8, respectively. It is noteworthy that neither Delta nor Epsilon GSTs are present in humans and other mammals or in plants.

Ecdysone is a steroid that serves as a master regulator in the control of development, involving molting, metamorphosis, and diapause, in ecdysozoan animals, which encompass insects and nematodes [18]. Following its synthesis, the ecdysone molecule is distributed to various tissues, where it is hydroxylated to form 20-hydroxyecdysone. Transcriptional gene regulation is effected by the binding of 20-hydroxyecdysone to a cognate nuclear receptor in target tissues. The biosynthesis of ecdysone originates in dietary cholesterol, and the accepted biosynthetic pathway is initiated by the 7,8-dehydrogenation of cholesterol and is terminated by a series of reactions catalyzed by different cytochrome P450 (Halloween) enzymes, leading to ecdysone and finally 20-hydroxyecdysone. In between, a number of chemical transformations take place, which remain partly unknown (black box in Figure 4).

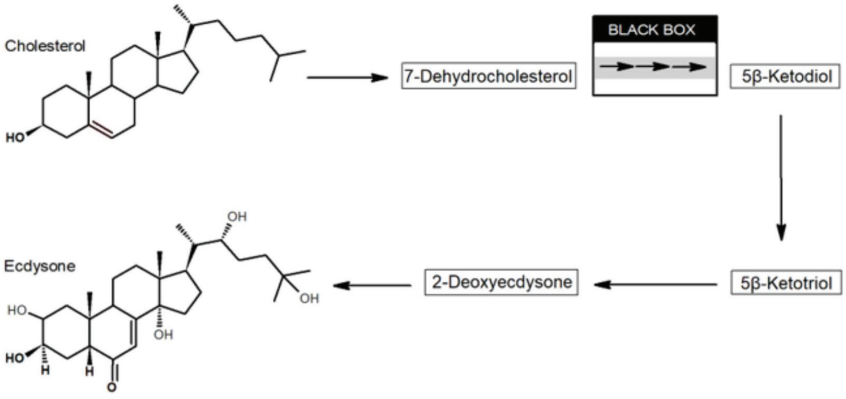

Figure 4. Biosynthetic pathway leading from cholesterol to the hormone ecdysone in insects. Established intermediates are indicated in boxes, whereas the black box includes several unidentified reactions and implicates the cytochrome P450 enzymes CYP6T3, CYP307A1, and CYP307A2 [31,32].

Following the dehydrogenation of cholesterol leading to 7-dehydrocholesterol (7dC), it has been hypothesized that reactions in the black box involve oxidation of the C3 hydroxyl group in 7dC to yield 3-oxo-7dC (cholesta-5,7-diene-3-one), which may undergo double-bond isomerization to cholesta-4,7-diene-3-one [31]. Both 3-oxo-7dC isomers are unstable, but it has been demonstrated that photosensitive, ketone-blocked derivatives release 3-oxo-7dC upon irradiation with UV light of a wavelength that is innocuous to the insect. Administered in vivo by this photolytic approach, 3-oxo-7dC is efficiently in-

corporated into ecdysteroids by both *D. melanogaster* and the tobacco hornworm moth *Manduca sexta* [31]. The three reactions leading from 5β-ketodiol to ecdysone are catalyzed by known cytochrome P450 enzymes present in the prothoracic gland. Ecdysone is released into the hemolymph and oxidized to 20-hydroxyecdysterone in peripheral tissues [32].

In 2014, two research groups identified the gene product of *Noppera-bo* as GSTE14 in *D. melanogaster* [3,4]. Like Halloween cytochrome P450 gene knockouts, null alleles of *Noppera-bo* result in embryonic lethality, embryonic cuticle abnormalities, and decreased ecdysteroid concentrations. Curiously, administration of either cholesterol or 20-hydroxyecdysterone rescues the phenotype, leaving the role of the enzyme Nobo (GSTE14) and the effect of knockdown of the gene unexplained. Niwa and coworkers have identified orthologous GSTs of the Epsilon class in numerous insects, but the presence of these orthologs is limited to the orders *Diptera* and *Lepidoptera* [14].

In addition to the well-established roles of ecdysteroids in metamorphosis and molting, recent investigations further demonstrate the crucial importance of ecdysone signaling for the insect proliferation [33]. For mosquitoes in particular, both oogenesis and larval development are critically dependent on ecdysone in both *An. gambiae* and *Ae. aegypti* [34]. Genetic modification of *An. gambiae* has demonstrated that disruption of the ecdysone pathway is associated with embryonic lethality midway through development [35]. Furthermore, a recent study of mosquito larvae demonstrated that larvicidal activity correlated with the inhibition of Nobo [6]. Since ecdysteroids are essential to molting and proliferation in insects, their biosynthesis is therefore a possible target for insect growth regulation and pest control.

The spread of insecticide resistance in *Anopheles* species has prompted the search for alternative sustainable approaches to controlling malaria. Pyrethroid resistance is, according to the WHO, currently the greatest biological threat to malaria control. Although new bed nets containing pyrethroid synergists or additional insecticides are slowly being introduced to tackle the loss of insecticidal activity of existing pyrethroid-only nets against increasingly resistant mosquitoes [36], it is clear that malaria control is in dire need of novel agents [24].

The structure of Nobo from *D. melanogaster* has been solved [9,14], and the enzyme was found to interact with steroid molecules structurally similar to the insect hormone ecdysone and its precursor cholesterol. We discovered that the *D. melanogaster* enzyme catalyzes a ketosteroid double-bond isomerization of 5-androsten-3,17-dione [9], but the catalytic efficiency was 20-fold lower than that of Nobo from *An. gambiae* reported here.

The GST Nobo enzyme is fundamental to the proliferation of dipteran and lepidopteran insects, being crucial for metamorphosis and oogenesis [37], and inhibitors of the enzyme can be expected to have similar lethal effects as demonstrated in homozygous Nobo null and Asp113Ala mutants in *D. melanogaster* [14]. These deleterious effects on ecdysteroidogenesis are noted by Nobo knockout or inhibition in a range of distantly related insect species. For example, similar lethal phenotypes are observed in *Bombyx mori* Nobo null insects [5]. In mosquitoes, inhibitors of the Nobo ortholog from the yellow-fever-transmitting mosquito *Ae. aegypti* are larvicidal to this insect and suppress the expression of the ecdysone-inducible gene E74B [6].

Globally, the number of malaria cases has stayed in excess of 200 million every year since 2000, but the tally of deaths has declined from 738,000 in the year 2000 to 409,000 in 2019. However, the number of fatalities has reportedly risen to 619,000 in 2021 according to the WHO. In spite of some reduced mortality in this period, the rate of improvement has stalled in many countries due to the emerging resistance of mosquito vectors to preventative measures. There is universal agreement that targeting the insects transmitting the infectious agent remains the mainstay in combating malaria, and novel insect growth regulators are urgently needed to supplement or replace pyrethroids and other insecticides currently used. Incisive studies of Nobo may pave the way for new agents to combat malaria by targeting the enzyme.

Author Contributions: B.M. conceived the study and wrote the manuscript with contributions from all other authors. Y.M. performed the kinetic studies. A.I. and B.S. assisted in the enzyme purification and provided materials. All authors contributed to the analysis and discussion of results. All authors have read and agreed to the published version of the manuscript.

Funding: The project was supported by a stipend from Wenner-Gren Foundations to Y.M. and grants to B.M. from the Swedish Research Council. The APC was funded by Stockholm University.

Data Availability Statement: Experimental data can be obtained from the authors by request.

Acknowledgments: Characterization of Nobo was initiated in our laboratory by Jessica Khin San and Kh. Nur E Sadid as students of the University of Skövde.

Conflicts of Interest: The authors declare no conflict of interest.

References

1. World Health Organization. *WHO Guidelines for Malaria*; World Health Organization (WHO): Geneva, Switzerland, 2021.
2. Ortelli, F.; Rossiter, L.C.; Vontas, J.; Ranson, H.; Hemingway, J. Heterologous expression of four glutathione transferase genes genetically linked to a major insecticide-resistance locus from the malaria vector *Anopheles gambiae*. *Biochem. J.* **2003**, *373*, 957–963. [CrossRef]
3. Chanut-Delalande, H.; Hashimoto, Y.; Pelissier-Monier, A.; Spokony, R.; Dib, A.; Kondo, T.; Bohere, J.; Niimi, K.; Latapie, Y.; Inagaki, S.; et al. Pri peptides are mediators of ecdysone for the temporal control of development. *Nat. Cell. Biol.* **2014**, *16*, 1035–1044. [CrossRef] [PubMed]
4. Enya, S.; Ameku, T.; Igarashi, F.; Iga, M.; Kataoka, H.; Shinoda, T.; Niwa, R. A halloween gene noppera-bo encodes a glutathione s-transferase essential for ecdysteroid biosynthesis via regulating the behaviour of cholesterol in Drosophila. *Sci. Rep.* **2014**, *4*, 6586. [CrossRef] [PubMed]
5. Enya, S.; Daimon, T.; Igarashi, F.; Kataoka, H.; Uchibori, M.; Sezutsu, H.; Shinoda, T.; Niwa, R. The silkworm glutathione s-transferase gene noppera-bo is required for ecdysteroid biosynthesis and larval development. *Insect. Biochem. Mol. Biol.* **2015**, *61*, 1–7. [CrossRef] [PubMed]
6. Inaba, K.; Ebihara, K.; Senda, M.; Yoshino, R.; Sakuma, C.; Koiwai, K.; Takaya, D.; Watanabe, C.; Watanabe, A.; Kawashima, Y.; et al. Molecular action of larvicidal flavonoids on ecdysteroidogenic glutathione s-transferase noppera-bo in Aedes aegypti. *BMC Biol.* **2022**, *20*, 43. [CrossRef]
7. Mannervik, B.; Danielson, U.H. Glutathione transferases—Structure and catalytic activity. *CRC Crit. Rev. Biochem.* **1988**, *23*, 283–337. [CrossRef]
8. Lindström, H.; Peer, S.M.; Ing, N.H.; Mannervik, B. Characterization of equine GST A3-3 as a steroid isomerase. *J. Steroid. Biochem. Mol. Biol.* **2018**, *178*, 117–126. [CrossRef]
9. Skerlova, J.; Lindström, H.; Gonis, E.; Sjödin, B.; Neiers, F.; Stenmark, P.; Mannervik, B. Structure and steroid isomerase activity of Drosophila glutathione transferase E14 essential for ecdysteroid biosynthesis. *FEBS Lett.* **2020**, *594*, 1187–1195. [CrossRef]
10. Mannervik, B.; Jemth, P. Measurement of glutathione transferases. In *Current Protocols in Toxicology*; Chapter 6; John Wiley & Sons: Hoboken, NJ, USA, 2001.
11. Pettersson, P.L.; Mannervik, B. The role of glutathione in the isomerization of Δ^5-androstene-3,17-dione catalyzed by human glutathione transferase A1-1. *J. Biol. Chem.* **2001**, *276*, 11698–11704. [CrossRef]
12. Johansson, A.S.; Mannervik, B. Human glutathione transferase A3-3, a highly efficient catalyst of double-bond isomerization in the biosynthetic pathway of steroid hormones. *J. Biol. Chem.* **2001**, *276*, 33061–33065. [CrossRef]
13. Raffalli-Mathieu, F.; Orre, C.; Stridsberg, M.; Hansson Edalat, M.; Mannervik, B. Targeting human glutathione transferase A3-3 attenuates progesterone production in human steroidogenic cells. *Biochem. J.* **2008**, *414*, 103–109. [CrossRef] [PubMed]
14. Koiwai, K.; Inaba, K.; Morohashi, K.; Enya, S.; Arai, R.; Kojima, H.; Okabe, T.; Fujikawa, Y.; Inoue, H.; Yoshino, R.; et al. An integrated approach to unravel a crucial structural property required for the function of the insect steroidogenic Halloween protein noppera-bo. *J. Biol. Chem.* **2020**, *295*, 7154–7167. [CrossRef]
15. Kuliopulos, A.; Mildvan, A.S.; Shortle, D.; Talalay, P. Kinetic and ultraviolet spectroscopic studies of active-site mutants of Δ^5-3-ketosteroid isomerase. *Biochemistry* **1989**, *28*, 149–159. [CrossRef] [PubMed]
16. Pollack, R.M. Enzymatic mechanisms for catalysis of enolization: Ketosteroid isomerase. *Bioorg. Chem.* **2004**, *32*, 341–353. [CrossRef]
17. Radzicka, A.; Wolfenden, R. A proficient enzyme. *Science* **1995**, *267*, 90–93. [CrossRef] [PubMed]
18. Pan, X.; Connacher, R.P.; O'Connor, M.B. Control of the insect metamorphic transition by ecdysteroid production and secretion. *Curr. Opin. Insect Sci.* **2021**, *43*, 11–20. [CrossRef]
19. Enya, S.; Yamamoto, C.; Mizuno, H.; Esaki, T.; Lin, H.K.; Iga, M.; Morohashi, K.; Hirano, Y.; Kataoka, H.; Masujima, T.; et al. Dual roles of glutathione in ecdysone biosynthesis and antioxidant function during larval development in Drosophila. *Genetics* **2017**, *207*, 1519–1532. [CrossRef]
20. Atkinson, H.J.; Babbitt, P.C. Glutathione transferases are structural and functional outliers in the thioredoxin fold. *Biochemistry* **2009**, *48*, 11108–11116. [CrossRef]

21. Dourado, D.F.; Fernandes, P.A.; Mannervik, B.; Ramos, M.J. Isomerization of Δ^5-androstene-3,17-dione into Δ^4-androstene-3,17-dione catalyzed by human glutathione transferase A3-3: A computational study identifies a dual role for glutathione. *J. Phys. Chem. A* **2014**, *118*, 5790–5800. [CrossRef]
22. Yabukarski, F.; Doukov, T.; Pinney, M.M.; Biel, J.T.; Fraser, J.S.; Herschlag, D. Ensemble-function relationships to dissect mechanisms of enzyme catalysis. *Sci. Adv.* **2022**, *8*, eabn7738. [CrossRef]
23. Mannervik, B.; Ismail, A.; Lindström, H.; Sjödin, B.; Ing, N.H. Glutathione transferases as efficient ketosteroid isomerases. *Front. Mol. Biosci.* **2021**, *8*, 765970. [CrossRef]
24. Ranson, H.; Lissenden, N. Insecticide resistance in African Anopheles mosquitoes: A worsening situation that needs urgent action to maintain malaria control. *Trends. Parasitol.* **2016**, *32*, 187–196. [CrossRef] [PubMed]
25. Josephy, P.D.; Mannervik, B. *Molecular Toxicology*, 2nd ed.; Oxford University Press: New York, NY, USA, 2006; pp. 333–364.
26. Koirala, B.K.S.; Moural, T.; Zhu, F. Functional and structural diversity of insect glutathione S-transferases in xenobiotic adaptation. *Int. J. Biol. Sci.* **2022**, *18*, 5713–5723. [CrossRef] [PubMed]
27. Ketterman, A.J.; Saisawang, C.; Wongsantichon, J. Insect glutathione transferases. *Drug Metab. Rev.* **2011**, *43*, 253–265. [CrossRef]
28. Adolfi, A.; Poulton, B.; Anthousi, A.; Macilwee, S.; Ranson, H.; Lycett, G.J. Functional genetic validation of key genes conferring insecticide resistance in the major African malaria vector, *Anopheles gambiae*. *Proc. Natl. Acad. Sci. USA* **2019**, *116*, 25764–25772. [CrossRef]
29. Ranson, H.; Hemingway, J. Mosquito glutathione transferases. *Methods Enzymol.* **2005**, *401*, 226–241.
30. Bresell, A.; Weinander, R.; Lundqvist, G.; Raza, H.; Shimoji, M.; Sun, T.H.; Balk, L.; Wiklund, R.; Eriksson, J.; Jansson, C.; et al. Bioinformatic and enzymatic characterization of the MAPEG superfamily. *FEBS J.* **2005**, *272*, 1688–1703. [CrossRef]
31. Warren, J.T.; O'Connor, M.B.; Gilbert, L.I. Studies on the black box: Incorporation of 3-oxo-7-dehydrocholesterol into ecdysteroids by Drosophila melanogaster and Manduca sexta. *Insect Biochem. Mol. Biol.* **2009**, *39*, 677–687. [CrossRef]
32. Kamiyama, T.; Niwa, R. Transcriptional regulators of ecdysteroid biosynthetic enzymes and their roles in insect development. *Front. Physiol.* **2022**, *13*, 823418. [CrossRef]
33. Swevers, L. An update on ecdysone signaling during insect oogenesis. *Curr. Opin. Insect. Sci.* **2019**, *31*, 8–13. [CrossRef] [PubMed]
34. Roy, S.; Saha, T.T.; Zou, Z.; Raikhel, A.S. Regulatory pathways controlling female insect reproduction. *Annu. Rev. Entomol.* **2018**, *63*, 489–511. [CrossRef]
35. Poulton, B.C.; Colman, F.; Anthousi, A.; Grigoraki, L.; Adolfi, A.; Lynd, A.; Lycett, G.J. Using the GAL4-UAS system for functional genetics in *Anopheles gambiae*. *J. Vis. Exp.* **2021**, *170*, e62131.
36. Grisales, N.; Lees, R.S.; Maas, J.; Morgan, J.C.; Wangrawa, D.W.; Guelbeogo, W.M.; N'Fale, S.; Lindsay, S.W.; McCall, P.J.; Ranson, H. Pyriproxyfen-treated bed nets reduce reproductive fitness and longevity of pyrethroid-resistant *Anopheles gambiae* under laboratory and field conditions. *Malar. J.* **2021**, *20*, 273. [CrossRef] [PubMed]
37. Baldini, F.; Gabrieli, P.; South, A.; Valim, C.; Mancini, F.; Catteruccia, F. The interaction between a sexually transferred steroid hormone and a female protein regulates oogenesis in the malaria mosquito *Anopheles gambiae*. *PLoS Biol.* **2013**, *11*, e1001695. [CrossRef] [PubMed]

biomolecules

MDPI

Review

Compounds Inhibiting Noppera-bo, a Glutathione *S*-transferase Involved in Insect Ecdysteroid Biosynthesis: Novel Insect Growth Regulators

Kana Ebihara [1] and Ryusuke Niwa [2,*]

[1] Degree Programs in Life and Earth Sciences, Graduate School of Science and Technology, University of Tsukuba, Tennodai 1-1-1, Tsukuba 305-8572, Ibaraki, Japan
[2] Life Science Center for Survival Dynamics, Tsukuba Advanced Research Alliance (TARA), University of Tsukuba, Tennodai 1-1-1, Tsukuba 305-8577, Ibaraki, Japan
* Correspondence: ryusuke-niwa@tara.tsukuba.ac.jp

Abstract: Glutathione *S*-transferases (GSTs) are conserved in a wide range of organisms, including insects. In 2014, an epsilon GST, known as Noppera-bo (Nobo), was shown to regulate the biosynthesis of ecdysteroid, the principal steroid hormone in insects. Studies on fruit flies, *Drosophila melanogaster*, and silkworms, *Bombyx mori*, demonstrated that loss-of-function mutants of *nobo* fail to synthesize ecdysteroid and die during development, consistent with the essential function of ecdysteroids in insect molting and metamorphosis. This genetic evidence suggests that chemical compounds that inhibit activity of Nobo could be insect growth regulators (IGRs) that kill insects by disrupting their molting and metamorphosis. In addition, because *nobo* is conserved only in Diptera and Lepidoptera, a Nobo inhibitor could be used to target IGRs in a narrow spectrum of insect taxa. Dipterans include mosquitoes, some of which are vectors of diseases such as malaria and dengue fever. Given that mosquito control is essential to reduce mosquito-borne diseases, new IGRs that specifically kill mosquito vectors are always in demand. We have addressed this issue by identifying and characterizing several chemical compounds that inhibit Nobo protein in both *D. melanogaster* and the yellow fever mosquito, *Aedes aegypti*. In this review, we summarize our findings from the search for Nobo inhibitors.

Keywords: glutathione *S*-transferases (GSTs); insecticide; insect growth regulator (IGR); mosquito; ecdysone; ecdysteroid; *Drosophila melanogaster*; *Aedes aegypti*; steroid; flavonoid

Citation: Ebihara, K.; Niwa, R. Compounds Inhibiting Noppera-bo, a Glutathione *S*-transferase Involved in Insect Ecdysteroid Biosynthesis: Novel Insect Growth Regulators. *Biomolecules* **2023**, *13*, 461. https://doi.org/10.3390/biom13030461

Academic Editor: Vladimir N. Uversky

Received: 30 December 2022
Revised: 20 February 2023
Accepted: 28 February 2023
Published: 2 March 2023

1. Introduction

Mosquitoes are responsible for the largest number of human deaths. They act as vectors for many pathogenic or parasitic infections such as malaria and dengue fever, which kill more than 700,000 people annually [1–3]. Therefore, it is essential to develop effective ways to control mosquito populations and prevent disease transmission. One method of mosquito control is to use insecticides that specifically act on cholinergic neurotransmission in insects and inhibit their motor functions. Organophosphates [4] and pyrethroids [5,6] are commonly used for mosquito control. However, some mosquitoes are developing resistance to them [7,8]. Therefore, instead of simply relying on a few insecticides, we must switch between multiple insecticides with different mechanisms of action and strategies to avoid the emergence of insecticide resistance. In this regard, the development of new insecticides with different chemical structures and mechanisms of action is required. Accordingly, the purpose of this review is to highlight an epsilon-class glutathione *S*-transferase (GST) in insects, the designated Noppera-bo (Nobo) [9–11], as a novel insecticide target.

2. Insect Growth Regulators (IGRs)

Insect growth regulators (IGRs) are drugs that exhibit high insecticidal or growth-inhibitory activity against insect pests, but have no effect on other organisms. IGRs cause death by

disrupting insect molting and metamorphosis [12]. Some of these target insect-specific structural materials, such as chitins, which are essential for formation of the cuticular layer, and insect hormones, which are required for molting and metamorphosis [13,14].

The Insect Resistance Action Committee (IRAC) classifies 34 groups of insecticides based on mode-of-action, identifying the following groups as IGRs.

(1) "Juvenile hormone mimics" (Group 7) regulate insect molting and metamorphosis by agonizing the action of juvenile hormones (JHs) and indispensable sesquiterpenoid hormones. Commercially used mimics include Methoprene [15–18], Fenoxycarb [19], and Pyriproxyfen [20–22]. These insecticides are effective against a variety of insect species, such as those belonging to the orders Diptera, Lepidoptera, Coleoptera, Orthoptera, and Hymenoptera [23].

(2) "Mite growth inhibitors affecting CHS1" (Group 10) [24], "Inhibitors of chitin biosynthesis affecting CHS1" (Group 15) [17], and "Inhibitors of chitin biosynthesis, type1" (Group 16) [25] inhibit chitin synthase 1 (CHS1) in the epidermis and prevent insects from molting, which leads to death. The CHS1 gene, which encodes enzymes that produce chitin in the cuticle, is found in the exoskeleton, and these insecticides target agricultural pests, such as mosquitoes, and mites.

(3) "Inhibitors of acetyl CoA carboxylase" (Group 23) disrupt the first reaction of lipid biosynthesis by inhibiting the enzyme, acetyl CoA carboxylase, resulting in death. The representative IGR, Spirodiclofen [26,27], developed as an acaricide, effectively controls a broad spectrum of sucking pests such as mosquitoes and mites.

(4) "Molting disruptor, Dipteran" (Group 17) causes irregular melanization and sclerotization of the cuticle, resulting in necrotic lesions, rupture of the insect body, and death in dipteran larvae. In this class, Cyromazine [28] is a widely used IGR, for which the target molecule is unknown.

(5) "Ecdysone receptor agonists" (Group 18) bind to the Ecdysone receptor, the nuclear receptor for active ecdysteroids that are indispensable in arthropods, including insects, but do not have significant physiological effects on other organisms [29]. Dibenzoylhydrazines are well-known commercially available ecdysone receptor agonists [14,30–32]. Dibenzoyl hydrazines include Tebufenozide, Methoxyfenozide, and Chromafenozide, which exhibit selective insecticidal activity against lepidopterans [32]. Although EcR is highly conserved in insects, the insecticidal activity of the Ecdysone receptor agonists is particularly high in lepidopteran insects, but weak in dipteran and coleopteran insects [33–35]. The emergence of resistance to these compounds has been reported [36].

The target molecule of IGRs is specific to insects, resulting in lower toxicity to non-target other animals, including humans, compared to other insecticides, thereby minimizing their impact on the environment [37]. IGRs classified in (2), (3), and (4) inhibit in vivo biosynthetic reactions through several mechanisms, while IGRs classified in (1) and (5) impact the binding of insect hormones, JHs and ecdysteroids by disrupting their receptors. However, no IGRs have yet been developed that target the biosynthesis of these hormones. Fortunately, in the past two decades, the biosynthetic pathways of JH and ecdysteroids and the enzymes involved have been identified and well characterized [38–40]. Therefore, IGR strategies that inhibit biosynthetic pathways rather than receptors are currently being considered [41]. In this review article, we focus on ecdysteroids, which are among the most crucial insect hormones.

3. Noppera-bo, the Ecdysteroidogenic GST

Ecdysteroids are arthropod steroid hormones, such as ecdysone and the more active 20-hydroxyecdysone, which regulate developmental and physiological processes in in-sects. Previous studies have shown that the amounts of active ecdysteroids, particularly 20E, in hemolymph fluctuate temporally during development [42]. Typically, surges of active ecdysteroid amounts are observed multiple times during development, which trigger temporal transitions in development, such as hatching, molting, metamorphosis, and eclosion.

During development, ecdysteroids are synthesized in the prothoracic gland (PG) from dietary cholesterol and plant sterol through multiple steps with various enzymes [39,43]. Ecdysteroid biosynthetic enzymes, including Nobo, collectively called Halloween enzymes [39], have been identified in *Drosophila melanogaster* and other insects over the past two decades [9–11]. Others include Neverland [44,45], non-molting glossy/Shroud [46], Spook/CYP307A1 [47,48], Spookier/CYP307A2 [48], Phantom/CYP306A1 [49,50], Disembodied/CYP302A1 [51], Shadow/CYP315A1 [51], and Shade/CYP314A1 [52]. *Spook*, *spookier*, *phantom*, *disembodied*, *shadow*, and *shade* encode cytochrome P450 monooxygenases, while others encode non-P450 type enzymes. All Halloween genes, except *shadow*, are specifically expressed in ecdysteroidgenic biosynthetic organs, including the PG and adult ovary, while *shade* is expressed in many peripheral tissues [39]. Genetic analyses of Halloween genes have been extensively conducted in *D. melanogaster*, and have revealed that the loss of Halloween genes causes embryonic or larval lethality due to defective ecdysteroid biosynthesis [53]. In the silkworm—*Bombyx mori*, a lepidopteran model insect—genetic mutants of *nobo* and *non-molting glossy/shroud* have been established. These also exhibit larval molting defects owing to the failure of ecdysteroid biosynthesis [11,46].

Among Halloween enzymes, Nobo is unique because it is the only ecdysteroidogenic enzyme belonging to the GST family, which are enzymes conserved in a wide range of organisms, from plants to animals [54–56]. GSTs generally catalyze conjugation of reduced glutathione (GSH) to substrates. Of the insect GSTs classified into six groups (delta, epsilon, sigma, theta, pi, and zeta) [57–60], Nobo belongs to the epsilon class. in vitro biochemical analysis has demonstrated that *D. melanogaster* Nobo (DmNobo; also known as GSTe14) exhibits steroid double-bond isomerase activity; however, corresponding steroid isomerization in vivo is unknown [61]. Although an endogenous substrate of Nobo has not yet been identified, genetic evidence strongly suggests that Nobo participates in cholesterol transport and/or metabolism [9–11]. Moreover, the requirement for GSH in ecdysteoid biosynthesis has also been confirmed; this is because a loss-of-function mutant of *glutamate-cysteine ligase catalytic subunit* (*gclc*), the critical enzyme for GSH biosynthesis, results in developmental lethality, partly due to a loss of ecdysteroid biosynthesis in *D. melanogaster* [62]. Thus, it is clear that GSH-dependent biochemical reactions mediated by Nobo are crucial for ecdysteroid biosynthesis in both dipteran and lepidopteran species. Of note, the developmental arrest phenotype observed in the loss-of-function mutant of *nobo* can be rescued by overexpression of *nobo* orthologs but not by the overexpression of other GST genes that do not belong to the Nobo family [10]. These observations suggest that, while most epsilon classes of GSTs have been reported to play a role in detoxification [63], Nobo is a GST specialized for ecdysteroid biosynthesis. Therefore, Nobo can be a target for IGRs that inhibit ecdysteroid biosynthesis (Figure 1).

GSTs are also used as tags to target proteins in genetic engineering, facilitating mass culture and purification of soluble recombinant proteins using an *Escherichia coli* expression system [64–66]. This is also the case for Nobo, as recombinant Nobo proteins can be easily produced by the *E. coli* expression system and purified using a commercially available conventional GSH column and gel-filtration chromatography [67–69]. Moreover, a high-throughput in vitro Nobo enzyme activity assay system has been established, which is optimal for screening inhibitors [67]. Taking advantage of these technical advances, Nobo is an attractive target for selective insecticides that kill only dipterans or lepidopterans, including mosquitoes, but does not kill beneficial insects, such as honeybees and ladybugs (Figure 1). In the remainder of this review, we focus on recent advances in the identification and characterization of compounds that inhibit enzymatic activity of DmNobo and yellow fever mosquito (*Aedes aegypti*) Nobo (AeNobo; also known as GSTe8), also known as *GSTe14* and *GSTe8*, respectively, and we discuss the search for vector mosquito-specific IGRs.

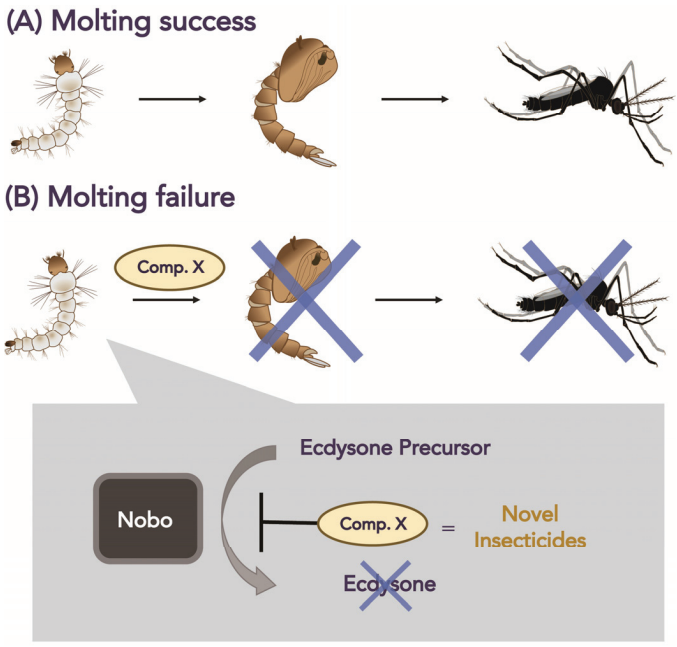

Figure 1. The action of a Nobo inhibitor affecting mosquito development. (**A**) Under normal conditions, mosquitoes are holometabolous insects, undergoing metamorphosis from larvae to pupae and finally to adulthood. Multiple molting stages occur during their development. (**B**) Exposure of early larvae to an inhibitor of Nobo (Comp. X) results in death prior to pupation. This phenomenon is attributed to the binding of Comp. X to Nobo, inhibiting ecdysteroid biosynthesis. Comp. X is anticipated to exhibit insecticidal efficacy as a novel IGR.

4. High-Throughput In Vitro Screening of Nobo Catalytic Activity

In general, several colorimetric and fluorometric methods have been used to detect GST activity in vitro. Conventional and typical substrates for colorimetric and fluorometric methods are 1-Chloro-2,4-dinitrobenzene (CDNB) [70,71] and monochlorobimane [72,73], respectively. However, both methods have low sensitivity and are unsuitable for high-throughput screening [41]. To overcome this low sensitivity, a novel fluorescent substrate, 3,4-DNADCF, was developed [67], which fluoresces approximately 54-fold upon GSH conjugation in the presence of GST. The enzymatic assay with 3,4-DNADCF was feasible even at a 1000-fold lower concentration than that of CDNB. Moreover, the high k_{cat}/K_M for 3,4-DNADCF is advantageous for the sensitive detection of GST enzymatic activity [67].

A high-throughput screening was conducted using 3,4-DNADCF with DmNobo recombinant proteins and a library of 9600 small-molecule compounds to identify inhibitors of DmNobo [69], and several inhibitors were identified [68,69,74]. Interestingly, these inhibitors included three steroid compounds, one of which was the mammalian steroid hormone 17 β-Estradiol (EST) [67]. EST is a strong inhibitor of DmNobo with 50% inhibitory concentration (IC_{50}) of 1.2 ± 0.1 μM; however, it does not inhibit human GST P1-1 [67]. Nonetheless, EST is an endocrine-disrupting chemical, which renders it difficult to use as an insecticide [75]. Therefore, EST serves as a model compound to clarify the general mode of action of DmNobo inhibitors.

5. 17β-Estradiol Inhibits *Drosophila melanogaster* Nobo Enzymatic Activity

In 2020, the crystal structure of DmNobo was reported by Bengt Mannervik's group and our group. The Mannervik group solved the co-crystal structure of DmNobo with GSH and 2-methyl-2,4-pentanediol, originating from the crystallization mother liquor

(Protein Data Bank (PDB):6T2T) [61]. Meanwhile, our group solved crystal structures of DmNobo: the apo form of DmNobo (PDB:6KEL), co-crystals with GSH (PDB:6KEN), EST (DmNobo-EST; PDB:6KEO), and both GSH and EST (PDB:6KEP) [68]. For any of these structures, like other GSTs generally, DmNobo forms a homodimer, conserving the GSH-binding pocket (G-site) and hydrophobic substrate-binding pocket (H-site). As expected, GSH is intercalated into the G-site, and EST and 2-methyl-2,4-pentanediol were bound to the H-sites.

Several amino acids in DmNobo interact with EST and GSH, via hydrophobic interaction with Phe39. However, the most important of these is the aspartate residue located at position 113 (Asp113), which is situated in the innermost region of the H-site (Figure 2A and Table 1). Specifically, the Oδ atom of Asp113 forms a hydrogen bond with the O3 atom in the hydroxyl group of EST [68]. The importance of the hydrogen bond between Asp113 and EST is also indicated by the fragment molecular orbital (FMO) method, which evaluates inter-fragment interaction energy [76–78]. Moreover, a point mutant DmNobo protein, in which Asp113 is replaced by alanine, has no loss of enzymatic activity even in the presence of 25 μM EST, providing bio-chemical evidence for the importance of hydrogen bonding between Asp113 and EST.

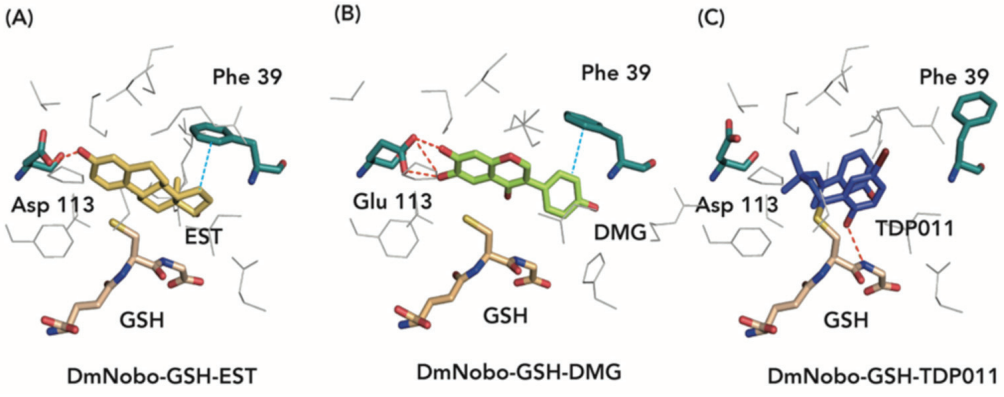

Figure 2. Characteristics of major Nobo inhibitors. Hydrogen bonds are represented by red lines, while hydrophobic interactions are represented by light blue lines. (**A**) EST (carbon atom depicted in yellow) interacts with DmNobo via Asp113 and forms a hydrogen bond. EST forms a hydrophobic interaction with Phe39. (**B**) DMG (carbon atom depicted in green) interacts with AeNobo via Glu113 and forms a hydrogen bond. DMG interacts hydrophobically with Phe39. (**C**) TDP011 (carbon atom depicted in blue) is glutathionylated, but lacks interactions with Asp 113 and Phe39, but it does interact with other hydrophobic amino acids (not shown).

Table 1. Characteristics of major Nobo inhibitors.

Compound	EST	DMG	TDP011
Protein	DmNobo	AeNobo	DmNobo
PDB ID: ID	6KEP	7EBW	7DB3
Glutathionylation [(a)]	NO	NO	YES
Interaction with Asp/Glu113	YES	YES	NO
Conformational change of Phe39	NO	NO	YES
IC_{50} (μM)	2.33 ± 0.08	0.293 ± 0.012	6.72 ± 1.48
Reference	Koiwai et al., 2020 [68]	Inaba et al., 2022 [69]	Koiwai et al., 2021 [74]

[(a)] Inhibitors bound to GSH.

The essentiality of Asp113 during *D. melanogaster* development has also been investigated using molecular genetics. A *D. melanogaster nobo* mutant allele carrying a D113A point mutation ($nobo^{Asp113Ala}$) was generated using CRISPR-Cas9-based knock-in. $Nobo^{Asp113Ala}$ mutant animals exhibited embryonic lethality, characterized by a naked cuticle structure and failure of head involution [68]. These phenotypes are very similar to features of Halloween mutants, which exhibit a complete loss of *nobo* function [9,10]. The level of mutated DmNobo protein from the $nobo^{Asp113Ala}$ allele was comparable to that of wild-type DmNobo protein in the prothoracic glands, indicating that the Asp113Ala mutation did not affect the stability of Nobo. Asp113 of Nobo sustains the intrinsic biochemical function of Nobo and regulates its normal development in *D. melanogaster*.

Notably, Asp113 is almost perfectly conserved among six dipteran and 13 lepidopteran species with Nobo sequences in public databases [68]. This observation is consistent with the functional importance of Asp113 in Nobo in vivo. The only exception among Nobo proteins is AeNobo, which has Glu113 instead of Asp113 in DmNobo. However, hydrogen bond interactions between Glu113 of AeNobo and some inhibitor compounds were observed.

6. Flavonoidal Compounds, Such as Desmethylglycitein, Inhibit *Aedes aegypti* Nobo Enzymatic Activity

After identifying EST as a DmNobo inhibitor, it was initially speculated that EST would also inhibit the enzymatic activity of AeNobo derived from the yellow fever mosquito, *A. aegypti*. However, this is not the case. The IC_{50} of EST against AeNobo is 21.3 μM, which is approximately 10-fold higher than against DmNobo [69]. Therefore, to identify inhibitors of AeNobo, a high-throughput screening against AeNobo recombinant protein was performed using a library of 9600 small molecule compounds [69]. The compound, 2′-hydroxyflavanone, was identified with an IC_{50} of 4.76 μM. The inhibitory activities of other subclasses of flavonoids, including flavanone, flavone, isoflavone, flavanol, isoflavan, and anthocyanidin, were also tested against AeNobo. More than half of the tested flavonoid compounds exhibited inhibitory activity against AeNobo with IC_{50}s less than 10 μM.

Three complex structures with three flavonoid inhibitors, daidzein (PDB:7EBU), luteolin (PDB:7EBV), and desmethylglycitein (DMG; IUPAC name:4′,6,7-trihy-droxyisoflavone; PDB:7EBW), were determined by X-ray crystallography. All three compounds formed hydrogen bonds with Glu113 in AeNobo (Figure 2B and Table 1 for DMG). Moreover, as in the case of DmNobo and EST, the enzymatic activity of a point mutation of the AeNobo protein substituting Glu113 with alanine was not inhibited by any of these flavonoids, even at a concentration of 25 μM. These results suggest that AeNobo Glu113 is essential for the inhibitory activity of flavonoids, as with Asp113.

Among the three flavonoids, DMG exhibits the strongest inhibitory activity against AeNobo, as the IC_{50} values of daidzein, luteolin, and DMG against AeNobo are 3.87 μM, 3.99 μM, and 0.287 μM, respectively. Although all of them form hydrogen bonds with Glu113 of Aenobo, the hydrogen bond itself cannot account for the difference in inhibitory activity between DMG and the other two. Our analysis suggests that a hydrophobic interaction between DMG and Phe39 of AeNobo is crucial for the higher inhibitory activity of DMG (Figure 2B and Table 1). Notably, the FMO calculation indicated a hydrophobic interaction between Phe39 of DmNobo and EST [61] (Figure 2A and Table 1).

A previous study reported that daidzein exhibited larvicidal activity against *A. aegypti* [79]. As DMG has stronger inhibitory activity against AeNobo than daidzein, it is expected to be a more effective larvicidal reagent. Indeed, this is the case, as the 50% leathal dose (LD_{50}) of DMG was approximately 9.39 ppm, whereas daidzein exhibited an LD_{50} of 85.8 ppm. These results suggest that inhibitory activities of flavonoids are correlated with their larvicidal activity. In addition, DMG-treated animals (2.5 ppm) exhibited growth delays and suppressed expression of the ecdysteroid-inducible gene, *E74B*, consistent with our expectation that DMG inhibits the ecdysteoidogenic GST Nobo. This is the first report of a flavonoid compound potentially inhibiting the ecdysteroid biosynthesis pathway.

Many flavonoid compounds, including daidzein, have estrogenic activity and activate estrogen receptors [80,81]. Estrogenic compounds, including daidzein, have been recognized as dangerous endocrine-disrupting chemicals that can harm other animals [75]; therefore, they cannot be used as insecticides. Interestingly, a previous study showed that DMG lacks estrogenic activity [81], suggesting that it may not be an endocrine disruptor like EST or daidzein. However, DMG is less active than commercially available insecticides that effectively control mosquitoes. Nevertheless, we expect that DMG may serve as a good starting point for the development of highly active and environmentally friendly IGRs.

7. Glutathionylation of DmNobo Inhibitors

From our studies on DmNobo-EST and AeNobo-flavonoid interactions, hydrogen bonds formed with Asp/Glu113 and a hydrophobic interaction with Phe39 are the important features to achieve high inhibitory activity against Nobo. However, our investigation revealed that neither of these interactions are an absolute prerequisite for inhibitory activity.

Inhibitors of DmNobo include not only EST, but also five non-steroidal compounds [74]: TDP011 (IUPAC name:4-bromo-2-[4-(3-methoxyphenyl)-2,2-dimethyl-5,6-dihydro-1H-pyrimidin-6-yl]phenol), TDP012 (IUPAC name:1-(4-fluorobenzyl)-1H-thieno [3,2-c][1,2]thiazin-4(3H)-one 2,2-dioxide), TDP013 (IUPAC name:2-(5-tert-butyl-2-methyl-benzenesulfonylamino)-benzoic acid), TDP015 (IUPAC name:6-(6,7-dihydrothieno [3,2-c]pyridin-5(4H)-yl)-3-pyridinamine), and TDP044 (IUPAC name:2,2′-(1,1-ethanediyl)bis(3-hydroxy-5,5-dimethyl-2-cyclohexen-1-one). Interactions between DmNobo and these five inhibitory compounds were investigated by X-ray crystallography, and three-dimensional structures of co-crystals of DmNobo with GSH and TDP011 (PDB:7BD3), TDP012 (PDB:7DB4), TDP013 (PDB:7DAY), and TDP015 (PDB:7DAZ) have been determined.

All four chemicals insert into the H-sites of DmNobo. Surprisingly, unlike EST, none of the four compounds form a hydrogen bond with Asp113 (Figure 2C and Table 1 for TDP011). Moreover, none of the four compounds interacted with Phe39. Instead, the position of Phe39 changed between the apo-form and the complex forms with these non-steroidal compounds. When they are present in the H-sites, the aromatic ring of Phe39 moves away from the compounds, preventing their interaction with Phe39 (Figure 2C and Table 1 for TDP011). These data imply that the inhibitory activity of these non-steroidal compounds is achieved by another mechanism.

Interestingly, TDP011, TDP012, and TDP015 (but not TDP013) intercalate into the H-site only when GSH is present at the G-site. Moreover, these three compounds bind covalently to GSH in DmNobo co-crystals, indicating that TDP011, TDP12, and TDP015 are glutathionylated in DmNobo proteins. Glutathionylation is a chemical reaction in which a covalent bond is formed between the thiol group of the cysteine of GSH and the substrate. Notably, covalent bonds are stronger than the chemical bonds often used in human drug development. These drugs, called covalent drugs, bind irreversibly to their target proteins and exhibit potent, sustained effects [82]. Accordingly, we now speculate that such glutathionylation may be indispensable for some compounds to exhibit inhibitory activity against Nobo, but further studies are needed to clarify this point. If this is true, the identification and characterization of such covalent "IGRs" against Nobo may be a new direction to develop more potent Nobo inhibitors. However, covalent drugs may react nonspecifically with off-target proteins or biological components, causing side effects. Therefore, it may be crucial to select chemical reactions that exhibit high selectivity for Nobo proteins in vivo.

8. Conclusions and Future Perspectives

We summarized ideas for a new IGR strategy against Nobo for insect GSTs. In our previous studies on the structure of Nobo inhibitors [68,69,74], three key features were identified: (i) hydrogen bonds formed with Asp/Glu113, (ii) a hydrophobic interaction with Phe39, and (iii) glutathionylation of compounds. Currently known Nobo inhibitors exhibit one or two of these features. To create a more potent Nobo inhibitor, we propose that a

stronger Nobo inhibitor can be developed by satisfying all three of these criteria. Currently, we are working on the identification and characterization of such compounds. We believe that this approach has potential to yield effective Nobo inhibitors for use as IGRs.

A variety of compounds with different chemical structures have been identified as inhibitors of DmNobo and AeNobo. Although the overall protein structures of DmNobo and AeNobo are similar, several amino acids surrounding the H-site differ between the two. Consequently, some DmNobo inhibitors exhibit weak hydrophobic interactions with AeNobo, resulting in low inhibitory activity. However, the differences in inhibitory activity among insect species cannot be solely attributed to the amino acid compositions or the size of their H-sites. Thus, the cause of the variation in inhibitory activity remains unknown. According to IRAC, commercially available IGRs, such as JH mimics, inhibitors of chitin biosynthesis, inhibitors of acetyl CoA carboxylase, and ecdysone receptor agonists, face resistance from certain species [7,8,65]. Moreover, insects that have acquired stronger resistance to IGRs may emerge more frequently in the future. Therefore, it is desirable to continuously develop IGRs with various mechanisms of action and to rotate their use with current insecticides.

Molecularly targeted insecticides, such as Nobo inhibitors, represent a safer and eco-friendly alternative, given their well-understood mode of action. To apply Nobo inhibitors as insecticides, it is imperative to undertake toxicity evaluations on both target and non-target insects. Furthermore, at the molecular level, Nobo inhibitors demonstrate greater potency than conventional GST inhibitors [83]. However, unlike existing IGRs, currently identified Nobo inhibitors are still less toxic to mosquitoes. For example, the LD_{50} of DMG, which is currently the most potent Nobo inhibitor, is approximately 10 ppm against *A. aegypti* larvae [69]. In contrast, the LD_{50} values for organophosphates and pyrethroids against mosquitoes are typically less than 0.1 ppm [84,85]. Therefore, a further combined approach, incorporating both in vitro and in vivo structural analysis, is required for a Nobo inhibitor with higher IGR activity.

As an additional curiosity, it is reported that the expression of Halloween genes is suppressed when JH mimics are administered to ex vivo cultured PGs from *D. melanogaster* and *B. mori* [86]. JH hormone mimics have also been reported as inhibitors of mosquitoes [15,17,18,23]. It is unclear whether JH mimics inhibit the enzymatic activity of Nobo, but if they inhibit the expression of Halloween genes, it is likely that they also inhibit Nobo. Since JH mimics possess multiple methyl groups, they are expected to have more hydrophobic interactions when bound to Nobo. On the other hand, the binding mode of the JH mimics is unknown, since few structures of JH mimics have been reported.

Lastly, it is crucial to identify the endogenous substrate of Nobo to completely understand its in vivo mode of action. The ligand is suspected to be a steroid that interacts with Asp/Glu113 of Nobo through a hydrogen bond and may be displaced from the H-site by Nobo inhibitors. Further studies are necessary to understand the chemical properties of the ligand and the relationship between the ligand, inhibitors, and Nobo proteins. These studies are important for any future use of Nobo inhibitors as IGRs.

Author Contributions: K.E. and R.N. wrote and revised the manuscript and approved the submitted version. All authors have read and agreed to the published version of the manuscript.

Funding: This work was supported by the Innovative Research Program Award from the Japan Society for Bioscience, Biotechnology, and Agrochemistry to RN, and by JST SPRING, Grant Number JPMJSP2124.

Acknowledgments: K.E. received a fellowship from the Support for Pioneering Research Initiated by the JST SPRING and a High Energy Accelerator Research Organization (KEK) Postgraduate Research Student Fellowship. We are also grateful to Steven D. Aird for technical editing.

Conflicts of Interest: The authors declare no conflict of interest.

References

1. Tolle, M.A. Mosquito-Borne Diseases. *Curr. Probl. Pediatr. Adolesc. Health Care* **2009**, *39*, 97–140. [CrossRef] [PubMed]
2. Guzman, M.G.; Gubler, D.J.; Izquierdo, A.; Martinez, E.; Halstead, S.B. Dengue Infection. *Nat. Rev. Dis. Prim.* **2016**, *2*, 16055. [CrossRef]
3. World Health Organization. *World Malaria Report: 20 Years of Global Progress and Challenges*; World Health Organization: Geneva, Switzerland, 2020; ISBN 978-92-4-001579-1.
4. Benelli, G. Research in Mosquito Control: Current Challenges for a Brighter Future. *Parasitol. Res.* **2015**, *114*, 2801–2805. [CrossRef] [PubMed]
5. Elliott, M. Synthetic Pyrethroids. In *Human Toxicology of Pesticides*; CRC Press: Boca Raton, FL, USA, 1977; Volume 42, pp. 1–28. [CrossRef]
6. WHO. *Safe Use of Pesticides: Fourteenth Report of the WHO Expert Committee on Vector Biology and Control*; World Health Organization—Technical Report Series; WHO: Geneva, Switzerland, 1991; Volume 813, pp. 1–27.
7. Moyes, C.L.; Vontas, J.; Martins, A.J.; Ng, L.C.; Koou, S.Y.; Dusfour, I.; Raghavendra, K.; Pinto, J.; Corbel, V.; David, J.P.; et al. Correction to: Contemporary Status of Insecticide Resistance in the Major Aedes Vectors of Arboviruses Infecting Humans. *PLoS Negl. Trop. Dis.* **2021**, *15*, e0009084. [CrossRef] [PubMed]
8. Marcombe, S.; Darriet, F.; Tolosa, M.; Agnew, P.; Duchon, S.; Etienne, M.; Tcha, M.M.Y.; Chandre, F.; Corbel, V.; Yébakima, A. Pyrethroid Resistance Reduces the Efficacy of Space Sprays for Dengue Control on the Island of Martinique (Caribbean). *PLoS Negl. Trop. Dis.* **2011**, *5*, e1202. [CrossRef]
9. Chanut-Delalande, H.; Hashimoto, Y.; Pelissier-Monier, A.; Spokony, R.; Dib, A.; Kondo, T.; Bohère, J.; Niimi, K.; Latapie, Y.; Inagaki, S.; et al. Pri Peptides Are Mediators of Ecdysone for the Temporal Control of Development. *Nat. Cell Biol.* **2014**, *16*, 1035–1044. [CrossRef]
10. Enya, S.; Ameku, T.; Igarashi, F.; Iga, M.; Kataoka, H.; Shinoda, T.; Niwa, R. A Halloween Gene Noppera-Bo Encodes a Glutathione S-Transferase Essential for Ecdysteroid Biosynthesis via Regulating the Behaviour of Cholesterol in Drosophila. *Sci. Rep.* **2014**, *4*, 6586. [CrossRef]
11. Enya, S.; Daimon, T.; Igarashi, F.; Kataoka, H.; Uchibori, M.; Sezutsu, H.; Shinoda, T.; Niwa, R. The Silkworm Glutathione S-Transferase Gene Noppera-Bo Is Required for Ecdysteroid Biosynthesis and Larval Development. *Insect Biochem. Mol. Biol.* **2015**, *61*, 1–7. [CrossRef] [PubMed]
12. Tunaz, H.; Uygun, N. Insect Growth Regulators for Insect Pest Control. *Turk. J. Agric. For.* **2004**, *28*, 377–387.
13. Vinson, S.B.; Plapp, F.W. Third Generation Pesticides. Potential for the Development of Resistance by Insects. *J. Agric. Food Chem.* **1974**, *22*, 356–360. [CrossRef]
14. Dhadialla, T.S.; Carlson, G.R.; Le, D.P. New Insecticides with Ecdysteroidal and Juvenile Hormone Activity. *Annu. Rev. Entomol.* **1998**, *43*, 545–569. [CrossRef] [PubMed]
15. Spielman, A.; Williams, C.M. Lethal Effects of Synthetic Juvenile Hormone on Larvae of the Yellow Fever Mosquito, Aedes Aegypti. *Science* **1966**, *154*, 1043–1044. [CrossRef] [PubMed]
16. Henrick, C.A.; Staal, G.B.; Siddall, J.B. Alkyl 3,7,11-Trimethyl-2,4-Dodecadienoates, a New Class of Potent Insect Growth Regulators with Juvenile Hormone Activity. *J. Agric. Food Chem.* **1973**, *21*, 354–359. [CrossRef] [PubMed]
17. Ho, C.M.; Wu, S.H.; Wu, C.C. Evaluation of the Control of Mosquitoes with Insect Growth Regulators. *Gaoxiong Yi Xue Ke Xue Za Zhi* **1990**, *6*, 366–374.
18. Minakuchi, C.; Riddiford, L.M. Insect Juvenile Hormone Action as a Potential Target of Pest Management. *J. Pestic. Sci.* **2006**, *31*, 77–84. [CrossRef]
19. Dorn, S.; Frischknecht, M.L.; Martinez, V.; Zurflüh, R.; Fischer, U. A Novel Non-Neurotoxic Insecticide with a Broad Activity Spectrum/Ein Neuartiges, Nicht-Neurotoxisches Insektizid Mit Einem Breiten Wirkungsspektrum. *Z. Für Pflanzenkrankh. Pflanzenschutz/J. Plant Dis. Prot.* **1981**, *88*, 269–275.
20. Hatakoshi, M.; Agui, N.; Nakayama, I. 2-[1-Methyl-2-(4-Phenoxyphenoxy) Ethoxy] Pyridine as a New Insect Juvenile Hormone Analogue: Induction of Supernumerary Larvae in *Spodoptera litura* (Lepidoptera: Noctuidae). *Appl. Entomol. Zool.* **1986**, *21*, 351–353. [CrossRef]
21. Hatakoshi, M.; Nakayama, I.; Riddiford, L.M. Penetration and Stability of Juvenile Hormone Analogues in *Manduca sexta*, L.: Lepidoptera: Sphingidae. *Appl. Entomol. Zool.* **1987**, *22*, 641–644. [CrossRef]
22. KAWADA, H.; KOJIMA, I.; SHINJO, G. Laboratory Evaluation of a New Insect Growth Regulator Pyriproxyfen, as a Cockroach Control Agent. *Med. Entomol. Zool.* **1989**, *40*, 195–201. [CrossRef]
23. Staal, G.B. Insect Growth Regulators with Juvenile Hormone Activity. *Annu. Rev. Entomol.* **1975**, *20*, 417–460. [CrossRef]
24. Yamada, T.; Kaeriyama, M.; Matsui, N.; Yoneda, H. Development of a New Miticide, Hexythiazox. *J. Pestic. Sci.* **1989**, *12*, 327–335. [CrossRef]
25. Asai, T.; Kajihara, O.; Fukada, M.; Maekawa, S. Studies on the Mode of Action of Buprofezin II. Effects on Reproduction of the Brown Planthopper, *Nilaparvata lugens* Stal (Homoptera: Delphacidae). *Appl. Entomol. Zool.* **1985**, *20*, 111–117. [CrossRef]
26. Lümmen, P.; Khajehali, J.; Luther, K.; Van Leeuwen, T. The Cyclic Keto-Enol Insecticide Spirotetramat Inhibits Insect and Spider Mite Acetyl-CoA Carboxylases by Interfering with the Carboxyltransferase Partial Reaction. *Insect Biochem. Mol. Biol.* **2014**, *55*, 1–8. [CrossRef] [PubMed]

27. Wybouw, N.; Kosterlitz, O.; Kurlovs, A.H.; Bajda, S.; Greenhalgh, R.; Snoeck, S.; Bui, H.; Bryon, A.; Dermauw, W.; Van Leeuwen, T.; et al. Long-Term Population Studies Uncover the Genome Structure and Genetic Basis of Xenobiotic and Host Plant Adaptation in the Herbivore Tetranychus Urticae. *Genetics* **2019**, *211*, 1409–1427. [CrossRef]
28. Hart, R.J.; Cavey, W.A.; Ryan, K.J.; Moore, B.; Strong, M.B. Technical Details of a New Sheep Blowfly Insecticide. *Wool Technol. Sheep Breed.* **1980**, *27*, 23–27.
29. Wing, K.D. RH 5849, a Nonsteroidal Ecdysone Agonist: Effects on a Drosophila Cell Line. *Science* **1988**, *241*, 467–469. [CrossRef]
30. Wing, K.D.; Slawecki, R.A.; Carlson, G.R. RH 5849, a Nonsteroidal Ecdysone Agonist: Effects on Larval Lepidoptera. *Science* **1988**, *241*, 470–472. [CrossRef]
31. Shimizu, B.I.; Nakagawa, Y.; Hattori, K.; Nishimura, K.; Kurihara, N.; Ueno, T. Molting Hormonal and Larvicidal Activities of Aliphatic Acyl Analogs of Dibenzoylhydrazine Insecticides. *Steroids* **1997**, *62*, 638–642. [CrossRef]
32. Carlson, G.R.; Dhadialla, T.S.; Hunter, R.; Jansson, R.K.; Jany, C.S.; Lidert, Z.; Slawecki, R.A. The Chemical and Biological Properties of Methoxyfenozide, a New Insecticidal Ecdysteroid Agonist. *Pest Manag. Sci.* **2001**, *57*, 115–119. [CrossRef]
33. Parihar, M.; Minton, R.L.; Flowers, S.; Holloway, A.; Morehead, B.E.; Paille, J.; Gissendanner, C.R. The Genome of the Nematode Pristionchus Pacificus Encodes Putative Homologs of RXR/Usp and EcR. *Gen. Comp. Endocrinol.* **2010**, *167*, 11–17. [CrossRef]
34. Tzertzinis, G.; Egañ, A.L.; Palli, S.R.; Robinson-Rechavi, M.; Gissendanner, C.R.; Liu, C.; Unnasch, T.R.; Maina, C.V. Molecular Evidence for a Functional Ecdysone Signaling System in *Brugia malayi*. *PLoS Negl. Trop. Dis.* **2010**, *4*, e625. [CrossRef] [PubMed]
35. Hill, R.J.; Billas, I.M.L.; Bonneton, F.; Graham, L.D.; Lawrence, M.C. Ecdysone Receptors: From the Ashburner Model to Structural Biology. *Annu. Rev. Entomol.* **2013**, *58*, 251–271. [CrossRef] [PubMed]
36. Uchibori-Asano, M.; Jouraku, A.; Uchiyama, T.; Yokoi, K.; Akiduki, G.; Suetsugu, Y.; Kobayashi, T.; Ozawa, A.; Minami, S.; Ishizuka, C.; et al. Genome-Wide Identification of Tebufenozide Resistant Genes in the Smaller Tea Tortrix, *Adoxophyes honmai* (Lepidoptera: Tortricidae). *Sci. Rep.* **2019**, *9*, 4203. [CrossRef] [PubMed]
37. Masih, S.C.; Ahmad, B.R. Insect Growth Regulators for Insect Pest Control. *Int. J. Curr. Microbiol. App. Sci.* **2019**, *8*, 208–218. [CrossRef]
38. Zhang, X.; Li, S.; Liu, S. Juvenile Hormone Studies in Drosophila Melanogaster. *Front. Physiol.* **2022**, *12*, 785320. [CrossRef]
39. Niwa, R.; Niwa, Y.S. Enzymes for Ecdysteroid Biosynthesis: Their Biological Functions in Insects and Beyond. *Biosci. Biotechnol. Biochem.* **2014**, *78*, 1283–1292. [CrossRef]
40. Kamiyama, T.; Niwa, R. Transcriptional Regulators of Ecdysteroid Biosynthetic Enzymes and Their Roles in Insect Development. *Front. Physiol.* **2022**, *13*, 823418. [CrossRef]
41. Fujikawa, Y.; Inoue, H. Exploration of Insect Growth Regulators Targeting Noppera-Bo, an Enzyme Involved in Ecdysteroid Biosynthesis. *Yakugaku Zasshi* **2018**, *138*, 1043–1048. [CrossRef]
42. Kozlova, T.; Thummel, C.S. Steroid Regulation of Postembryonic Development and Reproduction in Drosophila. *Trends Endocrinol. Metab.* **2000**, *11*, 276–280. [CrossRef]
43. Spindler, K.D.; Hönl, C.; Tremmel, C.; Braun, S.; Ruff, H.; Spindler-Barth, M. Ecdysteroid Hormone Action. *Cell. Mol. Life Sci.* **2009**, *66*, 3837–3850. [CrossRef]
44. Yoshiyama, T.; Namiki, T.; Mita, K.; Kataoka, H.; Niwa, R. Neverland Is an Evolutionally Conserved Rieske-Domain Protein That Is Essential for Ecdysone Synthesis and Insect Growth. *Development* **2006**, *133*, 2565–2574. [CrossRef]
45. Yoshiyama-Yanagawa, T.; Enya, S.; Shimada-Niwa, Y.; Yaguchi, S.; Haramoto, Y.; Matsuya, T.; Shiomi, K.; Sasakura, Y.; Takahashi, S.; Asashima, M.; et al. The Conserved Rieske Oxygenase DAF-36/Neverland Is a Novel Cholesterol-Metabolizing Enzyme. *J. Biol. Chem.* **2011**, *286*, 25756–25762. [CrossRef]
46. Niwa, R.; Namiki, T.; Ito, K.; Shimada-Niwa, Y.; Kiuchi, M.; Kawaoka, S.; Kayukawa, T.; Banno, Y.; Fujimoto, Y.; Shigenobu, S.; et al. Non-Molting Glossy/Shroud Encodes a Short-Chain Dehydrogenase/Reductase That Functions in the "Black Box" of the Ecdysteroid Biosynthesis Pathway. *Development* **2010**, *137*, 1991–1999. [CrossRef]
47. Namiki, T.; Niwa, R.; Sakudoh, T.; Shirai, K.I.; Takeuchi, H.; Kataoka, H. Cytochrome P450 CYP307A1/Spook: A Regulator for Ecdysone Synthesis in Insects. *Biochem. Biophys. Res. Commun.* **2005**, *337*, 367–374. [CrossRef] [PubMed]
48. Ono, H.; Rewitz, K.F.; Shinoda, T.; Itoyama, K.; Petryk, A.; Rybczynski, R.; Jarcho, M.; Warren, J.T.; Marqués, G.; Shimell, M.J.; et al. Spook and Spookier Code for Stage-Specific Components of the Ecdysone Biosynthetic Pathway in Diptera. *Dev. Biol.* **2006**, *298*, 555–570. [CrossRef] [PubMed]
49. Niwa, R.; Matsuda, T.; Yoshiyama, T.; Namiki, T.; Mita, K.; Fujimoto, Y.; Kataoka, H. CYP306A1, a Cytochrome P450 Enzyme, Is Essential for Ecdysteroid Biosynthesis in the Prothoracic Glands of Bombyx and Drosophila. *J. Biol. Chem.* **2004**, *279*, 35942–35949. [CrossRef]
50. Warren, J.T.; Petryk, A.; Marqués, G.; Parvy, J.P.; Shinoda, T.; Itoyama, K.; Kobayashi, J.; Jarcho, M.; Li, Y.; O'Connor, M.B.; et al. Phantom Encodes the 25-Hydroxylase of Drosophila Melanogaster and Bombyx Mori: A P450 Enzyme Critical in Ecdysone Biosynthesis. *Insect Biochem. Mol. Biol.* **2004**, *34*, 991–1010. [CrossRef] [PubMed]
51. Warren, J.T.; Petryk, A.; Marqués, G.; Jarcho, M.; Parvy, J.P.; Dauphin-Villemant, C.; O'Connor, M.B.; Gilbert, L.I. Molecular and Biochemical Characterization of Two P450 Enzymes in the Ecdysteroidogenic Pathway of Drosophila Melanogaster. *Proc. Natl. Acad. Sci. USA* **2002**, *99*, 11043–11048. [CrossRef]
52. Petryk, A.; Warren, J.T.; Marqués, G.; Jarcho, M.P.; Gilbert, L.I.; Kahler, J.; Parvy, J.P.; Li, Y.; Dauphin-Villemant, C.; O'Connor, M.B. Shade Is the Drosophila P450 Enzyme That Mediates the Hydroxylation of Ecdysone to the Steroid Insect Molting Hormone 20-Hydroxyecdysone. *Proc. Natl. Acad. Sci. USA* **2003**, *100*, 13773–13778. [CrossRef]

53. Chávez, V.M.; Marqués, G.; Delbecque, J.P.; Kobayashi, K.; Hollingsworth, M.; Burr, J.; Natzle, J.E.; Connor, M.B.O. The *Drosophila disembodied* gene controls late embryonic morphogenesis and codes for a cytochrome P450 enzyme that regulates embryonic ecdysone levels. *Development* **2000**, *127*, 4115–4126. [CrossRef]
54. Sheehan, D.; Meade, G.; Foley, V.M.; Dowd, C.A. Structure, Function and Evolution of Glutathione Transferases: Implications for Classification of Non-Mammalian Members of an Ancient Enzyme Superfamily. *Biochem. J.* **2001**, *360*, 1–16. [CrossRef]
55. Hayes, J.D.; Flanagan, J.U.; Jowsey, I.R. Glutathione transferases. *Annu. Rev. Pharmacol. Toxicol.* **2004**, *45*, 51–88. [CrossRef]
56. Hu, C.; Liu, J.Y.; Wang, W.; Mota-Sanchez, D.; He, S.; Shi, Y.; Yang, X.Q. Glutathione S-Transferase Genes Are Involved in Lambda-Cyhalothrin Resistance in *Cydia pomonella* via Sequestration. *J. Agric. Food Chem.* **2022**, *70*, 2265–2279. [CrossRef]
57. Fournier, D.; Bride, J.M.; Poirie, M.; Bergé, J.B.; Plapp, F.W.J. Insect Glutathione S-Transferases. Biochemical Characteristics of the Major Forms from Houseflies Susceptible and Resistant to Insecticides. *J. Biol. Chem.* **1992**, *267*, 1840–1845. [CrossRef]
58. Syvanen, M.; Zhou, Z.H.; Wang, J. ying Glutathione Transferase Gene Family from the Housefly Musca Domestica. *MGG Mol. Gen. Genet.* **1994**, *245*, 25–31. [CrossRef]
59. Ranson, H.; Claudianos, C.; Ortelli, F.; Abgrall, C.; Hemingway, J.; Sharakhova, M.V.; Unger, M.F.; Collins, F.H.; Feyereisen, R. Evolution of Supergene Families Associated with Insecticide Resistance. *Science* **2002**, *298*, 179–181. [CrossRef]
60. Ding, Y.; Ortelli, F.; Rossiter, L.C.; Hemingway, J.; Ranson, H. The Anopheles Gambiae Glutathione Transferase Supergene Family: Annotation, Phylogeny and Expression Profiles. *BMC Genom.* **2003**, *4*, 35. [CrossRef] [PubMed]
61. Škerlová, J.; Lindström, H.; Gonis, E.; Sjödin, B.; Neiers, F.; Stenmark, P.; Mannervik, B. Structure and Steroid Isomerase Activity of Drosophila Glutathione Transferase E14 Essential for Ecdysteroid Biosynthesis. *FEBS Lett.* **2020**, *594*, 1187–1195. [CrossRef]
62. Enya, S.; Yamamoto, C.; Mizuno, H.; Esaki, T.; Lin, H.K.; Iga, M.; Morohashi, K.; Hirano, Y.; Kataoka, H.; Masujima, T.; et al. Dual Roles of Glutathione in Ecdysone Biosynthesis and Antioxidant Function during Larval Development in Drosophila. *Genetics* **2017**, *207*, 1519–1532. [CrossRef] [PubMed]
63. Hemingway, J. The Molecular Basis of Two Contrasting Metabolic Mechanisms of Insecticide Resistance. *Insect Biochem. Mol. Biol.* **2000**, *30*, 1009–1015. [CrossRef] [PubMed]
64. RANSON, H.; PRAPANTHADARA, L.; HEMINGWAY, J. Cloning and Characterization of Two Glutathione S-Transferases from a DDT-Resistant Strain of Anopheles Gambiae. *Biochem. J.* **1997**, *324*, 97–102. [CrossRef] [PubMed]
65. Samra, A.; Kamita, S.; Yao, H.-W.; Cornel, A.; Hammock, B. Cloning and Characterization of Two Glutathione S-Transferases from Pyrethroid-Resistant Culex Pipiens. *Pest Manag. Sci.* **2012**, *68*, 764–772. [CrossRef]
66. Liu, J.; Yang, X.; Zhang, Y. Characterization of a Lambda-Cyhalothrin Metabolizing Glutathione S-Transferase CpGSTd1 from *Cydia pomonella* (L.). *Appl. Microbiol. Biotechnol.* **2014**, *98*, 8947–8962. [CrossRef]
67. Fujikawa, Y.; Morisaki, F.; Ogura, A.; Morohashi, K.; Enya, S.; Niwa, R.; Goto, S.; Kojima, H.; Okabe, T.; Nagano, T.; et al. A Practical Fluorogenic Substrate for High-Throughput Screening of Glutathione S-Transferase Inhibitors. *Chem. Commun.* **2015**, *51*, 11459–11462. [CrossRef] [PubMed]
68. Koiwai, K.; Inaba, K.; Morohashi, K.; Enya, S.; Arai, R.; Kojima, H.; Okabe, T.; Fujikawa, Y.; Inoue, H.; Yoshino, R.; et al. An Integrated Approach to Unravel a Crucial Structural Property Required for the Function of the Insect Steroidogenic Halloween Protein Noppera-Bo. *J. Biol. Chem.* **2020**, *295*, 7154–7167. [CrossRef] [PubMed]
69. Inaba, K.; Ebihara, K.; Senda, M.; Yoshino, R.; Sakuma, C.; Koiwai, K.; Takaya, D.; Watanabe, C.; Watanabe, A.; Kawashima, Y.; et al. Molecular Action of Larvicidal Flavonoids on Ecdysteroidogenic Glutathione S-Transferase Noppera-Bo in Aedes Aegypti. *BMC Biol.* **2022**, *20*, 43. [CrossRef] [PubMed]
70. Habig, W.H.; Pabst, M.J.; Jakoby, W.B. Glutathione S-Transferases. The First Enzymatic Step in Mercapturic Acid Formation. *J. Biol. Chem.* **1974**, *249*, 7130–7139. [CrossRef]
71. Robin, S.K.D.; Ansari, M.; Uppugunduri, C.R.S. Spectrophotometric Screening for Potential Inhibitors of Cytosolic Glutathione S-Transferases. *J. Vis. Exp.* **2020**, *164*, e61347. [CrossRef]
72. Kamencic, H.; Lyon, A.; Paterson, P.G.; Juurlink, B.H. Monochlorobimane Fluorometric Method to Measure Tissue Glutathione. *Anal. Biochem.* **2000**, *286*, 35–37. [CrossRef]
73. Ishkaeva, R.A.; Zoughaib, M.; Laikov, A.V.; Angelova, P.R.; Abdullin, T.I. Probing Cell Redox State and Glutathione-Modulating Factors Using a Monochlorobimane-Based Microplate Assay. *Antioxidants* **2022**, *11*, 391. [CrossRef]
74. Koiwai, K.; Morohashi, K.; Inaba, K.; Ebihara, K.; Kojima, H.; Okabe, T.; Yoshino, R.; Hirokawa, T.; Nampo, T.; Fujikawa, Y.; et al. Non-Steroidal Inhibitors of Drosophila Melanogaster Steroidogenic Glutathione S-Transferase Noppera-Bo. *J. Pestic. Sci.* **2021**, *46*, 75–87. [CrossRef] [PubMed]
75. Pinto, P.I.S.; Estêvão, M.D.; Power, D.M. Effects of Estrogens and Estrogenic Disrupting Compounds on Fish Mineralized Tissues. *Mar. Drugs* **2014**, *12*, 4474–4494. [CrossRef] [PubMed]
76. Kitaura, K.; Ikeo, E.; Asada, T.; Nakano, T.; Uebayasi, M. Fragment Molecular Orbital Method: An Approximate Computational Method for Large Molecules. *Chem. Phys. Lett.* **1999**, *313*, 701–706. [CrossRef]
77. Tanaka, S.; Mochizuki, Y.; Komeiji, Y.; Okiyama, Y.; Fukuzawa, K. Electron-Correlated Fragment-Molecular-Orbital Calculations for Biomolecular and Nano Systems. *Phys. Chem. Chem. Phys.* **2014**, *16*, 10310–10344. [CrossRef] [PubMed]
78. Tsukamoto, T.; Kato, K.; Kato, A.; Nakano, T.; Mochiduki, Y.; Fukuzawa, K. Implementation of Pair Interaction Energy Decomposition Analysis and Its Applications to Protein-Ligand Systems. *J. Comput. Chem. Jpn.* **2015**, *14*, 1–9. [CrossRef]
79. Rao, K.V.; Chattopadhyay, S.K.; Reddy, G.C. Flavonoids with Mosquito Larval Toxicity. *J. Agric. Food Chem.* **1990**, *38*, 1427–1430. [CrossRef]

80. Mbachu, O.C.; Howell, C.; Simmler, C.; Malca Garcia, G.R.; Skowron, K.J.; Dong, H.; Ellis, S.G.; Hitzman, R.T.; Hajirahimkhan, A.; Chen, S.N.; et al. SAR Study on Estrogen Receptor α/β Activity of (Iso)Flavonoids: Importance of Prenylation, c-Ring (Un)Saturation, and Hydroxyl Substituents. *J. Agric. Food Chem.* **2020**, *68*, 10651–10663. [CrossRef]
81. Murata, M.; Midorikawa, K.; Koh, M.; Umezawa, K.; Kawanishi, S. Genistein and Daidzein Induce Cell Proliferation and Their Metabolites Cause Oxidative DNA Damage in Relation to Isoflavone-Induced Cancer of Estrogen-Sensitive Organs. *Biochemistry* **2004**, *43*, 2569–2577. [CrossRef]
82. Singh, J.; Petter, R.C.; Baillie, T.A.; Whitty, A. The Resurgence of Covalent Drugs. *Nat. Rev. Drug Discov.* **2011**, *10*, 307–317. [CrossRef]
83. Shishido, Y.; Tomoike, F.; Kuwata, K.; Fujikawa, H.; Sekido, Y.; Murakami-Tonami, Y.; Kameda, T.; Abe, N.; Kimura, Y.; Shuto, S.; et al. A Covalent Inhibitor for Glutathione S-Transferase Pi (GSTP 1-1) in Human Cells. *ChemBioChem* **2019**, *20*, 900–905. [CrossRef]
84. Wang, Y.; An, M.; Stevens, K.M.; Liu, N. Insecticide Resistance in Alabama Populations of the Mosquito Aedes Albopictus. *J. Med. Entomol.* **2022**, *59*, 1678–1686. [CrossRef] [PubMed]
85. Ebrahimnejad, P.; Nikookar, S.H.; Fazeli-Dinan, M.; Payman Ziapour, S.; Farmoudeh, A.; Babaei, A.; Enayati, A. Preparation, Characterisation and Comparative Toxicity of Nanopermethrin against Anopheles Stephensi and Culex Pipiens. *Trop. Med. Int. Health* **2021**, *26*, 982–992. [CrossRef] [PubMed]
86. Zhang, T.; Song, W.; Li, Z.; Qian, W.; Wei, L.; Yang, Y.; Wang, W.; Zhou, X.; Meng, M.; Peng, J.; et al. Krüppel Homolog 1 Represses Insect Ecdysone Biosynthesis by Directly Inhibiting the Transcription of Steroidogenic Enzymes. *Proc. Natl. Acad. Sci. USA* **2018**, *115*, 3960–3965. [CrossRef] [PubMed]

MDPI
St. Alban-Anlage 66
4052 Basel
Switzerland
www.mdpi.com

Biomolecules Editorial Office
E-mail: biomolecules@mdpi.com
www.mdpi.com/journal/biomolecules

Academic Open
Access Publishing

mdpi.com

ISBN 978-3-7258-0454-2